Robust Multivariable Control of Industrial Production Processes: A Discrete-Time Multi-Objective Approach

Thesis submitted for the degree of
Doctor of Philosophy
at the University of Leicester

by

Ghassan Ali Murad BEng (Teesside) Msc, DIC (London)
Department of Engineering
University of Leicester

August 1995

ProQuest LLC
789 East Eisenhower Parkway
P.O. Box 1346
Ann Arbor, MI 48106-1346


LEICESTER UNIVERSITY LIBRARY

To my parents

Robust Multivariable Control of Industrial Production Processes: A Discrete-Time Multi-Objective Approach

Ghassan Ali Murad

Abstract

This thesis considers a number of important practical issues in the synthesis of discrete-time robust controllers for industrial processes. The work focuses on the control of an "unknown" SISO process (the IFAC 1993 benchmark), the design of robust model-based controllers for a MIMO industrial production process (a glass tube production process), and the design of robust MIMO controllers having integrated control and diagnostic capabilities.

The industrial case studies presented are realistic in the sense that their control problems do frequently arise in engineering situations. Explicit state-space formulae for $\mathcal{H}^\infty$-based one degree-of-freedom (1-DOF) and two degrees-of-freedom (2-DOF) robust controllers are derived. They provide robust stability with respect to left coprime factor perturbations, and for the 2-DOF case, a degree of robust performance in the sense of making the closed-loop system follow a desired reference model. Robust controllers for the "unknown" plant are designed using $\mathcal{H}^2$ and $\mathcal{H}^\infty$ optimization techniques. Explicit closed-loop performance is obtained by designing the weighting function parameters using numerical optimization techniques in the form of the method of inequalities.

Methods for designing $\mathcal{H}^\infty$-based controllers that can be directly implemented in the Internal Model Control (IMC) scheme are presented. Explicit state-space formulae for $\mathcal{H}^\infty$-based IMC 1-DOF and 2-DOF robust controllers which provide robust stability and robust performance with respect to left coprime factor perturbations, are derived.

A technique for discrete-time model reduction is presented, with two illustrative examples. The technique is used in a detailed study of the identification and control of the glass tube production process. The production process, especially for large tube measures, is ill-conditioned and contains large time delays. The model of the process reflects the transfer of two process inputs (mandrel pressure and drawing speed) to the tube dimensions (wall thickness and diameter). The models obtained from advanced multivariable identification are used for the design of robust IMC controllers for the process. The robust performance of the controller is demonstrated and a comparison is made with the present control system.

Finally, a framework for synthesizing robust controllers which have both control and actuator failure detection capabilities is presented. Simulation results for a MIMO design example are presented which demonstrate the feasibility of this integrated design approach.

Acknowledgements

First and foremost I would like to thank my supervisor Professor Ian Postlethwaite for all the guidance and support he gave me during the last four years. I am also indebted to Ian for his constructive criticism and reading of early drafts, and for his patience in reading such a large manuscript. I also wish to thank my co-supervisor Dr. Da-Wei Gu for his guidance and precious advice towards conducting my research.

Financial support for my research work came from the LUCIFER project organized by Philips Lighting, Netherlands, is gratefully acknowledged. In addition, I would like to thank my "project colleagues": Heinz Falkus (Eindhoven University of Technology), Richard Hakvoort (Delft University of Technology), Peter van Overschee (Catholic University Leuven), Erick van Bracht (Delft University of Technology), and Jobert Ludlage and Professor Ton Backx (SETPOINT-IPCOS) for many interesting discussions during the course of the project. I was also fortunate enough to have numerous informative visits to the industrial site of Philips Lighting in Aachen, Germany, and the Eindhoven University of Technology and SETPOINT-IPCOS, both in the Netherlands. In addition, I was able to visit the industrial site of Philips Lighting in Winschoten, Netherlands. I thank them all for their hospitality.

I would also like to thank my friends and colleagues with whom I have worked and socialized, in particular the "control group": Byung-Wook Choi, John Geddes, Jong-Lik Lin, Weining Feng, Daniel Walker, Abdul-Wahed Saif, Chris Edwards, Neale Prescott Foster, James Whidborne, Song-Joo Goh, Shuzhi Ge, Timothy Fitzpatrick, Raza Samar, Colin Paterson, Mark Tucker, Alex Smerlas, Jens Kawaleke, Ahmet Ucar, Xiao Yun, Aamer Bhatti, Sujit Bag, and the "biomedical group": Paul Goodyer, Dave Sewell, Tuan Tran. I would also like to thank my fellow 5-A-Side footballers for their contribution towards creating a friendly social atmosphere. Thanks to Dr. Michael Green, for sparking off my interest in Robust Multivariable Control whilst at Imperial College, and thanks to Tim Frankcom (Bahrain Telecommunications) for introducing me to the field of Control Engineering.

Finally, I thank my parents for being the constant source of moral support, and I also thank Jane Foreman for her support and great company.

Contents

1 Introduction **1**

1.1 General Introduction 1

1.2 An Overview of Robust $\mathcal{H}^\infty$ Control 3

1.3 Contribution and Summary of the Thesis 4

2 Robust Control System Design **9**

2.1 Introduction 9

2.2 $\mathcal{H}^2$ and $\mathcal{H}^\infty$-Optimal Control 10

2.2.1 Standard Regulator Problem 10

2.2.2 Problem Definition 11

2.3 $\mathcal{H}^2$-Optimal Control 12

2.3.1 The $\mathcal{H}^2$-Optimal Control Problem 12

2.3.2 The LQG Problem 14

2.4 $\mathcal{H}^\infty$-Optimal Control 19

2.4.1 Model Uncertainty Structures 19

2.4.2 The $\mathcal{H}^\infty$-Optimal Control Problem 20

2.4.3 The $\mathcal{H}^\infty$ Mixed Sensitivity Problem 24

2.4.4 Solution to the $\mathcal{H}^\infty$-Control Problem 24

2.4.5 Robust Performance 31

2.5 Summary 35

3 Robust Control with Normalized Coprime Factor Perturbations 36

3.1 Introduction 36

3.2 Special Control Problems 37

3.2.1 $\mathcal{H}^\infty$ Full Information Control 37

3.2.2 Disturbance Feedforward Problem 41

3.3 $\mathcal{H}^\infty$ 1-DOF Normalized Coprime Factor Design Approach 42

3.3.1 Robust Stabilization of Left Coprime Factorization 43

3.3.2 Controller Formulae 46

3.3.3 An $\mathcal{H}^\infty$ Loop Shaping Design Procedure (LSDP) 51

3.4 $\mathcal{H}^\infty$ 2-DOF Design Approach 52

3.4.1 The 2-DOF Design Configuration 53

3.4.2 The 2-DOF Controller Formulae and Structure 55

3.5 Summary 58

4 Robust Multi-Objective Control of an Unknown Industrial Plant 61

4.1 Introduction 61

4.2 Problem Statement 62

4.2.1 Specifications 63

4.2.2 Simulation 63

4.2.3 Linear Models and Open-loop Analysis 64

4.3 An Introduction to the Method of Inequalities 65

4.3.1 The Method of Inequalities (MOI) 65

4.3.2 An Algorithm for Solving MOI 68

4.4 Proposed Design Methods Using MOI for Multi-Objective Control . . . 69

4.4.1 PI/PID Controller Design 69
4.4.2 Weighting Parameter Design for the LQG 71
4.4.3 Weighting Parameter Design for the $\mathcal{H}^\infty$-Mixed Sensitivity Problem 73
4.4.4 Weighting Parameter Design for the LSDP 75
4.4.5 Weighting Parameter and Prefilter Design for the LSDP 76
4.4.6 Weighting Parameter Design for the 2-DOF LSDP 78
4.5 Controller Design and Simulation Results 80
4.5.1 Closed-Loop Performance Functionals and Design Criteria 81
4.5.2 Results obtained for all Stress Levels 82
4.6 Summary 97

5 Robust Internal Model-Based Controller Design **99**

5.1 Introduction 99
5.2 The Internal Model Control (IMC) Scheme 100
5.2.1 Stability Conditions for IMC 102
5.2.2 Relationship of IMC with Standard Unit Feedback 104
5.2.3 Performance of IMC 105
5.3 A Linear Quadratic - Implicit Model Following Approach 109
5.4 An $\mathcal{H}^\infty$ 1-DOF Design Approach 112
5.4.1 Traditional $\mathcal{H}^\infty$ Design Formulation for IMC 112
5.4.2 An IMC Formulation and Controller Synthesis of the Normalized Coprime Factor Design Procedure 119
5.4.3 Controller Formulae 120
5.5 An $\mathcal{H}^\infty$ 2-DOF Design Approach 123
5.5.1 2-DOF Controllers 123

5.5.2 An IMC Formulation and Controller Synthesis of the 2-DOF Design Approach 124

5.6 Summary 130

6 A Direct Approach to Discrete-Time Model Reduction 132

6.1 Introduction 132

6.2 Discrete-Time Model Reduction 134

6.3 A State-Space Balancing Transformation 140

6.4 Coprime Factor Model Reduction 146

6.5 Numerical Examples 152

6.6 Summary 157

7 Robust Process Identification of a Glass Tube Production Process 158

7.1 Introduction 158

7.2 Description of the Process 160

7.3 Identification by Advanced Multivariable Methods 164

7.3.1 A Minimal Polynomial Approach 164

7.3.2 A State-Space Approach 165

7.3.3 A Robust Control Oriented Approach 165

7.3.4 An Integrated Identification Approach 165

7.4 Data Pre-processing and Identification Experiments 166

7.4.1 Pre-processing of the Identification Data 166

7.4.2 Identification Experiments 167

7.5 Model Estimation and Validation 174

7.6 Summary 179

8 Applying Robust IMC Control to a Glass Tube Production Process 180

8.1 Introduction 180
8.2 Glass Tube Design Study 181
8.2.1 An Overview of the Control Problem 181
8.2.2 Open-Loop Analysis of the Process 182
8.2.3 Design Specifications 190
8.3 A Comparison with the Existing Control System 191
8.4 Controller Design Procedure 200
8.5 Simulation Results 203
8.5.1 Measure 1 204
8.5.2 Measure 2 204
8.5.3 Measure 3 206
8.6 Summary 213

9 A Robust Design Approach to Integrated Controls and Diagnostics 214

9.1 Introduction 214
9.2 Types of Failure Models 217
9.2.1 Actuator Failure 217
9.2.2 Sensor Failure 218
9.3 Control and Diagnostic Design Objectives 218
9.4 The Four Degrees-Of-Freedom Controller 223
9.4.1 A Generalized Regulator Framework 223
9.4.2 The Compatibility of the 4-DOF Controller Parameterization with the Youla Parameterization 224
9.5 $\mathcal{H}^2$-Optimal Control and Diagnostics 228
9.6 $\mathcal{H}^\infty$-Optimal Control and Diagnostics 231
9.6.1 Robust Synthesis of the 4-DOF Controller 232

9.6.2 Design Example 234
9.7 Summary 239

10 Conclusions and Future Work **240**

10.1 Concluding Remarks 240
10.2 Suggestions for Future Work 242

A Preliminary Mathematical Background **246**

A.1 Nomenclature 246
A.2 Basic System Theory 248
A.2.1 Transfer Functions 248
A.2.2 Controllability and Observability 248
A.2.3 All-Pass Transfer Function Matrices 249
A.3 The Discrete-Time Algebraic Riccati Equation 250
A.3.1 Symplectic Matrices 250
A.3.2 The Riccati Operator 251
A.4 Coprime Factorization 252
A.5 Internal Stability and Well-Posedness 254

B Proof of Results from Chapter 6 **256**

B.1 Proof of (6.18) 256
B.2 Proof of (6.20) 258

References **264**

Chapter 1

Introduction

1.1 General Introduction

In the process industry numerous types of processes are being controlled and monitored to produce manufactured products within desired specifications. The main task of the control engineer, with the aid of appropriate sensors, controllers and actuators, is to improve the performance of the plant or process. A block diagram of a general control system is shown in Figure 1.1. Since the sensor signals affect the particular plant to be

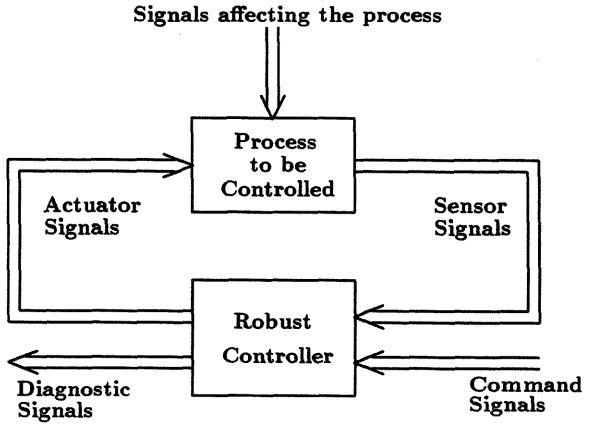

Figure 1.1: A General Control System.

controlled *via* the controller and the actuators, the control scheme shown in Figure 1.1

is called a closed-loop system. If the control scheme has no sensors and only generates actuator signals from the command signals alone, it is called an open-loop system. Finally, a system that has no actuators and produces only operator display signals by processing sensor signals alone, is sometimes called a monitoring or a diagnostic system.

The great flexibility of software-based control algorithms has made possible the synthesis of highly sophisticated controllers, including model-based controllers, which can control single-input single-output (SISO) systems with better robustness margins than simple controllers, and can solve complex multi-input multi-output (MIMO) control problems. In addition to improved control, additional functions such as adaptation and failure diagnosis can also be handled by modern algorithms as will be seen later. The need for these functions is strong in manufacturing and the process industries where there are ever increasing demands to improve quality and flexibility of production. In this thesis, a framework for synthesizing robust controllers, robust model-based controllers, and an integrated robust controller-diagnostic pair is presented and studied in detail. Industrial case studies are used to evaluate these functions and some important issues on model reduction and multivariable identification will also be addressed.

The presentation is entirely in discrete-time. The motivation behind this is that most new controllers are now implemented digitally. A natural approach to the discrete-time problem is to transform it into a continuous-time one *via* the bilinear transformation $s = \frac{z-1}{z+1}$, to design a continuous-time controller and then to transform back to discrete-time *via* the inverse map $z = \frac{1+s}{1-s}$. However, although this procedure is valid, a number of disadvantages have been noted in [41]:

1) The bilinear transformation cannot be used for time-varying problems.

2) Since properness is not preserved by the bilinear transformation, special care needs to be taken to avoid nonproper controllers.

3) Although the bilinear transformation will lead to controller formulae for the discrete-time synthesis problem, there are theoretical advantages to be gained from a solution in *natural coordinates.*

With these in mind we propose to work primarily in discrete-time.

1.2 An Overview of Robust $\mathcal{H}^\infty$ Control

After almost 15 years of development to produce more sophisticated yet realistic control methods, robust control has gained a high level of acceptance with applications in a range of industrial practices. In general, controllers differ in complexity and effectiveness. Simple controllers such as proportional plus derivative plus integral (PID) are widely used in industrial applications and their adjustment requires just a simple model of the dynamic behaviour of the plant to be controlled [119, 5]. A major draw back in the design of PID controllers, however, is that there is no direct incorporation of model uncertainty in the synthesis which inevitably limits the robustness of the closed-loop system.

Researchers in the 1930's and 1940's developed methods suitable for SISO systems [9, 80]. The designed controllers were expected to be insensitive to plant/model mismatch and perform well enough under unmeasured disturbances. However, extensions of these SISO methods to MIMO systems were found to be inadequate. In general, MIMO systems are difficult to control due to the presence of interaction. The problem is often further complicated by the presence of large time delays and process non-linearities. Several approaches have appeared in the control literature in recent years that overcome many of these MIMO difficulties. In the 1960's more sophisticated control methods such as optimal control theory (i.e Linear Quadratic Guassian - LQG) were developed. LQG could nicely handle MIMO systems, but was sometimes sensitive to small perturbations, leading to poor performance and possibly instability if implemented on a real plant. This demonstrated the need to directly incorporate model uncertainty into the controller design procedure so that *robust* controllers could be synthesized. Motivated by this need to address uncertainty in a systematic way, the $\mathcal{H}^\infty$ problem was formulated by [117]. This problem was then further developed by many researchers, and has proved to be an effective framework for analyzing robustness and a powerful tool for control system design under unstructured uncertainty. The structured uncertainty problem, originally formulated in [17], has further highlighted the differences between MIMO systems and SISO systems and has led to the analysis and design of MIMO systems using structured singular value analysis and synthesis, also known as μ-analysis and synthesis. Controllers synthesized *via* these sophisticated design methods were first

used in aerospace systems, and are now being introduced into other industrial systems.

$\mathcal{H}^\infty$ control is a frequency domain theory and it has been shown in [13, 30, 92] that important frequency domain problems in control system design can be formulated as $\mathcal{H}^\infty$-optimization problems. Such problems include for example the minimization of the sensitivity transfer function in a minimax approach, and the optimization of robustness for unstructured uncertainty. Mathematically speaking, the $\mathcal{H}^\infty$ control problem is to minimize a weighted infinity norm of some closed-loop transfer function or a combination of transfer functions over a set of controllers satisfying the internal stability requirement. The set of stabilizing controllers was first parameterized by Youla *et al* in [113]. With this Youla parameterization and some inner-outer factorizations, the $\mathcal{H}^\infty$-optimization problem can be simplified to a general distance problem [12] and in special cases, the general distance problem becomes the Nehari extension problem [74]. This special case is also known as the one-block distance problem, the most general case being a four-block problem. The first method available to solve the general four-block distance problem was proposed by [19] where the method resulted in high-order controllers compared to the plant order. A more elegant method introduced by [37] and [22] solves the problem in a suboptimal sense and only requires the solution to two Riccati equations for each level of optimality, γ. An attractive property regarding this solution is that it synthesizes suboptimal controllers with the same order as the plant. The situation has been further simplified by [62] where for a particular design problem optimal controllers can be synthesized without performing any iterations on the optimality level γ.

1.3 Contribution and Summary of the Thesis

A common aim in the process industry is to increase the levels of automation in production processes which must be highly flexible. Good control strategies are therefore essential. In turn good control strategies require a good understanding of the dynamic behaviour of the processes under consideration. However, with the aid of existing advanced identification techniques and emerging control methods, good mathematical models can be derived and advanced control strategies designed to further improve the performance and flexibility of industrial processes. The aim of the present study is:

1) To present some useful and improved methods for tuning and designing weighting functions in $\mathcal{H}^2$ and $\mathcal{H}^\infty$ optimization methods.

2) To present an approach which enables the direct design of robust internal model-based controllers in the framework of robust control theory.

3) To present an approach which enables the design of integrated controls and diagnostics in the framework of robust control theory.

4) To present a direct discrete-time model reduction approach suitable for reducing non-minimal high-order controllers.

5) To design and test a SISO control system and a MIMO control system on industrial case studies in order to asses the newly presented methods.

Details of the mathematical notation used, together with preliminary results pertaining to basic system theory, discrete-time algebraic Riccati equations, coprime factorization, and internal stability and well-posedness are given in Appendix A. The chapter contents can be summarized as follows:

Chapter 2 – In this chapter, an overview will be given on robust control. Well known results on discrete-time $\mathcal{H}^2$-optimal control, $\mathcal{H}^\infty$-optimal control, and μ-synthesis will be summarized. The majority of these results will be extensively applied in Chapter 4.

Chapter 3 – In this chapter, robust control using normalized coprime factor plant descriptions is investigated. There are two contributions. The first is to formulate, in a one degree-of-freedom (1-DOF) setting, the discrete-time problem of robust stabilization with respect to uncertainty in a normalized left coprime factorization of the plant. The steps are analogous to those in [106], where the problem was first formulated with respect to uncertainty in a normalized right coprime factorization. Suboptimal and optimal controllers are derived. The second contribution is to formulate, in a two degrees-of-freedom (2-DOF) setting, the discrete-time robust stablization problem with respect to uncertainty in a normalized left coprime factorization. Only suboptimal controllers are derived. The continuous-time problem was investigated by [47] and [108]. This second contribution has already been presented at the American Control Conference [93] and both contributions form part of a Journal paper under preparation.

Chapter 4 – In this chapter, the robust control techniques discussed in Chapters 2 & 3 will be applied to an "unknown" industrial plant, namely the IFAC 1993 benchmark problem proposed by [39]. These control techniques, which can also be cast as analytical optimization design methods, generally have weights which are adjusted by the designer in order to get a good design. This adjustment is often by trial and error and can be time consuming. To circumvent this problem, it is advantageous to combine analytical and numerical methods so that numerical search techniques, such as the method of inequalities (MOI) [115], can be used to find good weighting parameters for the analytical optimization problem. The main contribution is to describe how MOI can be combined with the various analytical optimization design methods discussed in Chapters 2 & 3 in order to provide a powerful multi-objective mixed optimization controller design method. Its application to the "unknown" industrial plant is described in detail. The majority of this work have been presented at the IFAC World Congress 1993 [85], in [109], and published in Automatica [86] and the International Journal of Control [110].

Chapter 5 – In this chapter, internal model control (IMC) concepts for stable plants are presented and some background material given in [67] will be summarized. We will only consider MIMO systems and show how the IMC can be implemented. However, more detailed developments of IMC controller design will not be discussed; they can be found in [67]. The main contribution is to present a framework to directly synthesize robust IMC controllers using $\mathcal{H}^\infty$-optimization methods. The $\mathcal{H}^\infty$ methods used include the 1-DOF and 2-DOF loop shaping approaches with coprime factor uncertainty. For the 1-DOF case, suboptimal and optimal IMC controllers are derived, and for the 2-DOF case only a suboptimal IMC controller is derived. The latter approach will be presented at the European Control Conference [71] and the majority of the work of this chapter is being prepared for submission to a Journal for consideration.

Chapter 6 – In this chapter, discrete-time model reduction is considered. A sophisticated approach towards the design of high-order discrete-time controllers, especially high-order IMC controllers, is given by $\mathcal{H}^2$ and $\mathcal{H}^\infty$ optimization techniques. The designed controllers, using these techniques, may be more complex than it would be reasonable to implement. In some cases such controllers can also be non-minimal resulting

in numerical difficulties when common model reduction algorithms are used. The main contribution is to propose a direct discrete-time model reduction approach. The approach will be based on combining existing numerical algorithms resulting in a reliable approach with numerical robustness for computing a balanced singular perturbational approximation of a stable state-space system that might be close to being non-minimal. The algorithm can be used for unstable systems by applying it separately to the factors in a normalized coprime factorization as proposed by [63]. The continuous-time results given in [63] will be extended and formulated in a discrete-time setting in this chapter. The majority of the work in this chapter is being prepared for submission to a Journal for consideration.

Chapter 7 – In this chapter, a detailed case study on the application of advanced multivariable identification to a glass tube production process will be presented. In this process the dimensions of the tube, *wall thickness* and *diameter*, are directly influenced by two process inputs, *mandrel pressure* and *drawing speed* (Figure 7.1). The response of the process to changes in the inputs can only be measured after a rather long period of time compared to the process dynamics. This large time delay is caused by the fact that no sensors are available for measuring the dimensions at high temperature, hence measurement is only possible at much lower temperatures. For the control of such a process, a good model is required, especially as the time delays in the measurements are of the order of the process dynamics, if not higher. So for accurate control of the tube dimensions, a good mathematical model is required. The main contribution is to directly apply existing advanced multivariable identification schemes [6, 27, 81, 44] to real identification data extracted from identification experiments carried out on the glass tube production process. The proposed identification procedure used in this chapter was presented at the Third Philips Conference on Applications of Systems and Control Theory [26].

Chapter 8 – In this chapter, the main contribution is to present a detailed case study on the application of robust IMC control (using the techniques from Chapter 5) to the glass tube production process (using the models from Chapter 7). In the study the open-loop behaviour of the production process is analyzed and a comparison with the present control system is discussed. A design procedure which combines the proposed

IMC design approach with the method of inequalities (MOI) is described. Finally, detailed results are given of the proposed control system applied to the production process. Earlier controller design results were presented at the IFAC World Congress 1993 [70], the European Control Conference 1993 [72], and in [73]. Some of the latest results were presented in [71] and [26].

Chapter 9 – In this chapter, the design problem of integrated controls and diagnostics is considered. The foundation for such an approach was presented in [77] where it was proposed to use a four degrees-of-freedom (4-DOF) controller. This controller has 2 types of input and 2 types of output (rather than one of each). The additional controller output is viewed as a diagnostic output (see Figure 1.1) which is monitored to detect and isolate failures in the sensors or actuators. The main contribution is to formulate a design approach to integrate controls and diagnostics in the now standard robust control theory framework. This enables the synthesis of the 4-DOF controller in a single step approach. The majority of the results in this chapter have been submitted to the IFAC World Congress 1996 for consideration.

Chapter 10 – In this chapter, general conclusions are drawn together with suggestions for future work.

Chapter 2

Robust Control System Design

2.1 Introduction

The aim of this chapter is to introduce and summarize some well known results on $\mathcal{H}^2$ & $\mathcal{H}^\infty$-optimal control, and μ-synthesis. The presentation of this chapter serves two main purposes: First, most of the main results on $\mathcal{H}^2$, $\mathcal{H}^\infty$, and μ will be extensively applied in Chapter 4. Second, some of the $\mathcal{H}^\infty$ results will be needed in Chapters 3, 5 and 9. The theory of Linear Quadratic Guassian (LQG) control (a special problem of $\mathcal{H}^2$) has been analyzed in more detail in [4, 54, 53]. State-space solutions of the discrete-time $\mathcal{H}^\infty$ problem were first derived in [49, 58, 96]. The results presented in this chapter follow those from [49]. An extensive discussion of the μ-analysis and synthesis can be found in [17, 20, 21, 7, 82] for the continuous-time case. The discrete-time analogues can be found in [14].

The organization of this chapter is as follows. Section 2.2 will introduce the $\mathcal{H}^2$ and $\mathcal{H}^\infty$-optimal control problem. In Section 2.3, the complete solution to the $\mathcal{H}^2$ control problem is presented. In this section, it will be shown that the LQG problem is a special case of the $\mathcal{H}^2$ problem. In Section 2.4, the complete solution to the $\mathcal{H}^\infty$ control problem is presented. In this section, different representations of modelling errors are introduced, various design objectives and solutions are formulated, and the robust performance problem is discussed. Finally, a summary is given in Section 2.5.

2.2 $\mathcal{H}^2$ and $\mathcal{H}^\infty$-Optimal Control

$\mathcal{H}^2$ and $\mathcal{H}^\infty$ controller synthesis enables the desired frequency response characteristics to be optimally shaped. Since the 2-norm and ∞-norm are intimately related to the singular values, robustness considerations are simply incorporated into the control design. Additionally, results obtained by several authors [41, 22, 4, 91, 57, 62, 38] make the computation of $\mathcal{H}^2$ and $\mathcal{H}^\infty$ controllers in an interactive design environment a reality.

2.2.1 Standard Regulator Problem

There are many ways in which feedback design problems can be cast as $\mathcal{H}^2$ and $\mathcal{H}^\infty$ optimization problems. It is very useful therefore to have a standard problem formulation into which most problems may be manipulated. Such a general formulation is shown in Figure 2.1, and is known as the standard regulator problem [19]. The system

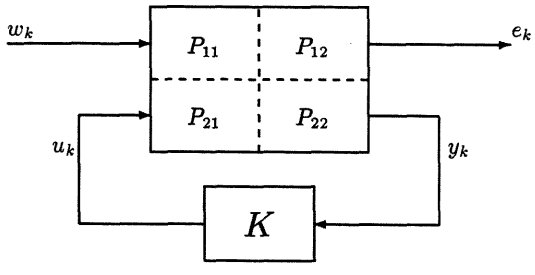

Figure 2.1: Standard Regulator Problem.

is described as

$$\begin{bmatrix} e_k \\ y_k \end{bmatrix} = P(z) \begin{bmatrix} w_k \\ u_k \end{bmatrix} = \begin{bmatrix} P_{11}(z) & P_{12}(z) \\ P_{21}(z) & P_{22}(z) \end{bmatrix} \begin{bmatrix} w_k \\ u_k \end{bmatrix} \tag{2.1}$$

$$u_k = K(z)y_k \tag{2.2}$$

with the state-space realization of P is

$$P \stackrel{s}{=} \left[\begin{array}{c|cc} A & B_1 & B_2 \\ \hline C_1 & D_{11} & D_{12} \\ C_2 & D_{21} & D_{22} \end{array}\right] \tag{2.3}$$

The signals are: u_k the control variables, y_k the measured variables, w_k the exogenous signals, and e_k the control objectives. The closed-loop transfer function matrix from w_k to e_k is given by the linear fractional transformation [87, 88]

$$e_k = \mathcal{F}_l(P, K)w_k \tag{2.4}$$

where

$$\mathcal{F}_l(P, K) = P_{11} + P_{12}K(I - P_{22}K)^{-1}P_{21} \tag{2.5}$$

The standardized plant P includes the plant model, all weighting matrices and the interconnection structure for the particular problem being solved. The standard regulator problem is then:

- Find all realizable controllers K which stabilize the closed-loop and achieve the ∞-norm objective

  $$\| F_l(P, K) \|_\infty < \gamma$$

  for some $\gamma > 0$.

By considering the dimensions of w_k, u_k, e_k and y_k, three special cases of the standard problem can be identified. If P_{12} and P_{21} are square, then the standard problem is called a 1-block problem. For a sensible control problem, P_{12} will be either a tall or square matrix, and P_{21} will be either flat or square. If P_{12} or P_{21} is square, but not both, then the standard problem is called a 2-block problem. If neither P_{12} nor P_{21} is square, then the standard problem is called a 4-block problem.

2.2.2 Problem Definition

Let the following assumptions be made on (2.3):

A1) (A, B_2) is stabilizable and (C_2, A) is detectable.

A2) D_{12} has full column rank and there exists a matrix $D_\perp$ such that $[\, D_{12} \quad D_\perp \,]$ is unitary.

A3) D_{21} has full row rank and there exists a matrix $\tilde{D}_\perp$ such that $\begin{bmatrix} D_{21} \\ \tilde{D}_\perp \end{bmatrix}$ is unitary.

A4) The matrix

$$\begin{bmatrix} A - e^{j\theta} I & B_2 \\ C_1 & D_{12} \end{bmatrix}$$

has full column rank for all $\theta \in [-\pi, \pi)$.

A5) The matrix

$$\begin{bmatrix} A - e^{j\theta} I & B_1 \\ C_2 & D_{21} \end{bmatrix}$$

has full row rank for all $\theta \in [-\pi, \pi)$.

A6) D_{22} is equal to zero.

A1 is necessary and sufficient to guarantee the existence of stabilizing controllers. A2 indicates that all the control signals are penalized. A3 is the dual of A2. A4 and A5 guarantee the existence of solutions to certain Riccati equations. In the case where $D_{12}^T C_1 = 0$, A4 can be replaced by assuming that (C_1, A) has no unobservable modes on the unit circle. Similarly, if $B_1 D_{21}^T = 0$, A5 can be replaced by assuming that (A, B_1) has no uncontrollable modes on the unit circle. The assumption $D_{22} = 0$ is not necessary but introduced for simplicity. It implies that there is no direct transmission from the control input to the measured output.

2.3 $\mathcal{H}^2$-Optimal Control

2.3.1 The $\mathcal{H}^2$-Optimal Control Problem

Consider the system

$$\begin{aligned} x_{k+1} &= Ax_k + Bu_k \\ y_k &= Cx_k + Du_k \end{aligned} \tag{2.6}$$

with the $n_p \times n_m$ transfer function matrix

$$G(z) = D + C(zI - A)^{-1}B \tag{2.7}$$

Suppose the system (2.6) is driven by white noise of unit intensity,

$$E\{u_k u_\tau^T\} = I\delta_{k-\tau} \tag{2.8}$$

The expected output power is then given by

$$\begin{aligned} E\left\{\lim_{N\to\infty}\frac{1}{2N}\sum_{k=-N}^{N} y_k^T y_k\right\} &= E\left\{\lim_{N\to\infty}\frac{1}{2N}\sum_{k=-N}^{N}\mathbf{tr}(y_k y_k^T)\right\} \\ &= \frac{1}{2\pi}\int_{-\pi}^{\pi}\mathbf{tr}\left(G(e^{j\theta})G^T(e^{-j\theta})\right)d\theta \\ &= \|G\|_2^2 \end{aligned} \tag{2.9}$$

The $\mathcal{H}^2$-norm can also be expressed in terms of the singular values of the transfer function matrix G as

$$\|G\|_2 = \left(\frac{1}{2\pi}\int_{-\pi}^{\pi}\sum_{i=1}^{n}\sigma_i(G(e^{j\theta}))^2 d\theta\right)^{1/2} \tag{2.10}$$

where $n = \min\{n_p, n_m\}$. Thus by minimizing the 2-norm, the output power of the system due to a unit intensity white noise input is minimized.

The standard $\mathcal{H}^2$ regulator problem is then [42]:

- Find a controller $K_{opt} \in \mathcal{K}$ such that

$$\|\mathcal{F}_l(P, K_{opt})\|_2 \leq \|\mathcal{F}_l(P, K)\|_2 \tag{2.11}$$

  $\forall\, K \in \mathcal{K}$, where $\mathcal{K}$ denotes the set of all controllers which achieve internal stability of the closed-loop.

This is known as the $\mathcal{H}^2$-optimization problem. The standardized plant P includes all weighting matrices, the plant model and the interconnection structure associated with the type of problem being solved.

2.3.2 The LQG Problem

An important special case of the $\mathcal{H}^2$-optimal control is that of the LQG regulator, which is considered by the following stochastic system

$$\begin{aligned} x_{k+1} &= Ax_k + Bu_k + w_{p_k} \\ y_k &= Cx_k + v_{s_k} \end{aligned} \tag{2.12}$$

where u_k is a control input, w_{p_k} and v_{s_k} are the process and measurement noise inputs which have constant power spectral density matrices W and V, respectively. They are also taken to be white, uncorrelated and of unit intensity

$$E\left\{\begin{bmatrix} w_{p_k} \\ v_{s_k} \end{bmatrix} \begin{bmatrix} w_{p_\tau}^T & v_{s_\tau}^T \end{bmatrix}\right\} = \begin{bmatrix} I & 0 \\ 0 & I \end{bmatrix} \delta_{k-\tau} \tag{2.13}$$

and y_k is the vector of measurements. A feedback controller is desired such that the performance measure

$$J_{lqg} = E\left\{\lim_{N\to\infty} \frac{1}{N} \sum_{k=0}^{N} \left(x_k^T Q x_k + u_k^T R u_k\right)\right\} \tag{2.14}$$

is minimized, where $Q \geq 0$ and $R \geq 0$. This is known as the LQG cost function which is the sum of the steady-state mean-square weighted state x_k, and the steady-state mean-square weighted actuator signal u_k.

The framework of the LQG problem can be cast as follows [11]. The weighted plant state x_k and actuator signal u_k can be extracted as the regulated output, *e.g.*

$$e_k = \begin{bmatrix} Q^{\frac{1}{2}} x_k \\ R^{\frac{1}{2}} u_k \end{bmatrix} \tag{2.15}$$

The exogenous input consists of the process and measurement noises, which are represented as

$$\begin{bmatrix} w_{p_k} \\ v_{s_k} \end{bmatrix} = \begin{bmatrix} W^{\frac{1}{2}} \\ V^{\frac{1}{2}} \end{bmatrix} w_k \tag{2.16}$$

with w_k a white noise signal. So the P matrix can be set up as the transfer function matrix from w_k and u_k to e_k and y_k. This is easily seen to be given by

$$\begin{bmatrix} x_{k+1} \\ e_k \\ y_k \end{bmatrix} = \left[\begin{array}{c|cc|c} A & W^{\frac{1}{2}} & 0 & B \\ \hline Q^{\frac{1}{2}} & 0 & 0 & 0 \\ 0 & 0 & 0 & R^{\frac{1}{2}} \\ \hline C & 0 & V^{\frac{1}{2}} & 0 \end{array}\right] \begin{bmatrix} x_k \\ w_k \\ u_k \end{bmatrix} \tag{2.17}$$

This is shown in Figure 2.2. Since w_k is a white noise signal, the LQG cost is simply

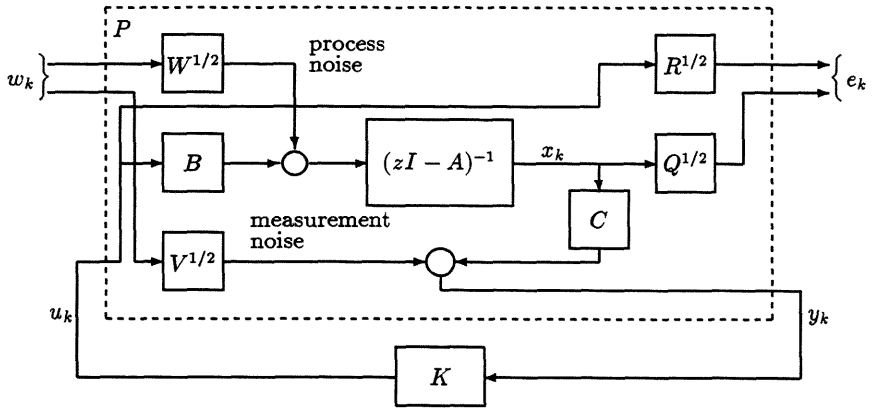

Figure 2.2: Standard Regulator LQG Problem.

the variance of e_k, which is given by

$$J_{lqg} = \| e_k \|_2^2 \tag{2.18}$$

A standard assumption for the LQG problem is that the plant is controllable from each of u_k and w_k, observable from each of e_k and y_k, and in order to satisfy the full column and row rank assumptions on D_{12} and D_{21}, the weights used for the actuator signal and the sensor noise, R and V, need to be > 0. The following extra assumptions are made:

A7) $D_{12}^T [C_1 \quad D_{12}] = [0 \quad I]$

A8) $\begin{bmatrix} B_1 \\ D_{21} \end{bmatrix} D_{21}^T = \begin{bmatrix} 0 \\ I \end{bmatrix}$

A9) $D_{11} = 0$

It follows from these assumptions that A4 reduces to the condition that (C_1, A) has no unobservable modes on the unit circle, and A5 reduces to the condition that (A, B_1) has no uncontrollable modes on the unit circle. Assumption A7 is quite common in the LQG literature and amounts to assuming that there is no cross term in the formula for $\| e_k \|_2^2$ and the penalty on the control input u_k is normalized. Assumption A8 is the dual of assumption A7 and is analogous to the standard assumption in the Kalman filtering

problem that the process noise and the measurement noise are uncorrelated and that the measurement noise is non-singular and normalized. Assumption A9 implies that there is no direct transmission from the exogenous input w_k to the regulated output e_k. The extra assumptions made require the definition of a scaled control input $u_k R^{-\frac{1}{2}}$ and a scaled measurement vector $V^{-\frac{1}{2}} y_k$. This gives the scaled P matrix, P_s as

$$\begin{bmatrix} x_{k+1} \\ e_k \\ V^{-\frac{1}{2}} y_k \end{bmatrix} = \left[\begin{array}{c|cc|c} A & W^{\frac{1}{2}} & 0 & BR^{-\frac{1}{2}} \\ \hline Q^{\frac{1}{2}} & 0 & 0 & 0 \\ 0 & 0 & 0 & I \\ \hline V^{-\frac{1}{2}} C & 0 & I & 0 \end{array}\right] \begin{bmatrix} x_k \\ w_k \\ u_k R^{-\frac{1}{2}} \end{bmatrix} \tag{2.19}$$

With the above assumptions in force, there is a unique controller that minimizes the LQG objective. The two symplectic pairs of matrices, H_2 and J_2, are defined as

$$H_2 := \left[\begin{pmatrix} A & 0 \\ -C_1^T C_1 & I \end{pmatrix}, \begin{pmatrix} I & B_2 B_2^T \\ 0 & A^T \end{pmatrix}\right] \tag{2.20}$$

$$J_2 := \left[\begin{pmatrix} A^T & 0 \\ -B_1 B_1^T & I \end{pmatrix}, \begin{pmatrix} I & C_2^T C_2 \\ 0 & A \end{pmatrix}\right] \tag{2.21}$$

Since (A, B_2) is stabilizable and (C_1, A) has no unobservable modes on the unit circle, it follows that $H_2 \in dom(RIC)$ (see Appendix A). Also, since (C_2, A) is detectable and (A, B_1) has no uncontrollable modes on the unit circle, it follows that $J_2 \in dom(RIC)$. For the LQG set up of (2.19), (2.20) and (2.21) may be rewritten as

$$H_2 := \left[\begin{pmatrix} A & 0 \\ -Q & I \end{pmatrix}, \begin{pmatrix} I & BR^{-1}B^T \\ 0 & A^T \end{pmatrix}\right] \tag{2.22}$$

$$J_2 := \left[\begin{pmatrix} A^T & 0 \\ -W & I \end{pmatrix}, \begin{pmatrix} I & C^T V^{-1} C \\ 0 & A \end{pmatrix}\right] \tag{2.23}$$

then X satisfies the control algebraic Riccati equation

$$A^T X (I + BR^{-1}B^T X)^{-1} A - X + Q = 0 \tag{2.24}$$

and Y satisfies the filter algebraic Riccati equation

$$AY(I + C^T V^{-1} CY)^{-1} A^T - Y + W = 0 \tag{2.25}$$

Equations (2.24) and (2.25) may also be recognized as the LQ control and Kalman filter Riccati equations, with X and Y being their unique positive definite solutions,

respectively. Furthermore, define

$$R_c = (I + R^{-\frac{1}{2}} B^T X B R^{-\frac{1}{2}}) \tag{2.26}$$

$$F = -R_c^{-1} R^{-\frac{1}{2}} B^T X A \tag{2.27}$$

The inverse of R_c exists, since it is positive definite and F may be rewritten as

$$F = -R^{-\frac{1}{2}} B^T X (I + B R^{-1} B^T X)^{-1} A \tag{2.28}$$

Also, define

$$R_f = (I + V^{-\frac{1}{2}} C Y C^T V^{-\frac{1}{2}}) \tag{2.29}$$

$$H = -A Y C^T V^{-\frac{1}{2}} R_f^{-1} \tag{2.30}$$

The inverse of R_f also exists and H may be rewritten as

$$H = -A(I + Y C^T V^{-1} C)^{-1} Y C^T V^{-\frac{1}{2}} \tag{2.31}$$

Both (2.28) and (2.31) are similarly recognized as the LQ optimal feedback and the Kalman filter gain matrices, respectively. The matrices F and H exist, and the closed-loop is internally stable, provided the systems with state-space realizations $(A, B, Q^{\frac{1}{2}})$ and $(A, W^{\frac{1}{2}}, C)$ are stabilizable and detectable.

By reversing the input and output scaling, the familiar LQG optimal controller is given by

$$K_{lqg} \stackrel{s}{=} \left[\begin{array}{c|c} A - B R^{-1} B^T X \tilde{F} - \tilde{H} Y C^T V^{-1} C & \tilde{H} Y C^T V^{-1} \\ \hline -R^{-1} B^T X \tilde{F} & 0 \end{array}\right] \tag{2.32}$$

where

$$\tilde{F} = (I + B R^{-1} B^T X)^{-1} A \tag{2.33}$$

$$\tilde{H} = A(I + Y C^T V^{-1} C)^{-1} \tag{2.34}$$

with the following main properties:

1) The state-feedback is a constant gain.

2) The filter is an observer.

3) The gains are obtained as solutions to two Riccati equations.

4) The controller has a separation structure.

5) The controller has the same degree as the plant.

The basic LQG controller scheme is shown in Figure 2.3 [4]. This has the desired structure of a two degrees-of-freedom compensator scheme. For the full-order state

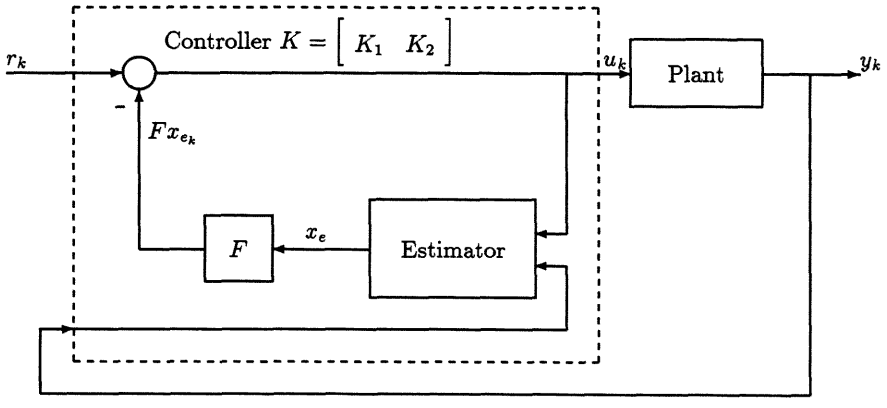

Figure 2.3: The Basic LQG Controller Scheme.

estimator case, the state equations are

$$\begin{aligned} x_{e_{k+1}} &= (A - BF - HC)x_{e_k} + Br_k - Hy_k \\ u_k &= -Fx_{e_k} + r_k \end{aligned} \tag{2.35}$$

The transfer function matrix of the controller, linking $\begin{bmatrix} r_k \\ y_k \end{bmatrix}$ to u_k, is

$$K(z) = -F(zI - A + BF + HC)^{-1}[B \quad H] + [I \quad 0] = [K_1(z) \quad K_2(z)] \tag{2.36}$$

There is no guarantee in the LQG theory that the controller of (2.35) and (2.36) will be open-loop stable. But if the controller is open-loop stable, then it can be implemented with the controller K_1 acting as a pre-filter and the controller K_2 acting as a feedback controller.

2.4 $\mathcal{H}^\infty$-Optimal Control

2.4.1 Model Uncertainty Structures

Allowing for modelling errors which may be caused by slowly varying parameters, non-linear effects, unmodelled dynamics and the like when designing for linear MIMO controllers, have received considerable attention. In classical feedback design, the problem of model uncertainty is dealt with by defining stability margins by means of gain and phase margins. Furthermore, stability is only maintained through the phase margin at the unity gain cross-over frequency. But by using unstructured uncertainty, a much broader frequency range which is of interest for robust control, can be included within the model uncertainty. By unstructured uncertainty, we mean that the only available knowledge about the uncertainty is that:

1) It can be represented by an unknown stable transfer function matrix Δ.

2) The magnitude of a possible perturbation is bounded by a frequency dependent magnitude bound $\delta(e^{j\theta})$, that is

$$\bar{\sigma}\left[\Delta(e^{j\theta})\right] \leq \delta(e^{j\theta}) \text{ for } \theta \in [-\pi, \pi) \tag{2.37}$$

Figure 2.4 gives some possible representations of unstructured uncertainty that can be used in the design process [18]. For all cases, G and Δ represent the nominal model and the uncertainty, respectively. Each configuration will generate a class of linear time invariant systems G_Δ centred on G, in which the true process G_t will lie.

- For the additive uncertainty,

$$G_\Delta = G + \Delta \text{ and } P = \begin{bmatrix} 0 & I \\ I & G \end{bmatrix} \tag{2.38}$$

- For input multiplicative uncertainty,

$$G_\Delta = G(I + \Delta) \text{ and } P = \begin{bmatrix} 0 & I \\ G & G \end{bmatrix} \tag{2.39}$$

- For output multiplicative uncertainty,

$$G_\Delta = (I + \Delta)G \text{ and } P = \begin{bmatrix} 0 & G \\ I & G \end{bmatrix} \tag{2.40}$$

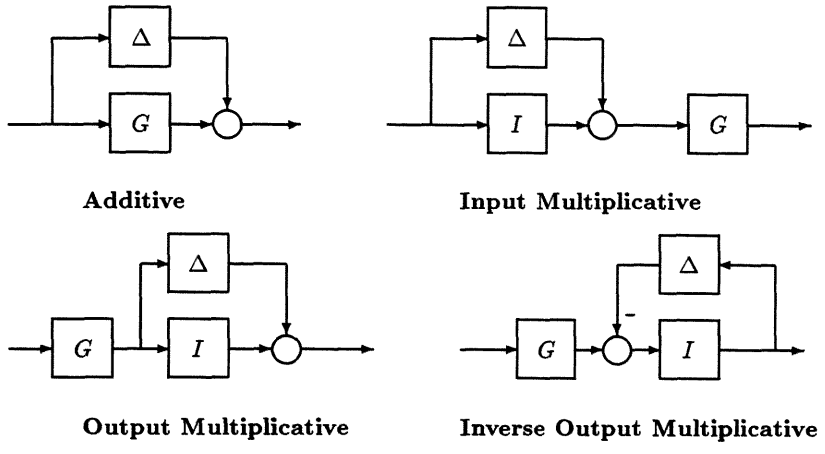

Figure 2.4: Model Uncertainty Representation.

- For inverse output multiplicative uncertainty,

$$G_\Delta = (I + \Delta)^{-1} G \text{ and } P = \begin{bmatrix} I & G \\ I & G \end{bmatrix} \tag{2.41}$$

2.4.2 The $\mathcal{H}^\infty$-Optimal Control Problem

The $\mathcal{H}^\infty$ specification of performance objectives can be cast as follows. Consider the prototype control configuration in Figure 2.5. From the loop diagram,

$$y_k = (I + GK)^{-1} d_k + (I + GK)^{-1} GK(r_k - n_k) \tag{2.42}$$

The tracking error $y_k - r_k$ is given by

$$y_k - r_k = (I + GK)^{-1}(d_k - r_k) - (I + GK)^{-1} GK n_k \tag{2.43}$$

The two transfer function matrices

$$S = (I + GK)^{-1} \text{ and } T = (I + GK)^{-1} GK \tag{2.44}$$

clearly play an important role in the loop. They are called the sensitivity and complementary sensitivity matrices, respectively. S is the inverse of the so-called return

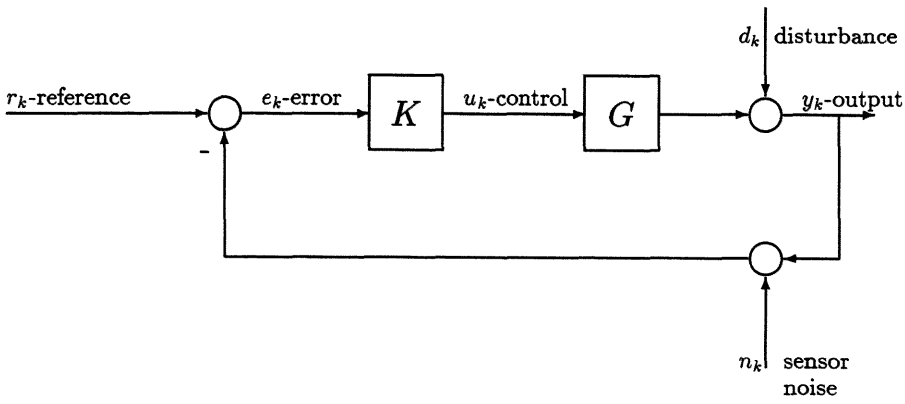

Figure 2.5: A Prototype Feedback System.

difference matrix $I + GK$, whilest T is the inverse of the so-called inverse return difference $I + (GK)^{-1}$. It is often desired to track references and reject disturbances, that is $(y_k - r_k)$ is required to be *small* and the effect of d_k on y_k should also be small.

A signal may be said to be small if it doesn't have much energy. The energy of a signal ξ_k is defined by

$$\begin{aligned} \| \xi_k \|_2^2 &= \sum_{k=0}^{\infty} \xi_k^T \xi_k \\ &= \frac{1}{2\pi} \int_{-\pi}^{\pi} \xi^T(e^{-j\theta}) \xi(e^{j\theta}) d\theta \end{aligned} \tag{2.45}$$

Thus to make tracking errors *small*, it is required that

$$\| y_k - r_k \|_2 < \epsilon \tag{2.46}$$

for some $\epsilon > 0$. Assuming there is no sensor noise, $y_k - r_k = S(d_k - r_k)$. In order to ensure (2.46), one needs to know the energy gain of the system. The ∞-norm is the worst case energy gain

$$\begin{aligned} \| S \|_\infty &= \max_{\xi_k \neq 0} \frac{\| S\xi_k \|_2}{\| \xi_k \|_2} \\ &= \max_{\theta} \bar{\sigma} \left[S(e^{j\theta}) \right] \end{aligned} \tag{2.47}$$

Equation (2.47) relates the ∞-norm problem to singular values: for scalar systems, the ∞-norm is the peak of the Bode magnitude plot. It follows from the definition that

$$\| y_k - r_k \|_2 \leq \| S \|_\infty \| d_k - r_k \|_2 \tag{2.48}$$

Therefore, by making

$$\| S \|_\infty < \gamma \tag{2.49}$$

for some $\gamma > 0$, the objective (2.46) is ensured for all disturbances such that

$$\| d_k - r_k \|_2 < \frac{\epsilon}{\gamma} \tag{2.50}$$

The smaller γ is made, the larger the disturbance energy the system will tolerate. From (2.45), we notice that all frequencies contribute to the energy equally - it is not possible to discriminate between high frequency and low frequency energy. To do this, a frequency weighting is introduced. If $\hat{W}$ is a low-pass filter, then

$$\left\| \hat{W} \xi_k \right\|_2 < \delta \tag{2.51}$$

for some $\delta > 0$, describes a class of signals of high energy content at high frequency (since low frequency energy is attenuated by the low-pass filter $\hat{W}$). Similarly, $\left\| \hat{W}^{-1} \xi_k \right\|_2$ describes a class of signals with high energy content at low frequency.

Tracking and disturbance attenuation objectives are typically most important at low frequency, so for some low-pass filter $\hat{W}_1$ known as a frequency weight, it is desired that

$$\left\| \hat{W}_1 (y_k - r_k) \right\|_2 < \epsilon \tag{2.52}$$

This will be achieved by requiring

$$\left\| \hat{W}_1 S \right\|_\infty < \gamma \tag{2.53}$$

Sensor noise influences the system *via* the complementary sensitivity matrix T. To ensure sensor noise, usually a high frequency signal, is attenuated, it is required that, for some low-pass weight $\hat{W}_2$

$$\left\| \hat{W}_2^{-1} T \right\|_\infty < \gamma \tag{2.54}$$

The $\mathcal{H}^\infty$ specification of robustness objectives can be cast as follows. In $\mathcal{H}^\infty$ control theory, one explicitly takes into account the fact that the model is not an accurate representation of the true system. A design is based on the model, and then implemented on the true system, which may be nonlinear, time-varying, or otherwise different from the model. This fact needs to be taken into account. The preservation of loop properties despite model uncertainty is known as *robustness*. The basic robustness definition can be stated as follows:

- Suppose the nominal model and the system have the same number of unstable poles, and that the controller makes the nominal loop stable. The actual loop will be stable provided the relative model error Δ satisfies

$$\| \Delta T \|_\infty < 1 \text{ (see Figure 2.6)}$$

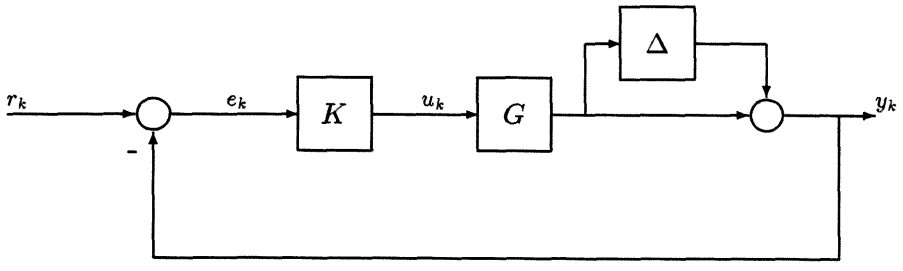

Figure 2.6: Relative Error Representation.

As with signals, one needs to be able to frequency shape the error, since at some frequencies the model will be more accurate than at others. Suppose one thinks of the model being less accurate at high frequency, and choose a low-pass filter $\hat{W}_2$ so that

$$\left\| \hat{W}_2 \Delta \right\|_\infty < 1 \tag{2.55}$$

is a reasonable description of the relative model error. Then one needs to ensure

$$\left\| \hat{W}_2^{-1} T \right\|_\infty < 1 \tag{2.56}$$

for stability to be guaranteed. The relative error can be represented in other ways (as shown in Section 2.4.1), depending on the plant and on the designer's objective.

2.4.3 The $\mathcal{H}^\infty$ Mixed Sensitivity Problem

It was seen that performance and robustness objectives for feedback systems can be posed as $\mathcal{H}^\infty$ norm constraints on the sensitivity and complementary sensitivity matrices. In order to achieve multiple objectives, *e.g.*, performance and robustness, one needs to take both into account. One way of doing this is the so-called mixed sensitivity problem:

- Find a controller K such that the loop is stable and

$$\left\| \begin{array}{c} \gamma^{-1}\hat{W}_1 S \\ \hat{W}_2^{-1} T \end{array} \right\|_\infty < 1 \tag{2.57}$$

  To maximize performance, γ should be made as small as possible.

Objectives, such as sensitivity and complementary sensitivity, can be approximated as constraints on the open-loop singular values - the singular values of GK.

The standard $\mathcal{H}^\infty$ regulator problem is then:

- Find all realisable controller K which stabilize the closed-loop and achieve the infinity norm objective

$$\| \mathcal{F}_l(P, K) \|_\infty < \gamma \tag{2.58}$$

This is known as the $\mathcal{H}^\infty$-optimization problem. The standardized plant P includes all weighting matrices, the plant model and the interconnection structure associated with the type of problem being solved.

2.4.4 Solution to the $\mathcal{H}^\infty$-Control Problem

All Stabilizing Controllers

Suppose K in the standard control configuration has the following state-space realization

$$K \stackrel{s}{=} \left[\begin{array}{c|c} \hat{A} & \hat{B} \\ \hline \hat{C} & \hat{D} \end{array}\right] \tag{2.59}$$

then together with the state-space realization of the standard augmented plant P, the system A-matrix for the standard control configuration is given by [19]

$$\tilde{A} = \begin{bmatrix} A & 0 \\ 0 & \hat{A} \end{bmatrix} + \begin{bmatrix} B_2 & 0 \\ 0 & \hat{B} \end{bmatrix} \begin{bmatrix} I & -\hat{D} \\ -D_{22} & I \end{bmatrix}^{-1} \begin{bmatrix} 0 & \hat{C} \\ C_2 & 0 \end{bmatrix} \tag{2.60}$$

where the matrix inverse exists under the assumption that the system is well-posed. The standard control configuration is therefore internally stable if $\tilde{A}$ is stable.

Under the assumption that P_{22} is stabilizable and detectable, it is well-known that the set of all stabilizing controllers for P in the standard control configuration can be parameterized by adding stable dynamics $Q \in \mathcal{RH}^\infty$ to an observer-based state-feedback stabilizing compensator for P as shown in Figure 2.7, where F and H are the state-feedback and observer constant gain matrices, respectively. Mathematically, the set of all stabilizing controllers can be characterized in terms of the left and right coprime factorizations of P_{22} , usually referred to as the Youla parametrization [113]. All stabilizing controllers of P in the standard control configuration are given by

$$\begin{aligned} K &= (Y + MQ)(X + NQ)^{-1} \\ &= (\tilde{X} + Q\tilde{N})^{-1}(\tilde{Y} + Q\tilde{M}) \end{aligned} \tag{2.61}$$

for any stable Q, where $(N, M, \tilde{N}, \tilde{M}, X, Y, \tilde{X}, \tilde{Y})$ are $\mathcal{RH}^\infty$ matrices and satisfy the double Bezout identity

$$\begin{bmatrix} \tilde{X} & -\tilde{Y} \\ -\tilde{N} & \tilde{M} \end{bmatrix} \begin{bmatrix} M & Y \\ N & X \end{bmatrix} = \begin{bmatrix} I & 0 \\ 0 & I \end{bmatrix} \tag{2.62}$$

The Model-Matching Problem

Consider the standard control configuration shown in Figure 2.7, where the input and output vectors of $-Q$ are denoted as y_{1_k} and u_{1_k}, respectively. Also, $-Q$ here can be interpreted as a stable compensator to be designed. Let $T = \begin{bmatrix} T_{11} & T_{12} \\ T_{21} & T_{22} \end{bmatrix}$ be partitioned according to the input and output vectors $\begin{bmatrix} w_k \\ u_{1_k} \end{bmatrix}$ and $\begin{bmatrix} e_k \\ y_{1_k} \end{bmatrix}$, respectively, with the

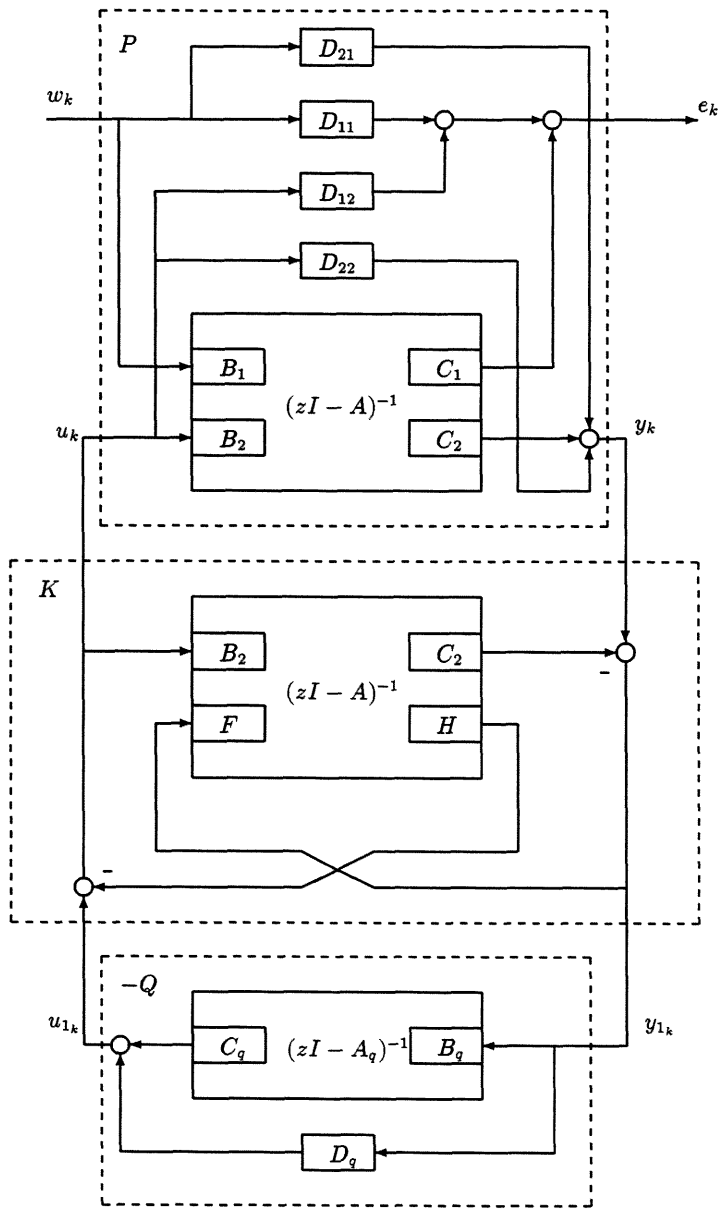

Figure 2.7: The Set of all Stabilizing Controllers.

following realization [29]:

$$T \stackrel{s}{=} \left[\begin{array}{cc|cc} A+B_2F & -B_2F & B_1 & B_2 \\ 0 & A+HC_2 & B_1+HD_{21} & 0 \\ \hline C_1+D_{12}F & -D_{12}F & D_{11} & D_{12} \\ 0 & C_2 & D_{21} & 0 \end{array}\right] \tag{2.63}$$

where F and H have been chosen so that $(A+B_2F)$ and $(A+HC_2)$ are stable. From (2.63), it is clear that T_{22} is identically zero, and therefore the transfer function from w_k to e_k, when K is stabilizing, is given by

$$F_l(P,K) = F_l(T,-Q) = T_{11} - T_{12}QT_{21} \tag{2.64}$$

for some $Q \in \mathcal{RH}^\infty$. The parameterization for stabilizing K has transformed the transfer function from w_k to e_k, which is nonlinear in K, to an affine function in Q. The standard problem

$$\min_{K-stabilizing} \| F_l(P,K) \|_\infty \tag{2.65}$$

is therefore equivalent to the affine optimization

$$\min_{Q\in\mathcal{RH}^\infty} \| T_{11} - T_{12}QT_{21} \|_\infty \tag{2.66}$$

This is called a model-matching Problem [19, 12].

Consider a standard 1-block model-matching problem, in which T_{12} and T_{21} are square. The constant matrices F and H in (2.63) can be chosen so that T_{12} and T_{21} are inner and co-inner respectively, that is

$$T_{12}T_{12}^* = I \text{ and } T_{21}^*T_{21} = I \tag{2.67}$$

Therefore, because the $\mathcal{L}^\infty$-norm is invariant under multiplication by a square inner matrix, pre- and post-multiplication in (2.66) by T_{12}^* and T_{21}^* results in the problem

$$\min_{Q\in\mathcal{RH}^\infty} \| R - Q \|_\infty \tag{2.68}$$

where

$$R = T_{12}^*T_{11}T_{21}^* \tag{2.69}$$

This is a Nehari problem where the objective is to find the closest Q to R. Q is of course an element of $\mathcal{RH}^\infty$, whereas R is generally an element of $\mathcal{RL}^\infty$. By construction R can be made completely unstable.

The 1-block problem arises when the number of external inputs, n_w, is equal to the number of measurements, n_y, used by the controller, and when the number of regulated variables, n_e, is equal to the number of control inputs to the plant, n_u (the requirement that $n_y = n_u$ is not necessary). For example, the sensitivity minimization problem

$$\min_{K-stabilizing} \left\| \hat{W}_1 S \right\|_\infty \tag{2.70}$$

and the robust stabilization problem

$$\min_{K-stabilizing} \left\| \hat{W}_2^{-1} T \right\|_\infty \tag{2.71}$$

fall into this category.

For a 2-block problem, which arises when T_{12} is square and T_{21} is nonsquare (T_{12} nonsquare and T_{21} square), the corresponding distance problem is

$$\min_{Q\in\mathcal{RH}^\infty} \left\| \begin{bmatrix} R_{11} - Q & R_{12} \end{bmatrix} \right\|_\infty \quad \left(\min_{Q\in\mathcal{RH}^\infty} \left\| \begin{bmatrix} R_{11} - Q \\ R_{21} \end{bmatrix} \right\|_\infty \right) \tag{2.72}$$

The 2-block problem arises when either $n_2 > n_u$ and $n_w = n_y$, or $n_w > n_y$ and $n_2 = n_u$. Typical 2-block minimization problems are those with a combination of sensitivity and complementary sensitivity functions.

For a 4-block problem, which arises when both T_{12} and T_{21} are nonsquare, the corresponding distance problem is

$$\min_{Q\in\mathcal{RH}^\infty} \left\| \begin{bmatrix} R_{11} - Q & R_{12} \\ R_{21} & R_{22} \end{bmatrix} \right\|_\infty \tag{2.73}$$

The 4-block problem arises when $n_w > n_y$ and $n_e > n_u$. A method for solving this problem may be found in [19] and [52].

State-Space Solution

Contrary to the $\mathcal{H}^2$ (LQG) problem, the controller will not be optimal, however, for practical purposes we will be content with a suboptimal solution which in some cases

is more useful. The assumptions A1-A8 still hold. A state-space representation of P is given by

$$\begin{aligned} x_{k+1} &= Ax_k + B_1 w_{worst_k} + B_2 u_k \\ e_k &= C_1 x_k + D_{11} w_{worst_k} + D_{12} u_k \\ y_k &= C_2 x_k + D_{21} w_{worst_k} + D_{22} u_k \end{aligned} \tag{2.74}$$

Lets define the following two symplectic pairs of matrices

$$H_\infty := \left[\begin{pmatrix} A & 0 \\ -C_1^T D_\perp D_\perp^T C_1 & I \end{pmatrix}, \begin{pmatrix} I & B_2 B_2^T - \gamma^{-2} B_1 B_1^T \\ 0 & A^T \end{pmatrix} \right] \tag{2.75}$$

$$J_\infty := \left[\begin{pmatrix} A^T & 0 \\ -B_1 \tilde{D}_\perp^T \tilde{D}_\perp B_1^T & I \end{pmatrix}, \begin{pmatrix} I & C_2^T C_2 - \gamma^{-2} C_1^T C_1 \\ 0 & A \end{pmatrix} \right] \tag{2.76}$$

and the two algebraic Riccati equations

$$X_\infty = A^T X_\infty \left[I + (B_2 B_2^T - \gamma^{-2} B_1 B_1^T) X_\infty \right]^{-1} A + C_1^T D_\perp D_\perp^T C_1 \tag{2.77}$$

$$Y_\infty = A Y_\infty \left[I + (C_2^T C_2 - \gamma^{-2} C_1^T C_1) Y_\infty \right]^{-1} A^T + B_1 \tilde{D}_\perp^T \tilde{D}_\perp B_1^T \tag{2.78}$$

If $H_\infty \in dom(RIC)$, $J_\infty \in dom(RIC)$, $X_\infty = RIC(H_\infty)$, and $Y_\infty = RIC(J_\infty)$, then we can define the gain matrix F_∞ and the gain matrix L_∞ as

$$F_\infty := \begin{pmatrix} F_{\infty_1} \\ F_{\infty_2} \end{pmatrix} = -(R + B^T X_\infty B)^{-1} B^T X_\infty A \tag{2.79}$$

$$L_\infty := \begin{pmatrix} L_{\infty_1} & L_{\infty_2} \end{pmatrix} = A Y_\infty C^T (\tilde{R} + C Y_\infty C^T)^{-1} \tag{2.80}$$

where

$$B = [B_1 \quad B_2], \; C = \begin{bmatrix} C_1 \\ C_2 \end{bmatrix}, \; R = \begin{bmatrix} -\gamma^2 I_{n_w} & 0 \\ 0 & I \end{bmatrix}, \text{ and } \tilde{R} = \begin{bmatrix} -\gamma^2 I_{n_z} & 0 \\ 0 & I \end{bmatrix} \tag{2.81}$$

Suppose that $\left(R + B^T X_\infty B\right)$ has a J_{n_w, n_u}-factorization [40] given by

$$R + B^T X_\infty B = \begin{bmatrix} T_{11}^T & T_{21}^T \\ 0 & T_{22}^T \end{bmatrix} \begin{bmatrix} -I_{n_w} & 0 \\ 0 & I_{n_u} \end{bmatrix} \begin{bmatrix} T_{11} & 0 \\ T_{21} & T_{22} \end{bmatrix} \tag{2.82}$$

then it follows that the following identities hold

$$\begin{aligned} T_{22}^T T_{22} &= I + B_2^T X_\infty B_2 \\ T_{22}^T T_{21} &= B_2^T X_\infty B_1 \\ T_{11}^T T_{11} &= T_{21}^T T_{21} + \gamma^2 I - B_1^T X_\infty B_1 \end{aligned} \tag{2.83}$$

Also define $Z_\infty := I - \gamma^{-2} Y_\infty X_\infty$. Next, the set of auxiliary variables are defined. We assume that the problem is normalized so that $\gamma = 1$. Let E be any matrix that satisfies

$$E^T E = I - T_{11}^T T_{11} \tag{2.84}$$

Define

$$\begin{aligned} N &:= \begin{pmatrix} N_{11} & N_{12} \\ N_{21} & N_{22} \end{pmatrix} = \begin{pmatrix} E\tilde{D}_\perp^T & ED_{21}^T \\ T_{21}\tilde{D}_\perp^T & T_{21}D_{21}^T \end{pmatrix} \\ M_2 &:= C_2 + D_{21}F_{\infty_1} \\ U_\infty &:= I + M_2 Y_\infty Z_\infty^{-T} M_2^T \\ V_\infty &:= -N_{12}U_\infty^{-1} M_2 Y_\infty Z_\infty^{-T}[F_{\infty_2}^T T_{22}^T + M_2^T N_{22}^T] - N_{11}N_{21}^T \\ W_\infty &:= I - N_{11}N_{11}^T - N_{12}M_2 Y_\infty Z_\infty^{-T} M_2^T U_\infty^{-1} N_{12}^T \end{aligned} \tag{2.85}$$

There exists a stabilizing controller such that $\| \mathcal{F}_l(P,K) \|_\infty < 1$ if, and only if, the following three conditions hold:

1) H_∞ has no eigenvalues on the unit disc, $X_\infty \geq 0$, and $(R + B^T X_\infty B)$ has a J_{n_w,n_u}-factorization.

2) J_∞ has no eigenvalues on the unit disc, $Y_\infty \geq 0$, and $(\tilde{R} + CY_\infty C^T)$ has a J_{n_e,n_y}-factorization.

3) The spectral radius condition $\rho(X_\infty Y_\infty) < 1$ is satisfied.

Given the above, all rational admissible controllers are given by $\mathcal{F}_l(K,Q)$ with $Q \in \mathcal{RH}^\infty$, $\| Q \|_\infty < 1$ and K equal

$$K \stackrel{s}{=} \left[\begin{array}{c|cc} \bar{A} & \bar{B}_1 & \bar{B}_2 \\ \hline \bar{C}_1 & \bar{D}_{11} & \bar{D}_{12} \\ \bar{C}_2 & \bar{D}_{21} & 0 \end{array}\right] \tag{2.86}$$

where

$$\bar{D}_{11} = T_{22}^{-1}(V_\infty^T W_\infty^{-1} N_{12} - N_{22} + T_{22}F_{\infty_2} Y_\infty Z_\infty^{-T} M_2^T) U_\infty^{-1} \tag{2.87}$$

$\bar{D}_{12}$ is any matrix satisfying

$$\begin{aligned} \bar{D}_{12}\bar{D}_{12}^T &= T_{22}^{-1}(I - N_{21}N_{21}^T - N_{22}N_{22}^T)T_{22}^{-1} \\ &\quad -F_{\infty_2} Y_\infty Z_\infty^{-T} F_{\infty_2}^T - T_{22}^{-1} V_\infty^T W_\infty^{-T} V_\infty T_{22}^{-T} \\ &\quad \times (T_{22}^{-1}N_{22} - F_{\infty_2} Y_\infty Z_\infty^{-T} M_2^T) U_\infty^{-1} (T_{22}^{-1}N_{22} - F_{\infty_2} Y_\infty Z_\infty^{-T} M_2^T)^T \end{aligned} \tag{2.88}$$

$\bar{D}_{21}$ is any matrix that satisfies

$$\bar{D}_{21}^T \bar{D}_{21} = U_\infty^{-1} - U_\infty^{-1} N_{12}^T W_\infty^{-1} N_{12} U_\infty^{-1} \tag{2.89}$$

The rest of the matrices defining K are given by

$$\begin{aligned}
\bar{B}_2 &= Z_\infty^{-1}(B_2 + L_{\infty_1} D_{21})\bar{D}_{12} \\
\bar{B}_1 &= -Z_\infty^{-1} L_{\infty_2} + \bar{B}_2 \bar{D}_{12}^{-1} \bar{D}_{11} \\
\bar{C}_2 &= -\bar{D}_{21}(C_2 + D_{21} F_{\infty_1}) \\
\bar{C}_1 &= F_{\infty_2} + \bar{D}_{11} \bar{D}_{21}^{-1} \bar{C}_2 \\
\bar{A} &= A + B F_\infty + \bar{B}_1 \bar{D}_{21}^{-1} \bar{C}_2
\end{aligned} \tag{2.90}$$

The central suboptimal controller $K_{central}$ equal

$$K_{central} \stackrel{s}{=} \left[\begin{array}{c|c} A + B F_\infty + \bar{B}_1 \bar{D}_{21}^{-1} \bar{C}_2 & -Z_\infty^{-1} L_{\infty_2} + \bar{B}_2 \bar{D}_{12}^{-1} \bar{D}_{11} \\ \hline F_{\infty_2} + \bar{D}_{11} \bar{D}_{21}^{-1} \bar{C}_2 & \bar{D}_{11} \end{array}\right] \tag{2.91}$$

For the case where $\gamma \neq 1$, (2.91) is calculated *via* γ-iteration using the bisection method [10]. Given a high and low value of γ, the bisection method is used to iterate on the value of γ to approach the optimal $\mathcal{H}^\infty$ control design.

2.4.5 Robust Performance

In this subsection a review of the methods for analyzing the stability and performance properties of interconnected systems subject to norm-bounded structured uncertainty is briefly covered, together with the synthesis of the final suboptimal controller. Any linear interconnection of inputs, outputs, and uncertainty perturbations can be rearranged to fit the interconnection structure of Figure 2.8 [17].

Some important design problems cannot be formulated as $\mathcal{H}^\infty$ problems. In particular, the problem of achieving robust performance, namely the maintenance of performance objectives - not merely stability - in the presence of unmodelled perturbations, is one such problem. The solution to this problem requires the minimization of the so-called structured singular value, $\mu(\mathcal{M})$ of a transfer function matrix $\mathcal{M}$, and this can be very different from $\bar{\sigma}(\mathcal{M})$.

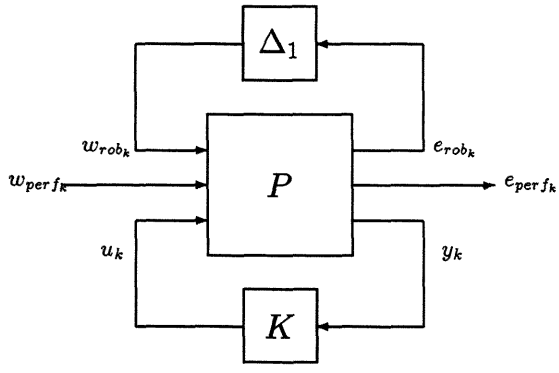

Figure 2.8: General Interconnection with Norm-bound Structured Uncertainty.

As in Section 2.2, P describes a plant augmented with all the weighting functions on the inputs and outputs used to scale the norm-bounds to 1. K is a controller mapping the measurements, y_k, to the plant control inputs, u_k. Δ_1 is the norm-bounded structured uncertainty perturbation, and the mapping $w_{rob_k} \rightarrow e_{rob_k}$ characterizes the uncertainty model being used. The mapping $w_{perf_k} \rightarrow e_{perf_k}$ characterizes the desired performance. The objective is to check if a controller, K, achieves robust performance, where robust performance is defined as achieving stability and performance over the entire set of norm-bounded perturbations. Hence, robust performance is achieved if K stabilizes $\mathcal{F}_u(P, \Delta_1), \forall \Delta_1 \in \mathbf{B\Delta_1}$ and $\| \mathcal{F}_u(\mathcal{F}_l(P, K), \Delta_1) \|_\infty < 1$, $\forall \Delta_1 \in \mathbf{B\Delta_1}$, where $\mathbf{B\Delta_1} = \{\Delta \in \mathbf{\Delta_1} : \bar{\sigma}(\Delta) < 1\}$ [7].

A matrix function μ will now be discussed which can be used to analyze the stability and performance properties of the interconnection structure in Figure 2.8. Define $\mathcal{M} = \mathcal{F}_l(P, K)$. Note that all of the matrices in Figure 2.8 are functions of a frequency parameter θ. The loop from $e_{perf_k} \rightarrow w_{perf_k}$ will now be closed with a complex full block and define the matrix function μ at a single frequency θ_0. Referring to Figure 2.9 - P, K, and Δ at θ_0 will be evaluated. It will be assumed that w_{rob_k} and e_{rob_k} are of equal dimensions n_1, and similarly that w_{perf_k} and e_{perf_k} are of equal dimensions n_2. If this is not the case then augmentation of the rows or columns of $\mathcal{F}_l(P, K)$ by zeros will be used to force the previous conditions.

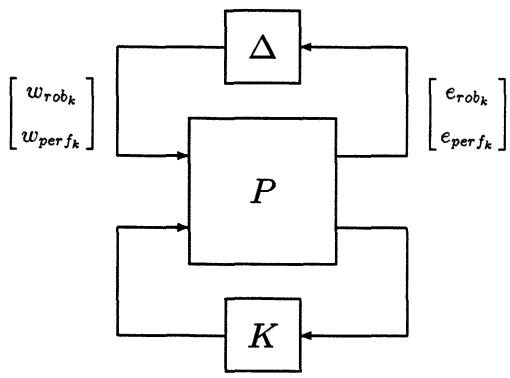

Figure 2.9: General Interconnection for μ-Analysis and Synthesis.

Let F_1 be the number of complex full blocks in the uncertainty perturbation Δ_1. Then the set $\mathbf{\Delta_1}$ is defined as

$$\mathbf{\Delta_1} \equiv \left\{\Delta_1 : \Delta_1 = \textbf{ diag } (\Delta_{k_1}, ..., \Delta_{k_{F_1}}), \Delta_{k_i} \in \mathcal{C}^{k_i \times k_i}\ i = 1, ..., F_1\right\} \tag{2.92}$$

where $\sum_{i=1}^{F_1} k_i = n_1$. Now the robust performance block structure can be defined by augmenting the uncertainty perturbation Δ_1 by a complex full block

$$\mathbf{\Delta} \equiv \left\{\Delta : \Delta = \textbf{ diag } (\Delta_1, \Delta_2), \Delta_1 \in \mathbf{\Delta_1}, \Delta_2 \in \mathcal{C}^{n_2 \times n_2}\right\} \tag{2.93}$$

μ can now be defined on the robust performance block structure Δ as

$$\mu_{\mathbf{\Delta}}(\mathcal{M}(e^{j\theta_0})) = \begin{cases} \left(\min\limits_{\Delta(e^{j\theta_0}) \in \mathbf{\Delta}} \{\bar{\sigma}(\Delta(e^{j\theta_0})) : \det(I + \mathcal{M}(e^{j\theta_0})\Delta(e^{j\theta_0})) = 0\}\right)^{-1} \\ 0 \text{ if no } \Delta \text{ satisfies } \det(I + \mathcal{M}(e^{j\theta_0})\Delta(e^{j\theta_0})) = 0 \end{cases} \tag{2.94}$$

Now with the previous definitions in mind, a precise definition of robust performance can be made

$$\begin{aligned} \mu_{\mathbf{\Delta}}(\mathcal{M}(e^{j\theta_0})) < 1 &\iff \mu_{\mathbf{\Delta_1}}(\mathcal{M}_{11}(e^{j\theta_0})) < 1 \\ &\iff \max_{\Delta_1 \in \mathbf{B\Delta_1}} \mu_{\mathbf{\Delta_2}}(\mathcal{F}_u(\mathcal{M}(e^{j\theta_0}), \Delta_1)) < 1 \end{aligned} \tag{2.95}$$

where $\mu_{\mathbf{\Delta_2}}(.) \equiv \bar{\sigma}(.)$ because of the block structure of $\mathbf{\Delta_2}$.

If $\mu_{\mathbf{\Delta_1}}(\mathcal{M}_{11}(e^{j\theta_0})) < 1$ and $\mathcal{M}(e^{j\theta_0})$ is stable, then there are no $\Delta_1 \in \mathbf{B\Delta_1}$ which can destabilize $\mathcal{F}_u(\mathcal{M}(e^{j\theta_0}), \Delta(e^{j\theta_0}))$ and if $\mu_{\mathbf{\Delta_2}}(\mathcal{F}_u(\mathcal{M}(e^{j\theta_0}), \Delta_1)) < 1$ then performance is

achieved at θ_0 since $\left\| \mathcal{F}_u(\mathcal{M}(e^{j\theta_0}), \Delta_1) \right\|_\infty < 1 \ \forall \Delta_1 \in \mathbf{B}\mathbf{\Delta_1}$. Hence, the above demonstrates the equivalence of $\mu_{\mathbf{\Delta}}(\mathcal{M}(e^{j\theta_0})) < 1$ and robust performance.

In the sequel it will be useful to establish an upper bound for μ. With this in mind the following set is defined

$$\mathcal{D} \equiv \{D \in \mathbf{\Delta} : D = \ \mathbf{diag}\ (d_1 I_{k_1}, ..., d_{F_1} I_{k_{F_1}}, I_{n_2}), d_i \in \mathcal{R},\ d_i > 0,\ i = 1, ..., F_1\} \quad (2.96)$$

where $\mathcal{D}$ is a set of diagonal, positive matrices whose structure matches that of the plant perturbation. It is clear from (2.93) and (2.96) that elements of $\mathcal{D}$ and Δ commute. The upper bound for μ can now be written as

$$\mu_{\mathbf{\Delta}}(\mathcal{M}(e^{j\theta_0})) \leq \inf_{D \in \mathcal{D}} \bar{\sigma} \left(D\mathcal{M}(e^{j\theta_0}) D^{-1} \right) \quad (2.97)$$

The following algorithm [7] will be used to find a controller satisfying $\mu_{\mathbf{\Delta}}(\mathcal{M}) < 1$. It is assumed that the weighted open-loop plant with the uncertainty and performance blocks (Figure 2.9) is given by P.

Algorithm (D-K iteration)

$x = -1$

do $x = x + 1$

if $x = 0$ **then**

$P_0 = P$

$K_0 = \arg \inf_{K \text{ stabilising}} \| \mathcal{F}_l(P_0, K) \|_\infty$

else

$D_x = \arg \inf_{D \in \mathcal{D}} \bar{\sigma} \left(D \mathcal{F}_l(P_{x-1}, K_{x-1}) D^{-1} \right)$

$$P_x = \begin{bmatrix} D_x & 0 \\ 0 & I_p \end{bmatrix} P_{x-1} \begin{bmatrix} D_x^{-1} & 0 \\ 0 & I_m \end{bmatrix}$$

$K_x = \arg \inf_{K \text{ stabilising}} \| \mathcal{F}_l(P_x, K) \|_\infty$

end

until $\| \mathcal{F}_l(P_x, K_x) \|_\infty - \| \mathcal{F}_l(P_{x-1}, K_{x-1}) \|_\infty <$ **tol**

It is noted that the controller is computed as the argument (arg) of the infimum (inf) in the above algorithm to mean that K_0 and K_x are some minimizers of $\| \mathcal{F}_l(P_0, K) \|_\infty$ and $\| \mathcal{F}_l(P_x, K) \|_\infty$, respectively. The computation of the D-scalings yield a matrix of frequency varying data points, since they are computed as the argument of the infimum. The multiplication of the D-scalings implied in the algorithm is done before the frequency varying data is fit to a transfer function. This prevents the states of the D-scalings from accumulating in each iteration of the algorithm.

Since the ∞-norm of the scaled system is norm non-increasing, the $D - K$ iteration will converge in a finite number of iterations. However, there is no *a priori* guarantee that the algorithm will converge to a global minimum. Suppose it converges on the N^{th} iteration. If $\| \mathcal{F}_l(P_N, K_N) \|_\infty < 1$, then $\mu_\Delta(\mathcal{F}_l(P, K_N)) < 1$, and K_N achieves robust performance. If $\mu_\Delta(\mathcal{F}_l(P, K_N)) \geq 1$ then the performance and uncertainty weights must be adjusted to either restrict the uncertainty or decrease the performance level and the $D - K$ iteration tried again.

2.5 Summary

In this chapter an extensive treatment of the main state-space results regarding the $\mathcal{H}^2$ and $\mathcal{H}^\infty$ problem have been presented, together with some well known results on the robust performance problem. The material was presented in order to use and apply these results in conjunction with other chapters.

Chapter 3

Robust Control with Normalized Coprime Factor Perturbations

3.1 Introduction

In Chapter 2, different ways for incorporating model uncertainty in the design procedure were discussed. The representation of the model set was given in terms of a nominal model and an additive model uncertainty or a multiplicative model uncertainty. These uncertainty representations are handicapped by the condition on the number of right-half plane poles. In addition, there can exist undesirable pole-zero cancellation between the nominal model and the $\mathcal{H}^\infty$ controller [94]. In this chapter, an alternative way of incorporating model uncertainty in the design procedure is presented. It involves representing the uncertainty as unknown stable transfer function matrix perturbations acting additively one on each of the elements of a particular right or left coprime factorization of the nominal plant model. This was first suggested in [105, 104]. There are no restrictions on the number of right-half plane poles and no pole-zero cancellations arise between the $\mathcal{H}^\infty$ controller and the nominal model for this representation of model uncertainty.

Various researchers, as in [62, 35] have thoroughly investigated this type of uncertainty representation. In [62] a parameterization of all controllers achieving suboptimal and optimal bounds was derived. A closed formula for the optimal bound was also derived, all with respect to uncertainty of a normalized left coprime factorization of the nominal plant model, in a continuous-time setting. In [106] the analogous discrete-time problem

was formulated with respect to uncertainty of a normalized right coprime factor plant description. The aim of this chapter is to follow similar steps to those in [106] to formulate the analogous discrete-time problem with respect to uncertainty of a normalized left coprime factor plant description, and to derive explicit state-space formulae for sub-optimal and optimal controllers. Also, explicit state-space formulae for an $\mathcal{H}^\infty$-based two degrees-of-freedom (2-DOF) robust controller will be derived. It will be shown that such a controller will provide robust stability against uncertainty of a normalized left coprime factor plant description and a high degree of good performance in the sense of making the closed-loop system match a pre-specified reference model. This problem was first investigated, in the continuous-time case, by [47] and [108].

The chapter is organized as follows. Section 3.2 introduces two special control problems which show that the parameterized closed-loop map decomposes into two natural components: State-feedback and Output Estimation. In Section 3.3, the 1-DOF normalized left coprime factor design approach is formulated. In Section 3.4, the 2-DOF normalized left coprime factor design approach is also formulated. Finally, a summary will be given in Section 3.5.

3.2 Special Control Problems

3.2.1 $\mathcal{H}^\infty$ Full Information Control

The full information problem describes the situation (Figure 3.1) where the controller K has access to both the present dynamic state x_k of the generalized plant P, and the current disturbance input w_k. The relationship between full information control, game theory and J-lossless factorizations is well documented for the discrete-time case in [107, 58]. Here, the J-lossless factorization results of [40], and the 1-DOF and 2-DOF design methodologies are invoked to parameterize $\mathcal{H}^\infty$ full information controls and the associated discrete-time $\mathcal{H}^\infty$ control Riccati equation for the case where $D_{11} \neq 0$. It is well-known [107] that the general system for the full information problem is described by the equations

$$x_{k+1} = Ax_k + B_1 w_k + B_2 u_k$$

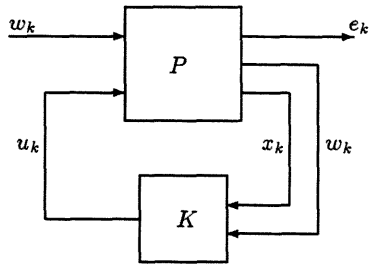

Figure 3.1: Full Information Control Structure.

$$e_k = C_1 x_k + D_{11} w_k + D_{12} u_k \tag{3.1}$$

The above is associated with J-lossless coprime factorization of [40] defining

$$\left[\begin{array}{c|c} A & B \\ \hline C & D \end{array}\right] := \left[\begin{array}{c|cc} A & B_1 & B_2 \\ \hline C_1 & D_{11} & D_{12} \\ 0 & I & 0 \end{array}\right] \tag{3.2}$$

and

$$J_{pq}(\gamma) := \begin{bmatrix} I_p & 0 \\ 0 & -\gamma^2 I_q \end{bmatrix} \tag{3.3}$$

The latter will simply be denoted by J. The $\mathcal{H}^\infty$ Full Information Control problem may be defined as follows: Given a performance level γ, find all possible controllers such that $\mathcal{F}_l(P,K) < \gamma$. This objective has the following interpretation: Find a control law $u_k = Ky_k$ such that

$$\sup_{w \in \mathcal{L}^2} (\| e_k \|_2^2 - \gamma^2 \| w_k \|_2^2) < 0 \tag{3.4}$$

With this interpretation, we can view the $\mathcal{H}^\infty$ Full Information Control problem as a game with w_k as the opponent and u_k as the minimizing input. The cost functional associated with the game Riccati difference equation is given by

$$V_0 = \sum_{k=0}^{N-1} (e_k^T e_k - \gamma^2 w_k^T w_k) + x_N^T P_N x_N \tag{3.5}$$

The terminal state weighting P_N is included in the cost functional to prevent the state vector from possibly becoming unbounded as N tends to infinity. Introducing Lagrange

multipliers λ_k, one can write

$$V_0 = \sum_{k=0}^{N-1} \left[(e_k^T e_k - \gamma^2 w_k^T w_k) - 2\lambda_{k+1}^T (x_{k+1} - Ax_k - B_1 w_k - B_2 u_k) \right] + x_N^T P_N x_N \quad (3.6)$$

Assuming the pair (C_1, A) has no unobservable poles on the unit circle, that is the term $D_{12}^T C_1 = 0$, the terminal state weighting P_N can be made zero and the expression given by (3.6) may be re-written as

$$V_0 = \sum_{k=0}^{N-1} \left[\begin{bmatrix} e_k^T & w_k^T \end{bmatrix} J \begin{bmatrix} e_k \\ w_k \end{bmatrix} - 2\lambda_{k+1}^T (x_{k+1} - Ax_k - B\phi_k) \right] \quad (3.7)$$

and

$$\begin{bmatrix} e_k \\ w_k \end{bmatrix} = \begin{bmatrix} C_1 & D_{11} & D_{12} \\ 0 & I & 0 \end{bmatrix}, \quad \begin{bmatrix} x_k \\ w_k \\ u_k \end{bmatrix} = \begin{bmatrix} C & D \end{bmatrix} \begin{bmatrix} x_k \\ \phi_k \end{bmatrix} \quad (3.8)$$

in which case

$$V_0 = \sum_{k=0}^{N-1} \left[(Cx_k + D\phi_k)^T J (Cx_k + D\phi_k) - 2\lambda_{k+1}^T (x_{k+1} - Ax_k - B\phi_k) \right] \quad (3.9)$$

The Euler-Lagrange equations

$$\begin{aligned} \frac{\partial V_o}{\partial x_k} &= 0, \ k = 1, 2, ..., N \\ \frac{\partial V_o}{\partial \phi_k} &= 0, \ k = 0, 1, ..., N-1 \end{aligned} \quad (3.10)$$

lead as N is made infinite, to the following discrete-time Riccati equation

$$\begin{aligned} X_\infty &= A^T X_\infty A + C^T J C - (C^T J D + A^T X_\infty B)(D^T J D + B^T X_\infty B)^{-1} \\ &\quad \times (D^T J C + B^T X_\infty A) \end{aligned} \quad (3.11)$$

This can be re-arranged to give the following expression

$$X_\infty = A^T X_\infty A + C^T J C - F^T (D^T J D + B^T X_\infty B) F \quad (3.12)$$

where

$$F = (D^T J D + B^T X_\infty B)^{-1} (D^T J C + B^T X_\infty A) \quad (3.13)$$

The term $(D^T J D + B^T X_\infty B)$ may be factorized [107], with $W = \begin{bmatrix} W_{11} & W_{12} \\ W_{21} & 0 \end{bmatrix}$, as

$$\begin{aligned} D^T J D + B^T X_\infty B &= \begin{bmatrix} W_{11}^T & W_{21}^T \\ W_{12}^T & 0 \end{bmatrix} \begin{bmatrix} I & 0 \\ 0 & -\gamma^2 I \end{bmatrix} \begin{bmatrix} W_{11} & W_{12} \\ W_{21} & 0 \end{bmatrix} \\ &= \begin{bmatrix} -\gamma^2 I + B_1^T X_\infty B_1 + D_{11}^T D_{11} & D_{11}^T D_{12} + B_1^T X_\infty B_2 \\ D_{12}^T D_{11} + B_2^T X_\infty B_1 & D_{12}^T D_{12} + B_2^T X_\infty B_2 \end{bmatrix} \end{aligned} \quad (3.14)$$

The terms of W are found by solving the two Cholesky factorizations

$$W_{12}^T W_{12} = D_{12}^T D_{12} + B_2^T X_\infty B_2 \tag{3.15}$$

$$\begin{aligned} W_{21}^T W_{21} = {} & \gamma^{-2}\left[(D_{11}^T D_{12} + B_1^T X_\infty B_2)(D_{12}^T D_{12} + B_2^T X_\infty B_2)^{-1}(D_{12}^T D_{11} + B_2^T X_\infty B_1)\right. \\ & \left. - D_{11}^T D_{11} + \gamma^2 I - B_1^T X_\infty B_1\right] \end{aligned} \tag{3.16}$$

and then

$$W_{11} = W_{12}^{-T}(D_{12}^T D_{11} + B_2^T X_\infty B_1) \tag{3.17}$$

The expression given in (3.13) may be re-written as

$$\begin{aligned} F &= W^{-1}J^{-1}W^{-T}(D^T JC + B^T X_\infty A) \\ &= \begin{bmatrix} 0 & W_{21}^{-1} \\ W_{12}^{-1} & -W_{12}^{-1}W_{11}W_{21}^{-1} \end{bmatrix} \begin{bmatrix} W_{12}^{-T}\Gamma_2 \\ -\gamma^{-2}W_{21}^{-T}\Gamma_1 + \gamma^{-2}W_{21}^{-T}W_{11}^T W_{12}^{-T}\Gamma_2 \end{bmatrix} \\ &= \begin{bmatrix} 0 & W_{21}^{-1} \\ W_{12}^{-1} & -W_{12}^{-1}W_{11}W_{21}^{-1} \end{bmatrix} \begin{bmatrix} L_1 \\ L_2 \end{bmatrix} \end{aligned} \tag{3.18}$$

where $\Gamma_1 = (D_{11}^T C_1 + B_1^T X_\infty A)$ and $\Gamma_2 = (D_{12}^T C_1 + B_2^T X_\infty A)$, $L_1 = W_{12}^{-T}\Gamma_2$ and $L_2 = \left(-\gamma^{-2}W_{21}^{-T}\Gamma_1 + \gamma^{-2}W_{21}^{-T}W_{11}^T W_{12}^{-T}\Gamma_2\right)$. The following theorem summarizes the results on the full information problem.

Theorem 3.2.1 [107] Given γ such that

$$\begin{aligned} & -\gamma^2 I + B_1^T X_\infty B_1 + D_{11}^T D_{11} - (D_{11}^T D_{12} + B_1^T X_\infty B_2)(D_{12}^T D_{12} + B_2^T X_\infty B_2)^{-1} \\ & (D_{12}^T D_{11} + B_2^T X_\infty B_1) < 0 \end{aligned}$$

where $X_\infty = X_\infty^T \geq 0$ satisfies (3.11), all internally stabilizing finite dimensional linear time-varying (FDLTV) controls u_k that satisfy $\| \mathcal{F}(P,K) \|_\infty < \gamma$ are generated by

$$u_k = -W_{12}^{-1}L_1 x_k - W_{12}^{-1}W_{11}w_k + \gamma W_{12}^{-1}\Theta\{\gamma W_{21}w_k + \gamma L_2 x_k\} \tag{3.19}$$

where $\Theta(z)$ is a stable causal FDLTV operator on $[0, N-1]$ and $\| \Theta(z) \|_\infty < \gamma^{-1}$.

The central full information control law, obtained by setting $\Theta(z) = 0$, is given by

$$u_k^* = -W_{12}^{-1}L_1 x_k - W_{12}^{-1}W_{11}w_k \tag{3.20}$$

(3.20) will guarantee a norm less than γ when both the states x_k and the disturbance input w_k are available for feedback.

3.2.2 Disturbance Feedforward Problem

In the event that the state x_k and the disturbance w_k are not available, an observer can be used to recover full information concerning the plant P, by reconstructing x_k and w_k from the output signal y_k. The measurement available to the controller is

$$y_k = C_2 x_k + D_{21} w_k + D_{22} u_k \tag{3.21}$$

When D_{21} is square, this equation can be inverted, and an estimate of w_k obtained in terms of u_k, y_k and an estimate of x_k. The problem is called disturbance feedforward, since in the case $C_2 = 0$, just the disturbance is measured.

The observer will be designed so that its state vector $\hat{x}_k$, which will be an estimate of P's true state x_k, will evolve according to the following equation

$$\hat{x}_{k+1} = A\hat{x}_k + B_1\hat{w}_k + B_2 u_k \tag{3.22}$$

where $\hat{w}_k$ is the observer estimate of w_k with $D_{22} = 0$, given by

$$\hat{w}_k = D_{21}^{-1}(y_k - C_2\hat{x}_k) \tag{3.23}$$

Substituting for y_k in (3.23) leads to the following equation for the disturbance estimation error

$$\hat{w}_k - w_k = D_{21}^{-1} C_2 (x_k - \hat{x}_k) \tag{3.24}$$

Also, subtracting (3.22) from $x_{k+1} = Ax_k + B_1 w_k + B_2 u_k$ and substituting from (3.24), one obtains

$$(\hat{x} - x)_{k+1} = (A - B_1 D_{21}^{-1} C_2)(\hat{x} - x)_k \tag{3.25}$$

which describes the propagation of the state estimation error. If $\hat{x}_o = x_o$, then (3.25) shows that the observer state will be identically equal to P's state vector x_k for all k, and hence $\hat{w}_k = w_k$ for all k, that is the observer will be able to reconstruct full information concerning P from y_k. Re-arranging these equations, the observer dynamics can be expressed as

$$\hat{x}_{k+1} = (A - B_1 D_{21}^{-1} C_2)\hat{x}_k + B_1 D_{21}^{-1} y_k + B_2 u_k \tag{3.26}$$

It is now possible to incorporate the observer with a suboptimal full information control law for $[\,P_{11} \quad P_{12}\,]$, which was obtained from (3.20). The controller separation structure is shown in Figure 3.2. So by substituting the estimated state $\hat{x}_k$ and disturbance $\hat{w}_k$ for the actual values in the suboptimal full information control law of (3.20), the following Certainty Equivalence control is obtained

$$u_k^* = -W_{12}^{-1}W_{11}\hat{w}_k - W_{12}^{-1}L_1\hat{x}_k \tag{3.27}$$

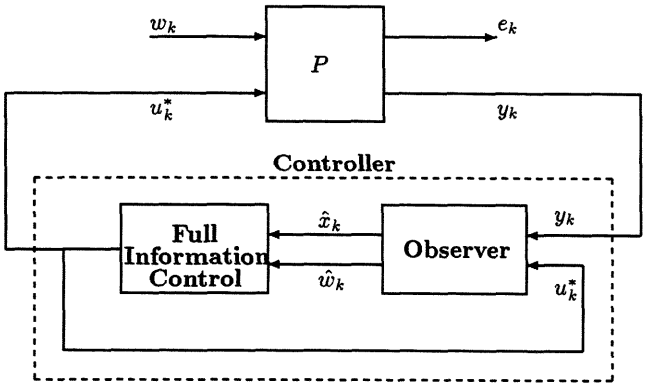

Figure 3.2: Controller Separation Structure.

3.3 $\mathcal{H}^\infty$ 1-DOF Normalized Coprime Factor Design Approach

A state-space construction for the normalized left coprime factorization and right coprime factorization can be obtained in terms of the solution to the two standard semi-definite algebraic Riccati equations

$$BR_1^{-1}B^T - P + \Phi P\Phi^T - \Phi PC^T Z_2^T Z_2 CP\Phi^T = 0 \tag{3.28}$$

$$C^T R_2^{-1}C - Q + \Phi^T Q\Phi - \Phi^T QBZ_1 Z_1^T B^T Q\Phi = 0 \tag{3.29}$$

respectively, where $Z_2^T Z_2 = (R_2 + CPC^T)^{-1}$, $Z_1 Z_1^T = (R_1 + B^T QB)^{-1}$, $P = P^T$ and $Q = Q^T$ are both the non-negative definite stabilizing solutions,

$R_1 = (I + D^T D)$, $R_2 = (I + DD^T)$ and $\Phi = (A - BR_1^{-1}D^T C)$. In detail, if

$$H = -(APC^T + BD^T)(R_2 + CPC^T)^{-1} \tag{3.30}$$

$$F = -(R_1 + B^T QB)^{-1}(B^T QA + D^T C) \tag{3.31}$$

then

$$\tilde{N} = Z_2 C(zI - A_H)^{-1}B_H + Z_2 D \tag{3.32}$$

$$\tilde{M} = Z_2 C(zI - A_H)^{-1}H + Z_2 \tag{3.33}$$

is a normalized left coprime factorization of G, where $A_H = (A + HC)$ and $B_H = (B + HD)$, and

$$N = C_F(zI - A_F)^{-1}BZ_1 + DZ_1 \tag{3.34}$$

$$M = Z_1 + F(zI - A_F)^{-1}BZ_1 \tag{3.35}$$

is a normalized right coprime factorization of G, where $A_F = (A + BF)$ and $C_F = (C + DF)$. Z_2 and Z_1 may be determined by performing a Cholesky Decomposition on

$$Z_2^T Z_2 = (R_2 + CPC^T)^{-1} \tag{3.36}$$

$$Z_1 Z_1^T = (R_1 + B^T QB)^{-1} \tag{3.37}$$

respectively.

3.3.1 Robust Stabilization of Left Coprime Factorization

A perturbed plant transfer function may be written as

$$G_\Delta = (\tilde{M} + \Delta_{\tilde{M}})^{-1}(\tilde{N} + \Delta_{\tilde{N}}) \tag{3.38}$$

In (3.38), the uncertainty associated with G is represented in terms of unknown stable transfer function perturbations acting additively one on each of the elements $\tilde{N}$ and $\tilde{M}$ of a left coprime factorization of G. This is clearly shown in Figure 3.3. The loop equations for Figure 3.3 can be written as

$$\begin{bmatrix} u_k \\ y_k \\ e_k \end{bmatrix} = \begin{bmatrix} \begin{bmatrix} K \\ I \end{bmatrix}(I - GK)^{-1}\tilde{M}^{-1} & \begin{bmatrix} I \\ G \end{bmatrix}(I - KG)^{-1}K \\ (I - GK)^{-1}\tilde{M}^{-1} & (I - GK)^{-1}GK \end{bmatrix} \begin{bmatrix} \phi_k \\ r_k \end{bmatrix} \tag{3.39}$$

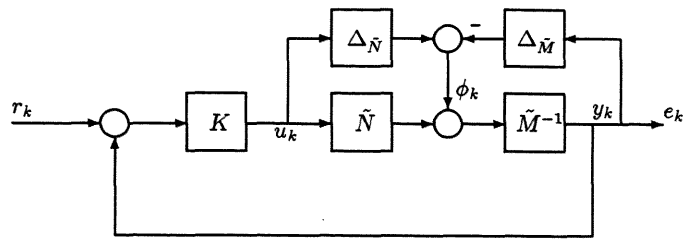

Figure 3.3: Left Coprime Factor Problem Formulation.

which is represented by an upper linear fractional transformation shown in Figure 3.4, where $\Delta = [\Delta_{\tilde{N}} \quad \Delta_{\tilde{M}}]$. Each transfer function element in $M(z) = \begin{bmatrix} M_{11}(z) & M_{12}(z) \\ M_{21}(z) & M_{22}(z) \end{bmatrix}$ is stable provided K is an internally stabilizing controller. The closed-loop transfer function from r_k to e_k shown in Figure 3.4 is given by

$$\mathcal{F}_u(M, \Delta) = M_{22} + M_{21}\Delta(I - M_{11}\Delta)^{-1}M_{12} \tag{3.40}$$

By the small gain theorem, the perturbed system in Figure 3.4 is guaranteed to be internally stable for a stable Δ, if $\| M_{11} \|_\infty < 1$. Hence, synthesizing an internally stabilizing K which minimizes $\| M_{11} \|_\infty$ corresponds to achieving optimal robust stabilization against left coprime factor perturbation.

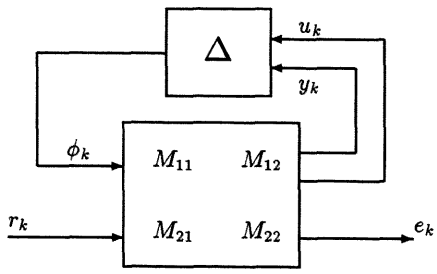

Figure 3.4: Left Coprime Factor Problem Formulation.

Substituting for K from (2.61) (with Q replaced by θ) into M_{11} gives

$$M_{11} = \begin{bmatrix} K \\ I \end{bmatrix} (\tilde{M} - \tilde{N}K)^{-1} = \begin{bmatrix} Y \\ X \end{bmatrix} + \begin{bmatrix} M \\ N \end{bmatrix} \theta \tag{3.41}$$

The problem of finding K which provides optimal robust stabilization can be converted into an optimal Hankel norm approximation problem [62]. Since $(\tilde{N}, \tilde{M})$ is normalized, $\begin{bmatrix} \tilde{N}^* \\ -\tilde{M}^* \end{bmatrix}$ is an all-pass extension for $\begin{bmatrix} M \\ N \end{bmatrix}$. Invoking the norm preserving properties of all-pass transfer function matrices, it follows that

$$\| M_{11} \|_\infty = \left\| \begin{matrix} R_{11} + \theta \\ -I \end{matrix} \right\|_\infty \tag{3.42}$$

where

$$R_{11} = \begin{bmatrix} M \\ N \end{bmatrix}^* \begin{bmatrix} Y \\ X \end{bmatrix} \tag{3.43}$$

(3.43) can be re-expressed as follows

$$R_{11} = Z_1^T \left[\begin{array}{c|c} A_F & B \\ \hline F & I \\ C_F & D \end{array}\right]^* \left[\begin{array}{c|c} A_F & -H \\ \hline F & 0 \\ C_F & I \end{array}\right] Z_2^{-1} \tag{3.44}$$

which may also be written as

$$\begin{aligned} R_{11}(z) \;=\; & Z_1^{-1}[-B^T(z^{-1}I - A_F^T)^{-1}(F^TF + C_F^TC_F)(zI - A_F)^{-1}H \\ & -(F + D^TC_F)(zI - A_F)^{-1}H + B^T(z^{-1}I - A_F^T)^{-1}C_F^T + D^T]Z_2^{-1} \end{aligned} \tag{3.45}$$

Writing the Q Riccati equation as

$$F^TF + C_F^TC_F = z(z^{-1}I - A_F^T)Q + A_F^TQ(zI - A_F) \tag{3.46}$$

it follows that

$$R_{11}(z) = Z_1^T \left[B^T(z^{-1}I - A_F^T)^{-1}(C_F^T - A_F^TQH) + D^T - B^TQH\right] Z_2^{-1} \tag{3.47}$$

Provided A_F is invertible, $R_{11}(z)$ has the following state-space realization

$$R_{11} \stackrel{s}{=} \left[\begin{array}{c|c} A_F^{-T} & (A_F^{-T}C_F^T - QH)Z_2^{-1} \\ \hline -Z_1^TB^TA_F^{-T} & Z_1^T(D^T - B^TA_F^{-T}C_F^T)Z_2^{-1} \end{array}\right] \tag{3.48}$$

The eigenvalues of A_F are the stable generalized eigenvalues of the following symplectic pencil

$$S_Q(\lambda) = \begin{bmatrix} \Phi & 0 \\ -C^T R_2^{-1} C & I \end{bmatrix} - \lambda \begin{bmatrix} I & BR_1^{-1}B^T \\ 0 & \Phi^T \end{bmatrix} \tag{3.49}$$

in which case, R_{11} is anti-stable. The optimal Hankel norm approximation results of [36] yields

$$\gamma_o^2 = \min_{\theta \in \mathcal{RH}^\infty} \left\| \begin{matrix} R_{11} + \theta \\ -I \end{matrix} \right\|_\infty^2 = 1 + \| R_{11} \|_H^2 = 1 + \lambda_{max}(W_c W_o) \tag{3.50}$$

where W_c and W_o are the controllability and observability Grammians of R_{11}, satisfying the Lyapunov equations

$$W_c - A_F^{-T} W_c A_F^{-1} = (A_F^{-T} C_F^T - QH)(Z_2^T Z_2)^{-1}(C_F A_F^{-1} - H^T Q) \tag{3.51}$$

$$W_o - A_F^{-1} W_o A_F^{-T} = (A_F^{-1} B)(Z_1 Z_1^T)(B^T A_F^{-T}) \tag{3.52}$$

Equations (3.51) and (3.52) can be solved explicitly in terms of the non-negative definite Riccati equations P and Q, that is

$$W_c = -Q(I + PQ) \tag{3.53}$$

$$W_o = -P(I + QP)^{-1} \tag{3.54}$$

Equation (3.53) can be proved by direct calculation of (3.51), and (3.54) can be proved by following Theorem 2 in [106]. Substituting (3.53) and (3.54) into (3.50), the lowest achievable (optimal) value of γ_o is given by

$$\gamma_o = (1 + \lambda_{max}(PQ))^{1/2} \tag{3.55}$$

3.3.2 Controller Formulae

Attention is now turned to the realization of suboptimal and optimal controllers which will provide some level of robust stability with respect to uncertainty of normalized left coprime factor plant description.

Suboptimal Controllers

A generator of all controllers achieving

$$\left\| \begin{bmatrix} K \\ I \end{bmatrix} (I - GK)^{-1} \tilde{M}^{-1} \right\|_\infty < \gamma \tag{3.56}$$

where $\gamma > \gamma_o$ can be obtained directly from the game theoretic formulae for suboptimal discrete-time $\mathcal{H}^\infty$ controllers derived in [58, 107].

The following general regulator formulation is now employed

$$P(z) = \begin{bmatrix} P_{11} & P_{12} \\ P_{21} & P_{22} \end{bmatrix} = \begin{bmatrix} 0 & I \\ \tilde{M}^{-1} & G \\ \tilde{M}^{-1} & G \end{bmatrix} \tag{3.57}$$

and P has the following state-space realization

$$\left[\begin{array}{c|c|c} A & B_1 & B_2 \\ \hline C_1 & D_{11} & D_{12} \\ \hline C_2 & D_{21} & D_{22} \end{array}\right] = \left[\begin{array}{c|c|c} A & -HZ_2^{-1} & B \\ \hline 0 & 0 & I \\ C & Z_2^{-1} & D \\ \hline C & Z_2^{-1} & D \end{array}\right] \tag{3.58}$$

Lemma 3.3.1 K internally stabilizes $\mathcal{F}_l(P,K)$ and $\| \mathcal{F}_l(P,K) \|_\infty < \gamma$ if, and only if, K internally stabilizes the transfer function matrix $M(z)$ in (3.39) and

$$\left\| \begin{bmatrix} K \\ I \end{bmatrix} (\tilde{M} - \tilde{N}K)^{-1} \right\|_\infty < \gamma$$

Proof

For P(z) given by (3.57), $\mathcal{F}_l(P,K) = \begin{bmatrix} K \\ I \end{bmatrix} (\tilde{M} - \tilde{N}K)^{-1}$. If $M(z)$ is stable, then so is $M_{11} = \begin{bmatrix} K \\ I \end{bmatrix} (\tilde{M} - \tilde{N}K)^{-1}$. Conversely, $\mathcal{F}_l(P,K)$ stable $\Rightarrow$ M_{11} stable $\Rightarrow$ $M_{11}\tilde{N}$ stable. This implies the stability of M. ■

A state-space realization of the central suboptimal controller for the 1-DOF control configuration under consideration will now be derived. We start with the following theorem.

Theorem 3.3.1 For the standardized plant described by (3.58) and satisfying assumptions A1, A2, A4 and A6 with D_{21} square, we have the following results:

1) There exist an internally stabilizing suboptimal controller $K(z)$ such that $\| \mathcal{F}_l(P,K) \|_\infty < \gamma$ if, and only if,

   i) $\gamma > \gamma_o$.

   ii) $-\gamma^2 I + B_1^T X_\infty B_1 + D_{11}^T D_{11} - B_1^T X_\infty B_2 (I + B_2^T X_\infty B_2)^{-1} B_2^T X_\infty B_1 < 0$
   where
   $X_\infty = X_\infty^T \geq 0$ satisfies (3.11).

2) When the conditions of part (1) are satisfied, the internally stabilizing suboptimal controller $K(z)$ satisfying $\| \mathcal{F}_l(P,K) \|_\infty < \gamma$ has the following state-space realization

$$K \stackrel{s}{=} \left[\begin{array}{c|c} O_{BX} A \left(I + PC^T C\right)^{-1} & O_{BX} A \left(I + PC^T C\right)^{-1} PC^T \\ \hline -B^T X_\infty O_{BX} A \left(I + PC^T C\right)^{-1} & -B^T X_\infty O_{BX} A \left(I + PC^T C\right)^{-1} PC^T \end{array}\right] \tag{3.59}$$

where $O_{BX} = \left(I + BB^T X_\infty\right)^{-1}$.

Proof

Part 1 (i): Straightforward.

Part 1 (ii) is a consequence of Theorem 3.2.1 and (3.58).

Part 2 : Lets consider the following observations. From (3.58) we have:

$$D_{12}^T D_{11} = 0, \quad D_{12}^T C_1 = 0, \quad D_{12}^T D_{12} = I \tag{3.60}$$

Now from (3.19) we have

$$\begin{aligned} W_{12}^{-1} W_{11} &= W_{12}^{-1} W_{12}^{-T} \left(D_{12}^T D_{11} + B_2^T X_\infty B_1\right) \\ (3.60) \Longrightarrow &= \left(W_{12}^T W_{12}\right)^{-1} B_2^T X_\infty B_1 \\ (3.15) \Longrightarrow &= \left(D_{12}^T D_{12} + B_2^T X_\infty B_2\right)^{-1} B_2^T X_\infty B_1 \\ (3.60) \Longrightarrow &= \left(I + B_2^T X_\infty B_2\right)^{-1} B_2^T X_\infty B_1 \end{aligned} \tag{3.61}$$

Also, from (3.19) we have

$$W_{12}^{-1} L_1 = W_{12}^{-1} W_{12}^{-T} \left(D_{12}^T C_1 + B_2^T X_\infty A\right)$$

$$
\begin{aligned}
(3.60) \Longrightarrow \quad &= \left(W_{12}^T W_{12}\right)^{-1} B_2^T X_\infty A \\
(3.15) \Longrightarrow \quad &= \left(D_{12}^T D_{12} + B_2^T X_\infty B_2\right)^{-1} B_2^T X_\infty A \\
(3.60) \Longrightarrow \quad &= \left(I + B_2^T X_\infty B_2\right)^{-1} B_2^T X_\infty A
\end{aligned} \tag{3.62}
$$

The central suboptimal control law given in (3.27) can now be written as

$$
\begin{aligned}
u_k^* &= -W_{12}^{-1} L_1 \hat{x}_k - W_{12}^{-1} W_{11} \hat{w}_k \\
(3.61)\&(3.62) \Longrightarrow u_k^* &= -\left(I + B_2^T X_\infty B_2\right)^{-1} B_2^T X_\infty A \hat{x}_k \\
&\quad -\left(I + B_2^T X_\infty B_2\right)^{-1} B_2^T X_\infty B_1 \hat{w}_k \\
&= -\left(I + B_2^T X_\infty B_2\right)^{-1} B_2^T X_\infty \left(A\hat{x}_k + B_1 \hat{w}_k\right) \\
(3.23) \Longrightarrow \quad &= -\left(I + B_2^T X_\infty B_2\right)^{-1} B_2^T X_\infty \left[A\hat{x}_k + B_1 D_{21}^{-1}\left(y_k - C_2 \hat{x}_k\right)\right] \\
&= -\left(I + B_2^T X_\infty B_2\right)^{-1} B_2^T X_\infty \\
&\quad \times \left[\left(A - B_1 D_{21}^{-1} C_2\right)\hat{x}_k + B_1 D_{21}^{-1} y_k\right] \\
&= C_k \hat{x}_k + D_k y_k
\end{aligned} \tag{3.63}
$$

where

$$
C_k = -\left(I + B_2^T X_\infty B_2\right)^{-1} B_2^T X_\infty \left(A - B_1 D_{21}^{-1} C_2\right) \tag{3.64}
$$

$$
D_k = -\left(I + B_2^T X_\infty B_2\right)^{-1} B_2^T X_\infty B_1 D_{21}^{-1} \tag{3.65}
$$

Now substituting for u_k^* from (3.63) in (3.26), the observer dynamics can be written as

$$
\begin{aligned}
\hat{x}_{k+1} &= \left(A - B_1 D_{21}^{-1} C_2\right)\hat{x}_k + B_1 D_{21}^{-1} y_k + B_2\left(C_k \hat{x}_k + D_k y_k\right) \\
&= \left(A - B_1 D_{21}^{-1} C_2 + B_2 C_k\right)\hat{x}_k + \left(B_1 D_{21}^{-1} + B_2 D_k\right) y_k \\
&= A_k \hat{x}_k + B_k y_k
\end{aligned} \tag{3.66}
$$

where

$$
A_k = A - B_1 D_{21}^{-1} C_2 + B_2 C_k \tag{3.67}
$$

$$
B_k = B_1 D_{21}^{-1} + B_2 D_k \tag{3.68}
$$

From (3.58), (3.64) becomes

$$
\begin{aligned}
C_k &= -\left(I + B^T X_\infty B\right)^{-1} B^T X_\infty (A + HC_2) \\
&= -\left(I + B^T X_\infty B\right)^{-1} B^T X_\infty (A - APC^T (I + CPC^T)^{-1} C) \\
&= -B^T X_\infty \left(I + BB^T X_\infty\right)^{-1} A (I + PC^T C)^{-1}
\end{aligned} \tag{3.69}
$$

and (3.65) becomes

$$\begin{aligned} D_k &= -(I + B^T X_\infty B)^{-1} B^T X_\infty H \\ &= -B^T X_\infty (I + BB^T X_\infty)^{-1} A (I + PC^T C)^{-1} PC^T \end{aligned} \tag{3.70}$$

Using (3.58), (3.64), and (3.65), (3.67) and (3.68) can be rewritten as

$$A_k = (I + BB^T X_\infty)^{-1} A (I + PC^T C)^{-1} \tag{3.71}$$

$$B_k = (I + BB^T X_\infty)^{-1} A (I + PC^T C)^{-1} PC^T \tag{3.72}$$

This completes the proof. ■

Optimal Controllers

The controller realization (3.59) becomes degenerate as γ approaches the optimal value of (3.55). This is accompanied by X_∞ being unbounded in the limit. Since [62]

$$X_\infty = \gamma^2 Q(\gamma^2 - 1) - PQ)^{-1} \tag{3.73}$$

the controller dynamics become after substituting (3.73) in (3.59)

$$x_{k+1} = ER^{-1} A \left(I + PC^T C\right)^{-1} x_k + ER^{-1} A \left(I + PC^T C\right)^{-1} PC^T y_k \tag{3.74}$$

$$u_k = -\gamma^2 B^T Q R^{-1} A \left(I + PC^T C\right)^{-1} x_k - \gamma^2 B^T Q R^{-1} A \left(I + PC^T C\right)^{-1} PC^T y_k \tag{3.75}$$

where

$$E = \left[(\gamma^2 - 1)I - PQ\right]^{-1} \tag{3.76}$$

$$R = \left[(\gamma^2 - 1)I - PQ + \gamma^2 BB^T Q\right]^{-1} \tag{3.77}$$

Clearly, when $\gamma = \gamma_o$, the left null spaces of the matrices A_k and B_k intersect and the realization of (3.59) contains r uncontrollable modes at the origin, r being the multiplicity of (3.55). These can be removed in the following manner. First, a singular value decomposition of E is performed as follows

$$\begin{bmatrix} U_1 & U_2 \end{bmatrix} \begin{bmatrix} \Sigma & 0 \\ 0 & 0 \end{bmatrix} \begin{bmatrix} V_1^T \\ V_2^T \end{bmatrix} = \left[(\gamma_o^2 - 1)I - PQ\right] \tag{3.78}$$

Then the state transition equation given in (3.74) becomes

$$x_{k+1} = U_1 \Sigma V_1^T R^{-1} A \left(I + PC^T C\right)^{-1} x_k + U_1 \Sigma V_1^T R^{-1} A \left(I + PC^T C\right)^{-1} PC^T y_k \tag{3.79}$$

Second, the uncontrollable modes can then be removed *via* the singular state transformation from x_k to ζ_k

$$x_k = U_1 \zeta_k \tag{3.80}$$

leading to a realization for the reduced-state-order central optimal controller

$$K_{opt} \stackrel{s}{=} \left[\begin{array}{c|c} \Sigma V_1^T R^{-1} A \left(I + PC^T C\right)^{-1} U_1 & \Sigma V_1^T R^{-1} A \left(I + PC^T C\right)^{-1} PC^T \\ \hline -\gamma_o^2 B^T Q R^{-1} A \left(I + PC^T C\right)^{-1} U_1 & -\gamma_o^2 B^T Q R^{-1} A \left(I + PC^T C\right)^{-1} PC^T \end{array}\right] \tag{3.81}$$

3.3.3 An $\mathcal{H}^\infty$ Loop Shaping Design Procedure (LSDP)

In practical design applications, an effective method is to reshape the plant frequency response in order to meet the closed-loop performance requirements. This loop shaping can be done by the following design procedure [62]:

1) Using a pre-compensator, W_1, and/or a post-compensator, W_2, the singular values of the nominal system G, are modified to give a desired loop shape. The nominal system and weighting functions W_1 and W_2 are combined to form the shaped system, G_s, where

$$G_s = W_2 G W_1 \tag{3.82}$$

It is assumed that W_1 and W_2 are such that G_s contains no hidden unstable modes.

2) A feedback controller, K, is synthesized which robustly stabilizes the normalized left coprime factorization of G_s, with a maximum stability margin ϵ_{max}, where $\epsilon_{max} = \frac{1}{\gamma_o}$.

3) The final feedback controller, K, is then constructed by combining the $\mathcal{H}^\infty$ controller K_∞, with the weighting functions W_1 and W_2 such that

$$K = W_1 K_\infty W_2 \tag{3.83}$$

It can be shown that the final controller does not significantly alter the specified loop shape provided a sufficiently small value of γ_o is achieved.

For a tracking problem, the reference signal is generally fed between K_∞ and W_1, so that the closed-loop transfer function between the reference r_k and the plant output y_k becomes

$$\frac{y(z)}{r(z)} = (I - G(z)K(z))^{-1}G(z)W_1(z)K_\infty(I)W_2(I), \tag{3.84}$$

where the reference r_k is connected through a gain $K_\infty(I)W_2(I)$ where

$$K_\infty(I)W_2(I) = \lim_{z\to 1} K_\infty(z)W_2(z), \tag{3.85}$$

to ensure unity steady-state gain.

3.4 $\mathcal{H}^\infty$ 2-DOF Design Approach

The objectives in control system design usually refer to internal stability of the control system, disturbance rejection, measurement noise attenuation, insensitivity to parameter variations, and reference signal tracking. These objectives may be achieved by one or 2-DOF schemes, but reference signal tracking often dictates the use of a 2-DOF controller. The philosophy of the 2-DOF scheme is to use a feedback controller K_2 to meet the requirements of internal stability, disturbance rejection, measurement noise attenuation, and sensitivity minimization. A prefilter K_1, is then applied to the reference signal, which optimizes the response of the overall system to the command input.

Sometimes for a 2-DOF controller design, a natural framework to adopt is that of an infinite-time model following task where the plant is forced to track, for example, a step response to a specified model. It may be for instance, that a flexible wing aircraft (the plant) is required to perform (after connection of feedforward and feedback control) in the same manner as a rigid body aircraft (the reference model). This approach was first proposed and developed for the continuous-time in [47], where in this 2-DOF framework, the feedback controller and prefilter are designed together in a single step *via* an $\mathcal{H}^\infty$ optimization framework. The feedback controller is used to meet the robust stability and disturbance rejection specifications, while the prefilter is used to shape the desired time responses of the closed-loop system, that is, it forces the plant model output to follow a reference model.

3.4.1 The 2-DOF Design Configuration

The 2-DOF configuration (Figure 3.5) includes a model matching problem in addition to the robust stability maximization problem outlined in Section (3.3). The controller K is partitioned as $K = [\,K_1 \quad K_2\,]$, where K_1 is the prefilter and K_2 the feedback controller. $M_o(z)$ is a reference model chosen to have ideal time-domain response characteristics, which the closed-loop system is desired to follow. $G_s = GW_1 = \tilde{M}^{-1}\tilde{N}$ is the shaped plant. For the 2-DOF configuration, we assume that the plant has no post-compensation as part of the weighting (*i.e.* $W_2 = I$). We shall later consider (Chapter 8) the case where W_2 may also be used in shaping the plant.

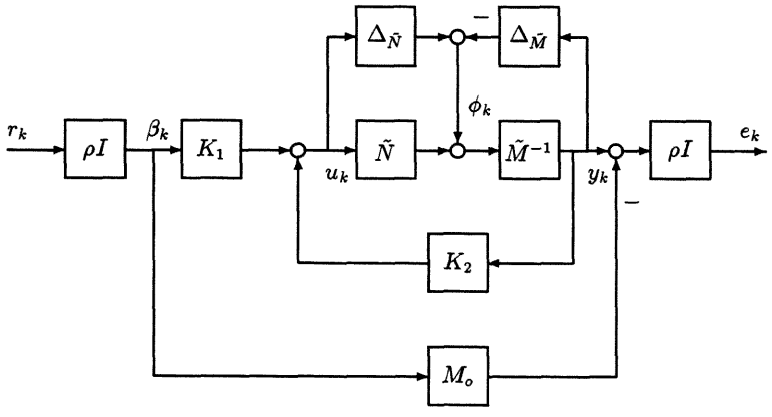

Figure 3.5: 2-DOF Design Configuration.

The problem is now formulated as a standard $\mathcal{H}^\infty$-optimization problem such that the ∞-norm of the transfer function matrix $\mathcal{F}_l(P,K)$ relating u_k, y_k, e_k to r_k, ϕ_k *via*

$$\left[\begin{array}{c|c} \rho(I - K_2G_s)^{-1}K_1 & K_2(I - G_sK_2)^{-1}\tilde{M}^{-1} \\ \rho(I - G_sK_2)^{-1}G_sK_1 & (I - G_sK_2)^{-1}\tilde{M}^{-1} \\ \hline \rho^2((I - G_sK_2)^{-1}G_sK_1 - M_o) & \rho(I - G_sK_2)^{-1}\tilde{M}^{-1} \end{array}\right] \tag{3.86}$$

is minimized. The (1,2) partition of (3.86) is associated with robust stability optimization and the (2,1) partition with model-matching. The aim is thus to provide robust

model following in addition to robust stability in the face of the coprime factor uncertainty. The (1,1) partition can interpreted as limiting actuator use when following references. The parameter ρ is a scaling used to emphasize the (2,1) partition of (3.86), thus emphasizing the model-matching part of the problem.

To set the problem in an $\mathcal{H}^\infty$-optimization framework, we shall first put it into the standard regulator form shown in Figure 2.1. As shown in the figure, w_k was the vector of all exogenous signals and e_k was the vector of all signals to be minimized, u_k was the vector of control signals and y_k was the vector of measurements available to the controller. For the 2-DOF case, $w_k = [r_k^T \quad \phi_k^T]^T$, $e_k = [u_k^T \quad y_k^T \quad e_k^T]^T$, and $y_k = [\beta_k^T \quad y_k^T]^T$. This is all apparent from the choice of the transfer function matrix (3.86) we seek to minimize. The generalized plant P is then given by

$$\begin{bmatrix} u_k \\ y_k \\ e_k \\ \beta_k \\ y_k \end{bmatrix} = \begin{bmatrix} P_{11} & P_{12} \\ P_{21} & P_{22} \end{bmatrix} \begin{bmatrix} r_k \\ \phi_k \\ u_k \end{bmatrix}$$

$$= \begin{bmatrix} 0 & 0 & I \\ 0 & \tilde{M}^{-1} & G_s \\ -\rho^2 M_o & \rho\tilde{M}^{-1} & \rho G_s \\ \rho I & 0 & 0 \\ 0 & \tilde{M}^{-1} & G_s \end{bmatrix} \begin{bmatrix} r_k \\ \phi_k \\ u_k \end{bmatrix} \tag{3.87}$$

Let the shaped plant $G_s(z)$ and the reference model $M_o(z)$ have state-space realizations $G_s \stackrel{s}{=} \left[\begin{array}{c|c} A_s & B_s \\ \hline C_s & 0 \end{array}\right]$ and $M_o \stackrel{s}{=} \left[\begin{array}{c|c} A_o & B_o \\ \hline C_o & 0 \end{array}\right]$, respectively, with M_o being stable. A state-space realization for (3.87) is then given by

$$P \stackrel{s}{=} \left[\begin{array}{c||c|c} A & B_1 & B_2 \\ \hline\hline C_1 & D_{11} & D_{12} \\ \hline C_2 & D_{21} & D_{22} \end{array}\right] = \left[\begin{array}{cc||cc|c} A_s & 0 & 0 & -HZ_2^{-1} & B_s \\ 0 & A_o & B_o & 0 & 0 \\ \hline\hline 0 & 0 & 0 & 0 & I \\ C_s & 0 & 0 & Z_2^{-1} & 0 \\ \rho C_s & -\rho^2 C_o & 0 & \rho Z_2^{-1} & 0 \\ \hline 0 & 0 & \rho I & 0 & 0 \\ C_s & 0 & 0 & Z_2^{-1} & 0 \end{array}\right] \tag{3.88}$$

The state vector x_k of P can be partitioned as $([\, x_{s_k}^T \quad x_{o_k}^T \,])^T$, where x_{s_k} is the state of the shaped plant G_s and x_{o_k} the state of the reference model M_o. Note that we have assumed the shaped plant G_s to be strictly proper.

3.4.2 The 2-DOF Controller Formulae and Structure

A state-space realization of the central suboptimal controller for the 2-DOF control configuration under consideration will now be derived. We start with the following theorem.

Theorem 3.4.1 For the standardized plant described by (3.88) and satisfying assumptions A1, A2, A4 and A6 with D_{21} square, we have the following results:

1) There exist an internally stabilizing suboptimal controller $K(z)$ such that $\| \mathcal{F}_l(P,K) \|_\infty < \gamma$ if, and only if,

   i) $\gamma > \sqrt{(1+\rho^2)\ \lambda_{max}\left[(Z_2 Z_2^T)^{-1}\right]}$.

   ii) $-\gamma^2 I + B_1^T X_\infty B_1 + D_{11}^T D_{11} - B_1^T X_\infty B_2 (I + B_2^T X_\infty B_2)^{-1} B_2^T X_\infty B_1 < 0$

   where

   $X_\infty = X_\infty^T \geq 0$ satisfies (3.11).

2) When the conditions of part (1) are satisfied, the internally stabilizing suboptimal controller $K(z)$ satisfying $\| \mathcal{F}_l(P,K) \|_\infty < \gamma$ has the following equations

$$\begin{aligned} \hat{x}_{s_{k+1}} &= A_s \hat{x}_{s_k} - H(y_k - C_s \hat{x}_{s_k}) + B_s u_k^* \\ x_{o_{k+1}} &= A_o x_{o_k} + B_o r_k \\ u_k^* &= O_s B_s^T [X_{\infty_{11}}(A_s + HC_s)\hat{x}_{s_k} + X_{\infty_{12}} A_o x_{o_k} \\ &\quad + X_{\infty_{12}} B_o r_k - X_{\infty_{11}} H y_k] \end{aligned} \tag{3.89}$$

where $O_s = -(I + B_s^T X_{\infty_{11}} B_s)^{-1}$.

Proof

Part 1 (i): A necessary condition [48] for the existence of an internally stabilizing suboptimal controller $K(z)$ is that $\gamma > \bar{\sigma}(D_\perp^T D_{11})$. Choosing $D_\perp = \begin{bmatrix} 0 & 0 \\ I & 0 \\ 0 & I \end{bmatrix}$ will ensure that $[\, D_{12} \quad D_\perp \,]$ is unitary. This implies that $D_\perp^T D_{11} = \begin{bmatrix} 0 & Z_2^{-1} \\ 0 & \rho Z_2^{-1} \end{bmatrix}$ and $\bar{\sigma}(D_\perp^T D_{11}) = \sqrt{(1+\rho^2)\ \lambda_{max}\left[(Z_2 Z_2^T)^{-1}\right]}$. Part 1 (ii) is a consequence of Theorem 3.3.1 and (3.88).

Part 2 : Lets consider the following observations. From (3.88) we have:

$$D_{12}^T D_{11} = 0, \quad D_{12}^T C_1 = 0, \quad D_{12}^T D_{12} = I \tag{3.90}$$

The solution X_∞ of the discrete Riccati equation can be partitioned conformally with $A = \left[\begin{array}{c|c} A_s & 0 \\ \hline 0 & A_o \end{array}\right]$, that is $X_\infty = \left[\begin{array}{c|c} X_{\infty_{11}} & X_{\infty_{12}} \\ \hline X_{\infty_{21}} & X_{\infty_{22}} \end{array}\right]$. We can thus write from (3.88)

$$B_2^T X_\infty = [\, B_s^T \quad 0\,] \begin{bmatrix} X_{\infty_{11}} & X_{\infty_{12}} \\ X_{\infty_{21}} & X_{\infty_{22}} \end{bmatrix} = [\, B_s^T X_{\infty_{11}} \quad B_s^T X_{\infty_{12}} \,] \tag{3.91}$$

and

$$B_2^T X_\infty B_2 = [\, B_s^T \quad 0\,] \begin{bmatrix} X_{\infty_{11}} & X_{\infty_{12}} \\ X_{\infty_{21}} & X_{\infty_{22}} \end{bmatrix} \begin{bmatrix} B_s \\ 0 \end{bmatrix} = B_s^T X_{\infty_{11}} B_s \tag{3.92}$$

so that (3.64) becomes

$$\begin{aligned} C_k &= -\left(I + B_s^T X_{\infty_{11}} B_s\right)^{-1} [\, B_s^T X_{\infty_{11}} \quad B_s^T X_{\infty_{12}} \,] \left(A - B_1 D_{21}^{-1} C_2\right) \\ &= -\left(I + B_s^T X_{\infty_{11}} B_s\right)^{-1} [\, B_s^T X_{\infty_{11}} \quad B_s^T X_{\infty_{12}} \,] \begin{bmatrix} A_s + H C_s & 0 \\ 0 & A_o \end{bmatrix} \\ &= -\left(I + B_s^T X_{\infty_{11}} B_s\right)^{-1} [\, B_s^T X_{\infty_{11}} (A_s + H C_s) \quad B_s^T X_{\infty_{12}} A_o \,] \\ &= [\, C_{k_{11}} \quad C_{k_{12}} \,] \end{aligned} \tag{3.93}$$

Similarly substituting for $B_2^T X_\infty$ and $B_2^T X_\infty B_2$ from above and for B_1 and D_{21} from (3.88) in (3.65), we get

$$\begin{aligned} D_k &= -\left(I + B_s^T X_{\infty_{11}} B_s\right)^{-1} [\, B_s^T X_{\infty_{11}} \quad B_s^T X_{\infty_{12}} \,] \begin{bmatrix} 0 & -H Z_2^{-1} \\ B_o & 0 \end{bmatrix} \begin{bmatrix} \rho I & 0 \\ 0 & Z_2^{-1} \end{bmatrix}^{-1} \\ &= -\left(I + B_s^T X_{\infty_{11}} B_s\right)^{-1} [\, \tfrac{1}{\rho} B_s^T X_{\infty_{12}} B_o \quad -B_s^T X_{\infty_{11}} H \,] \\ &= [\, D_{k_{11}} \quad D_{k_{12}} \,] \end{aligned} \tag{3.94}$$

Using (3.88) and (3.93), (3.67) can be written as

$$\begin{aligned} A_k &= \begin{bmatrix} A_s + HC_s & 0 \\ 0 & A_o \end{bmatrix} + \begin{bmatrix} B_s \\ 0 \end{bmatrix} \begin{bmatrix} C_{k_{11}} & C_{k_{12}} \end{bmatrix} \\ &= \begin{bmatrix} A_s + HC_s + B_s C_{k_{11}} & B_s C_{k_{12}} \\ 0 & A_o \end{bmatrix} \end{aligned} \tag{3.95}$$

Similarly for B_k substituting from (3.88) and (3.94) into (3.68), we have

$$\begin{aligned} B_k &= \begin{bmatrix} 0 & -HZ_2^{-1} \\ B_o & 0 \end{bmatrix} \begin{bmatrix} \rho I & 0 \\ 0 & Z_2^{-1} \end{bmatrix}^{-1} + \begin{bmatrix} B_s \\ 0 \end{bmatrix} \begin{bmatrix} D_{k_{11}} & D_{k_{12}} \end{bmatrix} \\ &= \begin{bmatrix} B_s D_{k_{11}} & -H + B_s D_{k_{12}} \\ \frac{1}{\rho} B_o & 0 \end{bmatrix} \end{aligned} \tag{3.96}$$

Using A_k and B_k from above, the observer dynamics (3.26) can be written as

$$\begin{aligned} \begin{bmatrix} \hat{x}_{s_{k+1}} \\ x_{o_{k+1}} \end{bmatrix} &= \begin{bmatrix} A_s + HC_s + B_s C_{k_{11}} & B_s C_{k_{12}} \\ 0 & A_o \end{bmatrix} \begin{bmatrix} \hat{x}_{s_k} \\ x_{o_k} \end{bmatrix} \\ &\quad + \begin{bmatrix} B_s D_{k_{11}} & -H + B_s D_{k_{12}} \\ \frac{1}{\rho} B_o & 0 \end{bmatrix} \begin{bmatrix} \beta_k \\ y_k \end{bmatrix} \end{aligned} \tag{3.97}$$

where we have split the observer state vector into the estimated state $\hat{x}_{s_k}$ of the shaped plant G_s, and the state x_{o_k} of the reference model M_o. Recall that the measurement y_k available to the controller consists of the scaled reference input β_k and the plant output y_k (as can be seen from (3.87)), and hence y_k has been replaced above by $[\beta_k^T \quad y_k^T]^T$. Using $\beta_k = \rho r_k$ (see Figure 3.5), we can re-write the observer state equation as

$$\begin{aligned} \begin{bmatrix} \hat{x}_{s_{k+1}} \\ x_{o_{k+1}} \end{bmatrix} &= \begin{bmatrix} A_s + HC_s + B_s C_{k_{11}} & B_s C_{k_{12}} \\ 0 & A_o \end{bmatrix} \begin{bmatrix} \hat{x}_{s_k} \\ x_{o_k} \end{bmatrix} \\ &\quad + \begin{bmatrix} \rho B_s D_{k_{11}} & -H + B_s D_{k_{12}} \\ B_o & 0 \end{bmatrix} \begin{bmatrix} r_k \\ y_k \end{bmatrix} \end{aligned} \tag{3.98}$$

The controller output equation (3.63) can be written as

$$u_k^* = \begin{bmatrix} C_{k_{11}} & C_{k_{12}} \end{bmatrix} \begin{bmatrix} \hat{x}_{s_k} \\ x_{o_k} \end{bmatrix} + \begin{bmatrix} \rho D_{k_{11}} & D_{k_{12}} \end{bmatrix} \begin{bmatrix} r_k \\ y_k \end{bmatrix} \tag{3.99}$$

(3.98) and (3.99) give a state-space realization of the suboptimal controller that is stabilizing and norm-bounding for the generalized plant of (3.88).

The controller state equation (3.98) can also be written as

$$\begin{bmatrix} \hat{x}_{s_{k+1}} \\ x_{o_{k+1}} \end{bmatrix} = \begin{bmatrix} A_s + HC_s & 0 \\ 0 & A_o \end{bmatrix} \begin{bmatrix} \hat{x}_{s_k} \\ x_{o_k} \end{bmatrix} + \begin{bmatrix} B_s & -H & 0 \\ 0 & 0 & B_o \end{bmatrix} \begin{bmatrix} u_k^* \\ y_k \\ r_k \end{bmatrix} \tag{3.100}$$

which shows clearly the controller structure. This completes the proof. ■

It is seen that the controller consists of an observer for the shaped plant G_s, which provides an estimate $\hat{x}_{s_k}$ for the state x_{s_k} of G_s; H being the observer gain. The observer is driven by the input and output of G_s, u_k^* and y_k, respectively. Also included in the controller dynamical equation is the state update equation of the reference model M_o. The model runs autonomously inside the controller, its state x_{o_k} being driven by the reference input r_k. Recall that the generalized plant P given in (3.88) has the state vector $[\,x_{s_k}^T \quad x_{o_k}^T\,]^T$. The controller has information regarding some of the states of P, *i.e.*, the ones corresponding to the reference model. These states are thus used directly – they need not be estimated. An observer, it turns out from (3.100), is constructed only for the estimation of the states of the shaped plant G_s.

The controller output equation (3.99) consists of a generalized state feedback that uses both the plant state estimate, and the reference model state. It is remarked here that in general, $\mathcal{H}^\infty$ suboptimal control problems cannot be solved by an observer-state feedback combination alone – a worst case disturbance estimate will also be used to generate the control. In the 2-DOF case under consideration however, it is the special structure of the generalized plant P (D_{21} square), that enables the controller to be written simply as an observer plus a state feedback. The controller structure is shown in Figure 3.6. For implementation of the control law, the weights W_1 and W_2 are cascaded with $K = [\,K_1 \quad K_2\,] = \left[\begin{array}{c|c} A_k & B_k \\ \hline C_k & D_k \end{array}\right]$ to yield the final controller

$$[\,W_1K_1 \quad W_1K_2W_2\,] \tag{3.101}$$

In addition, for perfect steady-state tracking, the pre-filter K_1 is scaled so that the steady-state gain from the reference to the output becomes unity.

3.5 Summary

In this chapter, a complete treatment was given of robust controller design for normalized left coprime factor plant description. The presentation had two main aims: The first was to re-formulate the work of [106] for the discrete-time normalized left coprime factorization using similar steps, and to derive central controllers with suboptimal and

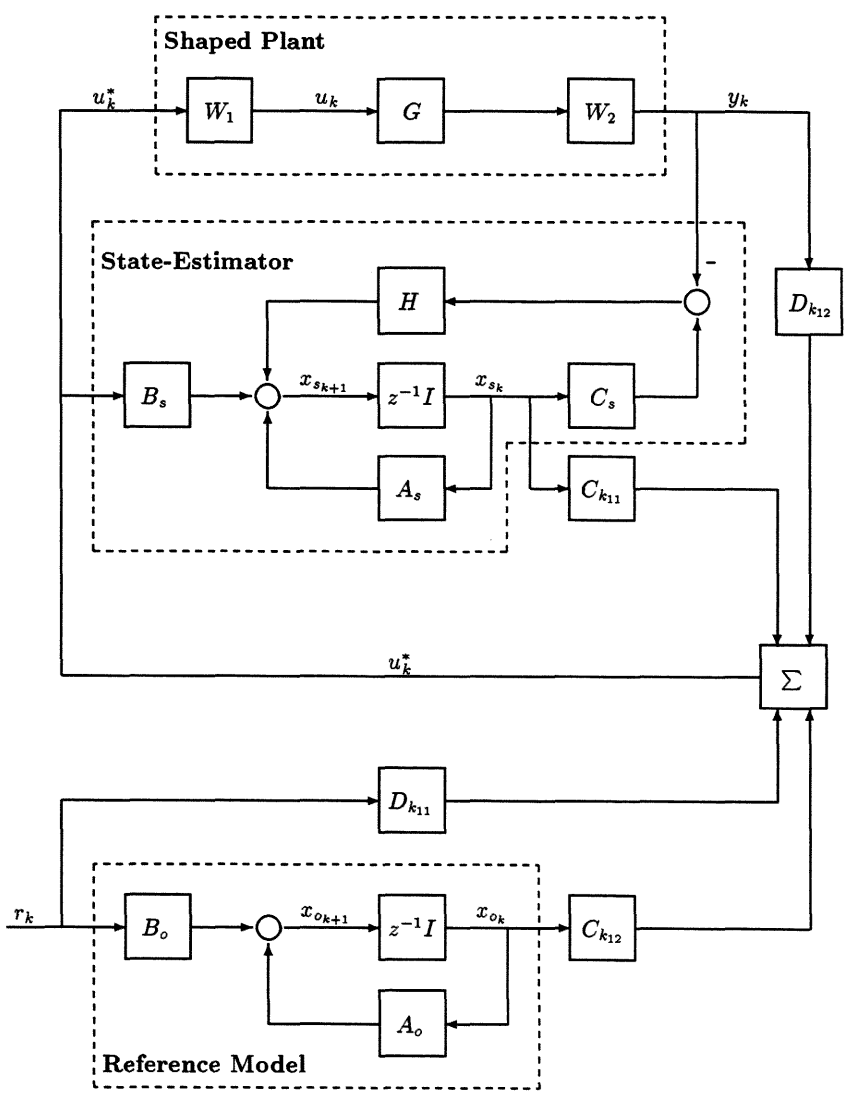

Figure 3.6: 2-DOF Controller Structure.

optimal bounds. The second was to formulate the 2-DOF normalized coprime factor design approach of [47] in discrete-time, and to analyze in more detail, the structure of the resulting 2-DOF suboptimal controller. Explicit state-space formulae for the controller were derived. This 2-DOF controller which achieves robust stability and model following requires the solution of only one indefinite Riccati equation, and its final structure consists of a combined state-estimator/state-feedback coupled with an explicit reference model.

In the next chapter, we shall demonstrate the robust control methods presented in Chapter 2 and this chapter on a SISO industrial case study.

Chapter 4

Robust Multi-Objective Control of an Unknown Industrial Plant

4.1 Introduction

The previous two chapters motivated the use of discrete-time $\mathcal{H}^\infty$ optimization as a method for designing robustly stabilizing controllers by incorporating several types of model uncertainty in the design procedure. In this chapter we are going to apply these methods to an "unknown" industrial plant (the IFAC 1993 benchmark).

The specifications for the IFAC 1993 benchmark control problem, Robust and Adaptive Control of an Unknown Industrial Plant [39] include stringent closed-loop performance requirements for a plant with parameters known only within a certain range. This means that a design method which explicitly considers *closed-loop* performance is desired. The method of inequalities (MOI) is a general-purpose, multi-objective design procedure in which closed-loop performance can be explicitly included in the design objectives. Most control problems, such as the IFAC 1993 benchmark, have significant plant uncertainty, and hence require robustness. This can be provided by use of a number of analytical optimization techniques. Thus, both explicit closed-loop performance and robustness can be obtained by combining the MOI with analytical optimization techniques. This can be simply done by using the MOI to design the weighting functions required for the practical implementation of analytical optimization methods, such as the Linear Quadratic Gaussian (LQG) problem or $\mathcal{H}^\infty$-optimization problems. This provides a powerful design framework for control system design problems such as the IFAC 1993

benchmark problem.

The aim of this chapter is to present designs for the problem achieved by the use of the MOI with several analytical optimization methods covered in Chapters 2 & 3. It also includes results for simple PID controllers designed using the MOI. The chapter also includes details of the combining of the various analytical optimization methods with the MOI.

Section 4.2 states the benchmark problem and gives the specifications and the linear models used for controller design. In Section 4.3, the method of inequalities (MOI) is described along with a summary of the moving boundaries process (MBP), which is the numerical search algorithm used by the MOI. In section 4.4 , a description is given of the design methods used and how they can be combined with the MOI; the methods include PI/PID controllers, an LQG method, the $\mathcal{H}^\infty$ mixed-sensitivity problem, the $\mathcal{H}^\infty$ LSDP and a 2-DOF LSDP extensions. Finally, the designs obtained for the benchmark problem using the various approaches are presented in Section 4.5. A gain adaptive scheme is also presented which improves the performance of the system at the most difficult operating conditions. Finally, a summary is given in Section 4.6.

4.2 Problem Statement

The benchmark is taken from [39] and can be briefly described as follows: One of the loops in a local company in Australia is a time-varying single-input single-output process. Depending on various production conditions, the loop operates at three different stress levels, with higher stress levels inducing larger time variations. The set-point to the loop is a square wave varying between +1 and -1 with a period of 20 seconds.

Until recently, the company was not aware of this loop's impact on product quality and has operated a simple unity gain controller.

New research results, however, have convincingly shown that the final product quality is directly linked to zero steady-state tracking error (modulo high frequency noise) and fast rise times. Thereby the plant output *must* remain within -1.5 and +1.5 *at all times*, otherwise damage is immediate. But it is actually preferable if the output remains

between -1.2 and +1.2 most of the time.

Unconfirmed spy reports claim that a competing company is succeeding in running the loop with rise times of 2 or 3 seconds and fast settling. So now the management of the local company would like to know if such performance, or possibly even better, can indeed be achieved.

4.2.1 Specifications

For each stress level, design a controller to achieve as fast a rise time as possible, subject to the following conditions:

1) The plant output must be within -1.5 and +1.5 at all times.

2) Zero steady state tracking error (modulo high frequency noise).

3) It is preferable if under/overshoot is around 0.2 most of the time (occasional large over/undershoots are acceptable as long as the output is within $\pm$ 1.5).

4) Fast settling time.

5) Plant input saturates at -5.0 and +5.0.

The set-point may be pre-filtered.

4.2.2 Simulation

The design is simulated *via* an accessible "black box" simulation code. The code for the supplied unity feedback controller is replaced with the final designed controller. The following points must be observed:

1) Due to noise and parameter variations, the response will be different every time the program is run (larger variations at higher stress levels).

2) A representative picture of the variations is achieved if the plant is simulated over at least 300 seconds.

3) The variations can be achieved by either simulating over a 300 second period, or by simulating several times over equivalently shorter periods. The latter is recommended for convenience.

4) The final design should be simulated by running the program at least 15 times over a 20 seconds period and plotting the 15 output curves on top of each other on a window scaled from 0 to 20 seconds on the horizontal and from -1.5 to +1.5 on the vertical axis. This should be done separately for each of the three stress levels, yielding a total of three windows with 15 curves each.

4.2.3 Linear Models and Open-loop Analysis

The nominal transfer function $G(s)$ of the plant is given by

$$G(s) = \frac{K(-T_2 s + 1)\omega_0^2}{(s^2 + 2\zeta\omega_0 s + \omega_0^2)(T_1 s + 1)} \tag{4.1}$$

where

$$T_1 = 5,\ T_2 = 0.4,\ \omega_0 = 5,\ \zeta = 0.3,\ K = 1$$

The transfer function of the plant for each stress level is also given by (4.1) with the following parameter variation intervals:

Stress Level	δT_1	δT_2	$\delta\omega_0$	$\delta\zeta$	δK
1	±0.20	±0.05	±1.50	±0.10	0
2	±0.30	±0.10	±2.50	±0.15	±0.15
3	±0.30	±0.15	±3.00	±0.15	±0.50

For stress level 1, the variations of the parameters are uniformly random within the indicated limits and the changes coincide with step changes in the set-point. For stress levels 2 & 3, the variations of the parameters are sinusoidal with indicated amplitudes and random phase changes. The complete transfer function $G_t(s)$ of the plant for each stress level is given by

$$G_t(s) = \frac{K(-T_2 s + 1)\omega_0^2}{(s^2 + 2\zeta\omega_0 s + \omega_0^2)(T_1 s + 1)} \frac{\omega_\delta^2}{(s^2 + 2\zeta_\delta\omega_\delta s + \omega_\delta^2)(T_1^\delta s + 1)(T_2^\delta s + 1)} \tag{4.2}$$

where

$$T_1^\delta = \frac{1}{8},\ T_2^\delta = \frac{1}{12},\ \omega_\delta = 15,\ \zeta_\delta = 0.6$$

The time domain open-loop responses for all stress levels are shown in Figure 4.1, where the dashed line indicates stress level 1, the dotted line indicates stress level 2, and the solid line indicates stress level 3. Also, the frequency domain open-loop responses for all stress levels are shown in the same figure, where the solid line indicates the complete transfer function and the dotted line indicates the nominal transfer function. The figure clearly indicates the high variations in static gains for stress levels 2 & 3.

4.3 An Introduction to the Method of Inequalities

Performance specifications for control and other engineering systems are frequently given in terms of algebraic or functional inequalities, rather than in the minimization of some objective function. For example, a control system may be required to have a rise time of less than 1 second, a settling time of less than 5 seconds, and an overshoot of less than 10%. In such cases, it is obviously more logical and convenient if the design problem is expressed explicitly in terms of such inequalities.

4.3.1 The Method of Inequalities (MOI)

The method of inequalities (MOI) [115] is a computer-aided multi-objective design approach, where desired performance is represented by such a set of algebraic inequalities, and where the aim of the design is to simultaneously satisfy these inequalities. The design problem is expressed as

$$\phi_i(p) \leq \varepsilon_i \quad \text{for} \quad i = 1, \ldots, n \tag{4.3}$$

where ε_i are real numbers, $p \in \mathcal{P}$ is a real vector $(p_1, p_2, \ldots, p_q)$ chosen from a given set $\mathcal{P}$ and ϕ_i are real functions of p. The functions ϕ_i are the *objective functions*, the components of p represent the *design parameters* and ε_i are the *design goals* which are chosen by the designer and represent the largest tolerable values of ϕ_i. The aim is the satisfaction of the set of inequalities in order that an acceptable design p is reached.

Each inequality $\phi_i(p) \leq \varepsilon_i$ of the set of inequalities (4.3) defines a set $\mathcal{S}_i$ of points in the q-dimensional space $\mathcal{R}^q$ and the co-ordinates of this space are $p_1, p_2, \ldots, p_q$, so

$$\mathcal{S}_i = \{p : \phi_i(p) \leq \varepsilon_i\}. \tag{4.4}$$

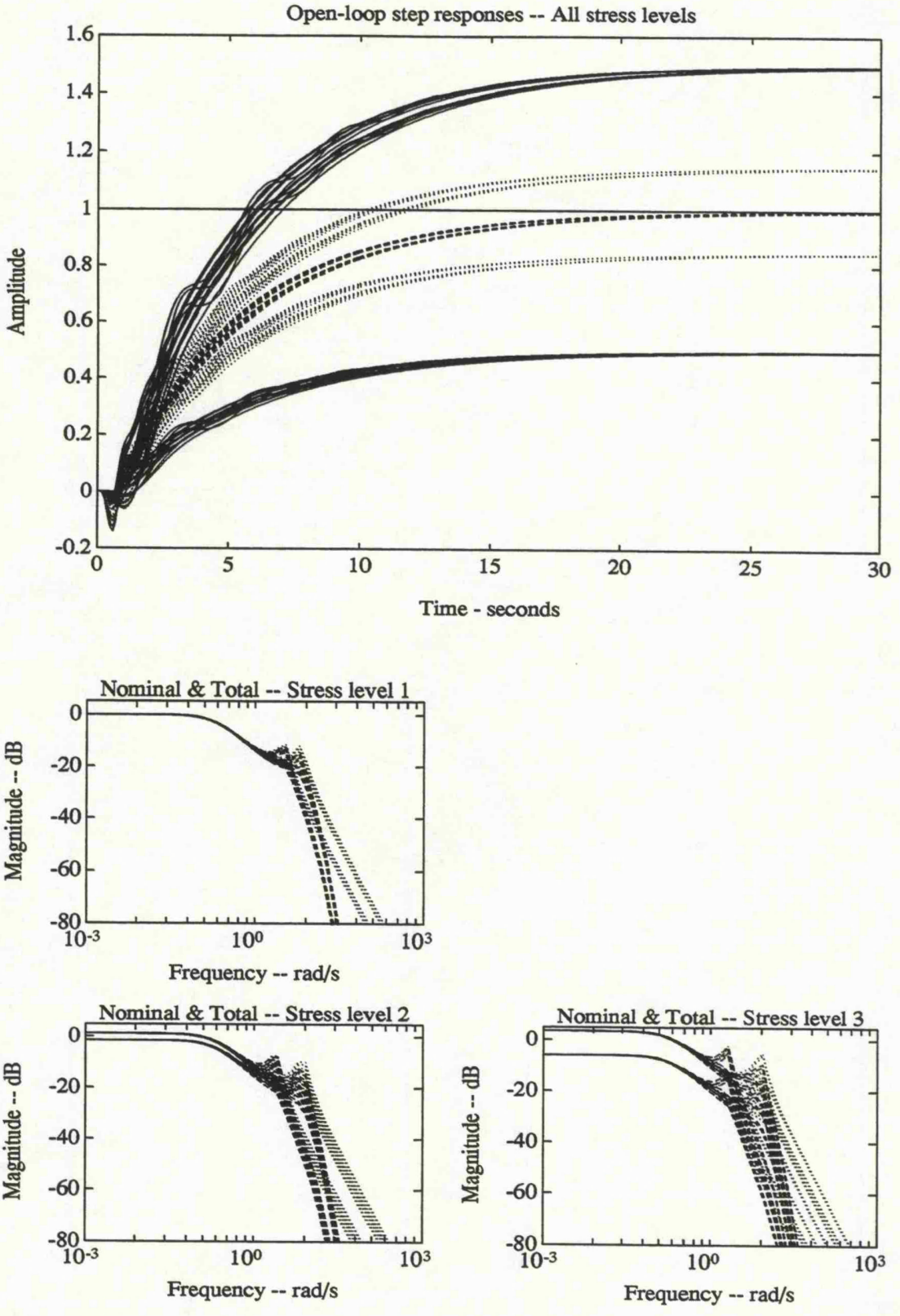

Figure 4.1: Open-loop Time and Frequency Responses.

The boundary of this set is defined by $\phi_i(p) = \varepsilon_i$. A point $p \in \mathcal{R}^q$ is a solution to the set of inequalities (4.3) if, and only if, it lies inside every set $\mathcal{S}_i$, $i = 1, 2, \ldots, n$ and hence inside the set $\mathcal{S}$ which denotes the intersection of all the sets $\mathcal{S}_i$,

$$\mathcal{S} = \bigcap_{i=1}^{n} \mathcal{S}_i \tag{4.5}$$

$\mathcal{S}$ is called the ***admissible set*** and any point p in $\mathcal{S}$ is called an ***admissible point*** denoted p_s. The objective is thus to find a point p such that $p \in \mathcal{S}$. Such a point satisfies the set of inequalities (4.3) and is said to be a solution. In general, a point p_s is not unique unless the subset $\mathcal{S}$ is a point in the space $\mathcal{R}^q$. In some cases, there is no solution to the problem, *i.e.* $\mathcal{S}$ is an empty set. It is then necessary to relax the boundaries of some of the inequalities, *i.e.* increase some of the numbers ε_i, until an admissible point p_s exists.

For control system design, the functions $\phi_i(p)$ may be functionals of the system step response, for example the rise time, overshoot or the integral absolute error, or functionals of the frequency response, such as the bandwidth. Until recently, in applications of the MOI, the design parameter p parameterized a fixed controller with a particular structure. However, in more recent applications [111, 72], p has parameterized the weighting functions required in $\mathcal{H}^\infty$-optimization problems.

They can also represent measures of system stability, such as the maximum real part of the closed-loop poles. Additional inequalities which arise from the physical constraints of the system can also be included, to restrict for example, the maximum control signal. In practice, the constraints on the design parameters p which define the set $\mathcal{P}$ are also included in the inequality set, *e.g.* to constrain the possible values of some of the design parameters, or to limit the search to stable controllers only.

The actual solution to the set of inequalities (4.3) may be obtained by means of numerical search algorithms, such as the moving boundaries process (MBP) [115]. The principles behind the MBP are described later. The procedure for obtaining a solution is interactive, in that it requires supervision and intervention from the designer. The designer needs to choose the dimension of the design parameter vector p and initial values for the design parameters. The progress of the search algorithm should be monitored, and, if a solution is not found, the designer may either change the starting point, amend

the size of the design vector, or relax some of the bounds ε. Alternatively, if a solution is easily found to improve the quality of the design, the bounds could be tightened or additional design objectives could be included in (4.3).

4.3.2 An Algorithm for Solving MOI

The moving boundaries process (MBP) algorithm can be used to numerically solve the inequalities (4.3). At each iteration, the process seeks to improve all the indices ϕ_i with unsatisfied bounds while keeping the other bounds satisfied.

The MBP proceeds from an arbitrary initial point to an admissible point, *i.e.* any point in the set $\mathcal{S}$, in an iterative way. Let p^k denote the value of p at the kth move. $\mathcal{S}_i^k$ is a set formed by the inequality $\phi_i(p) \leq \phi_i(p^k)$ with a boundary $\phi_i(p) = \phi_i(p^k)$. A step is taken from the point p^k to a trial point $\tilde{p}^k$. If for every $i = 1, 2, \ldots, m$, the boundary defined by $\phi_i(p) = \phi_i(\tilde{p}^k)$ is closer, or no further away from, the boundary of $\mathcal{S}_i^k$, then the point $\tilde{p}^k$ is accepted and becomes the new point p^{k+1}. After a sufficient number of successful steps, the boundary of $\mathcal{S}_i^k$ coincides with the boundary of $\mathcal{S}_i$ for every $i = 1, 2, \ldots, m$, and the problem is solved. Thus

$$\mathcal{S}^k = \bigcap_{i=1}^{m} \mathcal{S}_i^k \tag{4.6}$$

$$\mathcal{S}_i^k = \left\{ p : \phi_i(p) \leq \varepsilon_i^k \right\}, \qquad i = 1, 2, \ldots, m \tag{4.7}$$

$$\varepsilon_i^k = \begin{cases} \varepsilon_i & \text{if } \phi_i(p^k) \leq \varepsilon_i, \qquad i = 1, 2, \ldots, m \\ \phi_i(p^k) & \text{if } \phi_i(p^k) > \varepsilon_i, \qquad i = 1, 2, \ldots, m. \end{cases} \tag{4.8}$$

A step is taken from p^k to a trial point $\tilde{p}^k$. This point is a success and we set $p^{k+1} = \tilde{p}^k$ if, and only if,

$$\phi_i(\tilde{p}^k) \leq \varepsilon_i^k, \qquad i = 1, 2, \ldots, m \tag{4.9}$$

If any of the inequalities (4.9) do not hold, another trial point is made from p^k until a success occurs. When all the strict inequalities (4.9) hold, the boundaries of the set $\mathcal{S}^{k+1}$ would have moved closer to the boundaries of $\mathcal{S}$. The process is terminated when, after a sufficient number of successful steps, the boundaries of $\mathcal{S}^k$ converged to those of $\mathcal{S}$, *i.e.* when

$$\varepsilon_i^k = \varepsilon_i, \qquad i = 1, 2, \ldots, m \tag{4.10}$$

The original MBP [115] used the search scheme in [90] to generate trial points. Searches are conducted in a set of orthogonal directions, the descent directions being adjusted to maintain a direction of steepest descent.

An alternative scheme [79] uses a modified simplex method [75] for the search scheme. The following formulation makes all indices with unsatisfied bounds equally active at the start of each iteration; at the kth iteration, the following minimax problem is solved:

$$\min_{p} \max_{i} \left\{ \bar{\phi}_i = \frac{\phi_i(p) - \phi_i^g}{\phi_i^b - \phi_i^g},\ i = 1, 2, \ldots, m \text{ and } p \in \mathcal{P} \right\} \tag{4.11}$$

where

$$\phi_i^g = \begin{cases} \varepsilon_i & \text{if } \phi_i(p^k) > \varepsilon_i \\ \phi_i(p^k) - \delta & \text{if } \phi_i(p^k) \leq \varepsilon_i \end{cases} \tag{4.12}$$

$$\phi_i^b = \begin{cases} \phi_i(p^k) & \text{if } \phi_i(p^k) > \varepsilon_i \\ \varepsilon_i & \text{if } \phi_i(p^k) \leq \varepsilon_i \end{cases} \tag{4.13}$$

and δ is set to a small positive number.

The MBP using both search schemes has been implemented in MATLAB and both are used for the designs for the IFAC 1993 benchmark problem presented in Section 4.4.

4.4 Proposed Design Methods Using MOI for Multi-Objective Control

4.4.1 PI/PID Controller Design

The MOI can be used to find satisfactory controller parameters for fixed controllers, such as a PI or a PID controller in the simple feedback configuration shown in Figure 4.2.

For a PI controller, with $p = (p_1, p_2)$, the controller is parameterized as

$$K(p, z) = \frac{p_1 z + p_2}{z - 1} \tag{4.14}$$

and for a PID controller, with $p = (p_1, p_2, p_3, p_4)$, as

$$K(p, z) = \frac{z^2 p_1 + z p_2 + p_3}{(z - 1)(z + p_4)} \tag{4.15}$$

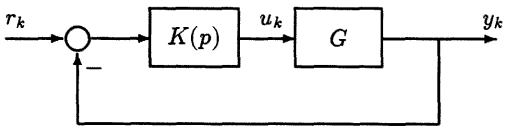

Figure 4.2: PI/PID Scheme.

The MBP can be implemented to find values of p which satisfy the inequalities (4.3). However, in general, if the closed loop system is unstable, the closed loop performance indices ϕ cannot be calculated, and no gradients exist to assist the search algorithm improve the values of ϕ. Hence, the search must be conducted in two stages; the first is to find a stability point, and the second is to find a solution to (4.3).

If (for a SISO system), $y_s(p,k)$ is the time response from which the functionals ϕ are calculated; then, from [115], a point p is a stability point if, and only if, the limit

$$y_s(p,\infty) = \lim_{k\to\infty} y_s(p,k) \tag{4.16}$$

exists and is finite. A different inequality set is thus required for the first stage to enable the MBP to yield a stability point. From [115], such an inequality is

$$\max_i |\lambda_i(p)| < 1 \quad \forall \quad \lambda_i(p) \in \Lambda(p) \tag{4.17}$$

where Λ denotes the set of all finite poles λ_i of the system closed loop transfer function. The MBP is used to solve (4.17), the first stage of the parameter search, and hence yield a stability point. The definition of a stability point can be extended for MIMO systems.

The design problem is thus stated as follows:

Problem

Stage 1 For the system of Figure 4.2, find a controller $K(p)$ such that

$$\phi_0(p) < 1 \tag{4.18}$$

where

$$\phi_0(p) = \max_i |\lambda_i(p)| \tag{4.19}$$

Stage 2 Find a $K(p)$ such that

$$\phi_i(p) \leq \varepsilon_i \quad \text{for} \quad i = 1, \ldots, m \tag{4.20}$$

where $\phi_i(p)$ are performance functionals of the closed-loop system, and ε_i are real numbers representing desired bounds on ϕ_i.

Design Procedure

A design procedure to solve the above problem is:

1) Define the plant G, and define the functionals ϕ_i.

2) Define the values of ε_i

3) Define the structure of the controller $K(p)$, *e.g.* a PI controller as in (4.14). Bounds should be placed on the values of p_i to ensure that $K(p)$ is implementable and to prevent undesirable pole/zero cancellations.

4) Define initial values of p_i.

5) Implement the MBP to find a $K(p)$ which satisfies inequality (4.18), *i.e.* locate a stability point. If no solution is found, try again with different initial values of p, or change the structure of the controller $K(p)$.

6) From a stability point, implement the MBP to find a $K(p)$ which satisfies inequality (4.20), *i.e.* locate an admissible point. If a solution is found, the design is satisfactory. If no solution is found, relax one or more of the bounds ε_i, change the initial values of p by returning to step (4) or change the structure of the controller by returning to step (3).

4.4.2 Weighting Parameter Design for the LQG

The quality of performance of the closed-loop system using the LQG design approach depends on the choice of:

1) The state and actuator signal weighting matrices Q and R, respectively.

2) The process and measurement noise covariance matrices W and V, respectively.

These weighting matrices, which appear explicitly in the problem formulation and final controller, are considered to be "tuning parameters" and are usually adjusted by the designer (using trial and error with experience and good insight) until a satisfactory design is obtained.

From the performance measure of (2.14), the weighting matrices of the LQ optimal feedback problem are given by

$$Q = C^T Q_c C \text{ and } N = \rho_c I_{n\times n} \tag{4.21}$$

where Q_c is a non-negative definite symmetric matrix given as $Q_c =$ **diag** $(q_{c_1}, \ldots, q_{c_r})$ and R is a positive definite symmetric matrix. The parameters $q_{c_1}, \ldots, q_{c_r}$ and ρ_c are the tuning parameters. Similarly, the weighting matrices of the Kalman filter problem are given by

$$W = BQ_f B^T \text{ and } V = \rho_f I_{n\times n} \tag{4.22}$$

where Q_f is a non-negative definite symmetric matrix given as $Q_f =$ **diag** $(q_{f_1}, \ldots, q_{f_r})$ and V is a positive definite symmetric matrix. The parameters $q_{f_1}, \ldots, q_{f_r}$ and ρ_f are the tuning parameters. So the weights Q, R, W, and V effectively represent the design parameters. By formulating the problem as in the MOI with the weights as the design parameters, the weighting parameter "tuning" is automated, and the control system can be designed for explicit *closed-loop* performance in both the time and frequency domains. The design problem is now stated as follows:

Problem

For the system of Figure 2.2, find a $(Q_c,\ \rho_c,\ Q_f,\ \rho_f)$ with $(Q_c, Q_f) \geq 0$ and $(\rho_c, \rho_f) > 0$ such that

$$\phi_i(Q_c, \rho_c, Q_f, \rho_f) \leq \varepsilon_i \quad \text{for} \quad i = 1, \ldots m, \tag{4.23}$$

where $\phi_i(Q_c, \rho_c, Q_f, \rho_f)$ are functionals of the closed-loop system, ε_i are real numbers representing desired bounds on ϕ_i. It should be noted that the pair $(A, B, Q_c^{\frac{1}{2}} C)$ and $(A, BQ_f^{\frac{1}{2}}, C)$ are assumed to be be stabilizable and detectable.

Design Procedure

A design procedure to solve the above problem is:

1) Define the plant G and the functionals ϕ_i.

2) Define the values of ε_i.

3) Define initial values of Q_c, ρ_c, Q_f, and ρ_f. Bounds should be placed on the design parameters to ensure that $(Q_c, Q_f) \geq 0$ and $(\rho_c, \rho_f) > 0$.

4) Implement the MBP to find a $(Q_c, \rho_c, Q_f, \rho_f)$ which satisfies inequality (4.23). If a solution is found, the design is satisfactory. If no solution is found, either relax one or more of the bounds ε_i, or try again with different initial values by repeating step (3).

5) With satisfactory weighting matrices Q, R, W, and V, a satisfactory controller is obtained from (2.32).

4.4.3 Weighting Parameter Design for the $\mathcal{H}^\infty$-Mixed Sensitivity Problem

The quality of performance of the closed-loop system using the $\mathcal{H}^\infty$ mixed sensitivity design problem, where the weighted cost function of (2.57) is minimized over the set of all stabilizing feedback controllers K, depends on the choice of the weighting functions $\hat{W}_1$ and $\hat{W}_2$ which are chosen to tailor the solution to meet the design specifications. The approach which was adopted here for the choice of the discrete-time frequency-dependent weighting function was to select it in the $s-domain$ and then use a bilinear transformation $z = \frac{2}{T}\frac{1+s}{1-s}$, where T is the sampling time, to convert to the $z-domain$.

The selection of frequency-dependent weights in $\mathcal{H}^\infty$ design is problem specific and therefore it is difficult to provide a definitive set of rules for building and modifying the weights. The general guide lines may be stated as follows:

1) Use only stable and diagonal weights.

2) Restrict the diagonal elements to be minimum phase, real rational functions.

Usually in the $\mathcal{H}^\infty$ mixed sensitivity design problem, for stopband shape adjustment, $\hat{W}_1$ is typically chosen to be a high-gain low-pass filter given by

$$\hat{W}_1 = \frac{w_1(s+w_2)}{(s+w_3)} \quad \text{for} \quad w_2 > w_3 \tag{4.24}$$

$\hat{W}_2$ is typically chosen as a high-pass filter given by

$$\hat{W}_2 = \frac{w_4(s+w_5)}{(s+w_6)} \quad \text{for} \quad w_5 < w_6 \tag{4.25}$$

in order to achieve robust stability with respect to high frequency model uncertainties. Finding suitable parameters $w = (w_1, w_2, w_3, w_4, w_5, w_6)$ for the frequency-dependent weights $\hat{W} = (\hat{W}_1, \hat{W}_2)$ can be cumbersome and time consuming. Hence, the $\mathcal{H}^\infty$ mixed sensitivity design approach can be incorporated with the method of inequalities to provide a more efficient and sensible way in selecting the weighting parameters, also to be known as the design parameters, in order to satisfy some set of closed-loop performance inequalities. The design problem is now stated as follows:

Problem

For the weighted system of (2.74), find a $\hat{W} = (\hat{W}_1, \hat{W}_2)$ such that

$$\gamma(\hat{W}) \leq \epsilon_\gamma \tag{4.26}$$

and

$$\phi_i(\hat{W}) \leq \varepsilon_i \quad \text{for} \quad i = 1, \ldots, m \tag{4.27}$$

where $\gamma(\hat{W})$ is the suboptimal value of γ satisfying (2.58), $\phi_i(\hat{W})$ are functionals of the closed-loop system, ϵ_γ, and ε_i are real numbers representing desired bounds on γ and ϕ_i, respectively. $\hat{W}$ is a pair of fixed order weighting functions with a real parameter vector w.

Design Procedure

A design procedure to solve the above problem is:

1) Define the plant G, and define the functionals ϕ_i.

2) Define the values of ϵ_γ and ε_i.

3) Define the form and order of the weighting functions $\hat{W}_1$ and $\hat{W}_2$ (*e.g.*, (4.24) & (4.25)). Bounds should be placed on the values of the parameters w to ensure that $\hat{W}_1$ and $\hat{W}_2$ are stable and minimum phase to prevent undesirable pole/zero cancellations. The form of the weighting functions should initially be a low-pass filter for $\hat{W}_1$ and a high-pass filter for $\hat{W}_2$.

4) Define initial values of w.

5) Implement the MBP to find a w which satisfies inequalities (4.26) and (4.27). If a solution is found, the design is satisfactory. If no solution is found, either increase the order of the weighting functions, relax one or more of the bounds ε_i, or try again with different initial values of w.

6) With satisfactory weighting functions $\hat{W}_1$ and $\hat{W}_2$, a satisfactory controller is obtained from (2.91).

4.4.4 Weighting Parameter Design for the LSDP

In the LSDP, the weighting functions are chosen by considering the open-loop response of the weighted plant, so effectively the weights W_1 and W_2 are the design parameters. This means that the design problem can be formulated as in the method of inequalities, with the weighting parameters used as the design parameters p to satisfy some set of closed-loop performance inequalities. The design problem is stated as follows:

Problem

For the system of Figure 3.3 with a plant weighted with W, find a W such that

$$\gamma_0(W) \leq \epsilon_\gamma \tag{4.28}$$

and

$$\phi_i(W) \leq \varepsilon_i \quad \text{for} \quad i = 1, \ldots, m \tag{4.29}$$

where

$$\gamma_0(W) = \inf_{K \text{ stabilizing}} \left\| \begin{bmatrix} W_1^{-1}K \\ W_2 \end{bmatrix} (I - GK)^{-1} \begin{bmatrix} W_2^{-1} & GW_1 \end{bmatrix} \right\|_\infty \tag{4.30}$$

and $\phi_i(W)$ are functionals of the closed-loop system, ϵ_γ, ε_i are real numbers representing desired bounds on γ_0 and ϕ_i respectively, and $W = (W_1, W_2)$, a pair of fixed order weighting functions with real parameters $w = (w_1, w_2, \ldots, w_q)$.

Design Procedure

A design procedure to solve the above problem is:

1) Define the plant G, and define the functionals ϕ_i.

2) Define the values of ε_γ and ε_i

3) Define the form and order of the of weighting functions W_1 and W_2. Bounds should be placed on the values of w_i to ensure that W_1 and W_2 are stable and minimum phase to prevent undesirable pole/zero cancellations. The order of the weighting functions, and hence the value of q, should initially be small.

4) Define initial values of w_i based on the open-loop frequency response of the plant.

5) Implement the MBP in conjunction with (3.81) and (3.55) to find a W which satisfies inequalities (4.28) and (4.29). If a solution is found, the design is satisfactory. If no solution is found, either increase the order of the weighting functions, relax one or more of the bounds ε_γ and ε_i, or try again with different initial values of w.

6) With satisfactory weighting functions W_1 and W_2, a satisfactory controller is obtained from (3.83).

4.4.5 Weighting Parameter and Prefilter Design for the LSDP

The procedure described in the previous section results in a 1-DOF control scheme. Improved performance for tracking systems may be obtained by including a pre-filter on the reference input. The proposed approach consists of adding a pre-filter K_p to a controller synthesized using the normalized coprime factor approach, as shown in Figure 4.3. The pre-filter is parameterized with a sub-set of the design parameters,

whilst the controller K is the solution to the weighted normalized coprime factor approach already described, with the weightings parameterized with the remaining design parameters. Note that the prefilter is scaled so that the closed-loop transfer function $(I - GK)^{-1}GW_1K_p$ is the unit matrix at steady state.

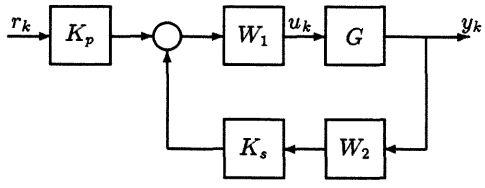

Figure 4.3: The 2-DOF Scheme using a Pre-filter.

The 2-DOF design problem is now stated as follows:

Problem

For the system of Figure 4.3, find a (W, K_p) such that

$$\gamma_0(W) \leq \epsilon_\gamma \tag{4.31}$$

and

$$\phi_i(W, K_p) \leq \varepsilon_i \quad \text{for} \quad i = 1, \ldots, m \tag{4.32}$$

where $\gamma_0(W)$ is as in (4.30), $\phi_i(W, K_p)$ are functionals of the 2-DOF closed-loop system, ϵ_γ, ε_i are real numbers representing desired bounds on γ_0 and ϕ_i, respectively, $W = (W_1, W_2)$ is a pair of fixed order weighting functions with real parameters $w = (w_1, w_2, \ldots, w_q)$ and K_p is a pre-filter with a fixed structure and order and with real parameters $p = (p_1, p_2, \ldots, p_r)$.

Design Procedure

A design procedure to solve the above problem is:

1) Define the plant G, and define the functionals ϕ_i.

2) Define the values of ε_γ and ε_i

3) Define the form and order of the weighting functions W_1 and W_2. Bounds should be placed on the values of w_i to ensure that W_1 and W_2 are stable and minimum phase to prevent undesirable pole/zero cancellations. The order of the weighting functions, and hence the value of q, should initially be small.

4) Define the form and order of the pre-filter K_p. Bounds may be placed on the values of p_i if desired. The order of the pre-filter transfer function, and hence the value of r, should initially be small.

5) Define initial values of w_i based on the open-loop frequency response of the plant. Define initial values of p_i.

6) Implement the MBP in conjunction with (3.81) and (3.55) to find a W and K_p which satisfy inequalities (4.31) and (4.32). If a solution is found, the design is satisfactory. If no solution is found, either increase the order of the weighting functions, relax one or more of the bounds ε_i, or try again with different initial values of w and p.

7) With satisfactory weighting functions W_1 and W_2, a satisfactory feedback controller is obtained from (3.83).

4.4.6 Weighting Parameter Design for the 2-DOF LSDP

The quality of performance of the closed-loop system using the 2-DOF design approach, based on a given sensible reference model to follow, primarily depends on two design parameters:

1) The weighting functions W_1 and W_2 which are used to shape the open-loop plant.

2) The scalar weighting parameter ρ given in (3.86).

Although closed-loop time domain specifications can be incorporated into the design through the desired reference model, finding suitable values for the parameters of the

weighting function pair $W = (W_1, W_2)$ and for the parameter ρ such that the behaviour of the closed-loop system closely mimics that of the reference model with a good stability margin can be difficult, cumbersome and time consuming. Hence, a design methodology, using the 2-DOF approach based on model-following combined with the normalized coprime factor design procedure, can be incorporated with the method of inequalities to provide a more efficient and powerful design procedure.

The design problem is now stated as follows:

Problem

For the system of Figure 3.5, find a (W,ρ) such that

$$\gamma_0(W) \leq \epsilon_{\gamma_0} \tag{4.33}$$

$$\gamma_1(W,\rho) \leq \epsilon_{\gamma_1} \tag{4.34}$$

and

$$\phi_i(W,\rho) \leq \varepsilon_i \quad \text{for} \quad i = 1,\ldots,m \tag{4.35}$$

where $\gamma_0(W)$ can be calculated using (3.55), $\gamma_1(W,\rho)$ is the suboptimal value of γ achieved by the $\mathcal{H}^\infty$ algorithm, and $\phi_i(W,\rho)$ are functionals of the closed-loop system, ϵ_{γ_0}, ϵ_{γ_1}, and ε_i are real numbers representing desired bounds on γ_0, γ_1, and ϕ_i, respectively. ρ is a scalar weighting parameter and W is a weighting function pair (W_1, W_2), each of fixed order with real parameters $w = (w_1, w_2, \ldots, w_q)$.

Design Procedure

The aim is to design a controller which ensures robust stability and robust performance. The procedure is:

1) Define the plant G and the functionals ϕ_i.

2) Define the values of ϵ_{γ_0}, ϵ_{γ_1} and ε_i.

3) Select the structure and order of the loop shaping weight W for the open-loop plant G. Bounds should be placed on the parameters w_i to ensure that W is stable and minimum phase.

4) Select the desired range for the scalar weighting parameter ρ of the 2-DOF problem in (3.86). The value of ρ should be ≥ 1.

5) Select a simple model M_0 which reflects the desired closed-loop system step response specifications. This is usually a diagonal matrix of first or second-order lags. The speed of response of the ideal model must be realistic, or the closed-loop system will have poor robust stability properties and the controller will produce excessive control signals.

6) Select the initial values of w & ρ.

7) Implement the MBP in conjunction with (3.98), (3.99),and (3.55) to find a W and ρ which satisfies inequalities (4.33), (4.34), and (4.35). If a solution is found, the design is satisfactory. If no solution is found, either increase the order of the weighting function, relax one or more of the bounds ϵ_{γ_0}, ϵ_{γ_1} and ϵ_i, or try again with different initial values of w & ρ.

8) With a satisfactory ρ and weighting functions W, a satisfactory controller is obtained from (3.101).

4.5 Controller Design and Simulation Results

In this section, the designs for the IFAC 1993 benchmark problem are described. The designs were completed using the 6 approaches described in Section 4.4, including μ-synthesis. The MOI was used to find the best design parameters for all the approaches except the μ synthesis approach, where computational limitations precluded this. The closed-loop performance functionals used to formulate the problem are defined in Section 4.5.1, along with the necessary prescribed bounds on the functionals. The results of the designs are presented in Section 4.5.2. The time-varying simulations for all the designs are presented; from these the worst overshoot, undershoot and rise time values are measured and presented in tables. The rise time is defined for this purpose as the time for the output to go from +0.8 to -0.8.

4.5.1 Closed-Loop Performance Functionals and Design Criteria

A set of closed-loop performance functionals $\{\phi_i(G_j,p),\ i = 1,2,\ldots,5\}$, are defined based on the design specifications given in Section 4.2.

The performance functionals $\phi_i(G_j,p)$, $i = 1,2,\ldots,5$ are calculated from the closed-loop time responses of the linear system to a reference step input of $+1$ with system initial conditions corresponding to a steady reference of -1, where G_j is a full time-invariant plant model at one of the vertices of the hyper-cube formed from the plant parameter ranges. The performance functionals $\phi_1(G_j,p)$ - $\phi_5(G_j,p)$ are measures of overshoot, undershoot, rise time, settling time, and control effort, respectively. If $y_s(G_j,p,t)$ is the plant output response, and $u_s(G_j,p,t)$ the plant input response, the functionals are defined as

$$\phi_1(G_j,p) = \max_t y_s(G_j,p,t) \tag{4.36}$$

$$\phi_2(G_j,p) = -\min_t y_s(G_j,p,t) \tag{4.37}$$

$$\phi_3(G_j,p) = \min\ t \quad \text{such that} \quad y_s(G_j,p,t) = 0.8 \tag{4.38}$$

$$\phi_4(G_j,p) = \max\ t \quad \text{such that} \quad |y_s(G_j,p,t) - 1| = 0.05 \tag{4.39}$$

$$\phi_5(G_j,p) = \max_t |u_s(G_j,p,t)| \tag{4.40}$$

The performance was calculated from linear time-invariant closed-loop responses for 6 plants, $G_j(j = 1,\ldots,6)$ with their parameters at the extremes of the parameter ranges, using the complete transfer function (4.2). The controllers were synthesized using the nominal plant model transfer function (4.1). The aim was to find design parameters which satisfied the inequalities for all 6 extreme plants.

From (4.3) and (4.36) - (4.40), the design criteria are

$$\phi_i(G_j,p) \leq \varepsilon_i \quad \text{for} \quad i = 1,\ldots,5, \quad j = 1,\ldots,6. \tag{4.41}$$

From the specifications given in Section 4.2, the undershoot, overshoot and control signal specifications are rigid, so bounds $\varepsilon_1, \varepsilon_2$ and ε_5 were fixed at 1.2, 1.2 and 5, respectively. The rise time and settling time specifications are less rigid, so ε_3 and ε_4 were increased or reduced depending on the stress level to obtain the best design. The "spy" reported

that rise times of 2 – 3 seconds were reported, so ε_3 was kept between these figures for stress levels 1 & 2.

4.5.2 Results obtained for all Stress Levels

Stress Level 1

The results of the time varying simulations for the various methods are shown in Figures 4.5 – 4.10. The approximate overshoot, undershoot and rise time values of the simulations are tabulated in Table 4.1.

All the designs met the specifications given in Section 4.2. The performance of all the designs are similar, except for the PI controller which had a slightly greater undershoot than the other designs.

Design Method	max. abs. overshoot	max. abs. undershoot	max. rise time (sec)
P+I	1.1	1.4	2.6
LQG	1.1	1.25	2.7
Mixed Sensitivity	1.25	1.3	2.5
1-DOF LSDP	1.1	1.25	2.7
Prefilter + LSDP	1.2	1.25	2.5
2-DOF LSDP	1.15	1.25	2.6
μ synthesis	1.2	1.3	2.2

Table 4.1: Simulation Performance - Stress Level 1

PI Controller – This controller

$$K(s) = 2.30 + \frac{0.52}{s} \tag{4.42}$$

met the performance requirements, although the undershoot was quite high. A PID controller with a better performance than the PI controller was not found.

LQG Controller – This controller designed with the weighting parameters

$$Q_c = 40.08,\ Q_f = 1.0,\ \rho_c = 1.0,\ \text{and}\ \rho_f = 1.0 \times 10^{-3} \tag{4.43}$$

met all the performance specifications. The undershoot bound was slightly exceeded in the simulations.

$\mathcal{H}^\infty$ (mixed sensitivity) Controller – This controller designed with the weighting functions

$$W_1(s) = \frac{0.0134s + 0.245}{(s + 0.445)(s + 0.530 \times 10^{-6})} \tag{4.44}$$

and

$$W_2(s) = \frac{(s + 0.630)(s + 5.985)}{(s + 5.506)(s + 2.246)} \tag{4.45}$$

met the performance specifications. The overshoot and undershoot bounds were slightly exceeded in the simulations.

1-DOF LSDP Controller – This controller with a weighting function

$$W_1(s) = 3.33 + \frac{1.68}{s}, \tag{4.46}$$

and $W_2 = 1$ met all the performance specifications. The undershoot bound was slightly exceeded in the simulations.

LSDP Controller with PreFilter – The performance functionals for the 1-DOF LSDP design were marginally improved upon by the inclusion of a prefilter. This improvement was not evident in the simulations, and thus they are not included.

2-DOF LSDP Controller – This controller designed with a weighting function

$$W_1(s) = \frac{707.25(s + 8.3 \times 10^{-3})}{s(142.5s + 1)} \tag{4.47}$$

$W_2 = 1$, $\rho = 1.0$, and $M_o(s) = \frac{1}{(0.8s+1)}$ met all the performance specifications. The undershoot bound was slightly exceeded in the simulations.

μ Controller – The μ-synthesis design met all the performance specifications. The undershoot bound was slightly exceeded in the simulations.

Stress Level 2

The simulation results are shown in Figures 4.11 – 4.16. The approximate overshoot, undershoot and rise time values of the simulations are tabulated in Table 4.2. The designs did not manage to meet the rise time specification of 2 – 3 seconds given in Section 4.2.

The PID controller which had greater rise time than the other designs, and the μ-synthesis resulted in a lower rise time, but at the expense of greater overshoot and undershoot. The other designs had comparable performance.

Design Method	max. abs. overshoot	max. abs. undershoot	max. rise time (sec)
PID	1.1	1.25	5.0
LQG	1.2	1.3	3.5
Mixed Sensitivity	1.25	1.3	3.5
1-DOF LSDP	1.1	1.15	4.0
2-DOF LSDP	1.2	1.17	3.7
μ synthesis	1.4	1.37	2.7

Table 4.2: Simulation Performance - Stress Level 2

PID Controller – A good PI controller was not found. The PID controller

$$K(s) = 1.311 + \frac{0.431}{s} + \frac{1.048s}{1 + 12.92s} \tag{4.48}$$

gave better results, but with a rise time slower than for other methods.

LQG Controller – This controller designed with the weighting parameters

$$Q_c = 38.08,\ Q_f = 1.217,\ \rho_c = 0.818,\ \text{and}\ \rho_f = 2.823 \times 10^{-3} \tag{4.49}$$

met almost all the performance specifications. The rise time and undershoot bound were slightly exceeded in the simulations.

$\mathcal{H}^\infty$ (mixed sensitivity) Controller – This controller designed with the weighting functions

$$W_1(s) = \frac{12.30 \times 10^{-3}s + 0.221}{(s + 0.445)(s + 0.5304 \times 10^{-6})} \tag{4.50}$$

and

$$W_2(s) = \frac{60s + 240}{s + 400} \tag{4.51}$$

met almost all the performance specifications. The rise time together with the overshoot and undershoot bounds were slightly exceeded in the simulations.

1-DOF LSDP Controller – This controller designed with a weighting function

$$W_1(s) = 1.941 + \frac{1.461}{s} \tag{4.52}$$

and $W_2 = 1$ met all the performance specifications. The undershoot bound was slightly exceeded in the simulations.

LSDP Controller with PreFilter – The performance functionals for the 1-DOF LSDP design were marginally improved upon by the inclusion of a prefilter. This improvement was not evident in the simulations, and thus they are not included.

2-DOF LSDP Controller – This controller designed with a weighting function

$$W_1(s) = \frac{300(s + 2.0 \times 10^{-2})}{s(150s + 1)} \tag{4.53}$$

$W_2 = 1$, $\rho = 1.0$, and $M_o(s) = \frac{1}{(s+1)}$ met almost all the performance specifications. The rise time was slightly exceeded in the simulations.

μ Controller – The μ-synthesis design met almost all the performance specifications. The overshoot and undershoot bounds were exceeded in the simulations, but the important bound of 1.5 was not. The rise time was shorter than for the other designs, but at the expense of the overshoot and undershoot.

Stress Level 3

The simulation results are shown in Figures 4.17 – 4.22. The approximate overshoot, undershoot and rise time values of the simulations are tabulated in Table 4.3. The designs were well outside the rise time specification of 2 – 3 seconds given in Section 4.2, although, using the MOI, the most important specification of maintaining the output to within the absolute value of 1.5 could be guaranteed, this could not be done with the μ-synthesis approach. Performance was improved considerably by including a gain adaptive scheme (discussed later), although this very occasionally resulted in outputs above the absolute value of 1.5.

PID Controller – A satisfactory PID controller was not found. The best controller was

$$K(s) = 0.816 + \frac{0.271}{s} + \frac{1.677s}{1 + 19.49s} \tag{4.54}$$

Design Method	max. abs. overshoot	max. abs. undershoot	max. rise time (sec)
PID	1.1	1.25	> 10
LQG	1.25	1.18	> 10
Mixed Sensitivity	1.15	1.2	> 10
1-DOF LSDP	1.3	1.25	10
Prefilter + LSDP	1.3	1.3	9
2-DOF LSDP	1.1	1.15	10
Adaptive	1.3	1.3	5.5

Table 4.3: Simulation Performance - Stress Level 3

This had a very long rise time and settling time.

LQG Controller – For the LQG method, weighting parameters which satisfied performance specifications were not found. The best weighting parameters were

$$Q_c = 28.07,\ Q_f = 1.659,\ \rho_c = 0.590,\ \text{and}\ \rho_f = 5.079 \times 10^{-3} \tag{4.55}$$

which did not satisfy the rise time and settling time performance specifications.

$\mathcal{H}^\infty$ (mixed sensitivity) Controller – Weighting functions for a satisfactory mixed sensitivity $\mathcal{H}^\infty$ controller were not found. The best weighting functions

$$W_1(s) = \frac{10.69 \times 10^{-3} s + 0.157}{(s + 0.6356)(s + 0.5304 \times 10^{-6})} \tag{4.56}$$

and

$$W_2(s) = \frac{61.5s + 240}{s + 400} \tag{4.57}$$

gave a very long rise time in the simulations.

1-DOF LSDP Controller – Satisfactory weighting functions for the 1-DOF LSDP were not found. The best weighting functions

$$W_1(s) = \frac{3.244s^2 + 1.844s + 1.662}{s(1.570s^2 + 1.666s + 1)} \tag{4.58}$$

and $W_2 = 1$, resulted in very long rise times.

LSDP Controller with PreFilter – The rise time for the 1-DOF LSDP design was marginally improved upon by the inclusion of a prefilter. The resulting weighting functions were

$$W_1(s) = \frac{3.390s^2 + 1.760s + 1.627}{s(1.459s^2 + 1.817s + 1)} \tag{4.59}$$

and $W_2 = 1$, and the prefilter was

$$K_p(s) = \frac{0.579s^2 + 1.092s + 1}{0.127s^2 + 0.647s + 1} \tag{4.60}$$

2-DOF LSDP Controller – The best 2-DOF LSDP controller had weighting functions

$$W_1(s) = \frac{420(s + 0.0342)}{s(148s + 1)} \tag{4.61}$$

$W_2 = 1$, $\rho = 1.2$, and $M_o(s) = \frac{1}{(2.8s+1)}$. The rise time specification was greatly exceeded in the simulations.

μ Controller – A sensible μ controller was not found.

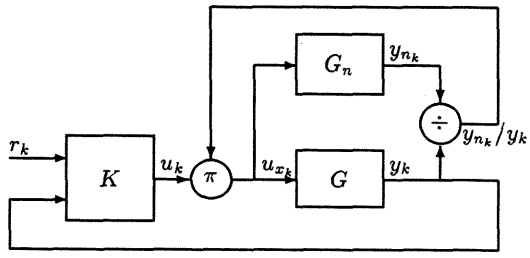

Figure 4.4: Adaptive Scheme.

Adaptive Gain Scheme – The performance of the system at stress level 3 can be improved by implementing the adaptive gain scheme shown in Figure 4.4. The plant gain is estimated by comparing the output of the plant y_k with the output of the nominal plant y_{n_k}. Thus the plant input becomes $u_{x_k} = (y_{n_k}/y_k)u_k$. As parameters other than the plant gain vary, and because there is significant measurement noise, the extra gain y_{n_k}/y_k was limited to $0.75 \leq y_{n_k}/y_k \leq 1.5$. This scheme was implemented with the mixed sensitivity $\mathcal{H}^\infty$ controller of stress level 3 and resulted in improved performance, as shown in in Figure 4.23, with a rise time of between about 3.5 and 5.3 seconds, and with occasional overshoot above 1.2, and which very rarely would be above 1.5.

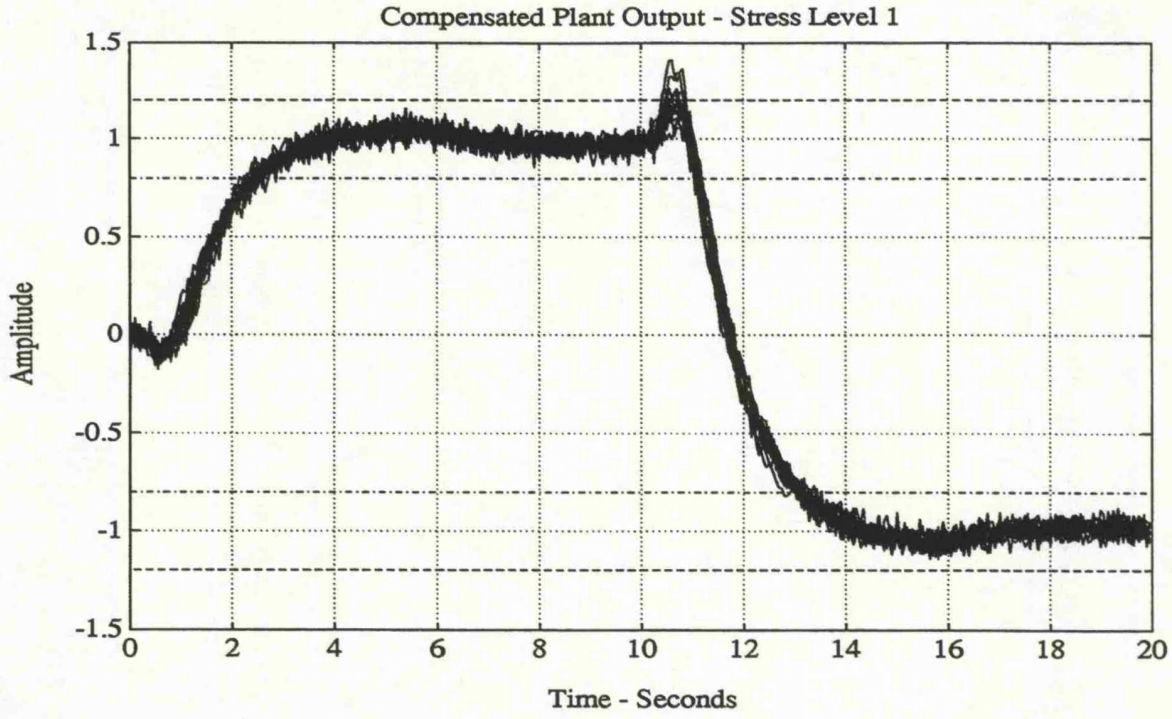

Figure 4.5: Simulations - Stress Level 1 - P+I Controller.

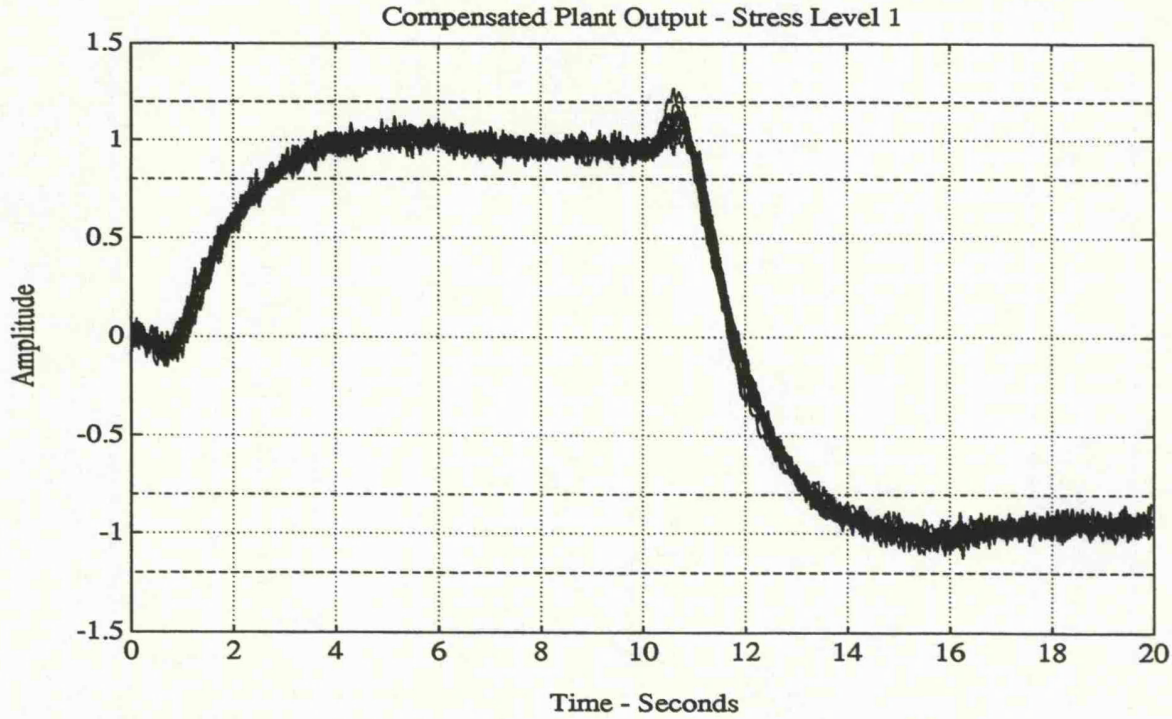

Figure 4.6: Simulations - Stress Level 1 - LQG Controller.

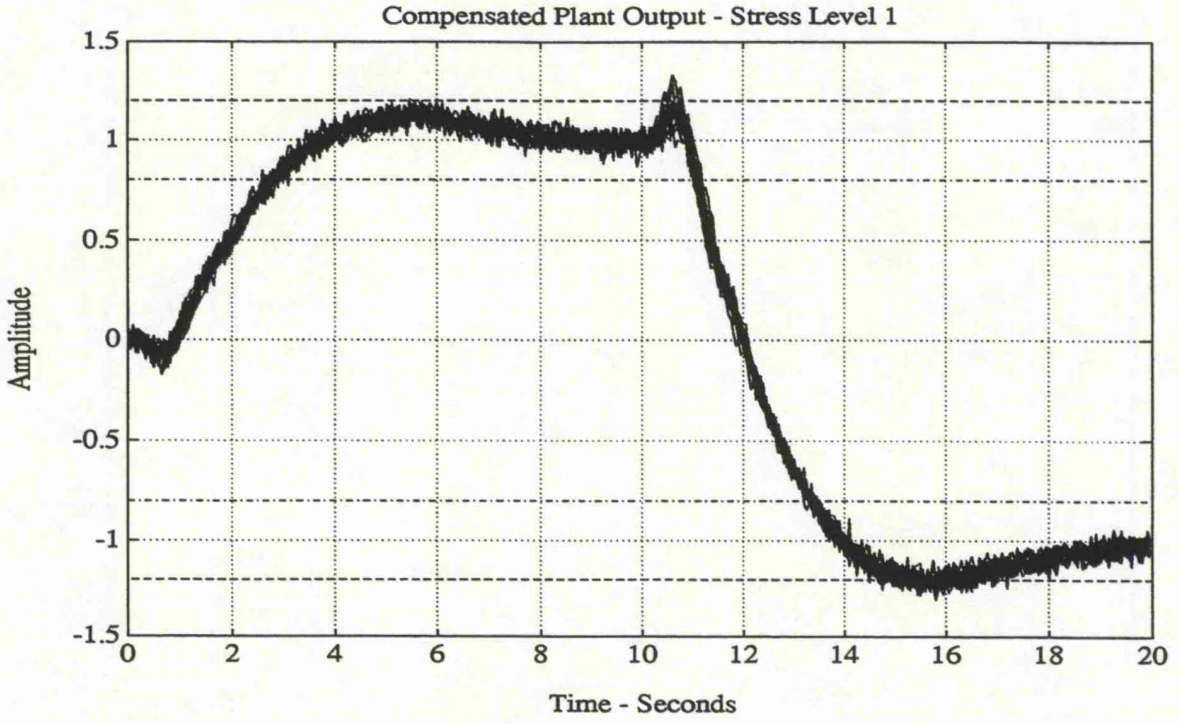

Figure 4.7: Simulations - Stress Level 1 - $\mathcal{H}^\infty$ (Mixed Sensitivity) controller.

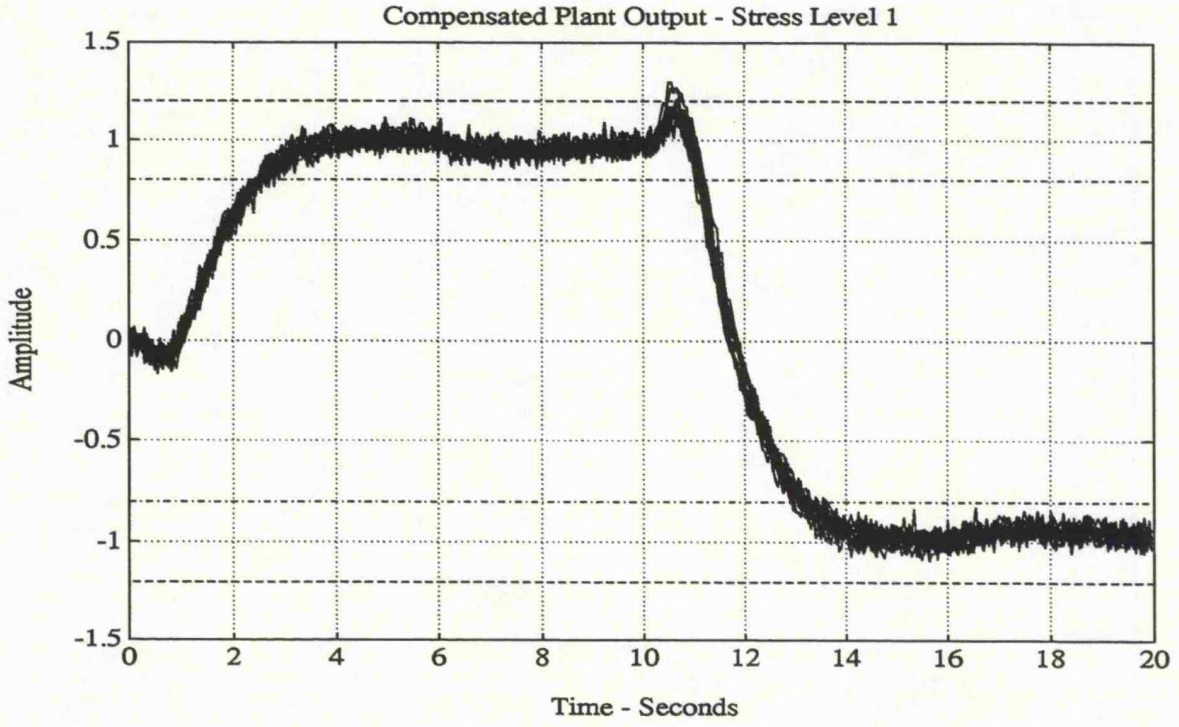

Figure 4.8: Simulations - Stress Level 1 - 1-DOF LSDP.

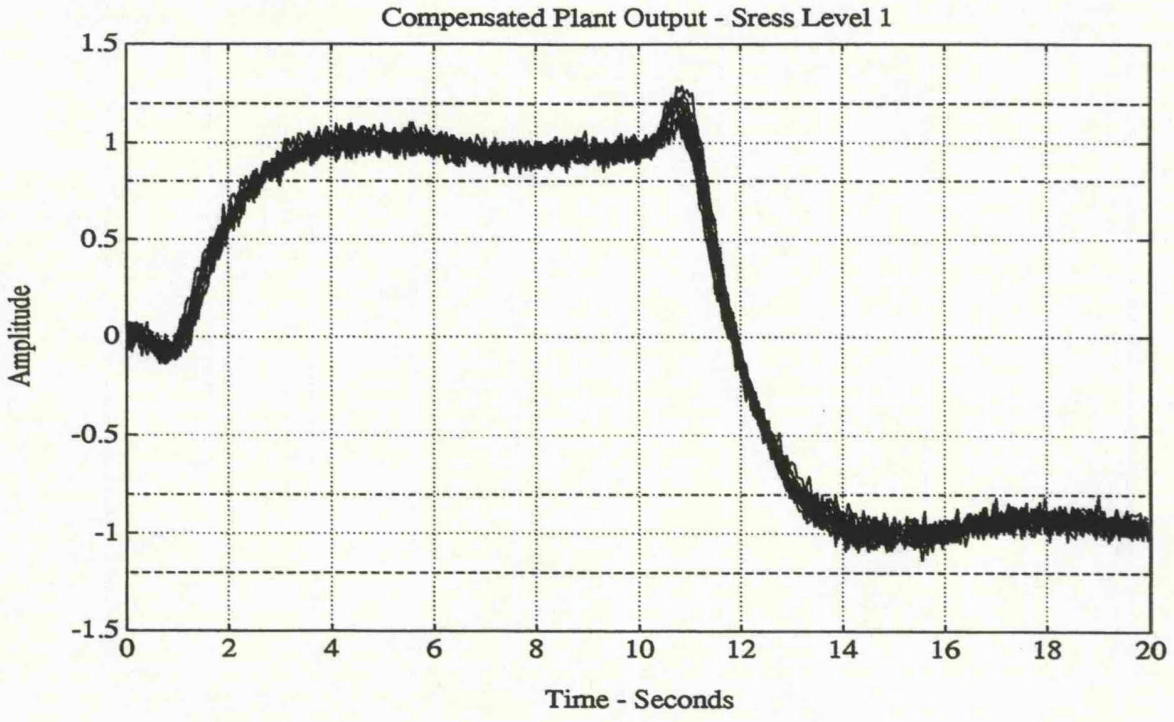

Figure 4.9: Simulations - Stress Level 1 - 2-DOF LSDP Controller.

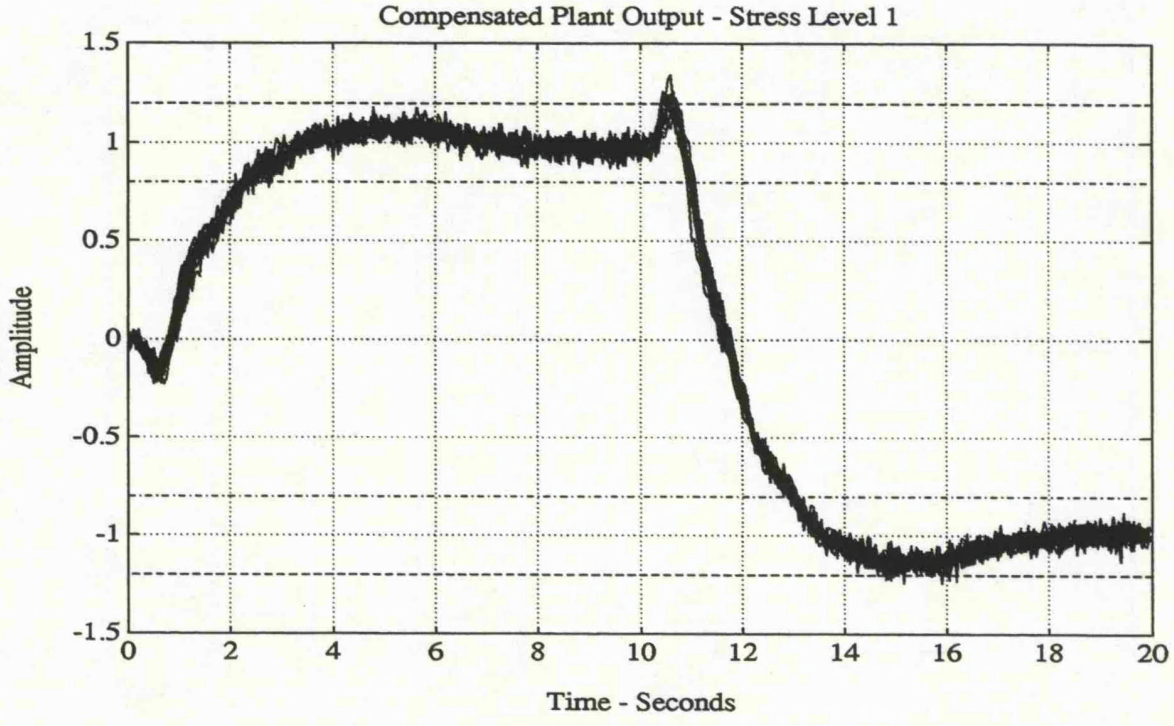

Figure 4.10: Simulations - Stress Level 1 - μ Controller.

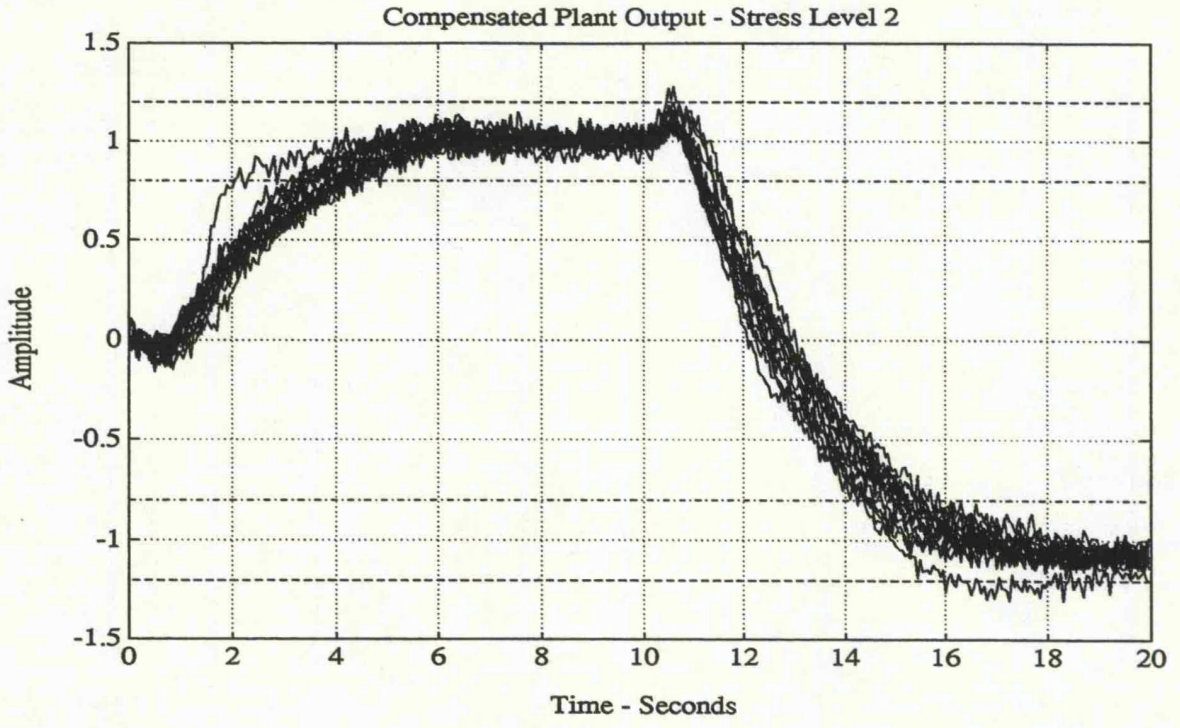

Figure 4.11: Simulations - Stress Level 2 - PID Controller.

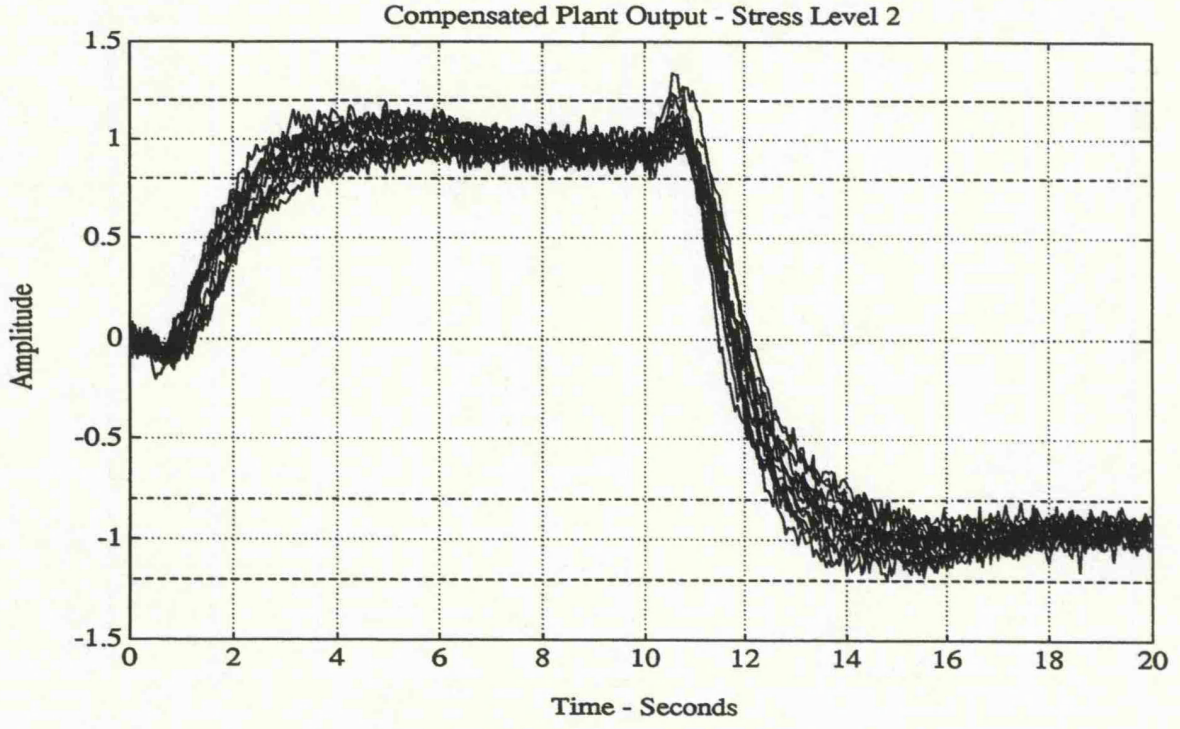

Figure 4.12: Simulations - Stress Level 2 - LQG Controller.

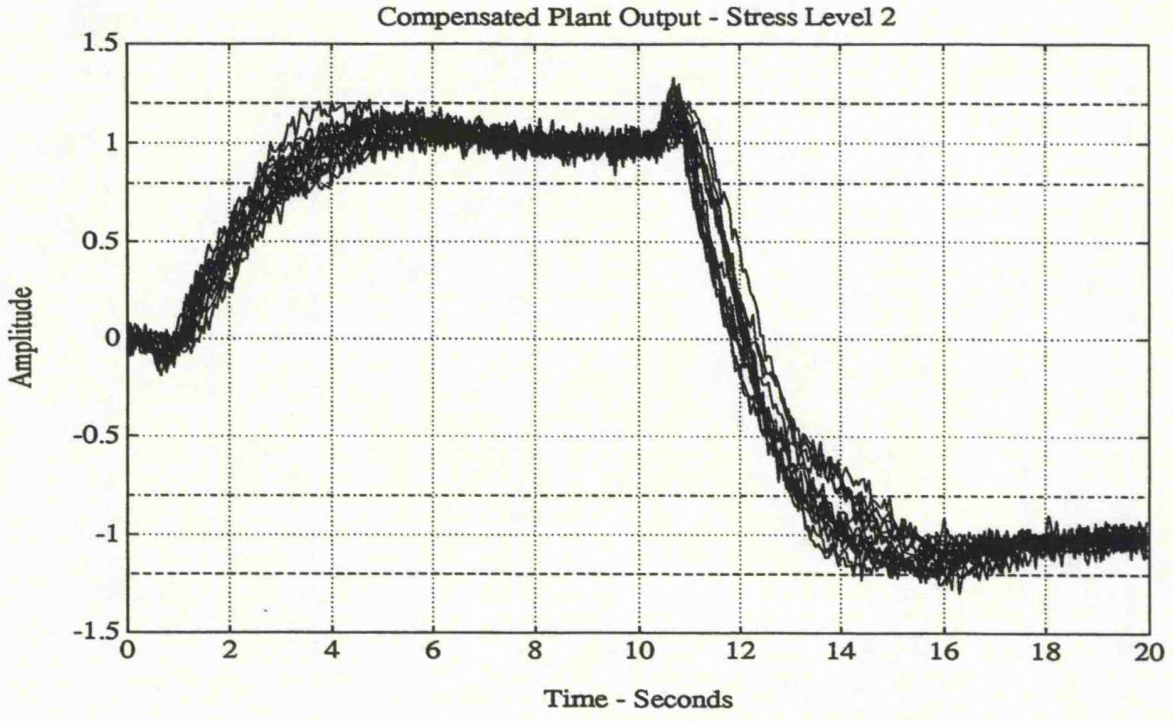

Figure 4.13: Simulations - Stress Level 2 - $\mathcal{H}^\infty$ (Mixed Sensitivity) controller.

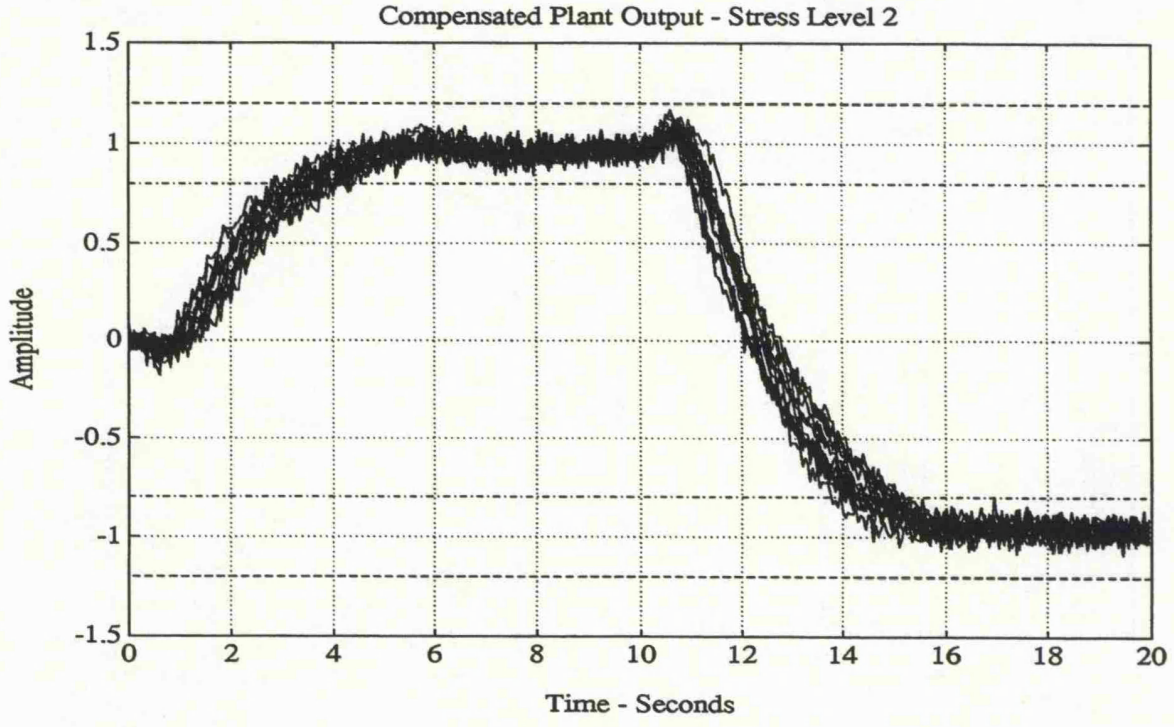

Figure 4.14: Simulations - Stress Level 2 - 1-DOF LSDP.

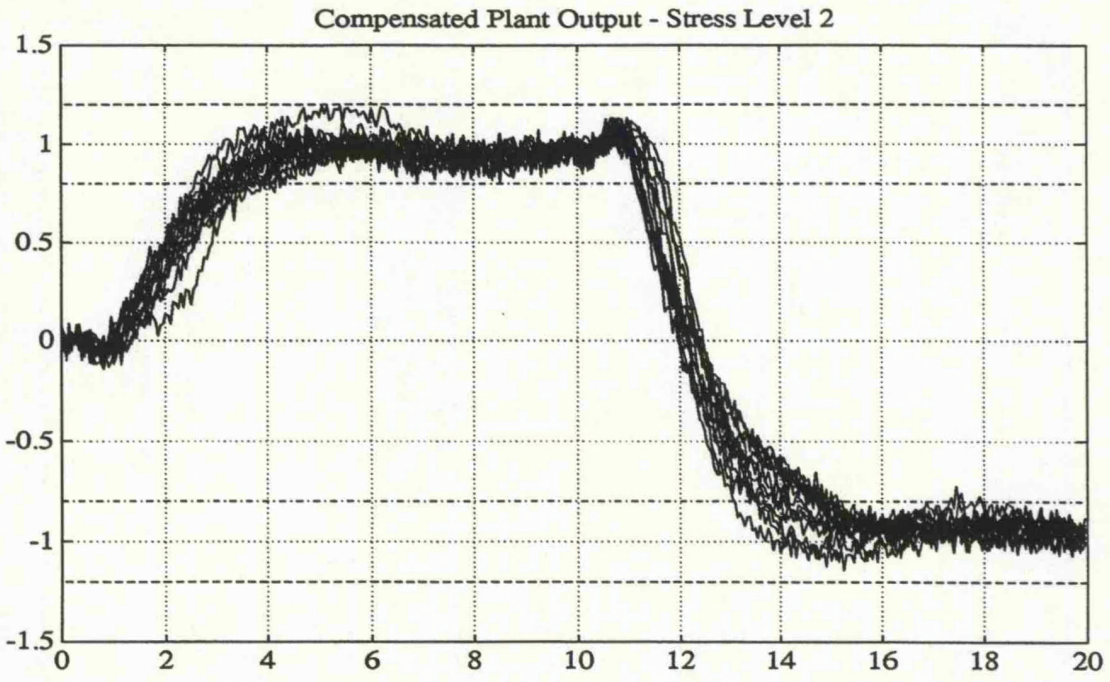

Figure 4.15: Simulations - Stress Level 2 - 2-DOF LSDP Controller.

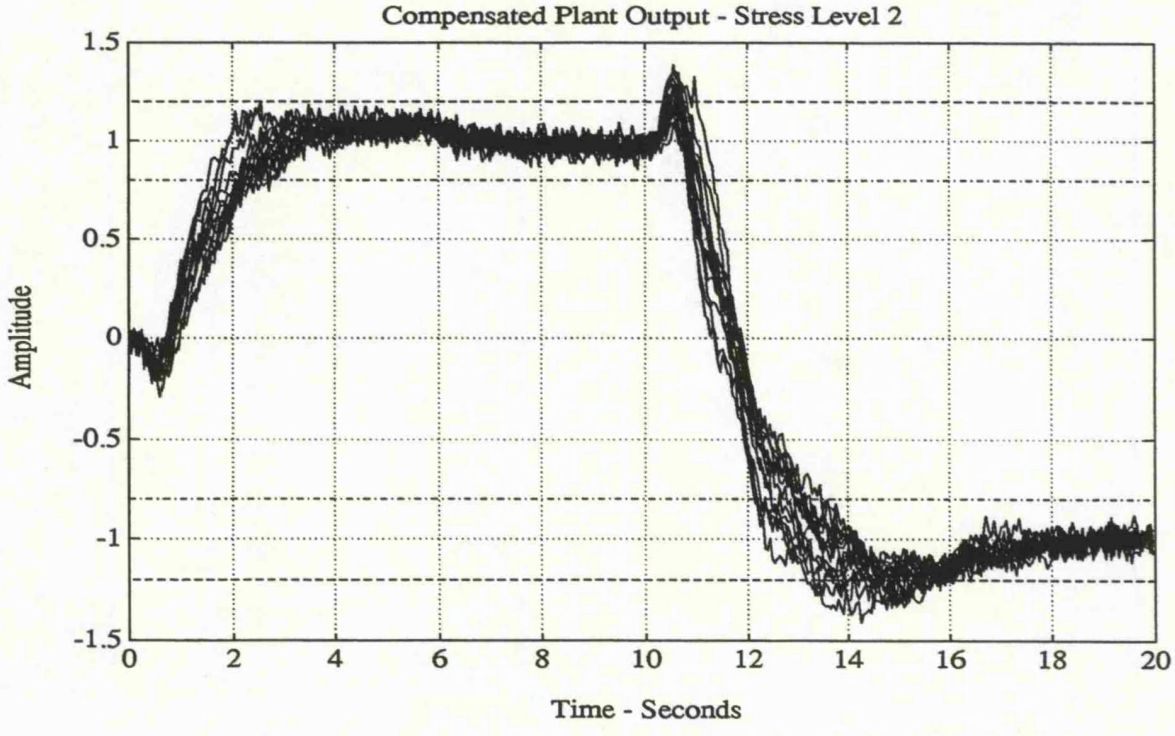

Figure 4.16: Simulations - Stress Level 2 - μ Controller.

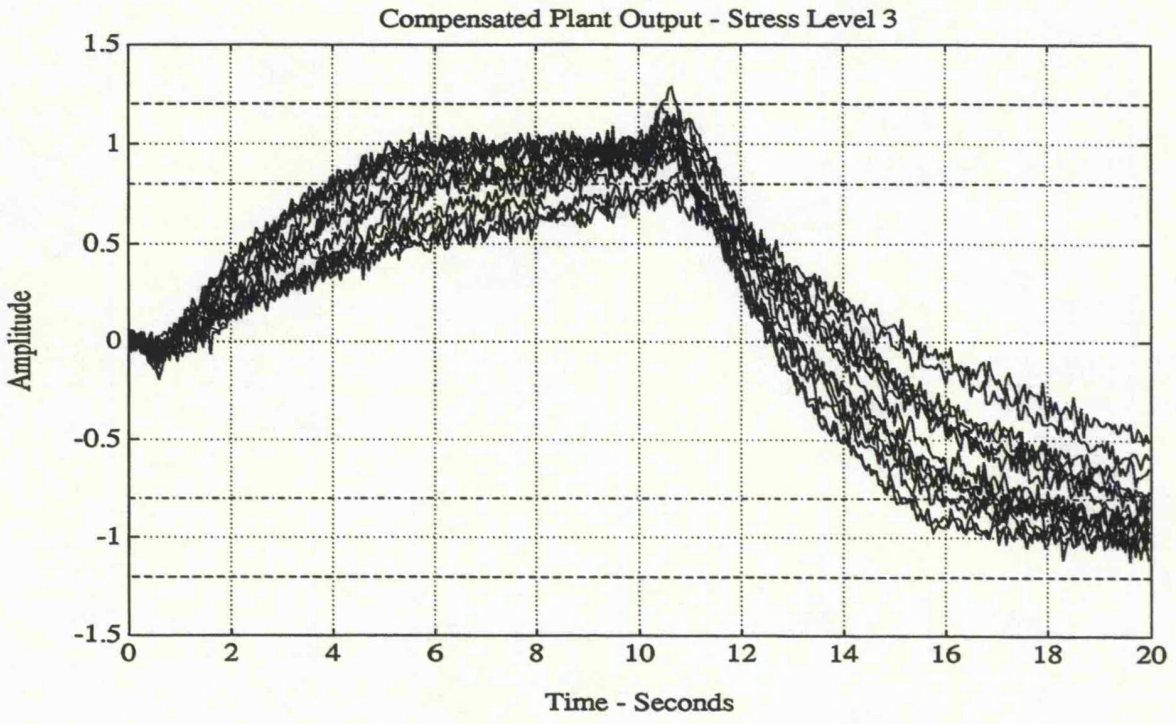

Figure 4.17: Simulations - Stress Level 3 - PID Controller.

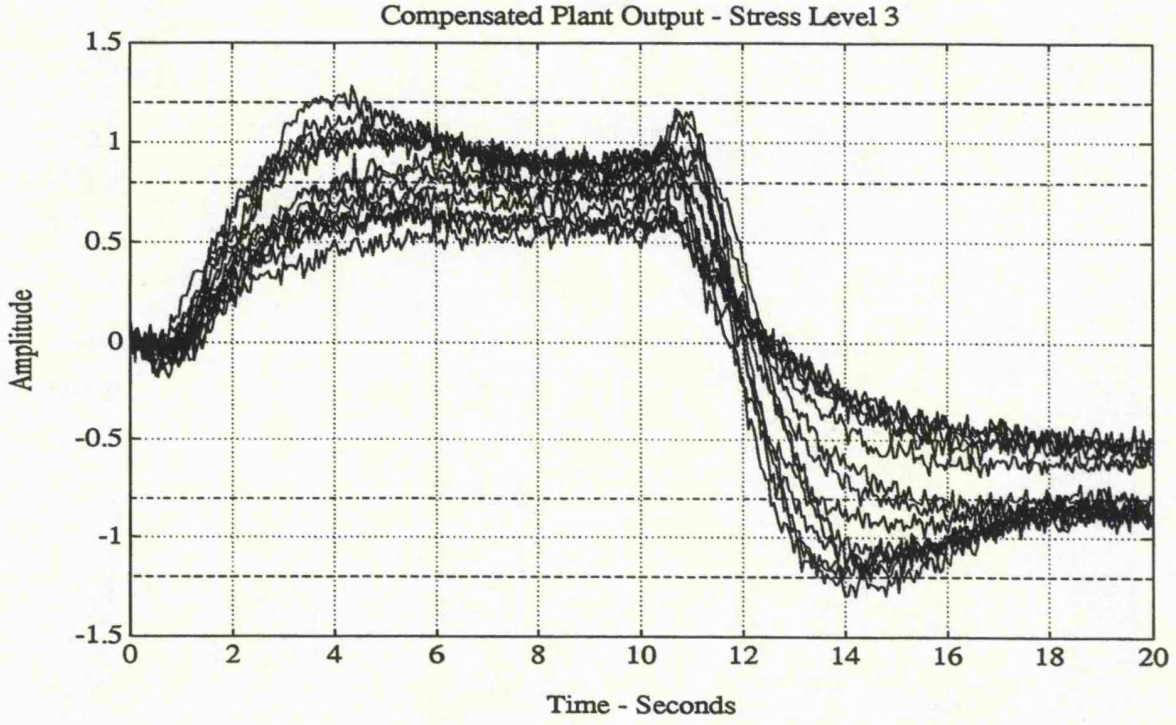

Figure 4.18: Simulations - Stress Level 3 - LQG Controller.

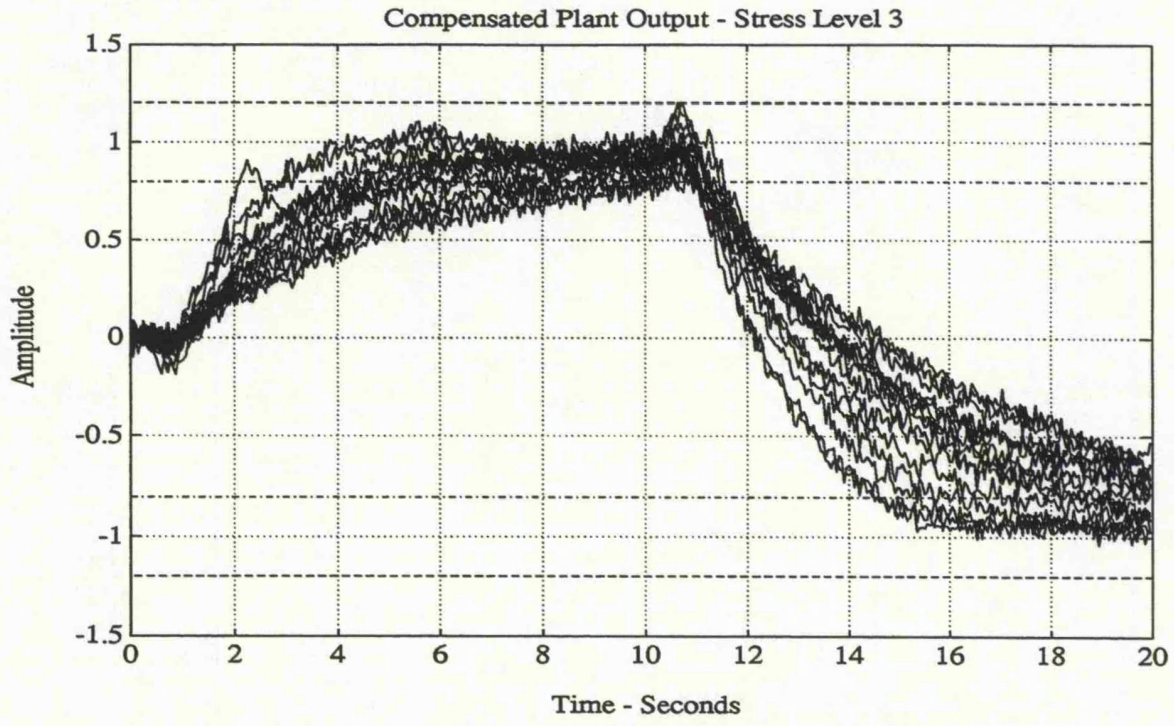

Figure 4.19: Simulations - Stress Level 3 - $\mathcal{H}^\infty$ (mixed sensitivity) controller.

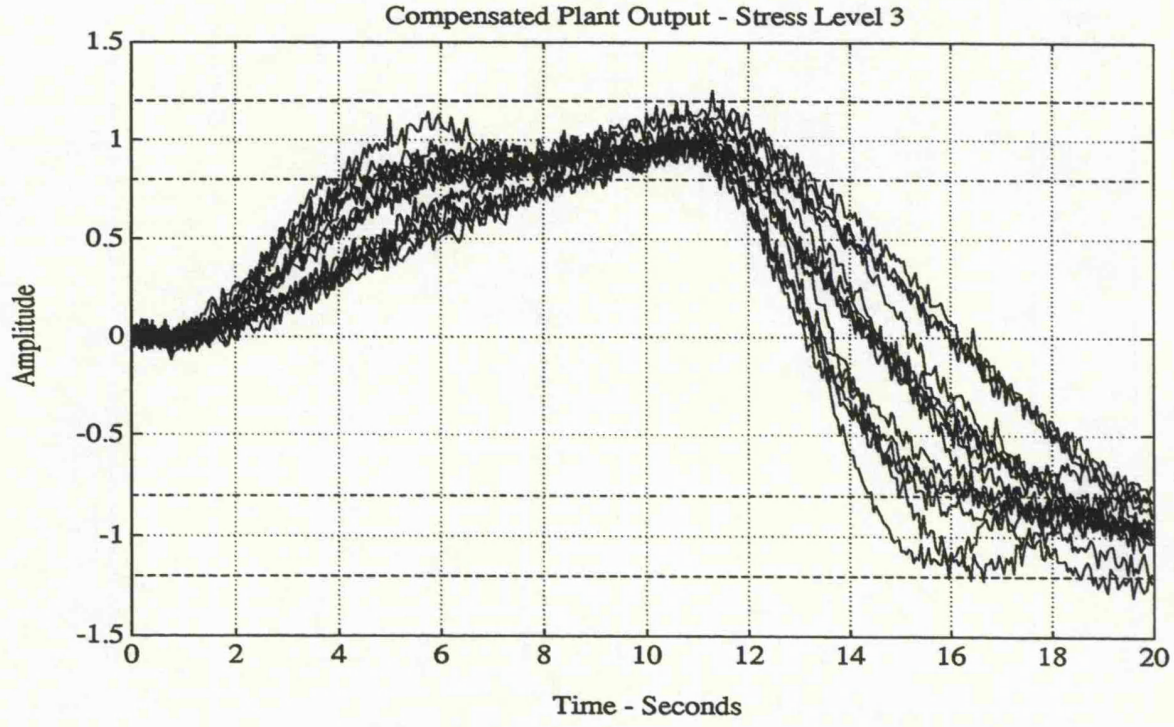

Figure 4.20: Simulations - Stress Level 3 - 1-DOF LSDP.

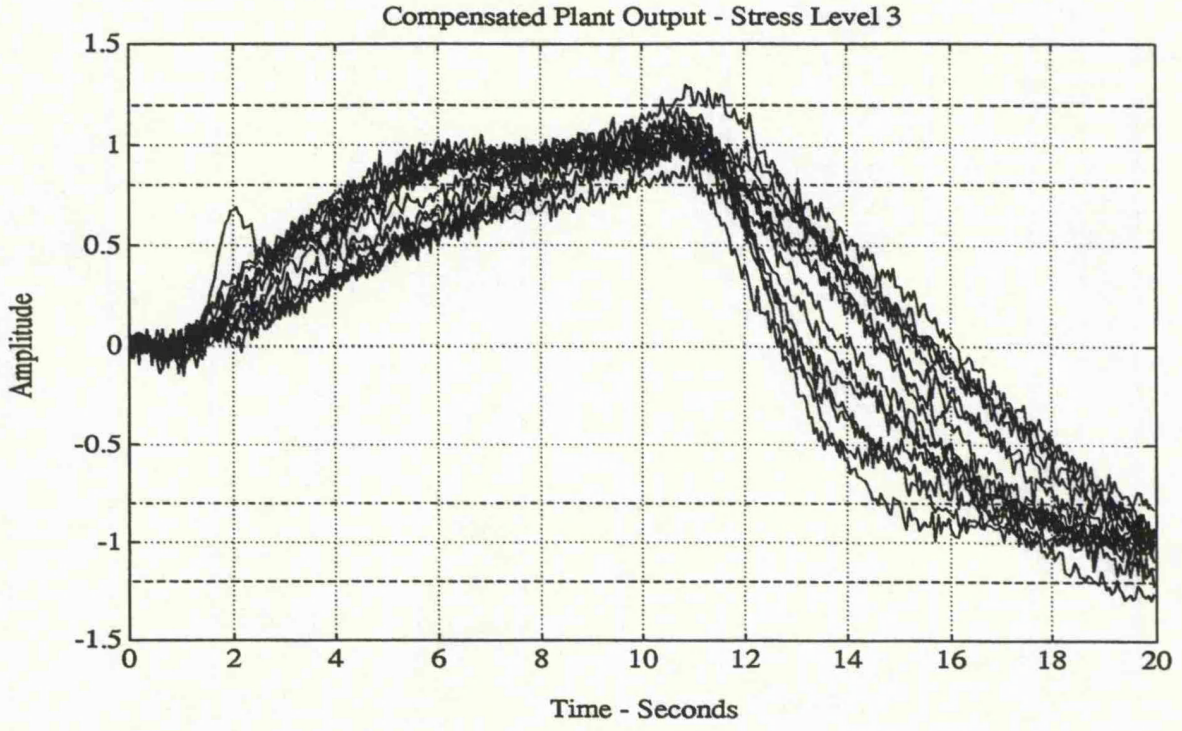

Figure 4.21: Simulations - Stress Level 3 - LSDP with Pre-filter.

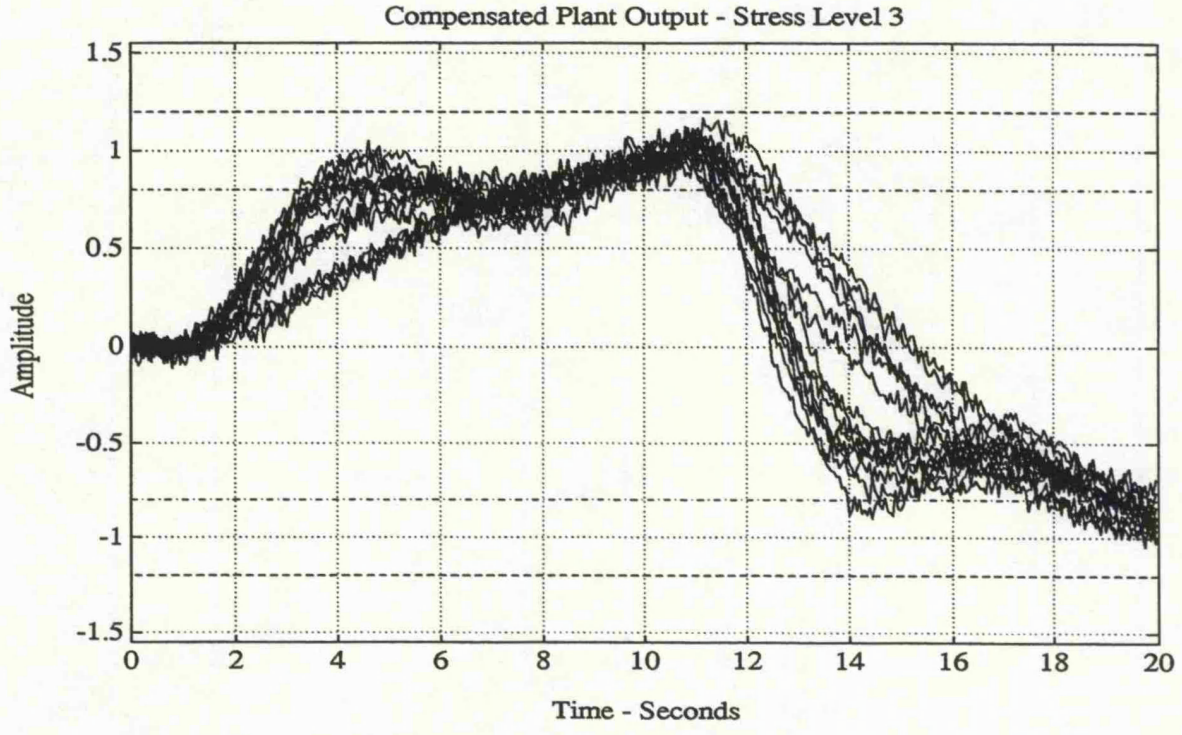

Figure 4.22: Simulations - Stress Level 3 - 2-DOF LSDP.

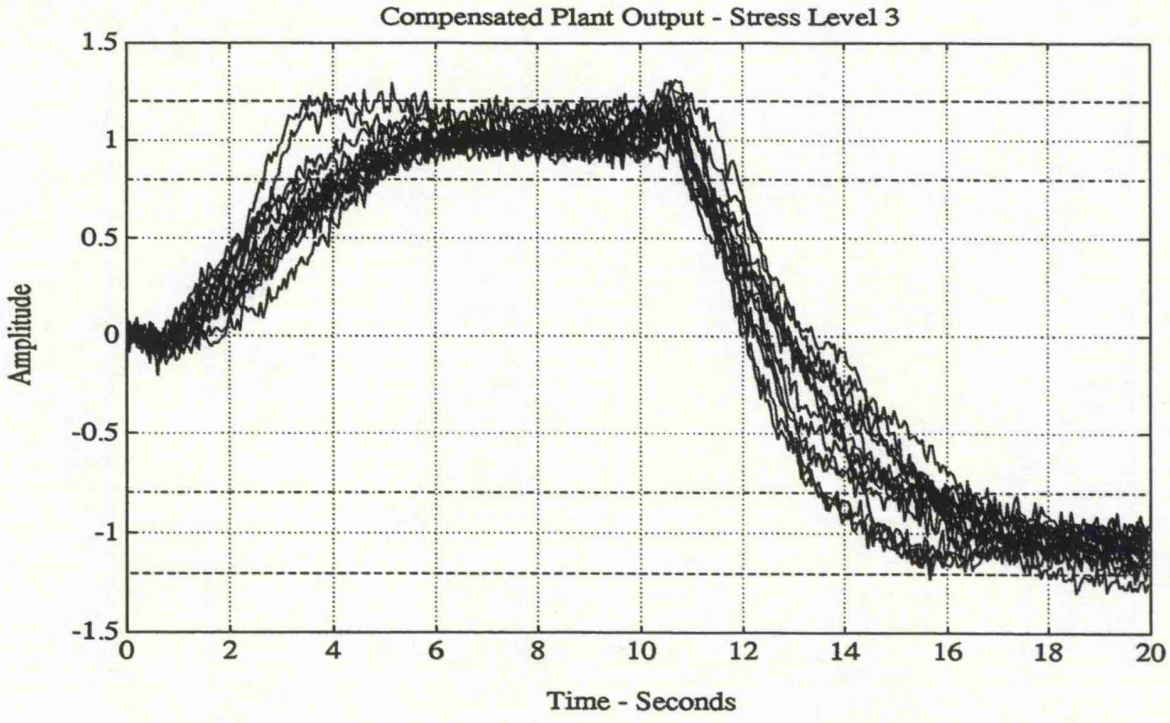

Figure 4.23: Simulations - stress level 3 $\mathcal{H}^\infty$ (mixed sensitivity) controller - (adaptive gain).

4.6 Summary

In this chapter, we considered the IFAC 1993 benchmark and it was shown that the MOI combined with the $\mathcal{H}^\infty$-optimization methods provided fixed controllers which achieved good robust performance for stress levels 1 & 2. The performance at stress level 3 was less satisfactory, but some improvement was obtained with the variable gain adaptive scheme, although at the expense of some robustness.

The formulation of the problem using the MOI makes the various trade-offs between the different performance requirements a simple matter, and can ensure that the rigid performance constraints are met.

The MOI provides an easy and effective method of designing the weighting functions for an analytical optimization problem. The $\mathcal{H}^\infty$-optimization methods gave better robustness than the LQG or the PID controller methods.

Because of the large parameter variations at stress level 3, it appears to be very difficult to obtain the required performance in terms of rise and settling times with fixed controllers. It is our hope that the "spy" observed the competitor's plant being run at stress level 1.

Chapter 5

Robust Internal Model-Based Controller Design

5.1 Introduction

In this chapter Internal Model Control (IMC) is presented for MIMO, discrete-time systems. We will show that the IMC scheme allows a controller design procedure, using the $\mathcal{H}^\infty$ optimization methods presented in Chapters 2 & 3, where good control performance and robust stability can be enhanced in a direct manner in the synthesis approach.

For stable plants, the parameterization of all stabilizing controllers has quite a long history. [78] used it to transform the closed-loop system into an open-loop one, and it was used in the same way by [117]. It is often referred to as the Q-parametrization and is very closely related to what the process control community calls IMC. The origin of the IMC scheme was provided by [31], where a process model placed in parallel with the real process is considered to be the main characteristic of the IMC scheme. The Smith predictor [95] also contains a process model in parallel with the real process. The advantages of such a scheme can be explained as follows. Consider the block diagram shown in Figure 5.1. The control system includes the two blocks labelled Q (the IMC controller) and G_m (the model). The control system has two inputs, r_k (the set-point) and y_{p_k} (the process output) and one output, u_k (the process input). The effect of the parallel path with the model is to subtract the effect of the process input from the process output. If for the moment the model is assumed to be a perfect representation of G_p (the process), then the feedback signal is equal to the influence of disturbances

(d_k) and is not affected by the action of the process input. Hence, the control system is in effect open-loop and the usual stability problems associated with feedback will disappear. The overall control system is stable if, and only if, the process and the IMC controller are both stable.

Regardless of what design technique is used, controllers are always designed based on information about the dynamic behaviour of the process. The accuracy of this information varies and is never perfect. Moreover, the dynamic behaviour of the process is time-varying and the changes are not fully captured in the models. Hence, it is most desirable that the IMC controller be insensitive to this kind of model uncertainty. The aim of this chapter is to formulate several approaches to directly synthesize, in an $\mathcal{H}^\infty$ setting, a robust IMC controller.

The organization of this chapter is as follows. Section 5.2 describes the principle of internal model control. In Sections 5.3, 5.4, and 5.5, three different approaches to directly synthesize robust IMC controllers are described and analyzed. The first approach (Section 5.3) is based on linear quadratic-implicit model following [6]. The second approach (Section 5.4) is based on synthesizing an IMC controller in a 1-DOF $\mathcal{H}^\infty$ setting, and within this approach, two different design methods are presented, the weighted 1, 2 and 4-block problem and the normalized left coprime factor design procedure. In the latter, suboptimal and optimal IMC-based controllers are derived. The third approach (Section 5.5) is based on synthesizing an IMC controller in a 2-DOF $\mathcal{H}^\infty$ setting *via* explicit model following and a coprime factor design framework. Also, explicit state-space formulae are derived for the precise structure of this controller. The controller structure is shown to comprise an observer, an on-line step response model, and a generalized state-feedback law. Such a combination results in a controller achieving, simultaneously, robust stability and robust model following. Finally, a summary is given in Section 5.6.

5.2 The Internal Model Control (IMC) Scheme

The Internal Model Control (IMC) scheme will be introduced, for stable systems only. It is frequently used as an alternative to classical feedback schemes. A comprehensive treatment on the IMC can be found in [67] and the references therein, these include

[32, 66, 33, 34, 24, 89]. The block diagram of the IMC loop is shown in Figure 5.1. Here G_p represents the real plant. In general G_p is not known exactly. The nominal model of the process, which is represented by G_m, is available. The signal d_k represents the effect of disturbances on the process output y_{p_k}. The measurement of y_{p_k} is corrupted by the measurement noise n_k. The controller Q determines the value of the control signal u_k. The control objective is to keep y_{p_k} close to the set-point r_k. For the sake of simplicity,

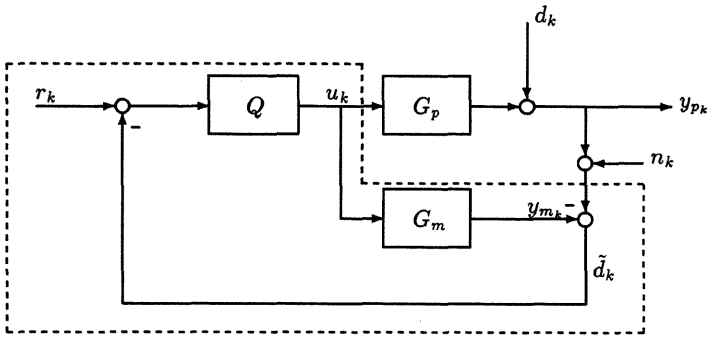

Figure 5.1: Internal Model Control Scheme.

exact knowledge of the output y_{p_k} is assumed ($n_k = 0$). The complete control system which may be implemented through computer software or analog hardware is contained in the dotted box in Figure 5.1. It includes the plant model G_m explicitly in addition to the controller Q, and so the control scheme is referred to as Internal Model Control, or IMC for short. The feedback signal is

$$\tilde{d}_k = (G_p - G_m)u_k + d_k \tag{5.1}$$

If the model is exact ($G_p = G_m$) and there are no disturbances ($d_k = 0$), then the model output y_{m_k} and the process output y_{p_k} are the same and the feedback signal $\tilde{d}_k$ is zero. Thus the control system is open-loop when there is no uncertainty (*i.e.* no model uncertainty and no unknown inputs d_k). This demonstrates that for stable processes feedback is only necessary because of uncertainty. The feedback signal $\tilde{d}_k$ expresses the uncertainty in the process.

The IMC scheme also demonstrates how to combine the advantages of feedback with those of feedforward. Assuming that $G_p = G_m$ and $d_k \neq 0$, it is clearly seen that $\tilde{d}_k = d_k$. Therefore, the IMC scheme of Figure 5.1 can be re-drawn as a model-matching problem (feedforward problem) as shown in Figure 5.2.

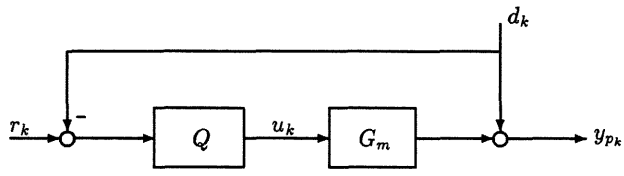

Figure 5.2: An Equivalent IMC Scheme.

5.2.1 Stability Conditions for IMC

In order to test for internal stability, the transfer functions between all possible system inputs and outputs are examined. From the block diagram of Figure 5.3, there are three independent system inputs and outputs. The independent inputs r_k, u_{1_k} and u_{2_k} are chosen together with independent outputs y_{p_k}, u_k and y_{m_k}. If there is no model error ($G_p = G_m$), then the inputs and outputs are related through the following transfer function matrix

$$\begin{bmatrix} y_{p_k} \\ u_k \\ y_{m_k} \end{bmatrix} = \begin{bmatrix} G_m Q & (I - G_m Q)G_m & G_m \\ Q & -QG_m & 0 \\ G_m Q & -G_m Q G_m & G_m \end{bmatrix} \begin{bmatrix} r_k \\ u_{1_k} \\ u_{2_k} \end{bmatrix} \tag{5.2}$$

The following theorem follows trivially by inspection.

Theorem 5.2.1 [67] Assume that the model is perfect ($G_p = G_m$). Then the IMC scheme in Figure 5.3 is internally stable if, and only if, both the plant G_p and the controller Q are stable. ■

It is clear from (5.2) that the implementation of the IMC scheme is only suitable for controlling stable processes. This is because the IMC system is effectively operating in

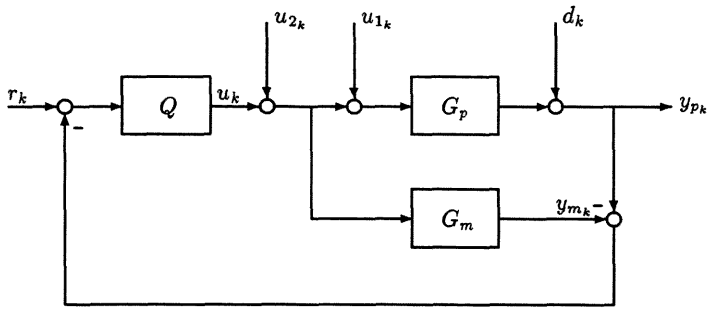

Figure 5.3: IMC Scheme for Deriving Internal Stability Conditions.

open-loop when there is no uncertainty, and since the stabilization of open-loop unstable systems requires feedback, the IMC scheme cannot be applied in this case.

It can be argued that the lack of model uncertainty is an artificial assumption. Uncertainty gives rise to feedback, and thus it could be possible to stabilize an unstable system with IMC. However, in any practical situation, it is unacceptable to rely on model uncertainty for stability [67]. It should be stated that the IMC scheme can still be used for unstable processes during the design [67].

In the case of a stable process, it is clear from (5.2) that internal stability is guaranteed by a stable controller. So the class of internally stabilizing controllers for the IMC scheme with a stable process is equal to the set of all stable transfer function matrices of appropriate dimensions. Furthermore, from the closed-loop transfer function matrices, it is clear that a perfect input-output behaviour can be accomplished, if it is possible to choose $Q = G_m^{-1}$. This is an important property of the IMC scheme. It can be stated that all effects which restrict the invertibility of a stable process are exactly the effects that limit the performance of the controlled process. This relation between closed-loop performance and invertibility of the process is much more direct than the relation with high gain in the unit feedback case.

5.2.2 Relationship of IMC with Standard Unit Feedback

The manipulations necessary to transform the block diagram in Figure 5.1 into the one in Figure 5.4 leave the signals u_k and y_{p_k} unaffected. Combining the two blocks Q and G_m in Figure 5.4 into one block K then the standard unit feedback control system is obtained with

$$K = Q(I - G_m Q)^{-1} \tag{5.3}$$

On the other hand, if two blocks of G_m are added to the standard unit feedback system

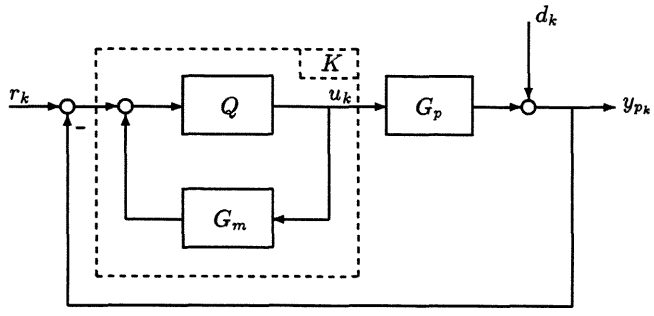

Figure 5.4: Alternate Representation of the IMC Scheme.

as shown in Figure 5.5, the signals u_k and y_{p_k} also remain unaffected. The IMC scheme follows with

$$Q = K(I + G_m K)^{-1} \tag{5.4}$$

Hence, in the way the outputs u_k and y_{p_k} respond to inputs r_k and d_k, the standard unit feedback scheme and the IMC scheme are entirely equivalent and the controllers K and Q are related through (5.3) and (5.4), respectively. If we consider the case that the real plant G_p is stable and exactly equals the plant model G_m:

1) Then assuming that the IMC scheme in Figure 5.1 is internally stable, the equivalent standard unit feedback scheme in Figure 5.4 is internally stable because the internal signals u_k and y_{p_k} are unaffected by the transformation.

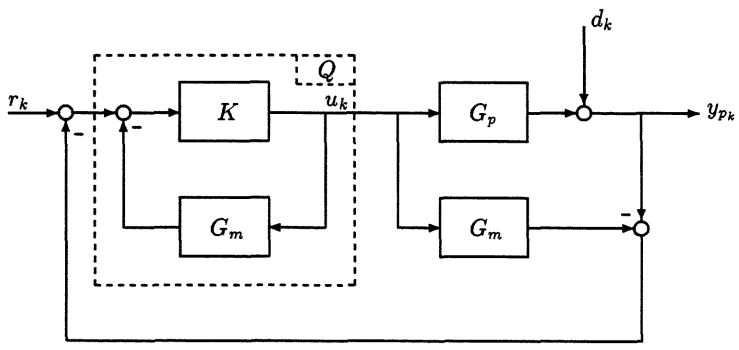

Figure 5.5: Alternate Representation of the IMC Scheme.

2) Then assuming that the standard unit feedback scheme in Figure 5.4 is internally stable, transfer function matrix (5.2) is stable and therefore Q defined by (5.4) is stable. Thus, the equivalent IMC scheme is internally stable.

5.2.3 Performance of IMC

For the IMC scheme in Figure 5.1 the following transfer functions relating inputs and outputs are easily found

$$y_{p_k} = G_pQ(I + (G_p - G_m)Q)^{-1}r_k + (I - G_mQ)(I + (G_p - G_m)Q)^{-1}d_k \tag{5.5}$$

The sensitivity function $S(z)$ relates the external inputs r_k and d_k to the error $e_k = y_{p_k} - r_k$

$$e_k = y_{p_k} - r_k = (I - G_mQ)(I + (G_p - G_m)Q)^{-1}(d_k - r_k) = S(z)(d_k - r_k) \tag{5.6}$$

The complementary sensitivity function $T(z)$ is found by subtracting $S(z)$ from unity

$$y_{p_k} = G_pQ(I + (G_p - G_m)Q)^{-1}r_k = T(z)r_k \tag{5.7}$$

When $G_p = G_m$, (5.6) and (5.7) reduce to

$$S(z) = I - G_mQ \tag{5.8}$$

$$T(z) = G_mQ \tag{5.9}$$

The classification of asymptotic closed-loop behaviour that defines "system type" is given by

$$Type\ m: \qquad \lim_{z\to 1} \frac{d^k}{dz^k}(I - G_m Q) = 0; \quad 0 \leq k < m \tag{5.10}$$

The following are then obtained from (5.10)

$$Type\ 1: \qquad \lim_{z\to 1} G_m Q = I \tag{5.11}$$

$$Type\ 2: \qquad \lim_{z\to 1} G_m Q = I \text{ and } \lim_{z\to 1} \frac{d}{dz}(G_m Q) = 0 \tag{5.12}$$

Thus, in order to track asymptotically constant inputs with zero steady-state error, the controller gain has to be the inverse of the model steady-state gain. The expressions (5.11) and (5.12) are necessary and sufficient for tracking steps and ramps with zero steady-state error, respectively, even when model error is present.

In some cases, the IMC controller Q is detuned to reduce its aggressiveness by augmenting it with a low-pass filter F_{lp} in a simple manner to give $\tilde{Q} = QF_{lp}$. In [33] they state that a first-order filter of the form

$$F_{lp}(z) = \frac{1 - \alpha_f}{1 - \alpha_f z^{-1}}, \ 0 \leq \alpha_f < 1 \tag{5.13}$$

may be used to stabilize the closed-loop system for a given plant/model mismatch. The filter constant α_f is given by

$$\alpha_f = e^{\frac{-T}{\tau_f}} \tag{5.14}$$

where T is the sampling period and τ_f is the filter time constant. The filter time constant can serve as a tuning parameter. So adjusting the parameters of F_{lp} is equivalent to adjusting the speed of the closed-loop response, that is with a good model, a high speed of response can be demanded from the system; but when the knowledge about the model is poor, then the speed of response has to be decreased. Thus, a suitable compromise must be found between robustness and dynamic performance. However, it is possible for the parameters of F_{lp} to be left for on-line adjustment.

Until now the discussion has been restricted to the nominal case. The behaviour of the process was completely described by the model behaviour. This however will never be the case in real life. Inevitably, there will be a difference between the nominal model and the real process, the so-called modelling error or perturbation, which is unknown. In the

IMC scheme, this modelling error can be usually expressed as an additive uncertainty $G_p = G_m + \Delta_a$. The modelling error can be represented in other ways (Chapter 2), but only the additive case will be discussed here. In general, an upper bound or some sort of structure is usually assumed on the uncertainty. If the additive perturbation Δ_a is present, the signal $\tilde{d}_k$ of (5.1) will not be equal to the disturbance d_k anymore, that is $\tilde{d}_k$ will contain an additional term due to the modelling error

$$\tilde{d}_k = \Delta_a u_k + d_k \tag{5.15}$$

The influence of this additive perturbation will also have to be taken into account in the output signal y_{p_k} as

$$y_{p_k} = (G_m + \Delta_a)u_k + d_k \tag{5.16}$$

Based on the above observations, the feedforward scheme in Figure 5.3 can be adapted to the perturbed case as shown in Figure 5.6.

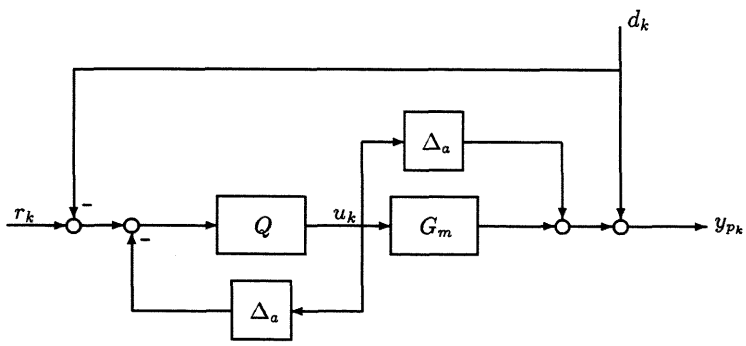

Figure 5.6: An Equivalent IMC Scheme with Additive Perturbation.

From this controller scheme, the signals of u_k and y_{p_k} are obtained as

$$u_k = Q(I + \Delta_a Q)^{-1}(r_k - d_k) \tag{5.17}$$

$$\begin{aligned} y_{p_k} &= G_m Q r_k + (I - G_m Q)d_k + G_m Q(I + \Delta_a Q)^{-1}\Delta_a Q(r_k - d_k) \\ &= (\Delta_a + G_m)Q(I + \Delta_a Q)^{-1} r_k + (I - G_m Q)(I + \Delta_a Q)^{-1} d_k \end{aligned} \tag{5.18}$$

From Figure 5.6, equations (5.17) and (5.18), it is seen that the feedforward scheme of Figure 5.3 has become a feedback scheme due to the feedback of Δ_a around the

Q. Therefore, internal stability of the control scheme is completely determined by $(I + \Delta_a Q)^{-1}$. That is, the stability of the loop, due to some permissible perturbation, is guaranteed with a stable controller if, and only if

$$\left|\mathbf{det}\left[I + \Delta_a(e^{j\theta})Q(e^{j\theta})\right]\right| > 0 \ , \theta \in [-\pi, \pi) \tag{5.19}$$

Since Q is stable and Δ_a is also stable by assumption, the control scheme becomes unstable only if one or more of the characteristic loci of $-Q\Delta_a$ encircles the point -1; a well known result from the generalized Nyquist theorem. Now, if $\lambda(Q\Delta_a)$ is any eigenvalue of $Q\Delta_a$, then

$$|\lambda(Q\Delta_a)| \leq \rho(Q\Delta_a) \leq \bar{\sigma}(Q\Delta_a) \tag{5.20}$$

and so no encirclement of -1 can occur if $\| Q\Delta_a \|_\infty < 1$. Now

$$\| Q\Delta_a \|_\infty \leq \| Q \|_\infty \| \Delta_a \|_\infty \tag{5.21}$$

and therefore there is no encirclement of -1 if

$$\bar{\sigma}(Q) < [\bar{\sigma}(\Delta_a)]^{-1} \tag{5.22}$$

The expression given in (5.22) can be regarded as a sufficient condition for stability of the loop. If an upper bound on the uncertainty $\bar{\sigma}\left[\Delta_a(e^{j\theta})\right] < |l_a(e^{j\theta})|$ is known, the following condition is an alternative to (5.22)

$$\bar{\sigma}\left[Q\right] < |l_a(e^{j\theta})|^{-1} \tag{5.23}$$

If both good tracking of r_k and good disturbance rejection are important in addition to the robust stability requirement, and if the dynamic characteristics of the two inputs r_k and d_k are substantially different, it is advantageous to introduce the 2-DOF IMC configuration as shown in Figure 5.7. The 2-DOF IMC scheme enables the separate design of the set-point behaviour of the closed-loop process from that of disturbance rejection. To see this, the 2-DOF IMC scheme of Figure 5.7 is analyzed in the following way. The effects of r_k and d_k on y_{p_k} are described by

$$y_{p_k} = G_p(I + Q_2(G_p - G_m))^{-1}Q_1 r_k + (I - G_m Q_2)(I + (G_p - G_m)Q_2)^{-1} d_k \tag{5.24}$$

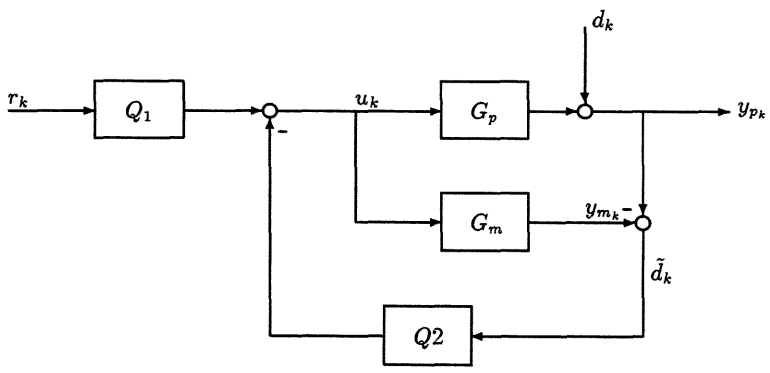

Figure 5.7: 2-DOF IMC Scheme.

For $G_p = G_m$, (5.24) becomes

$$y_{p_k} = G_m Q_1 r_k + (I - G_m Q_2) d_k \tag{5.25}$$

From (5.25) it is seen that, at least for the nominal case, the design of the controller Q_1 which is designed for set-point tracking, is independent of the controller Q_2 which designs for disturbance rejection. To ensure Type 1 behaviour, the controller Q_1 should be statically equal to the inverse of the model G_m. This is easily seen from the output equation $y_{p_k} = G_m Q_1 r_k$. From the final value theorem, it is required that $Q_1(1) = G_m(1)^{-1}$.

5.3 A Linear Quadratic - Implicit Model Following Approach

Consider the MIMO control system shown in Figure 5.8 [6]. The state-space of the real process is given by

$$\begin{aligned} x_{p_{k+1}} &= A_p x_{p_k} + B_p u_k \\ y_{p_k} &= C_p x_{p_k} + D_p u_k \\ y_k &= d_k + y_{p_k} \end{aligned} \tag{5.26}$$

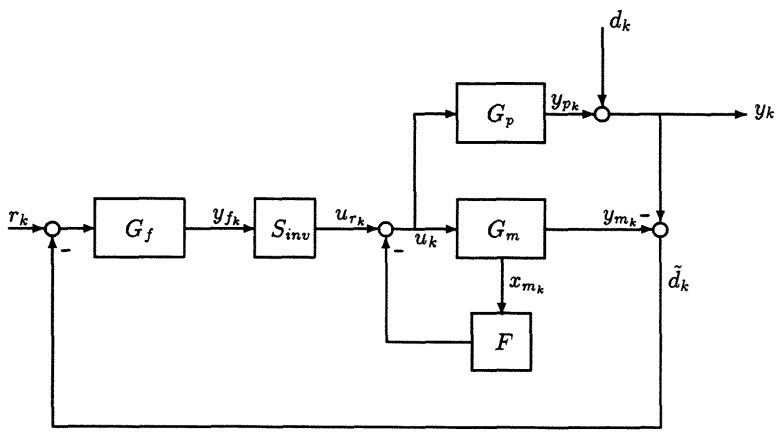

Figure 5.8: IMF Controller Implemented in the IMC Scheme.

The state-space of the process model is given by

$$\begin{aligned} x_{m_{k+1}} &= A_m x_{m_k} + B_m u_k \\ y_{m_k} &= C_m x_{m_k} + D_m u_k \end{aligned} \tag{5.27}$$

The dynamics of the process model are modified with a state-feedback controller F

$$u_k = u_{r_k} - F x_{m_k} \tag{5.28}$$

where F is designed *via* the following method:

Implicit Model Following (IMF) via Optimal Control

Given the system in (5.27) and the model

$$x_{n_{k+1}} = A_n x_{n_k} \tag{5.29}$$

we want to find the control law u_k such that $y_{m_k} \to x_{n_k}$. Define the performance index as

$$J = \sum_{k=0}^{\infty} (y_{m_{k+1}} - A_n y_{m_k})^T Q (y_{m_{k+1}} - A_n y_{m_k}) + u_k^T R u_k \tag{5.30}$$

where R is positive definite and Q is positive semi-definite. If the plant is controllable and the model is stable, the performance index is finite. Appropriate substitution in the performance index yields

$$J = \sum_{k=0}^{\infty} [\, x_{m_k}^T \quad u_k^T \,] \begin{bmatrix} W_{11} & W_{12} \\ W_{12}^T & W_{22} \end{bmatrix} \begin{bmatrix} x_{m_k} \\ u_k \end{bmatrix} \tag{5.31}$$

where

$$\begin{aligned} W_{11} &= (C_m A_m - A_n C_m)^T Q (C_m A_m - A_n C_m) \\ W_{12} &= (C_m B_m)^T Q (C_m A_m - A_n C_m) \\ W_{22} &= (C_m B_m)^T Q C_m B_m + R \end{aligned} \tag{5.32}$$

It is assumed that the initial condition of the state, $x(0) = x_o$, is determined by Gaussian white noise with intensity $E\{x_o x_o^T\} = I$. Minimizing the performance index over sequences of the process model inputs u_k, yields the standard LQ problem

$$\min_{u_k} \sum_{k=0}^{\infty} [\, x_{m_k}^T \quad u_k^T \,] \begin{bmatrix} W_{11} & W_{12} \\ W_{12}^T & W_{22} \end{bmatrix} \begin{bmatrix} x_{m_k} \\ u_k \end{bmatrix} \tag{5.33}$$

subject to closed-loop stability. This problem is known to have a solution of the form $u_k = F x_{m_k}$, where F is determined by

$$F = -(W_{22} + B_m^T P B_m)^{-1} (B_m^T P A_m + W_{12}) \tag{5.34}$$

where P is the positive definite solution of the Riccati equation

$$A_m^T P A_m - P + W_{11} - (A_m^T P B_m + W_{12})(W_{22} + B_m^T P B_m)^{-1} (A_m^T P B_m + W_{12})^T = 0 \tag{5.35}$$

The state-space realization for the controlled process is given by

$$\left[\begin{array}{c|c} A_m + B_m F & B_m \\ \hline C_m + D_m F & D_m \end{array}\right] \tag{5.36}$$

Since no demands on the input-output behaviour were considered in the optimization, the closed-loop behaviour will generally not be statically decoupled. Hence, to ensure static decoupling of the closed-loop, the realization of (5.36) is pre-multiplied with a static decoupler, S_{inv}, which happens to be the inverse of the steady-state of (5.36)

$$S_{inv} = \left[(C_m + D_m F)(I - A_m - B_m F)^{-1} B_m + D_m \right]^{-1} \tag{5.37}$$

and the final closed-loop realization yields

$$\left[\begin{array}{c|c} A_m + B_m F & B_m S_{inv} \\ \hline C_m + D_m F & D_m S_{inv} \end{array}\right] \tag{5.38}$$

The dynamics of the process considered between the input r_k and the output y_k will be modified accordingly, if the process and the model have the same input-output behaviour. The difference between the measured and simulated output signals may be considered to be an estimate for the process output noise $\tilde{d}_k$, the expression given in (5.1). The resulting error signal, when $\tilde{d}_k$ is compared with r_k is

$$e_k = r_k - \tilde{d}_k \tag{5.39}$$

This error signal may be filtered by a low-pass filter G_f as shown in Figure 5.8. The function of this filter is to:

1) Prevent the sensor noise from contaminating the control signal u_k.

2) Make the control scheme robust with respect to small modelling errors and to the changing characteristics of the process.

The controller could also be used as a dynamic compensator of the form $Q(z)$ with state-space realization

$$Q(z) \stackrel{s}{=} \left[\begin{array}{c|c} A_m + B_m F & B_m S_{inv} \\ \hline F & S_{inv} \end{array}\right] \tag{5.40}$$

Hence, the final IMC controller may be expressed as

$$Q_{final}(z) = Q(z) G_f(z) \tag{5.41}$$

5.4 An $\mathcal{H}^\infty$ 1-DOF Design Approach

5.4.1 Traditional $\mathcal{H}^\infty$ Design Formulation for IMC

The general structure of all stabilizing controllers given by (2.61) is depicted in Figure 5.9 [61]. This particular controller structure can be used if the plant G_p is unstable,

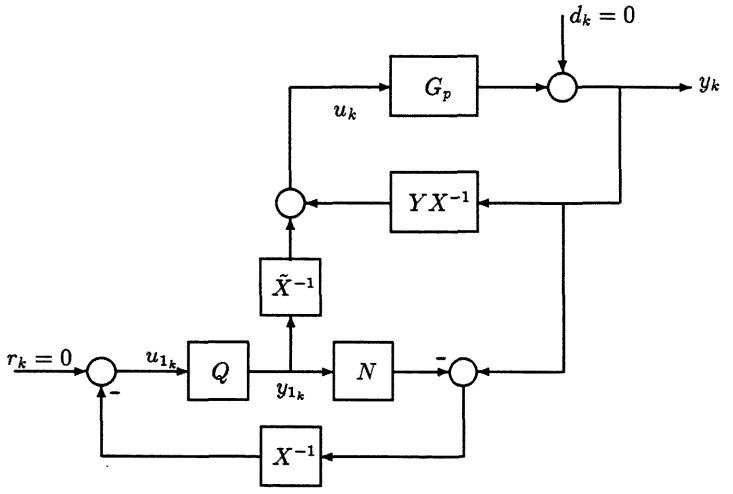

Figure 5.9: General Structure of Stabilizing Controllers ($Q \in \mathcal{RH}^\infty$).

but can be stabilized by YX^{-1}. The structure is re-drawn in Figure 5.10. Suppose the plant is stable, then one can take $N = G_m$, where G_m is the nominal model of the plant, $M = I$, $Y = 0$ and $X = I$. In this case the Bezout identity becomes

$$\begin{bmatrix} I & 0 \\ -G_m & I \end{bmatrix} \begin{bmatrix} I & 0 \\ G_m & I \end{bmatrix} = \begin{bmatrix} I & 0 \\ 0 & I \end{bmatrix} \tag{5.42}$$

and Figure 5.10 may be re-drawn as shown in Figure 5.11 which has a controller structure that can be used for stable systems. Also, (2.61) simplifies to $K = Q(I + G_m Q)^{-1}$, from which one obtains $Q = K(I - G_m K)^{-1}$, which is precisely the IMC controller discussed in Section 5.2. So for stable systems, Figure 5.9 is identical to that of Figure 5.1, which represents the IMC scheme. From these observations, it can be deduced that:

1) The IMC $\mathcal{H}^\infty$ controller design may be based on minimizing the following criterion function

$$\min_{Q \in \mathcal{RH}^\infty} \| \mathcal{F}_l(P_{imc}, Q) \|_\infty \tag{5.43}$$

where $\mathcal{F}_l(P_{imc}, Q)$ has the form

$$\mathcal{F}_l(P_{imc}, Q) = P_{imc_{11}} - P_{imc_{12}} Q (I + P_{imc_{22}} Q)^{-1} P_{imc_{21}} \tag{5.44}$$

2) For the IMC scheme all nominal criteria will lead to a model matching problem. This means that the transfer function matrix $P_{imc_{22}}$ is equal to zero, so the criterion function will be given by

$$\min_{Q \in \mathcal{RH}_\infty} \| P_{imc_{11}} - P_{imc_{12}} Q P_{imc_{21}} \|_\infty \tag{5.45}$$

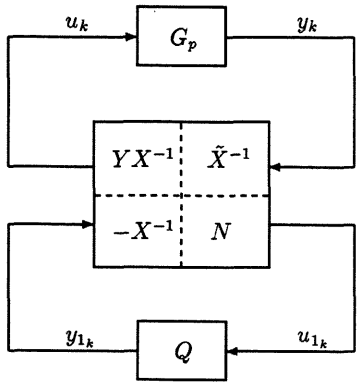

Figure 5.10: Controller Structure if the Plant is Unstable.

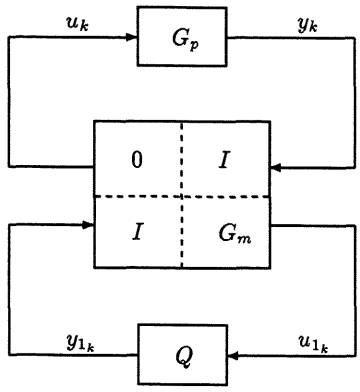

Figure 5.11: Controller Structure if the Plant is Stable.

In unity feedback schemes, the specifications on the properties of the process are demanded in open-loop (*i.e.* one demands large gain at low-frequency for performance

and small gain at high-frequency for robustness), but in the IMC scheme, the demands are directly put on the closed-loop transfer function matrix. This is seen from the fact that the criterion matrix $\mathcal{F}_l(P_{imc}, Q)$ is itself a closed-loop transfer function matrix. Except for the choice of the criterion function itself, one has the possibility to specify the demands by weighting both the input and the output of the criterion matrix. Suppose the criterion matrix is given by

$$T_{imc_{11}} - T_{imc_{12}} Q T_{imc_{21}} \tag{5.46}$$

then it is possible to weight both the input and the output by W_i and W_o, respectively as

$$W_o \left[T_{imc_{11}} - T_{imc_{12}} Q T_{imc_{21}} \right] W_i \tag{5.47}$$

The following is obtained for the standard augmented plant

$$P_{imc} = \begin{bmatrix} P_{imc_{11}} & P_{imc_{12}} \\ P_{imc_{21}} & 0 \end{bmatrix} = \begin{bmatrix} W_o & 0 \\ 0 & I \end{bmatrix} \begin{bmatrix} T_{imc_{11}} & T_{imc_{12}} \\ T_{imc_{21}} & 0 \end{bmatrix} \begin{bmatrix} W_i & 0 \\ 0 & I \end{bmatrix} \tag{5.48}$$

To ensure stability the weights are chosen to be stable and minimum phase. This is due to the fact that the original criterion matrix, after the design, will be expressed as

$$T_{imc} = \begin{bmatrix} T_{imc_{11}} & T_{imc_{12}} \\ T_{imc_{21}} & 0 \end{bmatrix} = \begin{bmatrix} W_o^{-1} & 0 \\ 0 & I \end{bmatrix} \begin{bmatrix} P_{imc_{11}} & P_{imc_{12}} \\ P_{imc_{21}} & 0 \end{bmatrix} \begin{bmatrix} W_i^{-1} & 0 \\ 0 & I \end{bmatrix} \tag{5.49}$$

Next, some examples on $\mathcal{H}^\infty$ problems in the IMC scheme will be presented.

Sensitivity Minimization – 1-Block Problem

Consider the IMC scheme shown in Figure 5.12. A plausible design objective is to find an internally stabilizing IMC controller Q which minimizes the worst-case excursion of the output signal y_k resulting from any disturbance d_k, and this could be achieved by solving the minimization problem

$$\min_{Q \in \mathcal{RH}^\infty} \| W_o (I - G_p Q) W_i \|_\infty \tag{5.50}$$

Since it is required that

$$\mathcal{F}_l(P_{imc}, Q) = W_o S W_i = W_o (I - G_p Q) W_i \tag{5.51}$$

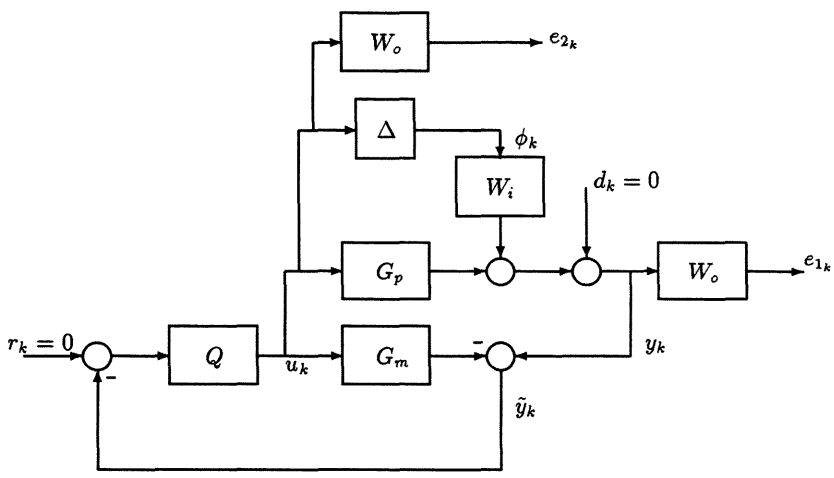

Figure 5.12: The 1-block and 2-block Problem in the IMC Scheme.

it can be deduced that

$$P_{imc_{11}} = W_o W_i, \quad P_{imc_{12}} = -W_o G_p, \quad P_{imc_{21}} = W_i, \quad P_{imc_{22}} = 0 \tag{5.52}$$

The state-space realization for this formulation is given by

$$P_{imc} \stackrel{s}{=} \left[\begin{array}{c|c} A_{w_o} & B_{w_o} \\ \hline C_{w_o} & D_{w_o} \end{array}\right] \left[\begin{array}{c|cc} A_p & 0_{n\times m} & B_p \\ \hline -C_p & I_{m\times m} & -D_p \\ 0_{r\times n} & I_{m\times m} & 0_{m\times r} \end{array}\right] \left[\begin{array}{c|c} A_{w_i} & B_{w_i} \\ \hline C_{w_i} & D_{w_i} \end{array}\right] \tag{5.53}$$

with (A_p, B_p, C_p, D_p) being the state-space realization of the plant G_p with dimensions $n \times n$, $n \times r$, $m \times n$ and $m \times r$, respectively, $(A_{w_i}, B_{w_i}, C_{w_i}, D_{w_i})$ and $(A_{w_o}, B_{w_o}, C_{w_o}, D_{w_o})$ being the state-space realization of input and output weightings, respectively. For the 1-block problem, the plant G_p is restricted to being square.

Mixed Performance and Robustness Objective – 2-Block Problem

Looking again at Figure 5.12, suppose the objective is to obtain good disturbance rejection and to maintain stability in the presence of unstructured additive uncertainty perturbations. That is, to keep both the sensitivity S and the IMC controller Q small

in magnitude. This could be achieved by solving the minimization problem

$$\min_{Q\in\mathcal{RH}^\infty} \left\| \begin{bmatrix} W_o(I - G_pQ)W_i \\ -W_oQW_i \end{bmatrix} \right\|_\infty \tag{5.54}$$

Since it is required that

$$\mathcal{F}_l(P_{imc}, Q) = \begin{bmatrix} W_oSW_i \\ -W_oQW_i \end{bmatrix} = \begin{bmatrix} W_o(I - G_pQ)W_i \\ -W_oQW_i \end{bmatrix} \tag{5.55}$$

it can be deduced that

$$P_{imc_{11}} = \begin{bmatrix} W_oW_i \\ 0 \end{bmatrix}, \quad P_{imc_{12}} = \begin{bmatrix} -W_oG_p \\ W_o \end{bmatrix}, \quad P_{imc_{21}} = W_i, \quad P_{imc_{22}} = 0 \tag{5.56}$$

The state-space realization for this formulation is given by

$$P_{imc} \stackrel{s}{=} \left[\begin{array}{c|c} A_{w_o} & B_{w_o} \\ \hline C_{w_o} & D_{w_o} \end{array}\right] \left[\begin{array}{c|cc} A_p & 0_{n\times m} & B_p \\ \hline -C_p & I_{m\times m} & -D_p \\ 0_{r\times n} & 0_{r\times m} & I_{r\times r} \\ 0_{r\times n} & I_{m\times m} & 0_{m\times r} \end{array}\right] \left[\begin{array}{c|c} A_{w_i} & B_{w_i} \\ \hline C_{w_i} & D_{w_i} \end{array}\right] \tag{5.57}$$

The size of the IMC controller Q will always be greater than the size of the classical feedback controller K. This can be easily seen from the expression given by (5.4) where its clear that $\mathbf{size}(Q) = \mathbf{size}(K) + \mathbf{size}(G_m)$, but by directly synthesizing an IMC controller to solve the 1-block or 2-block problem, we have $\mathbf{size}(Q) = \mathbf{size}(K)$. This can also be seen from the state-space realization given by (5.53) and (5.57).

The 4-Block Problem

Consider the IMC scheme shown in Figure 5.13. This approach considers not only output perturbations as in the 2-block problem but also input perturbations. In this case the minimization problem is

$$\min_{Q\in\mathcal{RH}^\infty} \left\| \begin{bmatrix} W_o(I - G_pQ)W_i & W_o(I - G_pQ)G_pW_i \\ -W_oQW_i & -W_oQG_pW_i \end{bmatrix} \right\|_\infty \tag{5.58}$$

This gives rise to designs with improved robustness properties, particularly at the control inputs, but can mean that performance can be degraded slightly. Since it is required that

$$\mathcal{F}_l(P_{imc}, Q) = \begin{bmatrix} W_oSW_i & W_oSG_pW_i \\ -W_oQW_i & -W_oTW_i \end{bmatrix} = \begin{bmatrix} W_o(I - G_pQ)W_i & W_o(I - G_pQ)G_pW_i \\ -W_oQW_i & -W_oQG_pW_i \end{bmatrix} \tag{5.59}$$

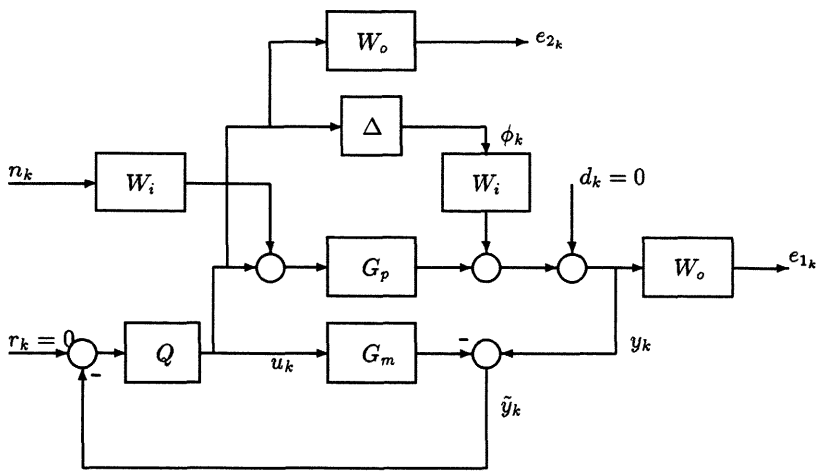

Figure 5.13: The 4-block Problem in the IMC Scheme.

it can be deduced that

$$P_{imc_{11}} = \begin{bmatrix} W_o W_i & W_o G_p \\ 0 & 0 \end{bmatrix}, \qquad P_{imc_{12}} = \begin{bmatrix} -W_o G_p \\ W_o \end{bmatrix}$$

$$P_{imc_{21}} = \begin{bmatrix} W_i & G_p W_i \end{bmatrix}, \qquad P_{imc_{22}} = 0 \tag{5.60}$$

The state-space realization for this formulation is given by

$$P_{imc} \stackrel{s}{=} \left[\begin{array}{c|c} A_{w_o} & B_{w_o} \\ \hline C_{w_o} & D_{w_o} \end{array}\right] \left[\begin{array}{ccc|cc} A_p & 0_{n\times n} & 0_{n\times m} & B_p & 0_{n\times r} \\ 0_{n\times n} & A_p & 0_{n\times r} & 0_{n\times m} & B_p \\ \hline C_p & -C_p & I_{m\times m} & D_p & -D_p \\ 0_{r\times m} & 0_{r\times n} & 0_{r\times m} & 0_{r\times m} & I_{r\times r} \\ C_p & 0_{m\times n} & I_{m\times m} & D_p & 0_{m\times r} \end{array}\right] \left[\begin{array}{c|c} A_{w_i} & B_{w_i} \\ \hline C_{w_i} & D_{w_i} \end{array}\right] \tag{5.61}$$

For this particular problem the size of the IMC controller Q will always be equal to that given by (5.4). This can be seen from the state-space realization given by (5.61).

The state-space realizations given by (5.53), (5.57) and (5.61) can be passed to standard $\mathcal{H}^\infty$ algorithms, where the solution is based *via* γ-iteration on solving two algebraic Riccati equations.

5.4.2 An IMC Formulation and Controller Synthesis of the Normalized Coprime Factor Design Procedure

The 1-DOF design approach proposed here is simply based on extending the Normalized Coprime Factor Design Procedure covered in Chapter 3 to the IMC scheme. The configuration used for the 1-DOF IMC design is shown schematically if Figure 5.14. It should be noted that in the design process:

1) The real plant G_p is equal to the plant model G_m.

2) G_m is pre- and/or post-multiplied by frequency-dependent weights W_1 and/or W_2, resectively, for the purpose of loop-shaping, that is $G_{m_s} = W_2 G_m W_1$.

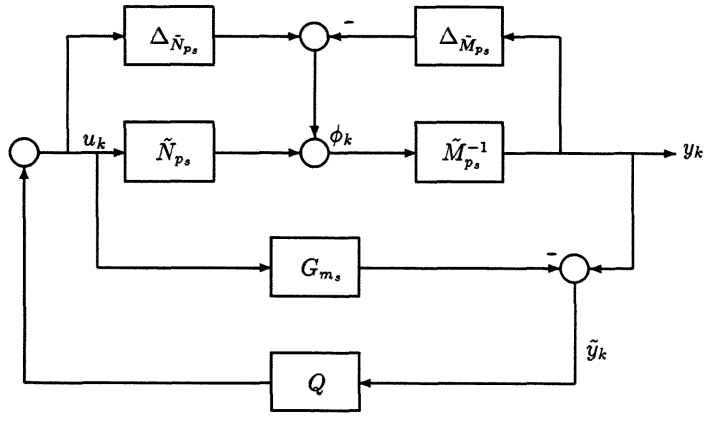

Figure 5.14: 1-DOF IMC Design Configuration.

The IMC design objective is to robustly stabilize the IMC scheme shown in Figure 5.14. This is possible if, and only if, (G_{p_s}, Q) is internally stable and

$$\left\| \begin{bmatrix} Q\tilde{M}_{p_s}^{-1} \\ (I + G_{p_s}Q)\tilde{M}_{p_s}^{-1} \end{bmatrix} \right\|_\infty \leq \gamma \tag{5.62}$$

Simple algebra from Figure 5.14 shows that

$$\begin{bmatrix} u_k \\ y_k \end{bmatrix} = \begin{bmatrix} Q\tilde{M}_{p_s}^{-1} \\ (I + G_{p_s}Q)\tilde{M}_{p_s}^{-1} \end{bmatrix} \phi_k \tag{5.63}$$

The 1-DOF IMC controller Q can be interpreted as $K(I-G_{p_s}K)^{-1}$, as shown in Section 5.2. Setting the problem up in the standard regulator framework gives

$$\begin{bmatrix} u_k \\ y_k \\ \tilde{y}_k \end{bmatrix} = \begin{bmatrix} P_{imc_{11}} & P_{imc_{12}} \\ P_{imc_{21}} & P_{imc_{22}} \end{bmatrix} \begin{bmatrix} \phi_k \\ u_k \end{bmatrix} = \begin{bmatrix} 0 & I \\ \tilde{M}_{p_s}^{-1} & G_{p_s} \\ \tilde{M}_{p_s}^{-1} & G_{p_s} - G_{m_s} \end{bmatrix} \begin{bmatrix} \phi_k \\ u_k \end{bmatrix} \tag{5.64}$$

which by defining

$$G_{p_s} \stackrel{s}{=} \left[\begin{array}{c|c} A_{p_s} & B_{p_s} \\ \hline C_{p_s} & 0 \end{array}\right] \text{ and } G_{m_s} \stackrel{s}{=} \left[\begin{array}{c|c} A_{m_s} & B_{m_s} \\ \hline C_{m_s} & 0 \end{array}\right] \tag{5.65}$$

gives the following realization for P_{imc}

$$P_{imc} \stackrel{s}{=} \left[\begin{array}{c||c|c} A & B_1 & B_2 \\ \hline\hline C_1 & D_{11} & D_{12} \\ \hline C_2 & D_{21} & D_{22} \end{array}\right] = \left[\begin{array}{cc||c|c} A_{p_s} & 0_{n\times n} & -HZ_2^{-1} & B_{p_s} \\ 0_{n\times n} & A_{m_s} & 0_{n\times m} & B_{m_s} \\ \hline\hline 0_{m\times n} & 0_{m\times n} & 0_{m\times m} & I_{r\times r} \\ C_{p_s} & 0_{m\times n} & Z_2^{-1} & 0_{m\times r} \\ \hline C_{p_s} & -C_{m_s} & Z_2^{-1} & D_{p_s} - D_{m_s} \end{array}\right] \tag{5.66}$$

The model $(A_{m_s}, B_{m_s}, C_{m_s})$ with dimensions $n \times n$, $n \times r$ and $m \times n$, respectively, may be replaced by $(A_{p_s}, B_{p_s}, C_{p_s})$, since $G_{p_s} = G_{m_s}$ by assumption.

5.4.3 Controller Formulae

Suboptimal and optimal IMC controllers will now be realized providing some level of robust stability with respect to uncertainty of normalized left coprime factor plant description.

Suboptimal Controllers

A generator of all controllers achieving

$$\left\| \begin{bmatrix} Q\tilde{M}_{p_s}^{-1} \\ (I + G_{p_s}Q)\tilde{M}_{p_s}^{-1} \end{bmatrix} \right\|_\infty < \gamma \tag{5.67}$$

where $\gamma > \gamma_o$ of (3.55) can be obtained directly from the game theoretic formulae for suboptimal discrete-time $\mathcal{H}^\infty$ controllers derived in [58, 107]. A state-space realization of the central suboptimal controller for the 1-DOF control configuration under consideration will now be derived. We start with the following theorem.

Theorem 5.4.1 For the standardized plant described by (5.66) and satisfying assumptions A1, A2, A4 and A6 with D_{21} square, we have the following results:

1) There exist an internally stabilizing suboptimal IMC controller $Q(z)$ such that $\| \mathcal{F}_l(P_{imc}, Q) \|_\infty < \gamma$ if, and only if,

   i) $\gamma > \gamma_o$.

   ii) $-\gamma^2 I + B_1^T X_\infty B_1 + D_{11}^T D_{11} - B_1^T X_\infty B_2 (I + B_2^T X_\infty B_2)^{-1} B_2^T X_\infty B_1 < 0$
   where
   $X_\infty = X_\infty^T \geq 0$ satisfies (3.11).

2) When the conditions of part (1) are satisfied, the internally stabilizing suboptimal IMC controller $Q(z)$ satisfying $\| \mathcal{F}_l(P_{imc}, Q) \|_\infty < \gamma$ has the following state-space realization $\left[\begin{array}{c|c} A_q & B_q \\ \hline C_q & D_q \end{array}\right]$ where

$$A_q = \left[\begin{array}{c|c} O_{BX_{11}} A_{p_s} O_{PC} & O_{BX_{11}} A_{p_s} O_{PC} P C_{p_s}^T C_{p_s} \\ \hline -B_{p_s} B_{p_s}^T X_{\infty_{11}} O_{BX_{11}} A_{p_s} O_{PC} & -B_{p_s} B_{p_s}^T X_{\infty_{11}} O_{BX_{11}} A_{p_s} O_{PC} P C_{p_s}^T C_{p_s} + A_{p_s} \end{array}\right] \tag{5.68}$$

$$B_q = \left[\begin{array}{c} O_{BX_{11}} A_{p_s} O_{PC} P C_{p_s}^T \\ \hline -B_{p_s} B_{p_s}^T X_{\infty_{11}} O_{BX_{11}} A_{p_s} O_{PC} P C_{p_s}^T \end{array}\right] \tag{5.69}$$

$$C_q = \left[\begin{array}{c|c} -B_{p_s}^T X_{\infty_{11}} O_{BX_{11}} A_{p_s} O_{PC} & -B_{p_s}^T X_{\infty_{11}} O_{BX_{11}} A_{p_s} O_{PC} P C_{p_s}^T C_{p_s} \end{array}\right] \tag{5.70}$$

and

$$D_q = -B_{p_s}^T X_{\infty_{11}} \left(I + B_{p_s} B_{p_s}^T X_{\infty_{11}}\right)^{-1} A_{p_s} \left(I + P C_{p_s}^T C_{p_s}\right)^{-1} P C_{p_s}^T \tag{5.71}$$

where $O_{BX_{11}} = \left(I + B_{p_s} B_{p_s}^T X_{\infty_{11}}\right)^{-1}$ and $O_{PC} = \left(I + P C_{p_s}^T C_{p_s}\right)^{-1}$.

Proof

Part 1 (i) and Part 1 (ii) where proven in Theorem 3.3.1.

Part 2 : The solution X_∞ of the discrete Riccati equation can be partitioned conformally with

$$A = \left[\begin{array}{c|c} A_{p_s} & 0 \\ \hline 0 & A_{p_s} \end{array}\right], \text{ that is } X_\infty = \left[\begin{array}{c|c} X_{\infty_{11}} & X_{\infty_{12}} \\ \hline X_{\infty_{12}}^T & X_{\infty_{22}} \end{array}\right].$$

Conjecture 5.4.1 It is noted, after many computational observations, that $X_{\infty_{12}} = 0$ and $X_{\infty_{22}} = 0$ are both solutions, and the solution X_∞ can be partitioned conformally as $X_\infty = \left[\begin{array}{c|c} X_{\infty_{11}} & 0 \\ \hline 0 & 0 \end{array}\right]$. ■

Following similar steps as in the proof of Part 2 of Theorem 3.3.1, equations (5.68) to (5.71) can be easily derived. ■

Optimal Controller

The controller realization (5.68) to (5.71) becomes degenerate as γ approaches the optimal value of (3.55). This is accompanied by $X_{\infty_{11}}$ being unbounded in the limit. Since

$$X_{\infty_{11}} = \gamma^2 Q(\gamma^2 - 1) - PQ)^{-1} \tag{5.72}$$

the controller dynamics become after substituting (5.72) in (5.68) to (5.71) and following similar steps as in Section 3.3.2, the reduced-state-order central optimal IMC controller will have a state-space realization given by $\left[\begin{array}{c|c} A_{q_r} & B_{q_r} \\ \hline C_{q_r} & D_{q_r} \end{array}\right]$ where

$$A_{q_r} = \left[\begin{array}{c|c} \Sigma V_1^T R^{-1} A_{p_s} O_{PC} U_1 & \Sigma V_1^T R^{-1} A_{p_s} O_{PC} P C_{p_s}^T C_{p_s} \\ \hline -\gamma_o^2 B_{p_s} B_{p_s}^T Q R^{-1} A_{p_s} O_{PC} U_1 & -\gamma_o^2 B_{p_s} B_{p_s}^T Q R^{-1} A_{p_s} O_{PC} P C_{p_s}^T C_{p_s} + A_{p_s} \end{array}\right] \tag{5.73}$$

$$B_{q_r} = \left[\begin{array}{c} \Sigma V_1^T R^{-1} A_{p_s} O_{PC} P C_{p_s}^T \\ \hline -\gamma_o^2 B_{p_s} B_{p_s}^T Q R^{-1} A_{p_s} O_{PC} P C_{p_s}^T \end{array}\right] \tag{5.74}$$

$$C_{q_r} = \left[\begin{array}{c|c} -\gamma_o^2 B_{p_s}^T Q R^{-1} A_{p_s} O_{PC} U_1 & -\gamma_o^2 B_{p_s}^T Q R^{-1} A_{p_s} O_{PC} P C_{p_s}^T C_{p_s} \end{array}\right] \tag{5.75}$$

and

$$D_{q_r} = -\gamma_o^2 B_{p_s}^T Q R^{-1} A_{p_s} O_{PC} P C_{p_s}^T \tag{5.76}$$

5.5 An $\mathcal{H}^\infty$ 2-DOF Design Approach

It is a trivial result that all 1-DOF stabilizing controllers can be generated as a subset of all 2-DOF controllers. So the theory for the class of all stabilizing 1-DOF controllers can be a special case for the class of all 2-DOF controllers [103].

5.5.1 2-DOF Controllers

Consider a nominal plant $\tilde{G}_m$ augmented as

$$\tilde{G}_m = \begin{bmatrix} 0 \\ G_m \end{bmatrix} \tag{5.77}$$

Consider also a coprime factorization in $\mathcal{RH}^\infty$

$$\tilde{G}_m = \begin{bmatrix} 0 \\ N \end{bmatrix} M^{-1} = \begin{bmatrix} I & 0 \\ 0 & \tilde{M}^{-1} \end{bmatrix} \begin{bmatrix} 0 \\ \tilde{N} \end{bmatrix} \tag{5.78}$$

Consider a proper stabilizing 2-DOF controller for (5.77) as

$$K = [K_1 \quad K_2] \tag{5.79}$$

with coprime factorizations in $\mathcal{RH}^\infty$ as

$$K = [0 \quad U] V^{-1} = \begin{bmatrix} I & 0 \\ 0 & \tilde{V}^{-1} \end{bmatrix} [0 \quad \tilde{U}] \tag{5.80}$$

such that the following Bezout identity is satisfied

$$\begin{bmatrix} V & 0 & U \\ 0 & I & 0 \\ -\tilde{N} & 0 & \tilde{M} \end{bmatrix} \begin{bmatrix} M & 0 & -\tilde{U} \\ 0 & I & 0 \\ N & 0 & \tilde{V} \end{bmatrix} = \begin{bmatrix} I & 0 & 0 \\ 0 & I & 0 \\ 0 & 0 & I \end{bmatrix} \tag{5.81}$$

and that

$$K(Q) = -(V + Q\tilde{N})^{-1}(U - Q\tilde{M}) \tag{5.82}$$

is the class of all proper stabilizing 2-DOF controllers for (5.77) characterized in terms of arbitrary

$$Q = [Q_1 \quad Q_2] \in \mathcal{RH}^\infty \tag{5.83}$$

As a consequence, the class of all stabilizing controllers $K(Q)$ of (5.82) for (5.77) can be partitioned as

$$\begin{aligned}[K_1(Q) \quad K_2(Q)] &= -(V+Q\tilde{N})^{-1}\left[[0 \quad U] - [Q_1 \quad Q_2]\begin{bmatrix} I & 0 \\ 0 & \tilde{M} \end{bmatrix}\right] \\ &= [(V+Q_2\tilde{N})^{-1}Q_1 \quad -(V+Q_2\tilde{N})^{-1}(U-Q_2\tilde{M})] \end{aligned} \tag{5.84}$$

If the nominal plant G_m is stable, then one can take $\tilde{N} = G_m$, $\tilde{M} = I$, $U = 0$ and $V = I$. In this case (5.84) simplifies to

$$[K_1(Q) \quad K_2(Q)] = [(I+Q_2G_m)^{-1}Q_1 \quad (I+Q_2G_m)^{-1}Q_2] \tag{5.85}$$

from which the 2-DOF IMC controller is obtained as

$$[Q_1(K) \quad Q_2(K)] = [(I-K_2G_m)^{-1}K_1 \quad (I-K_2G_m)^{-1}K_2] \tag{5.86}$$

and can then be directly implemented as shown previously in Figure 5.7 (except for a sign change, negative-feedback convention was used in Figure 5.7, and positive-feedback convention for the controller is used here).

5.5.2 An IMC Formulation and Controller Synthesis of the 2-DOF Design Approach

The 2-DOF IMC approach proposed here allows the feedback controller and prefilter to be designed together in a single step *via* an $\mathcal{H}^\infty$ optimization framework. The feedback controller is used to meet the robust stability and disturbance rejection specifications, while the prefilter is used to shape the desired time responses of the closed-loop system, that is to force the plant output to follow a reference model.

The configuration used for the 2-DOF design is shown schematically in Figure 5.15, which is the IMC formulation of the 2-DOF design approach. The control signal is given by

$$u_k = [Q_1 \quad Q_2]\begin{bmatrix} r_k \\ \tilde{y}_k \end{bmatrix} \tag{5.87}$$

in which Q_1 and Q_2 are the IMC prefilter and IMC feedback controller, respectively. The signals r_k and $\tilde{y}_k$ are the reference variable and the measured variable, respectively.

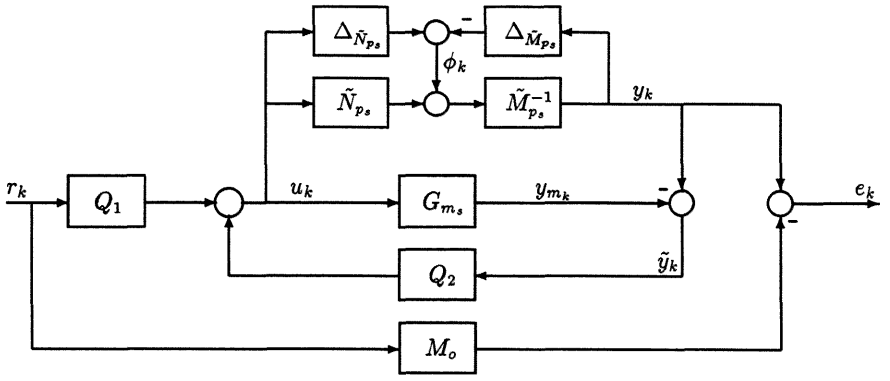

Figure 5.15: 2-DOF IMC Design Configuration.

Using similar arguments to those in Chapter 3, the purpose of the prefilter is to ensure that

$$\| G_{p_s} Q_1 - M_o \|_\infty \leq \gamma \tag{5.88}$$

and the transfer function $M_o(z)$ will also represent some desired closed-loop transfer function explicitly chosen by the designer to introduce time-domain specifications into the design process. Simple algebra from Figure 5.15 shows that

$$\begin{bmatrix} u_k \\ y_k \\ e_k \end{bmatrix} = \begin{bmatrix} Q_1 & Q_2 \tilde{M}_{p_s}^{-1} \\ G_{p_s} Q_1 & (I + G_{p_s} Q_2) \tilde{M}_{p_s}^{-1} \\ G_{p_s} Q_1 - M_o & (I + G_{p_s} Q_2) \tilde{M}_{p_s}^{-1} \end{bmatrix} \begin{bmatrix} r_k \\ \phi_k \end{bmatrix} \tag{5.89}$$

The 2-DOF IMC controller Q_1 and Q_2 can be interpreted as $(I - K_2 G_{p_s})^{-1} K_1$ and $(I - K_2 G_{p_s})^{-1} K_2$, respectively.

Setting the problem up in the standard regulator framework gives

$$\begin{bmatrix} u_k \\ y_k \\ e_k \\ r_k \\ \tilde{y}_k \end{bmatrix} = \begin{bmatrix} P_{imc_{11}} & P_{imc_{12}} \\ P_{imc_{21}} & P_{imc_{22}} \end{bmatrix} \begin{bmatrix} r_k \\ \phi_k \\ u_k \end{bmatrix}$$

$$= \begin{bmatrix} 0 & 0 & I \\ 0 & \tilde{M}_{p_s}^{-1} & G_{p_s} \\ -M_o & \tilde{M}_{p_s}^{-1} & G_{p_s} \\ I & 0 & 0 \\ 0 & \tilde{M}_{p_s}^{-1} & G_{p_s} - G_{m_s} \end{bmatrix} \begin{bmatrix} r_k \\ \phi_k \\ u_k \end{bmatrix} \tag{5.90}$$

Setting

$$M_o \stackrel{s}{=} \left[\begin{array}{c|c} A_o & B_o \\ \hline C_o & 0 \end{array}\right], G_{p_s} \stackrel{s}{=} \left[\begin{array}{c|c} A_{p_s} & B_{p_s} \\ \hline C_{p_s} & 0 \end{array}\right], \text{ and } G_{m_s} \stackrel{s}{=} \left[\begin{array}{c|c} A_{m_s} & B_{m_s} \\ \hline C_{m_s} & 0 \end{array}\right] \tag{5.91}$$

with M_o chosen to be stable and invertible, a state-space realization for (5.90) gives

$$P_{imc} \stackrel{s}{=} \left[\begin{array}{c|c|c} A & B_1 & B_2 \\ \hline C_1 & D_{11} & D_{12} \\ \hline C_2 & D_{21} & D_{22} \end{array}\right] = \left[\begin{array}{ccc||cc|c} A_{p_s} & 0_{n\times n} & 0_{n\times n_o} & 0_{n\times r_o} & -HZ_2^{-1} & B_{p_s} \\ 0_{n\times n} & A_{m_s} & 0_{n\times n_o} & 0_{n\times r_o} & 0_{n\times m} & B_{m_s} \\ 0_{n_o\times n} & 0_{n_o\times n} & A_o & B_o & 0_{n_o\times m} & 0_{n_o\times m} \\ \hline\hline 0_{m\times n} & 0_{m\times n} & 0_{m\times n_o} & 0_{m\times r_o} & 0_{m\times m} & I_{m\times r} \\ C_{p_s} & 0_{m\times n} & 0_{m\times n_o} & 0_{m\times r_o} & Z_2^{-1} & 0_{m\times r} \\ C_{p_s} & 0_{m\times n} & -C_o & 0_{m\times r_o} & Z_2^{-1} & 0_{m\times r} \\ \hline 0_{m\times n} & 0_{m\times n} & 0_{m\times n_o} & I_{r_o\times r_o} & 0_{r_o\times m} & 0_{m\times r} \\ C_{p_s} & -C_{m_s} & 0_{m\times n_o} & 0_{m\times r_o} & Z_2^{-1} & D_{p_s} - D_{m_s} \end{array}\right] \tag{5.92}$$

The model $(A_{m_s}, B_{m_s}, C_{m_s})$ has dimensions $n \times n$, $n \times r$ and $m \times n$, respectively, and the target model (A_o, B_o, C_o) has dimensions $n_o \times n_o$, $n_o \times r_o$ and $m_o \times n_o$, respectively. The states of G_{p_s} or G_{m_s} will be denoted by x_{s_k} and the states of M_o will be denoted by x_{o_k}.

2-DOF IMC Controller Structure

Using similar arguments to those in Chapter 3, a suboptimal full information control law for $[\, P_{imc_{11}} \quad P_{imc_{12}} \,]$ can be incorporated with an observer, since D_{21} is square. A state-space realization of the suboptimal internally stabilizing IMC controller for the 2-DOF control configuration under consideration will now be derived. We start with the following theorem.

Theorem 5.5.1 For the standardized plant described by (5.92) and satisfying assumptions A1, A2, A4 and A6 with D_{21} square, we have the following results:

1) There exists an internally stabilizing suboptimal controller $Q(z)$ such that $\| \mathcal{F}_l(P_{imc}, Q) \|_\infty < \gamma$ if, and only if,

   i) $\gamma > \sqrt{2\ \lambda_{max}\left[(Z_2 Z_2^T)^{-1}\right]}$.

   ii) $-\gamma^2 I + B_1^T X_\infty B_1 + D_{11}^T D_{11} - B_1^T X_\infty B_2 (I + B_2^T X_\infty B_2)^{-1} B_2^T X_\infty B_1 < 0$
   where
   $X_\infty = X_\infty^T \geq 0$ satisfies (3.11).

2) When the conditions of part (1) are satisfied, the internally stabilizing suboptimal controller $Q(z)$ satisfying $\| \mathcal{F}_l(P_{imc}, Q) \|_\infty < \gamma$ has the following equations

$$\begin{aligned}
\hat{x}_{s_{k+1}} &= A_{p_s}\hat{x}_{s_k} - H(\tilde{y}_k - C_{p_s}\hat{x}_{s_k}) + B_{p_s}u_k^* \\
x_{o_{k+1}} &= A_o x_{o_k} + B_o r_k \\
x_{s_{k+1}} &= A_{p_s} x_{s_k} + B_{p_s} u_k^* \\
u_k^* &= O_{p_s} B_{p_s}^T [X_{\infty_{11}}(A_{p_s} + HC_{p_s})\hat{x}_{s_k} + X_{\infty_{13}} A_o x_{o_k} - X_{\infty_{11}} HC_{p_s} x_{s_k} \\
&\quad + X_{\infty_{13}} B_o r_k - X_{\infty_{11}} H\tilde{y}_k] \qquad (5.93)
\end{aligned}$$

where $O_{p_s} = -(I + B_{p_s}^T X_{\infty_{11}} B_{p_s})^{-1}$.

Proof

Part 1 (i) and Part 1 (ii) where proven in Theorem 3.3.2.

Part 2 : The solution X_∞ of the discrete Riccati equation can be partitioned conformally with

$$A = \left[\begin{array}{cc|c} A_{p_s} & 0 & 0 \\ 0 & A_{p_s} & 0 \\ \hline 0 & 0 & A_o \end{array}\right], \text{ that is } X_\infty = \left[\begin{array}{cc|c} X_{\infty_{11}} & X_{\infty_{12}} & X_{\infty_{13}} \\ X_{\infty_{21}} & X_{\infty_{22}} & X_{\infty_{23}} \\ \hline X_{\infty_{31}} & X_{\infty_{32}} & X_{\infty_{33}} \end{array}\right].$$

Conjecture 5.5.1 It is noted, after many computational observations, that $X_{\infty_{12}} = 0$, $X_{\infty_{21}} = 0$, $X_{\infty_{22}} = 0$, $X_{\infty_{23}} = 0$, and $X_{\infty_{32}} = 0$ are all solutions, and the solution X_∞ can be partitioned conformally as $X_\infty = \left[\begin{array}{cc|c} X_{\infty_{11}} & 0 & X_{\infty_{13}} \\ 0 & 0 & 0 \\ \hline X_{\infty_{31}} & 0 & X_{\infty_{33}} \end{array}\right]$. ■

We can thus write from (5.92)

$$B_2^T X_\infty = [\, B_{p_s}^T \quad B_{p_s}^T \quad 0 \,] \begin{bmatrix} X_{\infty_{11}} & 0 & X_{\infty_{13}} \\ 0 & 0 & 0 \\ X_{\infty_{31}} & 0 & X_{\infty_{33}} \end{bmatrix} = [\, B_{p_s}^T X_{\infty_{11}} \quad 0 \quad B_{p_s}^T X_{\infty_{13}} \,] \tag{5.94}$$

and

$$B_2^T X_\infty B_2 = [\, B_{p_s}^T \quad B_{p_s}^T \quad 0 \,] \begin{bmatrix} X_{\infty_{11}} & 0 & X_{\infty_{13}} \\ 0 & 0 & 0 \\ X_{\infty_{31}} & 0 & X_{\infty_{33}} \end{bmatrix} \begin{bmatrix} B_{p_s} \\ B_{p_s} \\ 0 \end{bmatrix} = B_{p_s}^T X_{\infty_{11}} B_{p_s} \tag{5.95}$$

so that (3.64) becomes

$$\begin{aligned} C_q &= -\left(I + B_{p_s}^T X_{\infty_{11}} B_{p_s}\right)^{-1} [\, B_{p_s}^T X_{\infty_{11}} \quad 0 \quad B_{p_s}^T X_{\infty_{13}} \,] \left(A - B_1 D_{21}^{-1} C_2\right) \\ &= -\left(I + B_{p_s}^T X_{\infty_{11}} B_{p_s}\right)^{-1} [\, B_{p_s}^T X_{\infty_{11}} \quad 0 \quad B_{p_s}^T X_{\infty_{13}} \,] \begin{bmatrix} A_{p_s} + HC_{p_s} & HC_{p_s} & 0 \\ 0 & A_{p_s} & 0 \\ 0 & 0 & A_o \end{bmatrix} \\ &= -\left(I + B_{p_s}^T X_{\infty_{11}} B_{p_s}\right)^{-1} [\, B_{p_s}^T X_{\infty_{11}} (A_{p_s} + HC_{p_s}) \quad B_{p_s}^T X_{\infty_{11}} HC_{p_s} \quad B_{p_s}^T X_{\infty_{13}} A_o \,] \\ &= [\, C_{q_{11}} \quad C_{q_{12}} \quad C_{q_{13}} \,] \end{aligned} \tag{5.96}$$

Similarly substituting for $B_2^T X_\infty$ and $B_2^T X_\infty B_2$ from above and for B_1 and D_{21} from (5.92) in (3.65), we get

$$\begin{aligned} D_q &= -\left(I + B_{p_s}^T X_{\infty_{11}} B_{p_s}\right)^{-1} [\, B_{p_s}^T X_{\infty_{11}} \quad 0 \quad B_{p_s}^T X_{\infty_{13}} \,] \begin{bmatrix} 0 & -HZ_2^{-1} \\ 0 & 0 \\ B_o & 0 \end{bmatrix} \begin{bmatrix} I & 0 \\ 0 & Z_2^{-1} \end{bmatrix}^{-1} \\ &= -\left(I + B_{p_s}^T X_{\infty_{11}} B_{p_s}\right)^{-1} [\, B_{p_s}^T X_{\infty_{13}} B_o \quad -B_{p_s}^T X_{\infty_{11}} H \,] \\ &= [\, D_{q_{11}} \quad D_{q_{12}} \,] \end{aligned} \tag{5.97}$$

Using (5.92) and (5.96), (3.67) can be written as

$$\begin{aligned} A_q &= \begin{bmatrix} A_{p_s} + HC_{p_s} & HC_{p_s} & 0 \\ 0 & A_{p_s} & 0 \\ 0 & 0 & A_o \end{bmatrix} + \begin{bmatrix} B_{p_s} \\ B_{p_s} \\ 0 \end{bmatrix} [\, C_{q_{11}} \quad C_{q_{12}} \quad C_{q_{13}} \,] \\ &= \begin{bmatrix} A_{p_s} + HC_{p_s} + B_{p_s} C_{q_{11}} & HC_{p_s} + B_{p_s} C_{q_{12}} & B_{p_s} C_{q_{13}} \\ B_{p_s} C_{q_{11}} & A_{p_s} + B_{p_s} C_{q_{12}} & B_{p_s} C_{q_{13}} \\ 0 & 0 & A_o \end{bmatrix} \end{aligned} \tag{5.98}$$

Similarly for B_q substituting from (5.92) and (5.97) into (3.68), we get

$$\begin{aligned} B_q &= \begin{bmatrix} 0 & -HZ_2^{-1} \\ 0 & 0 \\ B_o & 0 \end{bmatrix} \begin{bmatrix} I & 0 \\ 0 & Z_2^{-1} \end{bmatrix}^{-1} + \begin{bmatrix} B_{p_s} \\ B_{p_s} \\ 0 \end{bmatrix} \begin{bmatrix} D_{q_{11}} & D_{q_{12}} \end{bmatrix} \\ &= \begin{bmatrix} B_{p_s}D_{q_{11}} & -H + B_{p_s}D_{q_{12}} \\ B_{p_s}D_{q_{11}} & B_{p_s}D_{q_{12}} \\ B_o & 0 \end{bmatrix} \end{aligned} \tag{5.99}$$

Using A_q and B_q from above, the IMC controller dynamics, using (3.66), can be written as

$$\begin{aligned} \begin{bmatrix} \hat{x}_{s_{k+1}} \\ x_{s_{k+1}} \\ x_{o_{k+1}} \end{bmatrix} &= \begin{bmatrix} A_{p_s} + HC_{p_s} + B_{p_s}C_{q_{11}} & HC_{p_s} + B_{p_s}C_{q_{12}} & B_{p_s}C_{q_{13}} \\ B_{p_s}C_{q_{11}} & A_{p_s} + B_{p_s}C_{q_{12}} & B_{p_s}C_{q_{13}} \\ 0 & 0 & A_o \end{bmatrix} \begin{bmatrix} \hat{x}_{s_k} \\ x_{s_k} \\ x_{o_k} \end{bmatrix} \\ &\quad + \begin{bmatrix} B_{p_s}D_{q_{11}} & -H + B_{p_s}D_{q_{12}} \\ B_{p_s}D_{q_{11}} & B_{p_s}D_{q_{12}} \\ B_o & 0 \end{bmatrix} \begin{bmatrix} r_k \\ \tilde{y}_k \end{bmatrix} \end{aligned} \tag{5.100}$$

where we have split the controller state vector into the estimated state $\hat{x}_{s_k}$ of the shaped plant G_{p_s}, the state x_{s_k} of the shaped plant G_{p_s}, and the state x_{o_k} of the reference model M_o. Equation (5.100) may be re-written as

$$\begin{aligned} \begin{bmatrix} \hat{x}_{s_{k+1}} \\ x_{s_{k+1}} \\ x_{o_{k+1}} \end{bmatrix} &= \begin{bmatrix} A_{p_s} + HC_{p_s} & HC_{p_s} & 0 \\ 0 & A_{p_s} & 0 \\ 0 & 0 & A_o \end{bmatrix} \begin{bmatrix} \hat{x}_{s_k} \\ x_{s_k} \\ x_{o_k} \end{bmatrix} \\ &\quad + \begin{bmatrix} B_{p_s} & B_{p_s}D_{q_{11}} & -H + B_{p_s}D_{q_{12}} \\ B_{p_s} & B_{p_s}D_{q_{11}} & B_{p_s}D_{q_{12}} \\ 0 & B_o & 0 \end{bmatrix} \begin{bmatrix} u_k^* \\ r_k \\ \tilde{y}_k \end{bmatrix} \end{aligned} \tag{5.101}$$

where the controller output equation u_k^* from (3.63) can be written as

$$u_k^* = \begin{bmatrix} C_{q_{11}} & C_{q_{12}} & C_{q_{13}} \end{bmatrix} \begin{bmatrix} \hat{x}_{s_k} \\ x_{s_k} \\ x_{o_k} \end{bmatrix} + \begin{bmatrix} D_{q_{11}} & D_{q_{12}} \end{bmatrix} \begin{bmatrix} r_k \\ \tilde{y}_k \end{bmatrix} \tag{5.102}$$

(5.101) and (5.102) give a state-space realization of the suboptimal IMC controller that is stabilizing and norm-bounding for the generalized plant of (5.92). This completes the proof. ■

The overall structure of the 2-DOF IMC controller is depicted in Figure 5.16.

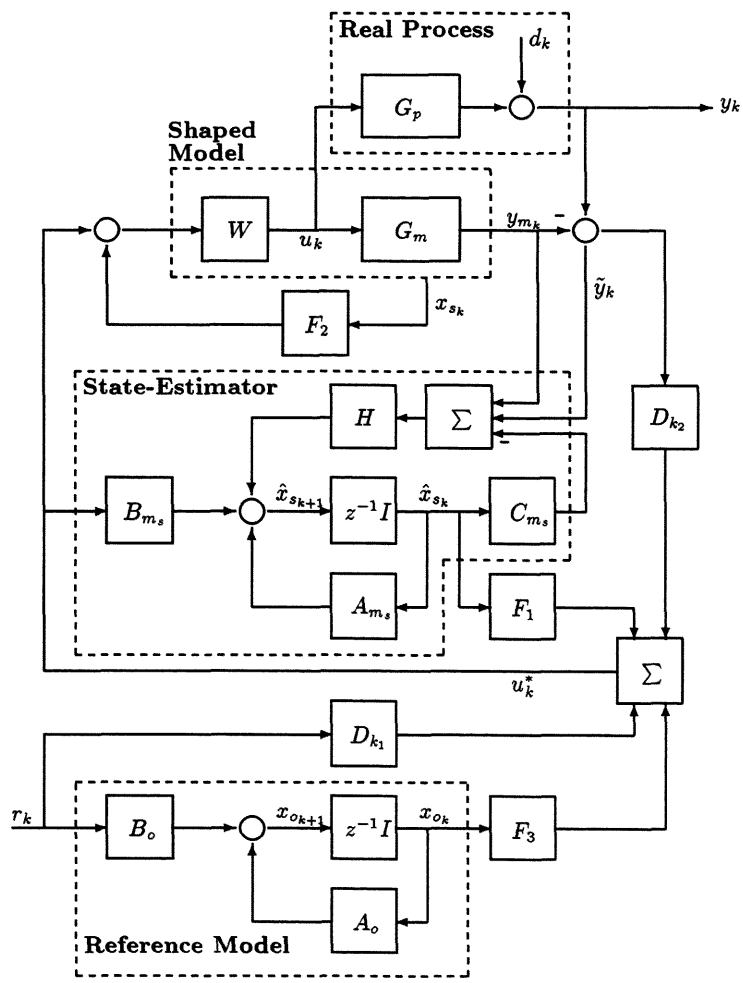

Figure 5.16: 2-DOF Controller Structure.

5.6 Summary

In this chapter, it was shown that for the IMC scheme all nominal criteria will lead to a model matching problem, and methods for directly synthesizing robust IMC controllers in an $\mathcal{H}^\infty$ setting were formulated. These include, for the 1-DOF case, the weighted

1-block, 2-block and 4-block problems together with the normalized left coprime factor design procedure. For the latter, explicit state-space formulae representing the IMC suboptimal and optimal controllers have been derived.

For the 2-DOF case, the principle of explicit model following and the coprime factor design framework have been used to synthesize a 2-DOF IMC controller. As in the 1-DOF case, explicit state-space formulae representing the IMC controller have been derived. This 2-DOF IMC controller which achieves robust stability and model following requires the solution to one Riccati equation and its final structure consists of a combined observer/state-feedback coupled with an explicit model. This controller will be designed, in a later chapter, for a MIMO industrial problem (a glass tube production process).

Chapter 6

A Direct Approach to Discrete-Time Model Reduction

6.1 Introduction

This chapter is concerned with discrete-time model reduction *via* order-reduction of a discrete-time coprime factor representation of a given model or controller. Balanced singular perturbational approximation will be considered rather than balanced truncation for reasons to be explained later in the chapter. Numerical issues will also be considered.

For discrete-time systems, balanced representations were first introduced in [68, 69] for the synthesis of minimum round-off noise, fixed point digital filters, where the problem of finding optimal word length to compromise between storage and quantization efficiencies was considered. In control systems terminology, storage and quantization effects correspond to controllability and observability properties, respectively. The best trade-off between high controllability with low observability and low controllability with high observability is provided by internally balanced representations. The states of such representations are balanced between controllability and observability. Thus they represent a convenient structure for model reduction since those states having weak controllability and observability can be neglected without causing any imbalance in controllability or observability properties of the remaining states.

Until now, most model-reduction techniques applied to discrete-time plants are ap-

proached indirectly by mapping the discrete-time model to the continuous-time domain *via* the bilinear transformation discussed in Chapter 1. Also, most techniques that require balancing are strictly limited to stable and minimal systems. Moreover, balancing is intrinsically badly conditioned for systems with nearly uncontrollable and/or nearly unobservable modes. The model-reduction approach presented here can be used directly to balance and residualize, *via* singular perturbational approximation, a non-minimal stable/unstable discrete-time plant. A model-reduction method suggested by [100, 97] can directly be used to compute a balanced singular perturbational approximation starting with either minimal or non-minimal discrete-time systems.

High-order discrete-time controllers are normally synthesized using the IMC approach presented in Chapter 5 and the robust design methods presented in Chapters 2 & 3. This is a major disadvantage for designing $\mathcal{H}^\infty$ based controllers. The aim of this chapter is to propose a discrete-time model reduction approach in order to alleviate the problem of implementing unnecessarily high-order controllers. This approach combines the algorithm of [56] for computing state-space balancing transformations directly from the state-space realization, and the algorithm of [45] for computing the solution of the real discrete-time non-negative definite Lyapunov equation. The combination of both algorithms results in a reliable method with enhanced numerical robustness for computing a balanced singular perturbational approximation of a stable state-space system that may be arbitrarily close to being unobservable and/or uncontrollable. The algorithms can then be enhanced in the normalized coprime factor model-reduction procedure of [63] which extends system balancing and truncation to unstable plants, giving a more reliable and powerful discrete-time model reduction approach that is capable of producing, in a direct manner, a good reduced-order discrete-time model.

The organization of this chapter is as follow. Preliminaries which include system balancing and discrete-time model reduction are briefly introduced in Section 6.2. Section 6.3 describes the state-space balancing transformation and the solution of the Lyapunov equation for the Cholesky factor. Section 6.4 describes the coprime factor model reduction procedure with main results extended to discrete-time systems, together with the proposed direct discrete-time model reduction algorithm, and Section 6.5 demonstrates the proposed algorithm on two industrial examples. Finally, a summary is given in

Section 6.6.

6.2 Discrete-Time Model Reduction

Consider a stable discrete-time system given by

$$\begin{aligned} x_{k+1} &= Ax_k + Bu_k \\ y_k &= Cx_k \end{aligned} \tag{6.1}$$

where A is $n \times n$, B is $n \times m$, and C is $p \times n$. The pair (A, B) and (C, A) are assumed to be controllable and observable, respectively. The associated controllability and observability Grammians of the system are

$$W_c = \sum_{k=0}^{\infty} A^k B B^T (A^k)^T \tag{6.2}$$

$$W_o = \sum_{k=0}^{\infty} (A^k)^T C^T C A^k \tag{6.3}$$

The system balancing is based upon the simultaneous diagonalization of the positive definite Grammians which is done by using a suitably chosen state similarity transformation [65]. Applying a non-singular transformation $x_k = T\hat{x}_k$, the system will be transformed to

$$\begin{aligned} \hat{x}_{k+1} &= \hat{A}\hat{x}_k + \hat{B}u_k \\ y_k &= \hat{C}\hat{x}_k \end{aligned} \tag{6.4}$$

where $\hat{A} = T^{-1}AT$, $\hat{B} = T^{-1}B$ and $\hat{C} = CT$. The corresponding Grammians of the transformed system are expressed as $\hat{W}_c = T^{-1}W_c(T^{-1})^T$ and $\hat{W}_o = T^T W_o T$. The eigenvalues of the matrix A are invariant under similarity transformation, but the eigenvalues of W_c and W_o are not. The transformation $x_k = T\hat{x}_k$ for which the matrices $\hat{W}_c$ and $\hat{W}_o$ are both diagonal is called a contragradient transformation. Since the matrix W_c is symmetric and positive definite, it may be reduced to

$$V_c^T W_c V_c = \Sigma_c^2 \tag{6.5}$$

where V_c is an orthogonal matrix and Σ_c is a diagonal matrix with positive entries, and because of the positive definiteness of the matrix

$$(V_c\Sigma_c)^T W_o (V_c\Sigma_c) \tag{6.6}$$

it is possible to find another orthogonal matrix U such that

$$U^T(V_c\Sigma_c)^T W_o(V_c\Sigma_c)U = \Sigma^2 \tag{6.7}$$

where Σ is a diagonal matrix with positive entries. Now it is easy to check that the expression

$$T_l = V_c\Sigma_c U\Sigma^{-l} \tag{6.8}$$

defines a family of contragradient transformations with

$$\begin{aligned} T_l^{-1}W_c(T_l^{-1})^T &= \Sigma^{2l} \\ T_l^T W_o T_l &= \Sigma^{2-2l} \end{aligned} \tag{6.9}$$

The diagonal elements of Σ are the positive square roots of the eigenvalues of the product W_cW_o since

$$T_l^{-1}W_cW_oT_l = \Sigma^2 \tag{6.10}$$

These elements are referred to as second-order modes and they are invariant under state similarity transformations.

The following three values of l, namely $l = 0, \frac{1}{2}$ and 1 are of special interest and correspond to:

$$\begin{array}{lllll} l = 0 & \hat{W}_c = I & \hat{W}_o = \Sigma^2 & \rightarrow & \text{input-normal coordinates} \\ l = \frac{1}{2} & \hat{W}_c = \Sigma & \hat{W}_o = \Sigma & \rightarrow & \text{internally balanced coordinates} \\ l = 1 & \hat{W}_c = \Sigma^2 & \hat{W}_o = I & \rightarrow & \text{output-normal coordinates} \end{array}$$

The most interesting of these is the contragradient transformation for $l = \frac{1}{2}$. The diagonal elements of Σ are called the Hankel singular values.

Let $\tilde{\sigma}_i$ be the Hankel singular values of the controllability and observability Grammian Σ. It is assumed that the state variables have been permuted so that $\tilde{\sigma}_{i+1} \leq \tilde{\sigma}_i$, $i = 1, \ldots, n-1$ and that the Grammian Σ of dimension $n \times n$ is partitioned in the format $\Sigma = \begin{bmatrix} \Sigma_1 & 0 \\ 0 & \Sigma_2 \end{bmatrix}$ where Σ_1 and Σ_2 are diagonal matrices of dimensions $r \times r$ and $n-r \times n-r$,

respectively. Then the balanced system can be partitioned as

$$\begin{bmatrix} x_1 \\ x_2 \end{bmatrix}_{k+1} = \begin{bmatrix} A_{11} & A_{12} \\ A_{21} & A_{22} \end{bmatrix} \begin{bmatrix} x_1 \\ x_2 \end{bmatrix}_k + \begin{bmatrix} B_1 \\ B_2 \end{bmatrix} u_k$$
$$y_k = [C_1 \quad C_2] \begin{bmatrix} x_1 \\ x_2 \end{bmatrix}_k \tag{6.11}$$

where A_{11}, is $r \times r$. Let u_1 and u_2 be the minimum norm ($\mathcal{L}^2$-norm) functions that drive the state from the origin to $[(x_1^T(\infty))_k \quad 0)]^T$ and $[0 \quad (x_2^T(\infty))_k]^T$, respectively, in the time interval $[0, \infty]$. It was shown in [65] that

$$\frac{\| u_2 \|_2}{\| u_1 \|_2} \geq \frac{\tilde{\sigma}_r}{\tilde{\sigma}_{r+1}} \frac{\| (x_2(\infty))_k \|_2}{\| (x_1(\infty))_k \|_2} \tag{6.12}$$

If $\tilde{\sigma}_r \gg \tilde{\sigma}_{r+1}$ and u_1 and u_2 have the same norms, it follows that

$$\| (x_2(\infty))_k \|_2 \ll \| (x_1(\infty))_k \|_2 \tag{6.13}$$

In other words, the part $(x_2)_k$ of the state is much less affected by the input than the part $(x_1)_k$.

Similarly, let y_1 and y_2 be the zero input responses of the outputs from the initial conditions $[(x_1^T(0))_k \quad 0]^T$ and $[0 \quad (x_2^T(0))_k]^T$, respectively. Then

$$\| y_2 \|_2 \ll \| y_1 \|_2 \tag{6.14}$$

if $\tilde{\sigma}_r \gg \tilde{\sigma}_{r+1}$ and $\| (x_1(0))_k \|_2 = \| (x_2(0))_k \|_2$. This means that the $(x_2)_k$ part of the state affects the output much less than the $(x_1)_k$ part.

It seems reasonable to assume that the $(x_2)_k$ part of the state does not affect the input-output behaviour of the system very much if $\tilde{\sigma}_{r+1} \ll \tilde{\sigma}_r$. This observation suggests that the subsystem $\{A_{11}, B_1, C_1\}$ be called the strong subsystem and the subsystem $\{A_{22}, B_2, C_2\}$ be called the weak subsystem. However, it was emphasised in [28] that the subsystems $\{A_{ii}, B_i, C_i\}$, $i = 1, 2$ are not internally balanced, as in the case of the continuous-time counterpart, and the submatrices Σ_i, $i = 1, 2$ are not balanced Grammians of the subsystems. These conditions prevent the direct extension of the continuous-time results of [65] to discrete-time systems. A good low-order approximation of the original system can be represented, as suggested in [28], by the singular

perturbational low-order approximation $\{\hat{A}, \hat{B}, \hat{C}, \hat{D}\}$, with

$$\begin{aligned} \hat{A} &= A_{11} + A_{12}(I - A_{22})^{-1}A_{21} \\ \hat{B} &= B_1 + A_{12}(I - A_{22})^{-1}B_2 \\ \hat{C} &= C_1 + C_2(I - A_{22})^{-1}A_{21} \\ \hat{D} &= C_2(I - A_{22})^{-1}B_2 \end{aligned} \tag{6.15}$$

Lemma 6.2.1 Let $G(z) = C(zI-A)^{-1}B$ be asymptotically stable and minimal with n-states. Let $G(z)$ be in balanced coordinates with the following balanced Grammian $\Sigma = \mathbf{diag}(\tilde{\sigma}_1, \tilde{\sigma}_2, ..., \tilde{\sigma}_n)$ and Hankel singular values $\tilde{\sigma}_1 \geq \tilde{\sigma}_2 \geq ... \geq \tilde{\sigma}_n > 0$. Let $r < n$ and partition $\Sigma = \mathbf{diag}(\Sigma_1, \Sigma_2)$, where $\Sigma_1 = \mathbf{diag}(\tilde{\sigma}_1, ..., \tilde{\sigma}_r)$ and $\Sigma_2 = \mathbf{diag}(\tilde{\sigma}_{r+1}, ..., \tilde{\sigma}_n)$. Let $G_{DT}(z) = C_1(zI-A_{11})^{-1}B_1$ be the r-state reduced order model obtained by directly truncating the balanced realization of $G(z)$ to r states. Let $G_{SPA}(z) = \hat{C}(zI-\hat{A})^{-1}\hat{B}+\hat{D}$ be the r-state reduced order model obtained by singular perturbational approximation of the balanced realization of $G(z)$. Let $G_{SPA_n}(z) = \hat{C}(zI - \hat{A})^{-1}\hat{B}$ be another r-state reduced order model obtained by the singular perturbational approximation of the balanced realization of $G(z)$. Then

1) $G_{DT}(z)$ is not in balanced coordinates, [84, 28].

2) $G_{SPA}(z)$ is in balanced coordinates with balanced Grammian Σ_1, [28].

3) If $\tilde{\sigma}_r > \tilde{\sigma}_{r+1}$ then $G_{DT}(z)$ is asymptotically stable and minimal, [84].

4) If $\tilde{\sigma}_r > \tilde{\sigma}_{r+1}$ then $G_{SPA}(z)$ is asymptotically stable and minimal, [28].

5) $\| G(z) - G_{DT}(z) \|_\infty \leq 2\ \mathbf{tr}[\Sigma_2]$, [1].

6) $\| G(z) - G_{SPA}(z) \|_\infty \leq 2\ \mathbf{tr}[\Sigma_2]$, [1, 59].

7) $\| G(z) - G_{SPA_n}(z) \|_\infty \leq 4\ \mathbf{tr}[\Sigma_2]$, [1, 59].

8) $\| G(z) \|_\infty < 2\ \mathbf{tr}[\Sigma]$, [1].

9) If $G(z)$ is **coinner (inner)**, then $G_{SPA}(z)$ is also **coinner (inner)**, [101].

■

An indirect approach to reduce a discrete-time model is as follows [2]:

1) The discrete-time state-space system $\{A, B, C\}$ is mapped to the continuous-time state-space system $\{\tilde{E}, \tilde{F}, \tilde{G}, \tilde{H}\}$ using the bilinear transformation with

$$\begin{aligned} \tilde{E} &= (I+A)^{-1}(A-I) \\ \tilde{F} &= \sqrt{2}(I+A)^{-1}B \\ \tilde{G} &= \sqrt{2}C(I+A)^{-1} \\ \tilde{H} &= -C(I+A)^{-1}B \end{aligned} \tag{6.16}$$

2) The continuous-time state-space system $\{\tilde{E}, \tilde{F}, \tilde{G}, \tilde{H}\}$ is transformed into a balanced state-space system $\{E, F, G, \tilde{H}\}$. This realization is a balanced realization with the same observability and controllability Grammians as its corresponding balanced discrete-time state-space system [36]. As a consequence both realizations have the same Hankel singular values and the same McMillan degree.

3) The ordered balanced realization is then partitioned as

$$\begin{aligned} \begin{bmatrix} \dot{x_1} \\ \dot{x_2} \end{bmatrix} &= \begin{bmatrix} E_{11} & E_{12} \\ E_{21} & E_{22} \end{bmatrix} \begin{bmatrix} x_1 \\ x_2 \end{bmatrix} + \begin{bmatrix} F_1 \\ F_2 \end{bmatrix} u \\ y &= \begin{bmatrix} G_1 & G_2 \end{bmatrix} \begin{bmatrix} x_1 \\ x_2 \end{bmatrix} + \tilde{H}u \end{aligned} \tag{6.17}$$

4) The reduced-order continuous-time state-space system is then mapped to the discrete-time system $\{\hat{A}, \hat{B}, \hat{C}, \hat{D}\}$ using the bilinear transformation. The corresponding balanced reduced-order discrete-time system is obtained (see Appendix B) with

$$\begin{array}{rcccl} \hat{A} &=& (I+E_{11})(I-E_{11})^{-1} &=& \hat{A}_{11} - \hat{A}_{12}(I+\hat{A}_{22})^{-1}\hat{A}_{21} \\ \hat{B} &=& \sqrt{2}(I-E_{11})^{-1}F_1 &=& \hat{B}_1 - \hat{A}_{12}(I+\hat{A}_{22})^{-1}\hat{B}_2 \\ \hat{C} &=& \sqrt{2}G_1(I-E_{11})^{-1} &=& \hat{C}_1 - \hat{C}_2(I+\hat{A}_{22})^{-1}\hat{A}_{21} \\ \hat{D} &=& \tilde{H} - G_1(I-E_{11})^{-1}F_1 &=& \hat{D} - \hat{C}_2(I+\hat{A}_{22})^{-1}\hat{B}_2 \end{array} \tag{6.18}$$

5) To guarantee that the DC gain of the reduced-model will be right, the obtained balanced continuous-time state-space system $\{E, F, G, \tilde{H}\}$ is approximated *via*

singular perturbational low-order approximation as follows

$$\begin{aligned}\hat{E} &= \hat{E}_{11} - \hat{E}_{12}\hat{E}_{22}^{-1}\hat{E}_{21} \\ \hat{F} &= \hat{F}_1 - \hat{E}_{12}\hat{E}_{22}^{-1}\hat{F}_2 \\ \hat{G} &= \hat{G}_1 - \hat{G}_2\hat{E}_{22}^{-1}\hat{E}_{21} \\ \hat{H} &= \tilde{H} - \hat{G}_2\hat{E}_{22}^{-1}\hat{F}_2 \end{aligned} \tag{6.19}$$

The corresponding reduced-order discrete-time system $\{\hat{A}, \hat{B}, \hat{C}, \hat{D}\}$ is then obtained using the bilinear transformation which in fact has the following singular perturbational low-order approximation structure (see Appendix B)

$$\begin{aligned}\hat{A} &= \hat{A}_{11} + \hat{A}_{12}(I - \hat{A}_{22})^{-1}\hat{A}_{21} \\ \hat{B} &= \hat{B}_1 + \hat{A}_{12}(I - \hat{A}_{22})^{-1}\hat{B}_2 \\ \hat{C} &= \hat{C}_1 + \hat{C}_2(I - \hat{A}_{22})^{-1}\hat{A}_{21} \\ \hat{D} &= \tilde{H} + \hat{C}_2(I - \hat{A}_{22})^{-1}\hat{B}_2 \end{aligned} \tag{6.20}$$

Lemma 6.2.2 Let $G(z) = C(zI-A)^{-1}B+D$ be a balanced system with a low frequency gain expressed by (letting $z = 1$) $L_{gain} = C(I - A)^{-1}B + D$, and a high frequency gain expressed by (letting $z = -1$) $H_{gain} = -C(I + A)^{-1}B + D$. Then

1) The reduced discrete-time system given in step 5 will always retain the low frequency gain.

2) The reduced discrete-time system given in step 4 will always retain the high frequency gain.

Proof

$L_{gain} = C(I - A)^{-1}B + D$ can be rewritten as

$$\begin{aligned} &= [C_1 \quad C_2]\begin{bmatrix} I - A_{11} & -A_{12} \\ -A_{21} & I - A_{22} \end{bmatrix}^{-1}\begin{bmatrix} B_1 \\ B_2 \end{bmatrix} + D \\ &= [C_1 \quad C_2]\begin{bmatrix} I & 0 \\ (I - A_{22})^{-1}A_{21} & I \end{bmatrix}\begin{bmatrix} I & 0 \\ -(I - A_{22})^{-1}A_{21} & I \end{bmatrix}\begin{bmatrix} I - A_{11} & -A_{12} \\ -A_{21} & I - A_{22} \end{bmatrix}^{-1} \\ &\quad \times \begin{bmatrix} I & -A_{12}(I - A_{22})^{-1} \\ 0 & I \end{bmatrix}\begin{bmatrix} I & A_{12}(I - A_{22})^{-1} \\ 0 & I \end{bmatrix}\begin{bmatrix} B_1 \\ B_2 \end{bmatrix} + D \end{aligned}$$

$$
\begin{aligned}
&= [C_1 + C_2(I-A_{22})^{-1}A_{21} \quad C_2]\left[\begin{bmatrix} I & A_{12}(I-A_{22})^{-1} \\ 0 & I \end{bmatrix}\begin{bmatrix} I-A_{11} & -A_{12} \\ -A_{21} & I-A_{22} \end{bmatrix}\right. \\
&\quad \left.\times \begin{bmatrix} I & 0 \\ (I-A_{22})^{-1}A_{21} & I \end{bmatrix}\right]^{-1}\begin{bmatrix} B_1 + A_{12}(I-A_{22})^{-1}B_2 \\ B_2 \end{bmatrix} + D \\
&= [C_r \quad C_2]\begin{bmatrix} I-(A_{11}+A_{12}(I-A_{22})^{-1}A_{21}) & 0 \\ 0 & (I-A_{22}) \end{bmatrix}^{-1}\begin{bmatrix} B_r \\ B_2 \end{bmatrix} + D \\
&= [C_r \quad C_2]\begin{bmatrix} (I-A_r)^{-1} & 0 \\ 0 & (I-A_{22})^{-1} \end{bmatrix}^{-1}\begin{bmatrix} B_r \\ B_2 \end{bmatrix} + D \\
&= C_r(I-A_r)^{-1}B_r + C_2(I-A_{22})^{-1}B_2 + D \\
&= C_r(I-A_r)^{-1}B_r + D_r
\end{aligned}
$$

Part 2 can be proven in a similar manner. This completes the proof. ■

6.3 A State-Space Balancing Transformation

A method for computing a balancing transformation is given as follows [55]:

1) Compute the Grammians from the discrete Lyapunov equations

$$AW_cA^T - W_c = -BB^T \tag{6.21}$$

$$A^TW_oA - W_o = -C^TC \tag{6.22}$$

2) Applying the Cholesky decomposition, the controllability Grammian is represented as

$$W_c = L_cL_c^T \tag{6.23}$$

where L_c is a lower triangular matrix. The observability Grammian is then transformed to the matrix $L_c^TW_oL_c$ which is reduced to the diagonal form

$$V^T(L_c^TW_oL_c)V = \Sigma^2 \tag{6.24}$$

This reduction is done by the QR decomposition method for symmetric matrices. Now it is easy to verify that

$$T = L_cV\Sigma^{-1/2} \tag{6.25}$$

is a balancing transformation such that

$$T^{-1}W_c(T^{-1})^T = T^TW_oT = \Sigma \tag{6.26}$$

3) The matrices of the balanced system are given by

$$\tilde{A} = T^{-1}AT = \Sigma^{1/2}V^T L_c^{-1} A L_c V \Sigma^{-1/2} \quad (6.27)$$

$$\tilde{B} = T^{-1}B = \Sigma^{1/2}V^T L_c^{-1} B \quad (6.28)$$

$$\tilde{C} = CT = C L_c V \Sigma^{-1/2} \quad (6.29)$$

A disadvantage of the above balancing algorithm is that the computation of the Grammian through (6.21) and (6.22) requires the evaluation of the matrices BB^T and C^TC which may not be positive definite due to some rounding errors making the computation of a full rank Cholesky factor impossible. An algorithm suggested by [45] (which will be explained in more detail later) can be applied to circumvent the problem of finding a unique Cholesky factor. The method suggests finding the Cholesky factor of the solution of a Lyapunov equation without explicit determination of the solution. This possibility was exploited in the algorithm of [56] which proceeds in the following way. The decompositions

$$W_c = L_c L_c^T \text{ and } W_o = L_o L_o^T \quad (6.30)$$

are found by the Hammerling algorithm [45], where the matrices W_c and W_o are not actually formed. The Hankel singular values in terms of L_o and L_c are

$$\begin{aligned} \lambda_i^{1/2}(W_o W_c) &= \lambda_i^{1/2}(L_o L_o^T L_c L_c^T) \\ &= \lambda_i^{1/2}((L_o^T L_c)^T (L_o^T L_c)) \\ &= \sigma_i(L_o^T L_c) \end{aligned} \quad (6.31)$$

This shows that the singular values of $L_o^T L_c$ are the positive square roots of the eigenvalues of the product $W_o W_c$, *i.e.* the second-order modes of the system. Using the singular value decomposition of the product $L_o^T L_c$ such that

$$L_o^T L_c = U \Sigma V^T \quad (6.32)$$

the balancing transformation matrix is determined as

$$T = L_c V \Sigma^{-1/2} \text{ and } T^{-1} = \Sigma^{-1/2} U^T L_o^T \quad (6.33)$$

So the new balanced state-space matrices are given by

$$\tilde{A} = T^{-1}AT = \Sigma^{-1/2}U^T L_o^T A L_c V \Sigma^{-1/2} \quad (6.34)$$

$$\tilde{B} = T^{-1}B = \Sigma^{-1/2}U^T L_o^T B \tag{6.35}$$

$$\tilde{C} = CT = CL_cV\Sigma^{-1/2} \tag{6.36}$$

Lemma 6.3.1 The system $\{\tilde{A}, \tilde{B}, \tilde{C}\}$ is a balanced realization of the discrete-time system $\{A, B, C\}$.

Proof

By considering (6.22), substituting for W_o from (6.30), pre- and post-multiplying by $V^T L_c^T$ and L_cV, respectively, we obtain

$$V^T L_c^T A^T L_o L_o^T A L_c V - V^T L_c^T L_o L_o^T L_c V = -V^T L_c^T C^T C L_c V \tag{6.37}$$

Substituting for $L_o^T L_c$ and $L_c^T L_o$ from (6.32) gives

$$V^T L_c^T A^T L_o L_o^T A L_c V - \Sigma^2 = -V^T L_c^T C^T C L_c V \tag{6.38}$$

Proceeding in a similar manner for (6.21) by pre- and post-multiplying by $U^T L_o^T$ and L_oU, respectively we obtain

$$U^T L_o^T A L_c L_c^T A^T L_o U - U^T L_o^T L_c L_c^T L_o U = -U^T L_o^T B B^T L_o U \tag{6.39}$$

Substituting for $L_o^T L_c$ and $L_c^T L_o$ from (6.32) gives

$$U^T L_o^T A L_c L_c^T A^T L_o U - \Sigma^2 = -U^T L_o^T B B^T L_o U \tag{6.40}$$

(6.34) implies that

$$\tilde{A}^T = \Sigma^{-1/2} V^T L_c^T A^T L_o U \Sigma^{-1/2} \tag{6.41}$$

Pre-multiplying by $\Sigma^{1/2}$, and post-multiplying by $\Sigma^{1/2}$ and U^T gives

$$\Sigma^{1/2}\tilde{A}^T\Sigma^{1/2}U^T = V^T L_c^T A^T L_o \tag{6.42}$$

which implies that

$$\begin{aligned}(V^T L_c^T A^T L_o)(L_o^T A L_c V) &= \Sigma^{1/2}\tilde{A}^T\Sigma^{1/2}U^T U\Sigma^{1/2}\tilde{A}\Sigma^{1/2} \\ &= \Sigma^{1/2}\tilde{A}^T\Sigma\tilde{A}\Sigma^{1/2}\end{aligned} \tag{6.43}$$

(6.36) can be re-expressed as

$$\tilde{C}\Sigma^{1/2} = CL_cV \tag{6.44}$$

which implies that

$$-(V^T L_c^T C^T)(C L_c V) = -\Sigma^{1/2}\tilde{C}^T\tilde{C}\Sigma^{1/2} \tag{6.45}$$

Substitution of (6.43) and (6.45) into (6.38) gives

$$\Sigma^{1/2}\tilde{A}^T\Sigma\tilde{A}\Sigma^{1/2} - \Sigma^2 = -\Sigma^{1/2}\tilde{C}^T\tilde{C}\Sigma^{1/2} \tag{6.46}$$

Pre- and post-multiplying (6.46) by $\Sigma^{-1/2}$ gives

$$\tilde{A}^T\Sigma\tilde{A} - \Sigma = -\tilde{C}^T\tilde{C} \tag{6.47}$$

Proceeding in a similar manner by substituting into (6.39) gives

$$\tilde{A}\Sigma\tilde{A}^T - \Sigma = -\tilde{B}\tilde{B}^T \tag{6.48}$$

It is therefore shown that the discrete system transformed by T and T^{-1} given in (6.34), (6.35), and (6.36) is in balanced form with Grammians equal to Σ. ■

Lemma 6.3.2 Let the internally balanced asymptotically stable system $\{\tilde{A}, \tilde{B}, \tilde{C}\}$ and the Grammian Σ be partitioned conformally as

$$\tilde{A} = \begin{bmatrix} \tilde{A}_{11} & \tilde{A}_{12} \\ \tilde{A}_{21} & \tilde{A}_{22} \end{bmatrix},\ \tilde{B} = \begin{bmatrix} \tilde{B}_1 \\ \tilde{B}_2 \end{bmatrix},\ \tilde{C} = [\tilde{C}_1 \quad \tilde{C}_2],\ \Sigma = \begin{bmatrix} \Sigma_1 & 0 \\ 0 & \Sigma_2 \end{bmatrix} \tag{6.49}$$

where $\tilde{A}_{11}$ and Σ_1 are $r \times r$ matrices. Then the slow singular perturbational approximation $\{\hat{A}, \hat{B}, \hat{C}, \hat{D}\}$ given by

$$\begin{aligned} \hat{A} &= \tilde{A}_{11} + \tilde{A}_{12}(I - \tilde{A}_{22})^{-1}\tilde{A}_{21} \\ \hat{B} &= \tilde{B}_1 + \tilde{A}_{12}(I - \tilde{A}_{22})^{-1}\tilde{B}_2 \\ \hat{C} &= \tilde{C}_1 + \tilde{C}_2(I - \tilde{A}_{22})^{-1}\tilde{A}_{21} \\ \hat{D} &= \tilde{C}_2(I - \tilde{A}_{22})^{-1}\tilde{B}_2 \end{aligned} \tag{6.50}$$

and the fast singular perturbational approximation $\{\tilde{A}_{22}, \tilde{B}_2, \tilde{C}_2\}$ of the system (6.49) will each define an internally balanced system with Grammians Σ_1 and Σ_2, respectively.

Proof

Let $S_1 = \begin{bmatrix} I & \tilde{A}_{12}(I - \tilde{A}_{22})^{-1} \\ 0 & I \end{bmatrix}$ and $S_2 = \begin{bmatrix} I & \tilde{A}_{21}^T(I - \tilde{A}_{22}^T)^{-1} \\ 0 & I \end{bmatrix}$. Partition (6.48) conformally as

$$\begin{bmatrix} \tilde{A}_{11} & \tilde{A}_{12} \\ \tilde{A}_{21} & \tilde{A}_{22} \end{bmatrix} \begin{bmatrix} \Sigma_1 & 0 \\ 0 & \Sigma_2 \end{bmatrix} \begin{bmatrix} \tilde{A}_{11}^T & \tilde{A}_{21}^T \\ \tilde{A}_{12}^T & \tilde{A}_{22}^T \end{bmatrix} - \begin{bmatrix} \Sigma_1 & 0 \\ 0 & \Sigma_2 \end{bmatrix} = \begin{bmatrix} \tilde{B}_1 \\ \tilde{B}_2 \end{bmatrix} [\tilde{B}_1^T \quad \tilde{B}_2^T] \tag{6.51}$$

Pre- and post-multiply (6.51) by S_1 and S_1^T, respectively. After some algebra, the $(1,1)$ block of the final expression will be given by

$$\hat{A}\Sigma_1\hat{A}^T - \Sigma_1 = -\hat{B}\hat{B}^T \tag{6.52}$$

with $(\hat{A}, \hat{B})$ as defined in (6.50), and the $(2,2)$ block will be given by

$$\tilde{A}_{22}\Sigma_2\tilde{A}_{22}^T - \Sigma_2 = -\tilde{B}_2\tilde{B}_2^T \tag{6.53}$$

Proceeding in a similar manner for (6.47) by partitioning it conformally as (6.51) and pre- and post-multiplying by S_2 and S_2^T, respectively, we obtain

$$\hat{A}^T\Sigma_1\hat{A} - \Sigma_1 = -\hat{C}^T\hat{C} \tag{6.54}$$

with $(\hat{A}, \hat{C})$ as defined in (6.50), and

$$\tilde{A}_{22}^T\Sigma_2\tilde{A}_{22} - \Sigma_2 = -\tilde{C}_2^T\tilde{C}_2 \tag{6.55}$$

From the balanced Lyapunov equations of (6.52), (6.53), (6.54) and (6.55), it is clear that the slow and fast singular perturbational approximations are both internally balanced with Grammians Σ_1 and Σ_2, respectively. ■

Solving the Lyapunov Equation for the Cholesky Factor

In some applications it is necessary to solve the Lyapunov equation

$$A^TXA - X = -C^TC \tag{6.56}$$

Since C^TC is non-negative definite, the above Lyapunov has a unique non-negative solution for X. Using the Cholesky decomposition, X can be factorized as

$$X = Y^TY \tag{6.57}$$

where Y is an upper triangular matrix. In solving (6.56), it is preferable to find the Cholesky factor Y *via* C rather than C^TC for the following reasons. First, when X is positive definite, its condition number with respect to inversion is

$$cond(X) = cond^2(Y) \tag{6.58}$$

That is why X may be more ill-conditioned than Y. Second, if it is possible to find Y directly from C, the loss of accuracy associated with the computation of C^TC will be avoided. The equation

$$A^T(Y^TY)A - (Y^TY) = -C^TC \tag{6.59}$$

can be solved directly for Y by the method of [45]. This method is based on the Bartels-Stewart algorithm and involves the reduction of the matrix A into real Schur form

$$S = U^TAU \tag{6.60}$$

where U is orthogonal and S is upper triangular. Let the QR decomposition of the matrix C be

$$C = Q\begin{bmatrix} R \\ 0 \end{bmatrix} \tag{6.61}$$

where Q is orthogonal and R upper triangular. According to (6.61)

$$C^TC = R^TR \tag{6.62}$$

so that R is a Cholesky factor of C^TC. Pre- and post-multiplying (6.59) by U^T and U, respectively, gives

$$U^TA^T(Y^TY)AU - U^T(Y^TY)U = -U^TC^TCU \tag{6.63}$$

From (6.60), $A = USU^T$, and (6.63) may be rewritten, by substituting for A and using (6.62), as

$$S^TU^T(Y^TY)US - U^T(Y^TY)U = -U^TR^TRU \tag{6.64}$$

which may be re-arranged as

$$S^T(\tilde{Y}^T\tilde{Y})S - \tilde{Y}^T\tilde{Y} = -\tilde{R}^T\tilde{R} \tag{6.65}$$

where $\tilde{Y}$ and $\tilde{R}$ are upper triangular matrices that satisfy

$$\tilde{Y}^T\tilde{Y} = U^T(Y^TY)U \tag{6.66}$$

$$\tilde{R}^T\tilde{R} = U^T(R^TR)U \tag{6.67}$$

The matrices $\tilde{Y}$ and $\tilde{R}$ can be found as the Cholesky factors of (6.66) and (6.67), respectively. It is noticed that it is not necessary to form the matrix $U^T(R^TR)U$ explicitly,

since RU can be formed and $\tilde{R}$ is found as an upper triangular matrix of the QR decomposition of RU. After $\tilde{Y}$ is found, the matrix Y is obtained in a similar manner from $\tilde{Y}U^T$. Equation (6.65) can be solved by a forward substitution for the elements of $\tilde{Y}$ without forming $\tilde{R}^T\tilde{R}$. To summarize, the method of [45] provides a method for solving equation (6.56) directly for the Cholesky factor, without the loss of accuracy associated with forming C^TC.

6.4 Coprime Factor Model Reduction

Most model reduction techniques require the original model to be stable. In the coprime factor model reduction procedure, the coprime factors are reduced. Since the coprime factors of any system are always stable, the method is applicable to unstable as well as stable systems. The procedure is:

1) Write G, the transfer function to be reduced (with degree n) as $G = \tilde{M}^{-1}\tilde{N}$.

2) Let the Hankel singular values of $[\tilde{N} \quad \tilde{M}]$ be $\tilde{\sigma}_1 \geq \tilde{\sigma}_2 \geq ... \geq \tilde{\sigma}_n > 0$ and define $\tilde{\Sigma} = \mathbf{diag}(\tilde{\sigma}_1, \tilde{\sigma}_2, ..., \tilde{\sigma}_n)$. Since the factorization is normalized, we have that $I > \tilde{\Sigma}$, so $1 > \tilde{\sigma}_i$. $r < n$ is then picked such that $\tilde{\sigma}_r > \tilde{\sigma}_{r+1}$. A balanced singular perturbational approximation can be performed in the usual way on $[\tilde{N} \quad \tilde{M}]$ to obtain a reduced order representation of the form $[\tilde{N}_r \quad \tilde{M}_r]$, or of the form $[\tilde{N}_{r_n} \quad \tilde{M}_{r_n}]$ with the same feedthrough (D) term as that of $[\tilde{N} \quad \tilde{M}]$.

3) Form the reduced-order transfer function G_r (with degree r) by $G_r = M_r^{-1}N_r$. Here, G_r is in fact a normalized left coprime factorization.

We now extend the continuous-time results given in [63] to their discrete-time counterpart.

Lemma 6.4.1 **[107]** Suppose $\{A, B, C\}$ is minimal, and let $H = -APC^T(I+CPC^T)^{-1}$ with P as the unique positive definite solution to the algebraic Riccati equation

$$APA^T - P - APC^T(I + CPC^T)^{-1}CPA^T + BB^T = 0$$

then (3.32) and (3.33) gives a normalized left coprime factorization. ■

Lemma 6.4.2 Given a realization $\{A, B, C\}$. Suppose $H = -APC^T(I + CPC^T)^{-1}$ with P the solution to the algebraic Riccati equation

$$APA^T - P - APC^T(I + CPC^T)^{-1}CPA^T + BB^T = 0$$

and $\bar{A} = A + HC$ has eigenvalues inside the open unit disc. Suppose further that

$$\left[\begin{array}{c|cc} \bar{A} & B & H \\ \hline Z_2C & 0 & Z_2 \end{array}\right] \tag{6.68}$$

is minimal. Then

1) P is the controllability Grammian for (6.68) and so is positive definite,

2) either

   i) $\{A, B, C\}$ is minimal, or

   ii) there exists a non-zero vector x and a complex number λ so that $A^Tx = \lambda x$, $B^Tx = 0$, $\bar{A}Px = \frac{1}{\lambda}Px$, and $|\lambda| > 1$.

Proof

It is clear that the algebraic Riccati equation can be rewritten as

$$\bar{A}P\bar{A}^T - P + HH^T + BB^T = 0 \tag{6.69}$$

which implies that P is the controllability Grammian for the controllable, stable pair

$$\left\{\bar{A}, [B \quad H]\right\}$$

and hence is positive definite. This proves part 1.

Observability of $\{Z_2C\,\bar{A}\}$ implies the observability for $\{C, A\}$. This can be shown by a simple PBH (Popov-Belevitch-Hautus) test. Now suppose $\{A, B\}$ is uncontrollable so there exists a non-zero vector x such that $A^Tx = \lambda x$ and $B^Tx = 0$. Rewriting the algebraic Riccati equation as

$$\bar{A}PA^T - P + BB^T = 0 \tag{6.70}$$

and post-multiplying this by x, we can conclude that $\frac{1}{\lambda}$ is an eigenvalue of $\bar{A}$ with a non-zero eigenvector Px. Hence $|\lambda| > 1$ since $\bar{A}$ has eigenvalues inside the open unit disc. This proves part 2. ■

Lemma 6.4.3 Let $\{A, B, C\}$ be minimal. Suppose $\bar{A} = A + HC$ has eigenvalues inside the open unit disc with $H = -APC^T(I + CPC^T)^{-1}$ and P as the positive solution to the algebraic Riccati equation

$$APA^T - P - APC^T(I + CPC^T)^{-1}CPA^T + BB^T = 0$$

Then the Hankel singular values of

$$[\tilde{N} \quad \tilde{M}] \stackrel{s}{=} \left[\begin{array}{c|cc} A + HC & B & H \\ \hline Z_2C & 0 & Z_2 \end{array}\right]$$

are strictly less than one.

Proof

The proof of this lemma uses a well-known result from Hankel operator theory [29].

Lemma 6.4.4 [29] Let

$$\| R(z) - X(z) \|_\infty = \| R^* \|_H = \tilde{\sigma}_1(R^*) \tag{6.71}$$

where $\tilde{\sigma}_1(.)$ denotes the maximum Hankel singular value, and $X(z) \in \mathcal{RH}^\infty$. Then there exist vectors $g(z)$ and $f(z) \in \mathcal{RH}^2$ independent of $X(z)$ such that

$$[R(z) - X(z)]\, g(z) = \tilde{\sigma}_1(R^*) f(z^{-1}) \tag{6.72}$$

■

The proof of Lemma 6.4.3 is then as follows. It is well known that

$$\| [\tilde{N} \quad \tilde{M}] \|_H \leq \| [\tilde{N} \quad \tilde{M}] \|_\infty \tag{6.73}$$

Also if the pair $[\tilde{N} \quad \tilde{M}]$ are normalized, then $\| [\tilde{N} \quad \tilde{M}] \|_\infty = 1$.

Suppose that $\| [\tilde{N} \quad \tilde{M}] \|_H = 1$, then from Lemma 6.4.4, there exists $g(z)$, $f(z) \in \mathcal{RH}^2$ such that

$$\begin{bmatrix} \tilde{N}^* \\ \tilde{M}^* \end{bmatrix} g(z) = f(z^{-1}) \tag{6.74}$$

that is, $R = \begin{bmatrix} \tilde{N}^* \\ \tilde{M}^* \end{bmatrix}$ and $X = 0$ in Lemma 6.4.4. But, one of the main requirements for a coprime factorization is that there exist U, $V \in \mathcal{RH}^\infty$ such that $U^*\tilde{N}^* + V^*\tilde{M}^* = I$. Pre-multiplying (6.74) by $[\,U^* \quad V^*\,]$ yields

$$g(z) = [\,U^* \quad V^*\,]\, f(z^{-1}) \tag{6.75}$$

which is a contradiction as the right-hand side of (6.75) $\notin \mathcal{RH}^2$. This contradiction implies $\|\,[\,\tilde{N} \quad \tilde{M}\,]\,\|_H \neq 1$, which is equivalent to saying that the maximum Hankel singular value is always less than one. Hence, the Hankel singular values of $[\,\tilde{N} \quad \tilde{M}\,]$ are strictly less than one, which completes the proof. ■

Conjecture 6.4.1 [101] Let $[\,\tilde{N} \quad \tilde{M}\,]$ be the normalized left coprime factors of the n-state full order model G. Also let $[\,\tilde{N}_r \quad \tilde{M}_r\,]$ be the r-state reduced order model obtained by singular perturbational approximation of the balanced realization of $[\,\tilde{N} \quad \tilde{M}\,]$. Then $[\,\tilde{N}_r \quad \tilde{M}_r\,]$ is left coprime and normalized. ■

Lemma 6.4.5 Let $[\,\tilde{N} \quad \tilde{M}\,]$ be the normalized left coprime factors of the model G. Let $[\,\tilde{N} \quad \tilde{M}\,]$ be in balanced coordinates with the following balanced Grammian $\tilde{\Sigma} = \mathbf{diag}(\tilde{\sigma}_1, \tilde{\sigma}_2, ..., \tilde{\sigma}_n)$ and Hankel singular values $\tilde{\sigma}_1 \geq \tilde{\sigma}_2 \geq ... \geq \tilde{\sigma}_n > 0$. Let $r < n$ and partition $\tilde{\Sigma} = \mathbf{diag}(\tilde{\Sigma}_1, \tilde{\Sigma}_2)$ where $\tilde{\Sigma}_1 = \mathbf{diag}(\tilde{\sigma}_1, ..., \tilde{\sigma}_r)$ and $\tilde{\Sigma}_2 = \mathbf{diag}(\tilde{\sigma}_{r+1}, ..., \tilde{\sigma}_n)$. Let $[\,\tilde{N}_r \quad \tilde{M}_r\,]$ be the r-state reduced order model obtained by singular perturbational approximation of the balanced realization of $[\,\tilde{N} \quad \tilde{M}\,]$ to r states. Let $[\,\tilde{N}_{r_n} \quad \tilde{M}_{r_n}\,]$ be the r-state reduced order model obtained by singular perturbational approximation of the balanced realization of $[\,\tilde{N} \quad \tilde{M}\,]$ with the same feedthrough (D) term, to r states. Then the frequency error bounds in Conjecture 6.2.1 apply:

$$\|\,[\,\tilde{N} - \tilde{N}_r \quad \tilde{M} - \tilde{M}_r\,]\,\|_\infty \leq 2\ \mathbf{tr}[\tilde{\Sigma}_2] \tag{6.76}$$

$$\|\,[\,\tilde{N} - \tilde{N}_{r_n} \quad \tilde{M} - \tilde{M}_{r_n}\,]\,\|_\infty \leq 4\ \mathbf{tr}[\tilde{\Sigma}_2] \tag{6.77}$$

this time in terms of $\tilde{\Sigma}_2$, the diagonal matrix of the neglected Hankel singular values of $[\,\tilde{N} \quad \tilde{M}\,]$.

Proof

This lemma follows immediately from Conjecture 6.4.5 and the $\mathcal{H}^\infty$ error bound for balanced singular perturbational approximations derived in [1, 59]. ■

Lemma 6.4.6 Let $[\,\tilde{N} \quad \tilde{M}\,]$ be the normalized left coprime factors of the model G. Let $[\,\tilde{N} \quad \tilde{M}\,]$ be in balanced coordinates with balanced Grammian $\tilde{\Sigma} = \mathbf{diag}(\tilde{\sigma}_1, \tilde{\sigma}_2, ..., \tilde{\sigma}_n)$ and Hankel singular values $\tilde{\sigma}_1 \geq \tilde{\sigma}_2 \geq ... \geq \tilde{\sigma}_n > 0$. Let $r < n$ and partition $\tilde{\Sigma} = \mathbf{diag}(\tilde{\Sigma}_1, \tilde{\Sigma}_2)$ where $\tilde{\Sigma}_1 = \mathbf{diag}(\tilde{\sigma}_1, ..., \tilde{\sigma}_r)$ and $\tilde{\Sigma}_2 = \mathbf{diag}(\tilde{\sigma}_{r+1}, ..., \tilde{\sigma}_n)$. Let $[\,\tilde{N}_r \quad \tilde{M}_r\,]$ be the r-state reduced order model obtained by singular perturbational approximation of the balanced realization of $[\,\tilde{N} \quad \tilde{M}\,]$ to r states. Let $\tilde{M}_r^{-1}$ be the r-state reduced order model of $\tilde{M}^{-1}$. Let G_r be the r-state reduced order model of G obtained by forming $G_r = \tilde{M}_r^{-1}\tilde{N}_r$. Then

$$\| G - G_r \|_\infty \leq \left\| M^{-1} \right\|_\infty (2\ \mathbf{tr}[\tilde{\Sigma}_2]) \left\| M_r^{-1} \right\|_\infty \tag{6.78}$$

Proof

We have $G - G_r = \tilde{M}^{-1}\tilde{N} - \tilde{M}_r^{-1}\tilde{N}_r$ which can be expressed, after some algebra, as

$$\begin{aligned} G - G_r &= \tilde{M}^{-1} [\,\tilde{N} - \tilde{N}_r \quad \tilde{M} - \tilde{M}_r\,] \begin{bmatrix} I \\ -G_r \end{bmatrix} \\ &= \tilde{M}^{-1} [\,\tilde{N} - \tilde{N}_r \quad \tilde{M} - \tilde{M}_r\,] \tilde{M}_r^{-1} \begin{bmatrix} \tilde{M}_r \\ -\tilde{N}_r \end{bmatrix} \end{aligned}$$

This implies that

$$\| G - G_r \|_\infty \leq \left\| \tilde{M}^{-1} \right\|_\infty \| \tilde{N} - \tilde{N}_r \quad \tilde{M} - \tilde{M}_r \|_\infty \left\| \tilde{M}_r^{-1} \right\|_\infty \left\| \begin{matrix} \tilde{M}_r \\ \tilde{N}_r \end{matrix} \right\|_\infty$$

Since the pair $(\tilde{N}_r, \tilde{M}_r)$ are normalized, $\left\| \begin{matrix} \tilde{M}_r \\ \tilde{N}_r \end{matrix} \right\|_\infty = 1$. By using the inequality given by (6.76), the inequality given by (6.78) will result. This can be regarded as a useful indication of how many states can be removed without extensively changing the input-output properties of G. ■

Proposed Discrete-time Model Reduction Algorithm

Problem: Given $G(z)$ with the state-space $\{A, B, C\}$ of degree n, stable/unstable, non-minimal with dimension $p \times n$, find an approximant $G_r(z)$ with the state-space $\{A_r, B_r, C_r, D_r\}$ of degree $r < n$.

Algorithm

1) Obtain a normalized left coprime factorization $(\tilde{N}, \tilde{M})$ of $G(z)$.

2) Perform the following state-space balancing algorithm on $[\tilde{N} \quad \tilde{M}]$. The coprime factors $\tilde{N}$ and $\tilde{M}$ can be formed using (3.32) and (3.33).

   i) Compute the Cholesky factors of the Grammians by the method proposed by [45].

   ii) Compute the singular value decomposition of the product of the Cholesky factors given in (6.32).

   iii) Form the balancing transformations using (6.33).

   iv) Form the balanced state-space matrices using (6.34), (6.35) and (6.36).

3) Apply the singular perturbational approximation technique on the balanced $[\tilde{N} \quad \tilde{M}]$ to obtain $[\tilde{N}_r \quad \tilde{M}_r]$. Suppose that the slow singular perturbational approximation of the following realization

$$[\tilde{N} \quad \tilde{M}] \stackrel{s}{=} \left[\begin{array}{c|cc} A+HC & B & H \\ \hline Z_2C & 0 & Z_2 \end{array}\right] \tag{6.79}$$

has been performed such that

$$\left[\begin{array}{c|cc} A+HC & B & H \\ \hline Z_2C & 0 & Z_2 \end{array}\right] \xrightarrow[residualized]{balanced} \left[\begin{array}{c|cc} \hat{A} & \hat{B}_1 & \hat{B}_2 \\ \hline \hat{C} & \hat{D}_1 & \hat{D}_2 \end{array}\right] = [\tilde{N}_r \quad \tilde{M}_r] \tag{6.80}$$

Then $\tilde{N}_r$ and $\tilde{M}_r$ are also left coprime and normalized.

4) Construct and use $G_r(z) = \tilde{M}_r^{-1}\tilde{N}_r$ as an approximant to $G(z)$.

$$\begin{aligned} \tilde{M}_r^{-1}\tilde{N}_r &\stackrel{s}{=} \left[\begin{array}{c|c} \hat{A}-\hat{B}_2\hat{D}_2^{-1}\hat{C} & \hat{B}_2\hat{D}_2^{-1} \\ \hline -\hat{D}_2^{-1}\hat{C} & \hat{D}_2^{-1} \end{array}\right] \times \left[\begin{array}{c|c} \hat{A} & \hat{B}_1 \\ \hline \hat{C} & \hat{D}_1 \end{array}\right] \\ &= \left[\begin{array}{cc|c} \hat{A} & 0 & \hat{B}_1 \\ \hat{B}_2\hat{D}_2^{-1}\hat{C} & \hat{A}-\hat{B}_2\hat{D}_2^{-1}\hat{C} & \hat{B}_2\hat{D}_1 \\ \hline \hat{D}_2^{-1}\hat{C} & -\hat{D}_2^{-1}\hat{C} & \hat{D}_2^{-1}\hat{D}_1 \end{array}\right] \end{aligned}$$

$$
\begin{aligned}
&= \left[\begin{array}{cc|c} \hat{A} & 0 & \hat{B}_1 \\ 0 & \hat{A}-\hat{B}_2\hat{D}_2^{-1}\hat{C} & \hat{B}_2\hat{D}_1-\hat{B}_1 \\ \hline 0 & -\hat{D}_2^{-1}\hat{C} & \hat{D}_2^{-1}\hat{D}_1 \end{array}\right] \\
&= \left[\begin{array}{c|c} \hat{A}-\hat{B}_2\hat{D}_2^{-1}\hat{C} & \hat{B}_2\hat{D}_1-\hat{B}_1 \\ \hline -\hat{D}_2^{-1}\hat{C} & \hat{D}_2^{-1}\hat{D}_1 \end{array}\right]
\end{aligned} \tag{6.81}
$$

which is a state-space realization of the approximant.

6.5 Numerical Examples

Two examples are presented to validate the model-reduction approach presented in this chapter. The first example arises from the design of a controller for a *glass tube production process*, and the second example arises from the design of a controller for a *high performance aero-engine*, both using discrete-time $\mathcal{H}^\infty$-optimization.

Example 1 – The controller is for a 2-input 2-output *glass tube production process* model. It has 32 states and it is non-minimal. The Hankel singular values of $[\tilde{N} \quad \tilde{M}]$ for this controller are given in Table 6.1. A good place to truncate this model is at 12 states. The singular values of the error function

$$E_{11}(z) = [\tilde{N}(z) - \tilde{N}_{12}(z) \quad \tilde{M}(z) - \tilde{M}_{12}(z)]$$

are shown in Figure 6.1, with a maximum value of 2.1311×10^{-4}. The singular values of the error function $E_{12}(z) = G(z) - G_{12}(z)$ are shown in Figure 6.2, with a maximum value of 1.5650×10^{-3}. Finally, the singular values of both the high and reduced-order controller are shown in Figure 6.3.

Example 2 – The controller is for a 3-input 3-output *high performance aero-engine* model. It has 30 states and it is non-minimal. The Hankel singular values $[\tilde{N} \quad \tilde{M}]$ of this controller are given in Table 6.1. A good place to truncate this model is at 13 states. The singular values of the error function

$$E_{21}(z) = [\tilde{N}(z) - \tilde{N}_{13}(z) \quad \tilde{M}(z) - \tilde{M}_{13}(z)]$$

are shown in Figure 6.4, with a maximum value of 1.4948×10^{-4}. The singular values of the error function $E_{22}(z) = G(z) - G_{13}(z)$ are shown in Figure 6.5, with a maximum

value of 1.6548×10^{-3}. Finally, the singular values of both the high and reduced-order controller are shown in Figure 6.6.

Example 1		**Example 2**	
1) 4.2482e-01	17) 9.8594e-06	1) 4.0694e-01	16) 2.8708e-05
2) 2.5171e-01	18) 3.6020e-06	2) 3.2597e-01	17) 8.0369e-07
3) 9.6639e-02	19) 2.2974e-06	3) 2.4179e-01	18) 3.8852e-07
4) 8.0217e-02	20) 1.5802e-06	4) 1.3627e-01	19) 2.0525e-07
5) 3.4282e-02	21) 1.2674e-06	5) 8.3641e-02	20) 3.7137e-08
6) 1.6642e-02	22) 5.6427e-07	6) 6.8822e-02	21) 1.2298e-08
7) 6.8411e-03	23) 1.5936e-07	7) 5.5705e-02	22) 2.1012e-09
8) 5.2274e-03	24) 5.4077e-08	8) 3.3439e-02	23) 4.3942e-12
9) 2.5324e-03	25) 1.9548e-08	9) 1.7371e-02	24) 6.3541e-13
10) 1.4173e-03	26) 8.3475e-09	10) 6.0502e-03	25) 1.5454e-14
11) 6.9009e-04	27) 6.3176e-10	11) 4.1995e-03	26) 8.1517e-17
12) 2.8681e-04	28) 3.8663e-10	12) 1.4436e-03	27) 1.0166e-18
13) 9.0396e-05	29) 6.9527e-11	13) 2.6330e-04	28) 4.2545e-29
14) 6.9483e-05	30) 1.4107e-11	14) 7.4916e-05	29) 3.5347e-31
15) 3.9909e-05	31) 1.2590e-24	15) 3.2171e-05	30) 8.4547e-32
16) 1.5268e-05	32) 1.5765e-25		

Table 6.1: Hankel Singular Values.

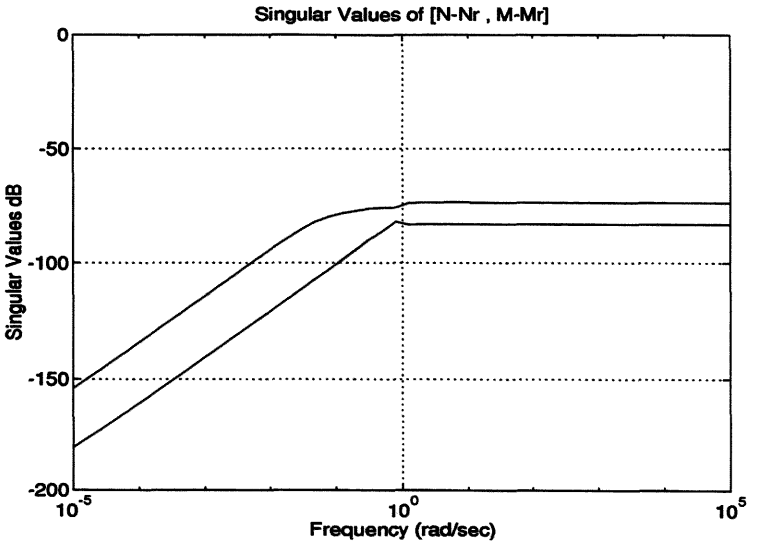

Figure 6.1: Singular Values of the Error Function $E_{11}(z)$.

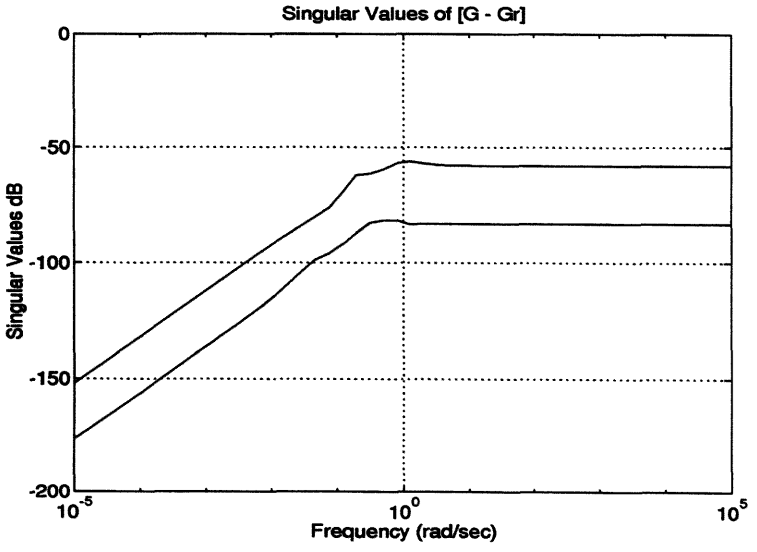

Figure 6.2: Singular Values of the Error Function $E_{12}(z)$.

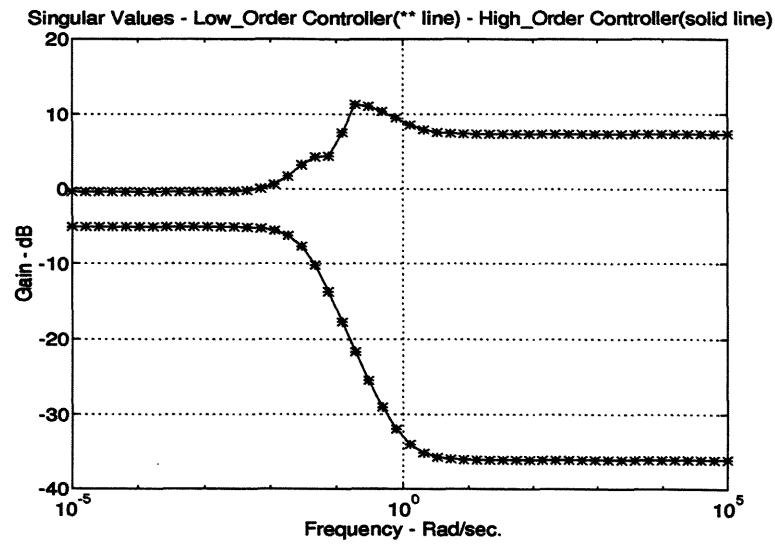

Figure 6.3: Singular Values of the Full and Reduced-order Controller.

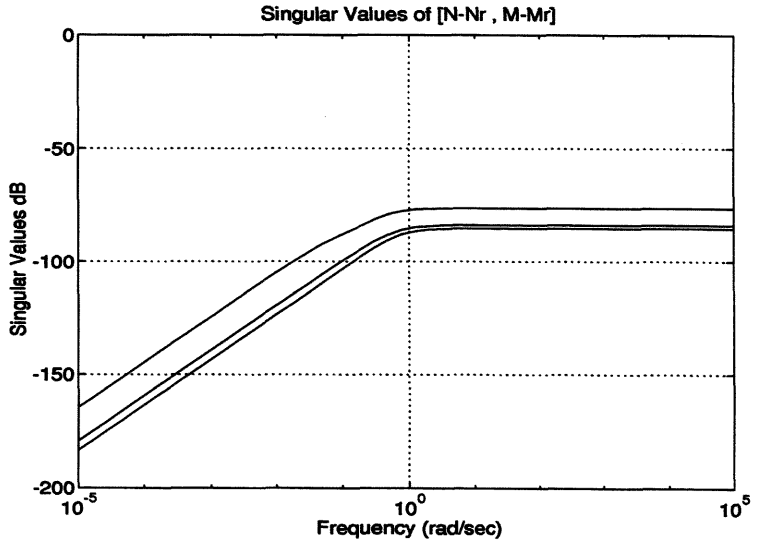

Figure 6.4: Singular Values of the Error Function $E_{21}(z)$.

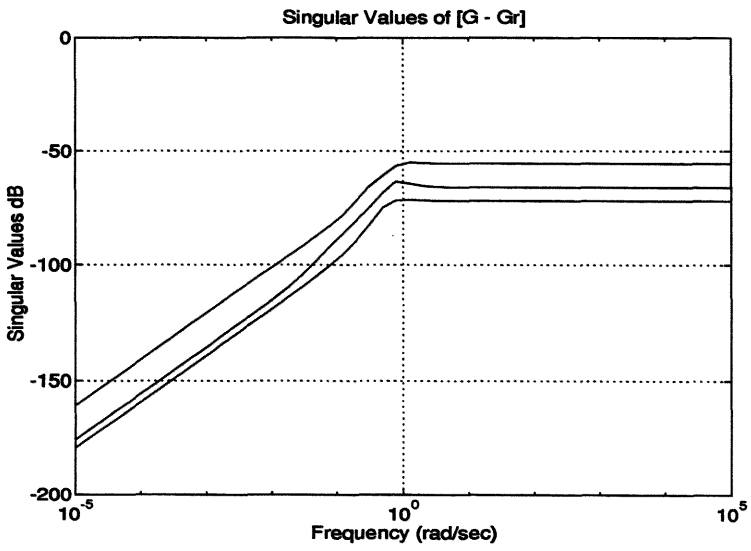

Figure 6.5: Singular Values of the Error Function $E_{22}(z)$.

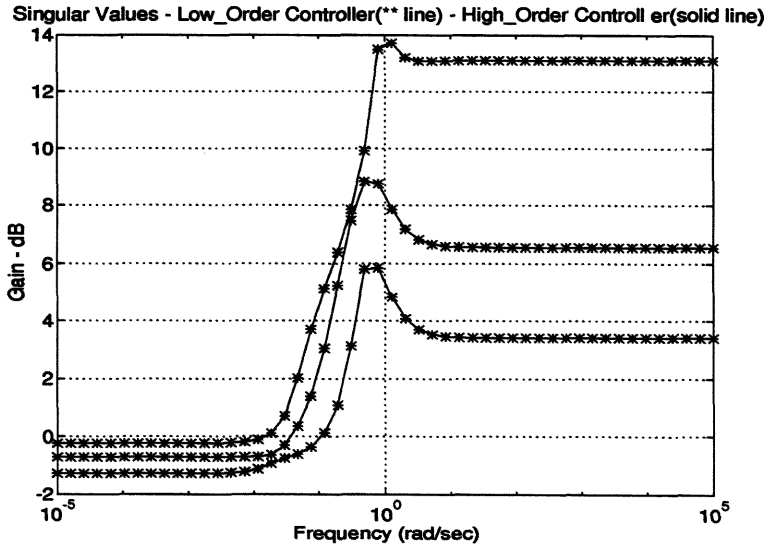

Figure 6.6: Singular Values of the Full and Reduced-order Controller.

6.6 Summary

In this chapter, a comprehensive treatment of discrete-time model reduction was presented with two main aims: The first was to describe two algorithms that can be used for the reliable computation of the balanced realization of a stable state-space model. By combining the two algorithms, assumptions about the controllability or observability of the original system can be dispensed with, since the Cholesky factors of the Grammians can be computed directly, given the state-space realization. The second was to combine the two algorithms together with a model-reduction approach based on normalized fractional representations thereby extending the continuous-time results of [63] to the discrete-time analogous.

The model-reduction approach was demonstrated successfully on two different examples. In Chapter 8, high-order IMC controllers will be synthesized for a glass tube production process with large time-delays. Such high-order controllers can be numerically ill-conditioned for performing model order-reduction. The proposed approach of this chapter will prove to be numerically reliable in finding low-order controllers in the case study of Chapter 8.

Chapter 7

Robust Process Identification of a Glass Tube Production Process

7.1 Introduction

This chapter is concerned with applying advanced identification to a MIMO industrial production process, in this case a *glass tube production process.* The process will be described in detail in order to provide an understanding of the dynamic behaviour. The treatment of data and design experiments which are relevant to the multivariable identification approach will be briefly described, but the main attention will be focused on the application of the identification approach in terms of the accuracy of the identified models.

Mathematical modelling of processes from experimental data is regarded as the field of system or process identification, and it is defined in [114] as follows: System identification is the determination, on the basis of input and output data, of a system (model) within a specified class of systems (models), to which the system under test is equivalent (in terms of a criterion). From this definition, it follows that the experimental modelling of a process can be divided into the following entities [27, 60]:

1) **Data**: Input-output data is recorded and treated from specially designed identification experiments and pre-processing stages in order to make the measured data well informative about the properties of the process of interest.

2) **Model Set**: The mathematical properties of the model together with the

availability of *a priori* knowledge, engineering intuition and insight have to be invoked to select a set of candidate models and an error criterion to define the accuracy of the models.

3) **Parameterization**: Within the selected set of models, the parameterization involves issues like selecting a suitable model structure and an appropriate model order.

4) **Optimization**: The identification method based on optimization defines the construction of the best model within the parameterized model set.

5) **Model Validation**: This is the process where the final judgement of the model quality is given. This relates the model behaviour to the *a priori* knowledge, the observed data which is independent of the data set used for the identification and its intended use.

Many different types of industrial processes do require some sort of control in order to meet the product specifications. In the last decade model-based multivariable control systems have been increasingly applied to industrial production processes. The application of these control systems can significantly reduce the tolerance of important product and process specifications and the transition times of the controlled process. To further improve the control system, the dynamics of a process should be accurately known. Both accurate models and knowledge of the corresponding model errors (due to process perturbations) are necessary for robust control system design. This knowledge can be obtained by advanced identification techniques. The designed robust controller then guarantees a certain performance for all systems within the identified uncertainty bounds. The aim of this chapter is to identify, with the aid of existing methods for data pre-treatment and advanced multivariable identification, a nominal model for a glass tube production process (operating at three working conditions) suitable for control system design.

The organization of this chapter is as follows. Section 7.2 gives a description of the glass tube production process. In Section 7.3, the main features of the advanced multivariable identification techniques will be briefly introduced; these include the Minimal

Polynomial Approach [27], the Subspace State-Space Approach [81], The Robust Control Oriented Approach [44]. In Section 7.4, the preliminary experiments for collecting *a priori* information are briefly outlined and analyzed, together with the pre-treatment of the measured data. In Section 7.5, the problem related to the final identification experiment which is for model estimation and model validation is discussed. Finally, a summary will be given in Section 7.6.

7.2 Description of the Process

In a special glass factory of Philips Lighting in the Netherlands, glass tubes are manufactured on so-called SQ (Sulvanian Quartz) furnaces. The main part of this process is outlined schematically in Figure 7.1. Glass is manufactured from very pure sand. After various processing and purification stages, the level of impurities in this sand is so low that it can be used as raw material of the glass tube. The sand is melted by indirect electrical heating, which yields sintering at the transition between the sand and the molten glass, and flows down through a spout where a mandrel is accurately positioned. Under pressure, gas is led through the hollow mandrel. The glass tube is pulled down due to gravity and supported by a drawing machine.

Shaping of the tube takes place at, and just below the end of the mandrel. The shape of the tube is determined by two output variables : the wall thickness and the diameter as a function of time. In the production process, 4 wall thickness (North, South, East and West) and 2 diameter (North/South and East/West) sensors measure the tube quality. Thus, the longitudinal shape of the tube is characterized by two important parameters, which will be taken as outputs to be controlled:

1) Average tube diameter (D).

2) Average tube wall thickness (W).

Both these outputs are influenced by many process conditions, which are all candidates for controlling inputs. These are:

1) Mandrel gas pressure.

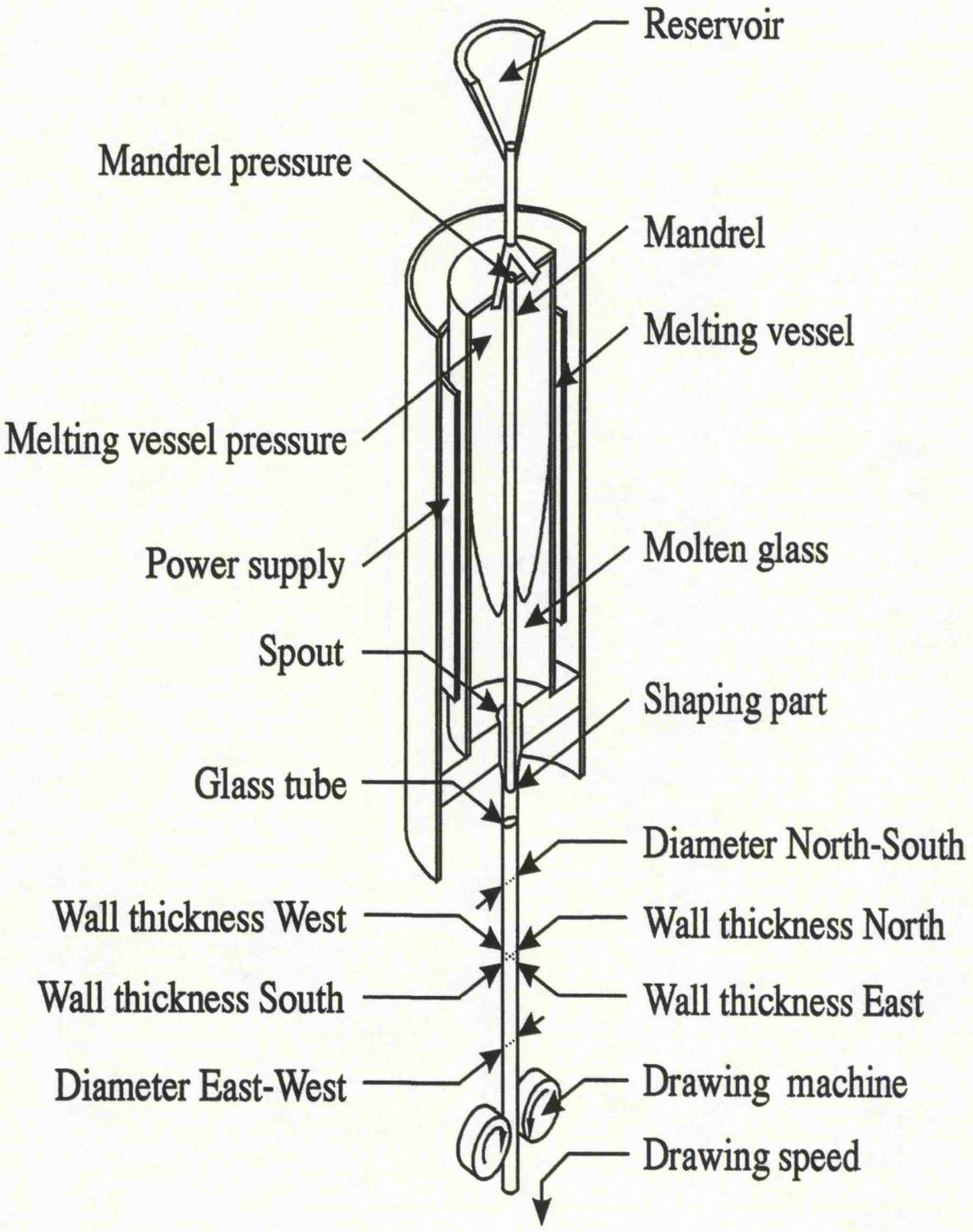

Figure 7.1: The Glass Tube Production Process.

2) Drawing speed.

3) Power applied to the furnace (temperature of the glass).

4) Melting vessel pressure.

5) Composition of the raw materials.

Preliminary process measurements have indicated that the shaping of the tube over the largest frequency range with the shortest time delays, was most directly influenced by two process conditions [6]:

1) Mandrel pressure (MP).

2) Drawing speed (DS).

Consequently these variables are taken as the controlling inputs.

The shaping part of the glass tube production process is a distributed parameter system. Shaping of the tube takes place when the glass has a relatively low viscosity. A physical model of the shaping part of the process may be obtained from two coupled partial difference equations:

1) First, there is a partial difference equation describing the flow of the glass from the mandrel to form a tube with specific dimensions as a function of mandrel pressure and drawing speed. In this difference equation the viscosity is an important position-dependent parameter. The viscosity is a non-linear function of temperature.

2) Second, there is a partial difference equation describing the temperature of the glass as a function of the power input. The velocity of the glass as a function of time and position is an important parameter in this partial difference equation.

Physical modelling of the process to describe the shaping of the tube in detail and over the full range of all possible operating points (determined by various diameter and wall thickness values), is very complex with many uncertain parameter values. For control

system design, however, it is often sufficient to have a model that describes the input-output behaviour of the process in the vicinity of its operating points. It is clear that the input-output behaviour of the tube process cannot be described *exactly* by a linear, lumped parameter model. Nevertheless, an attempt has been made to find a model that describes the process dynamics with sufficient accuracy for controller design. For this modelling, an advanced multivariable identification technique was applied. The model obtained was a set of linear, time-invariant difference equations which was considered to be a suitable approximation of the partial difference equations at that point of application where shaping of the tube takes place most frequently.

Shaping of the tube is a real MIMO process (Figure 7.2), and strong interactions between the different inputs and outputs exist:

1) An increase in the mandrel pressure results in an *increase* in diameter and a *decrease* in wall thickness.

2) An increase in the drawing speed results in a *decrease* of both diameter and wall thickness.

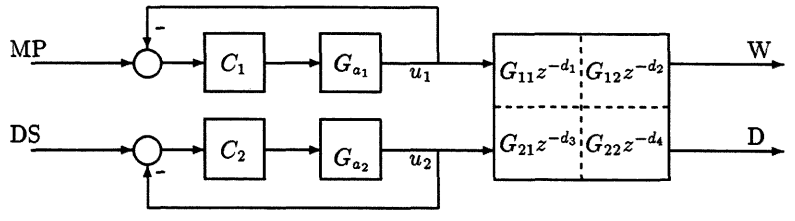

Figure 7.2: Open-loop Configuration of the Glass Tube Production Process.

The actuators of the mandrel pressure G_{a_1} and the drawing speed G_{a_2} are pre-controlled by PID controllers, C_1 and C_2, respectively. The inputs u_1 and u_2 that directly affect the process are fed back and control action is undertaken, if these measured inputs differ from their set-points. Also, there are time delays ($z^{-d_i}, i = 1,2,3,4$) in each element of the transfer function matrix shown in Figure 7.2. This is because the dimensions of the tube can only be measured when the glass has considerably cooled down.

Three different operating points were measured and taken to represent for the whole working range of the production process which includes more than 60 different operating points. For each of the 3 selected operating points, a state-space model is derived. The measurement signals are first pre-processed (Section 7.4); that is, the main obvious properties are removed from the measured data (delay, offset, low-frequency trends, etc.). This enables the identification algorithms to concentrate on the dynamic part of the process. Table 7.1 lists the selected measure for each of the three operating points. Because of the limited space, only the data for Measure 1 will be used for the analysis

Tube Measure	Diameter (mm)	Wall thickness (mm)
1	13	1
2	20	1
3	30.5	1.55

Table 7.1: Glass Tube Dimensions.

of model estimation.

7.3 Identification by Advanced Multivariable Methods

7.3.1 A Minimal Polynomial Approach

This identification approach [27] is based on minimizing the sum-squared prediction errors. In the classical approach for multivariable systems, however, structural indices are required for the polynomial model parameterization, which are very hard to estimate in practice. This problem can be avoided by adopting a minimal polynomial model structure. For this model structure, the structure estimation problem reduces to an order selection problem. In this way, a well known minimization criterion is formulated. In addition, it is possible to include specific structure knowledge as zero transfers, static gain optimization for predefined reference values, and to use multiple data sets for the model estimation, if data of several experiments are available. A clear disadvantage results from the fact that the solution is obtained by iterative non-linear optimization which is not guaranteed to converge to a globally optimum solution. Local minima of the

objective criterion and sensitivity to initial estimates are among the main drawbacks.

7.3.2 A State-Space Approach

This identification approach [81] is viewed as the better alternative to polynomial identification methods based on observability and/or controllability indices. This is especially true for high-order multivariable systems, for which it is not trivial to find a parameterization. With this approach, the *a priori* parameterization can be avoided. The order of the system is determined through the inspection of the dominant singular values of a matrix that is calculated during the identification. The state-space matrices are not calculated in their canonical forms (with a minimal number of parameters), but as full state-space matrices and is therefore simple to use. Another major advantage is that the algorithms are one shot algorithms (no iterations) which are therefore fast because no non-linear optimization is involved. A disadvantage of this method, however, is that there is no criterion for which these models are optimal.

7.3.3 A Robust Control Oriented Approach

This identification approach [44] is a two step method. The first step estimates uncertainty intervals of the frequency response of the system based on stochastic assumptions about the noise. In the second step, a nominal model is estimated on the basis of the uncertainty intervals using curve fitting techniques in the frequency domain. This approach provides very accurate models of the process. A major advantage is that bounds for the model errors are obtained in the frequency domain describing the model accuracy which can also be used for $\mathcal{H}^\infty$ control design. Computational complexity is, however, a clear disadvantage of this identification approach.

7.3.4 An Integrated Identification Approach

A user-friendly and efficient identification shell for industrial purposes can now be realized by combining the advantages of each of the developed identification methods:

1) **Initialization:** The State-Space approach provides accurate models in minimum time and it is easy to use.

2) **Optimization:** The Minimal Polynomial approach can be used to optimize the initial State-Space model and fix the static gains to the reference values for multiple data sets.

3) **Bounds:** Model error bounds required for $\mathcal{H}^\infty$ control system design can be computed with the Robust Control Oriented approach which also indicates the model accuracy.

7.4 Data Pre-processing and Identification Experiments

7.4.1 Pre-processing of the Identification Data

For the different identification experiments (Section 7.4.2), the following collected input and output signals are processed:

1)	Diameter (North/South)	(mm)
2)	Diameter (East/West)	(mm)
3)	Wall Thickness (North)	(mm)
4)	Wall Thickness (South)	(mm)
5)	Wall Thickness (West)	(mm)
6)	Wall Thickness (East)	(mm)
7)	Drawing Speed	(m/s)
8)	Mandrel Pressure	(mmH_2O)

The pre-processing of the collected process data involves the following steps [118]:

- **Peak Shaving:** This is required to reduce the effects of spikes (peaks due to *e.g.* loose contacts, power failure, cross-talk between cables etc.) on measured process signals. In industrial practice, spikes are often induced in the sensors and the long leads from the sensors to the measuring equipment. The spikes may have a large influence on the identification results and therefore have to be removed.

- **Trend Correction:** This is generally required as the measured process signals often show slow drifts or variations. In general, trends and drifts may a have a bad influence on the estimation results. They do not average out because of their low frequency behaviour and they will cause considerable bias of the model. This type of disturbance can be easily compensated for by simply applying feedback control. Hence, if the model is used for control design, there is no need to model this part of the signal.

- **Data Reduction:** The collected input and output signals may be reduced from 8 to 4 signals. This is done by averaging the two measured diameters 1) & 2) and averaging the four measured wall thicknesses 3), 4), 5) & 6).

- **Delay Correction:** This is required for model estimation in order to avoid identifying relatively high-order models. The time delays can be compensated for by simply shifting the input and output signals relative to each other. One of the signals is used as a reference and the remaining signals are shifted in time in order to compensate the delays.

- **Data Decimation:** This is the last step of the pre-processing stage and is also known as sample rate reduction. This step is necessary because redundancy has been built into the data by sampling faster than necessary. If there is noise energy in the high frequency band beyond the range of interest, the input and output signals are filtered with a low-pass Butterworth filter to cut it off.

7.4.2 Identification Experiments

Staircase Experiment

This type of experiment [118] is directed to test the range of linearity of the process, to find the static gains, and to have a rough estimation of the largest time constant. The estimate of the largest time constant is required to define the duration of an experiment directed to parameter estimation. Staircase test signals are applied to the selected process inputs. The time interval of one stair should allow the process to reach its steady-state.

For the glass tube production process, a data set of 16200 samples (mandrel pressure) and 33200 samples (drawing speed) were collected. An oversampling ratio of 20 was chosen for data pre-processing. Figure 7.3 shows a staircase test at the mandrel pressure and drawing speed. Clearly, the control inputs of the mandrel pressure and drawing speed were changed with block shaped orthogonal test signals of various amplitude levels balanced around nominal levels. Each block was kept at a constant level for at least 3 minutes with 2 or more amplitude levels both above and below the nominal level. The figure also shows the measured process outputs, average output diameter and average wall thickness. From these plots, it is clear that the glass tube production process behaves statically linear. Figure 7.4 shows the non-linear effects. In this figure, the steady-state values of the process, for each interval and input-output pair, are plotted with an asterisk. A 1st-order polynomial is fitted (solid line) to the measured steady-state values. Clearly, all the points can be approximately connected. Therefore, the system is approximately statically linear. The slopes of the plots are the estimated static gains listed in Table 7.2. The plus and minus signs stem from the physical nature

	Mandrel pressure	Drawing speed
Wall thickness	-0.0229	-6.0477
Diameter	0.3112	-65

Table 7.2: Static Gains.

of the inputs and outputs: An increase in mandrel pressure will cause a decrease (-) in wall thickness and an increase (+) in diameter; an increase in drawing speed will cause a decrease (-) in both wall thickness and diameter.

Free-Run Experiment

In this type of experiment [118] none of the inputs are activated. The process is simply running in open-loop. The outputs of the process should then be measured over a long period of time until the statistical properties of the measured output signals show no significant change. The main purpose of this experiment is to determine the standard deviations and the bounds of the noise on the measured inputs and outputs.

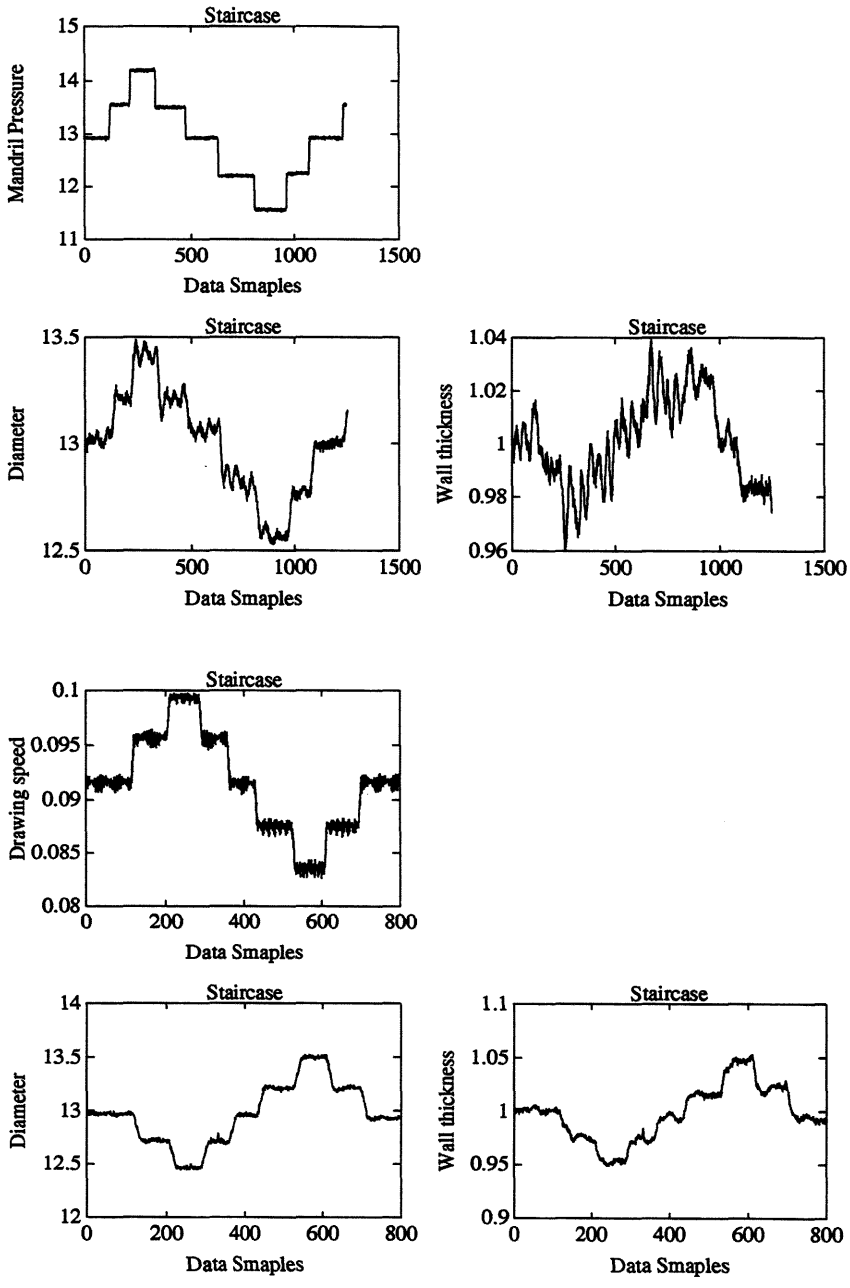

Figure 7.3: Staircase Experiment.

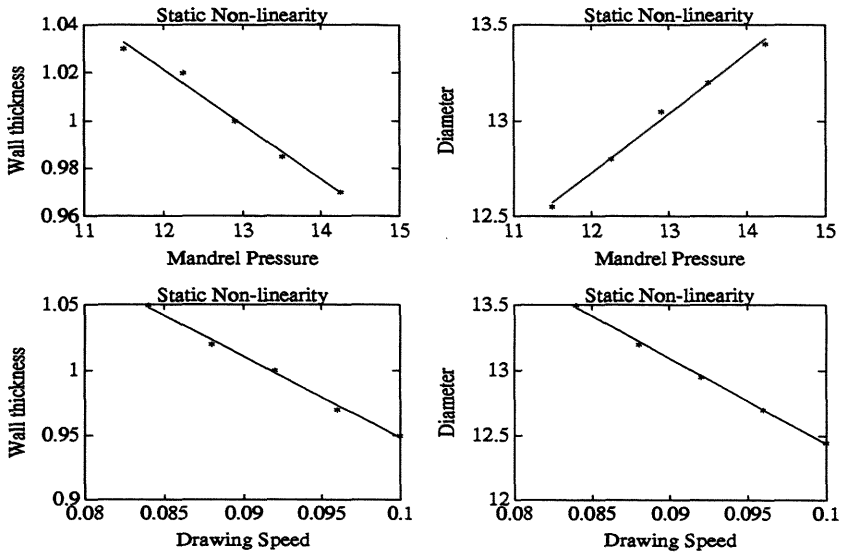

Figure 7.4: Static Non-linearity Test.

For the glass tube production process, measurements were taken of the average wall thickness and average output diameter without changing the drawing speed and mandrel pressure from their nominal values. The experiment covered about 45 minutes production time. This resulted in a data set of 15000 samples. An oversampling ratio of 10 was chosen for data pre-processing. Figure 7.5 shows the process input and output signals and the corresponding auto-correlation functions. Clearly, the measurement noise for the mandrel pressure is white, but the drawing speed is correlated. The peaks in this signal correspond to the rotation frequency of the measurement wheel. The auto-correlation functions of the wall thickness and diameter show the colouring of the output noise.

White Noise Experiment

This experiment [118] involves the application to the process inputs of a set of mutually independent Pseudo Random Binary Noise Sequence (PRBNS) test signals of proper length and high clock frequency. The length of the PRBNS test signal should at least

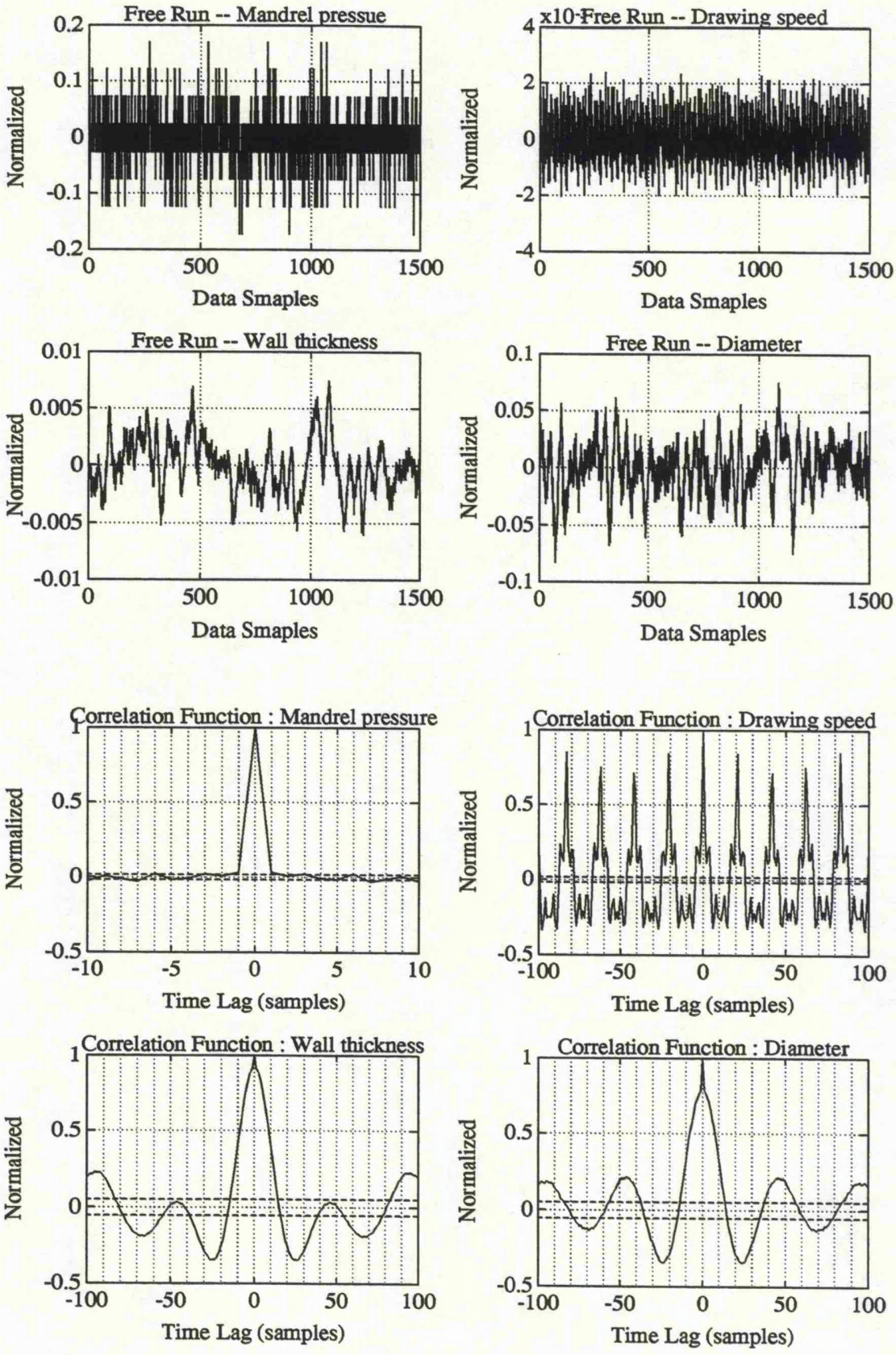

Figure 7.5: Free Run Experiment.

be 5-10 times the largest time constant estimated from the staircase experiment.. The clock frequency is determined on the basis of the staircase signal responses. The amplitudes of PRBNS signals are determined by the already estimated range of linearity for each input. The main purpose of this experiment serves for time delay estimation, model estimation, and model validation.

For the glass tube production process, PRBNS test signals were applied simultaneously to both the mandrel pressure and drawing speed. The experiment was planned to cover at least 45 minutes production time. This resulted in a data set of 15000 samples. An oversampling ratio of 10 was chosen for data pre-processing. Since the diameter sensors are located at different heights, the relative delay between the two diameter readings must be calculated before the average diameter signal is constructed. The time delay which corresponds to the peak value in the cross-correlation (Figure 7.6) between the North/South and East/West diameter signals defines this relative delay. The wall thickness sensors are installed at the same height, so the relative delay between the sensors are almost negligible.

From this experiment, the next step is to estimate the process time delays. They are determined by computing the cross-correlations between all the input and output signals as shown in Figure 7.6. The estimated process time delays are listed in Table 7.3. Finally, for model identification the first 700 samples were selected for the estimation data and the remaining data samples for the model validation. The input-output estimation data has been scaled to unit standard deviation and is shown in Figure 7.7.

	Mandrel pressure	Drawing speed
Wall thickness	60	50
Diameter	30	20

Table 7.3: Time Delays (samples).

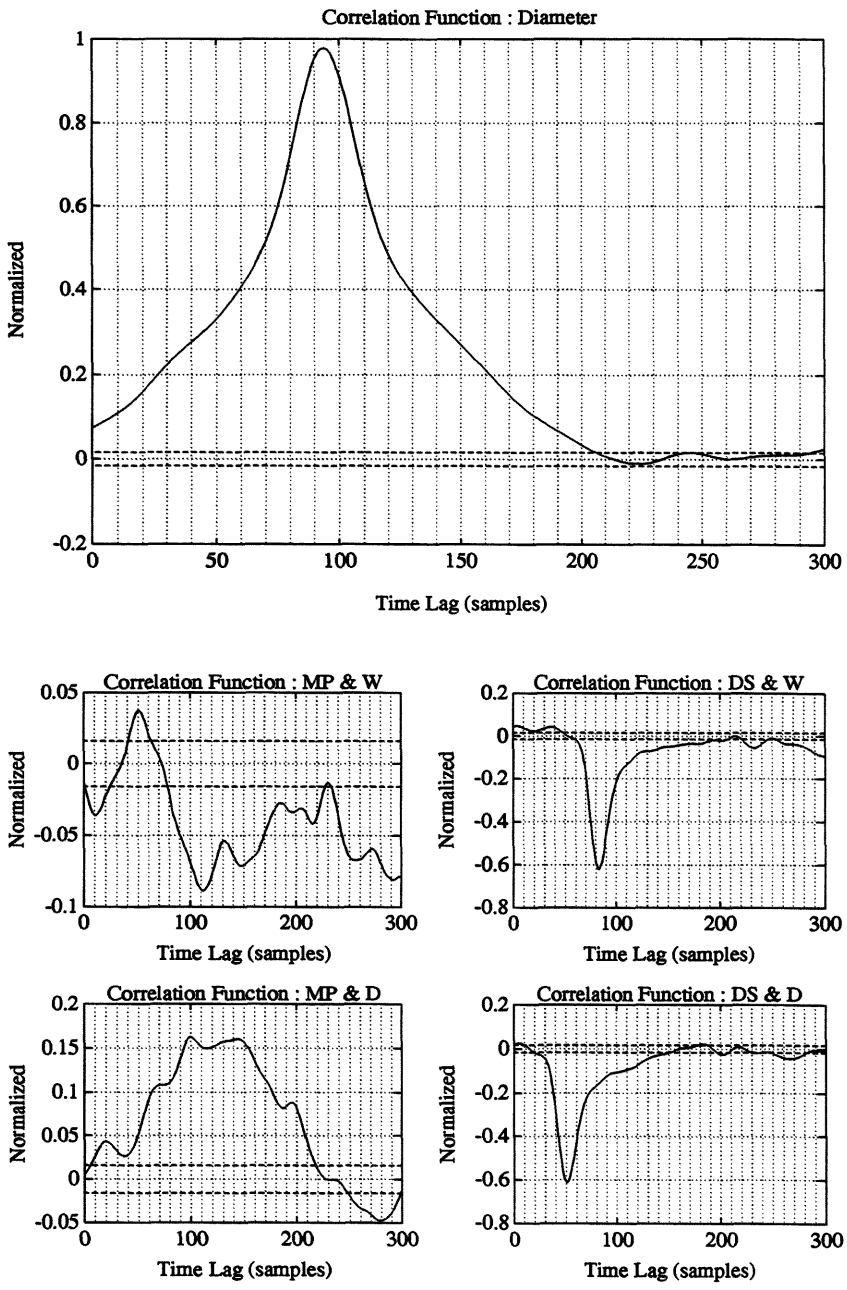

Figure 7.6: Estimating Time Delays: The dashed lines indicate 95% confidence intervals.

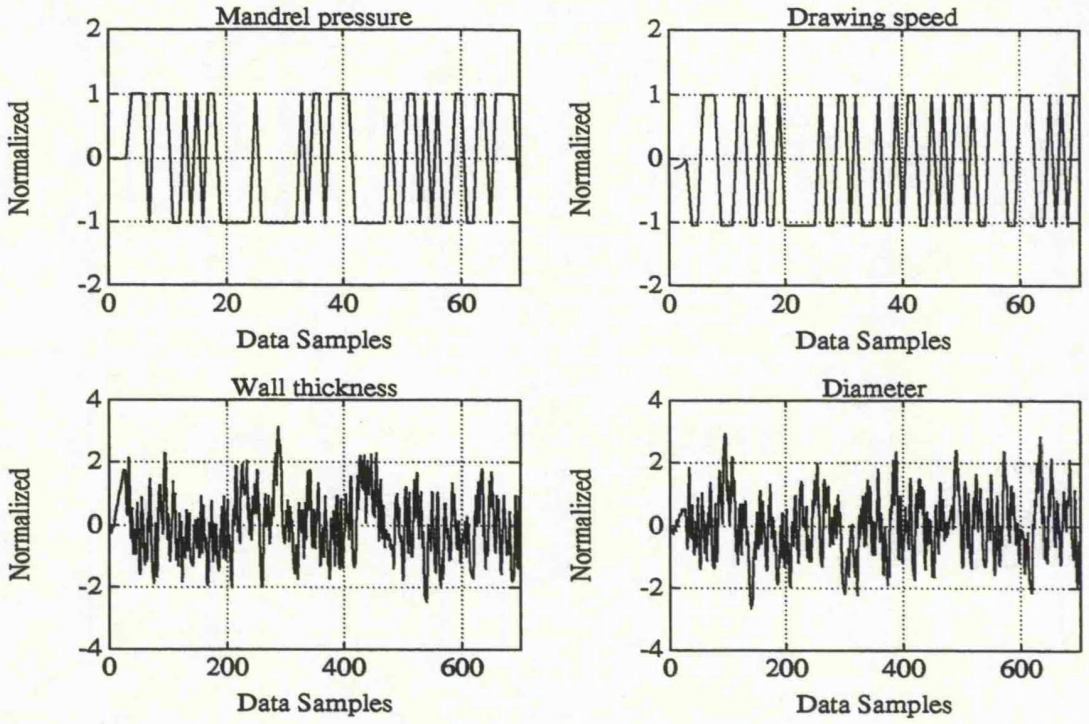

Figure 7.7: Estimation Data.

7.5 Model Estimation and Validation

For model estimation, the integrated identification approach discussed in Section 7.3 was followed. An initial model using the state-space approach was first calculated. The order of the model was selected based on the singular value decomposition of block Hankel matrices which can be built from the process input-output signals [81]. This is clearly shown in Figure 7.8. The next step is to optimize the initial model using the minimal polynomial approach. One of the major requirements for this approach is that the process input-output data is scaled in such a way that the white noise sequences disturbing the process have equal variance [27]. In order to obtain a model which is suitable for controller design and to obtain a white prediction error, a Box-Jenkins model structure [60] has been adopted. A *6-th* order process model and a *2-nd* order noise model were selected. Figure 7.9 shows the computed auto-correlation of the prediction error for the process outputs. This clearly indicates that the prediction error is almost white, since it is almost completely within the confidence intervals.

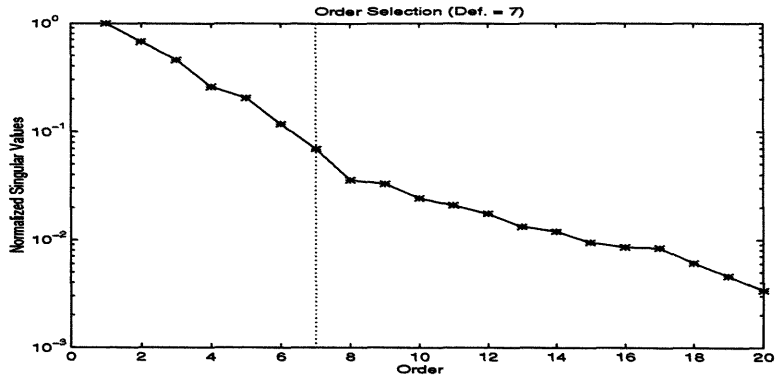

Figure 7.8: Initial Model-order Selection.

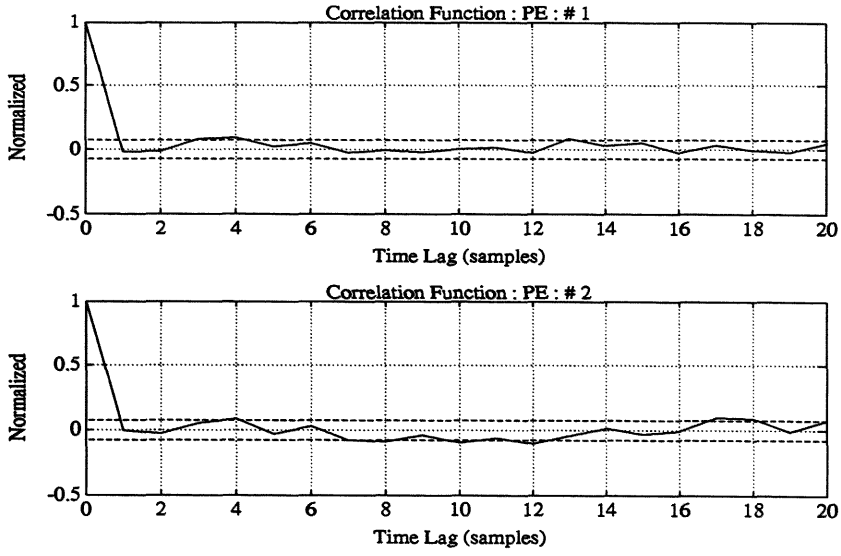

Figure 7.9: Auto-correlations of the Prediction Errors.

Standard deviation	σ_e	σ_v
Wall thickness	0.1820	0.1795
Diameter	0.1896	0.2069

Table 7.4: Model Validation.

For model validation, the prediction errors for both data sets, estimation and validation are shown in Figure 7.10. The prediction errors have been scaled to a normalized value by dividing by the standard deviation of the corresponding output. The standard deviations of these normalized prediction errors for both the estimation (σ_e) and the validation (σ_v) data set are listed in Table 7.4. This validation using an independent data set shows very clearly that a good accurate model of the glass tube production process has been obtained in the defined operating point. Another indication of the model accuracy is shown is Figure 7.11, where the cross-correlations between the prediction errors and the process inputs are computed. It is clear from this figure that no clear correlation is present.

Finally, a further indication of the model accuracy is shown in Figure 7.12. In this figure the magnitude plots of the process model are compared with the estimated spectra of the process input-output data for each transfer. The *6-th* order process model can accurately describe the dynamical behaviour of the glass tube production process. This minimal polynomial model of order $n = 6$ can then be converted into a state-space representation of order $n.\min(nu, ny)$, where nu and ny are the number of process inputs and outputs, respectively. To realize the smallest possible state-space system, a controller canonical form is selected [118]. A *12-th* order state-space model was obtained for Measures 1 & 2, and an *8-th* order model for Measure 3. The singular values for all measures are shown in Figure 7.13.

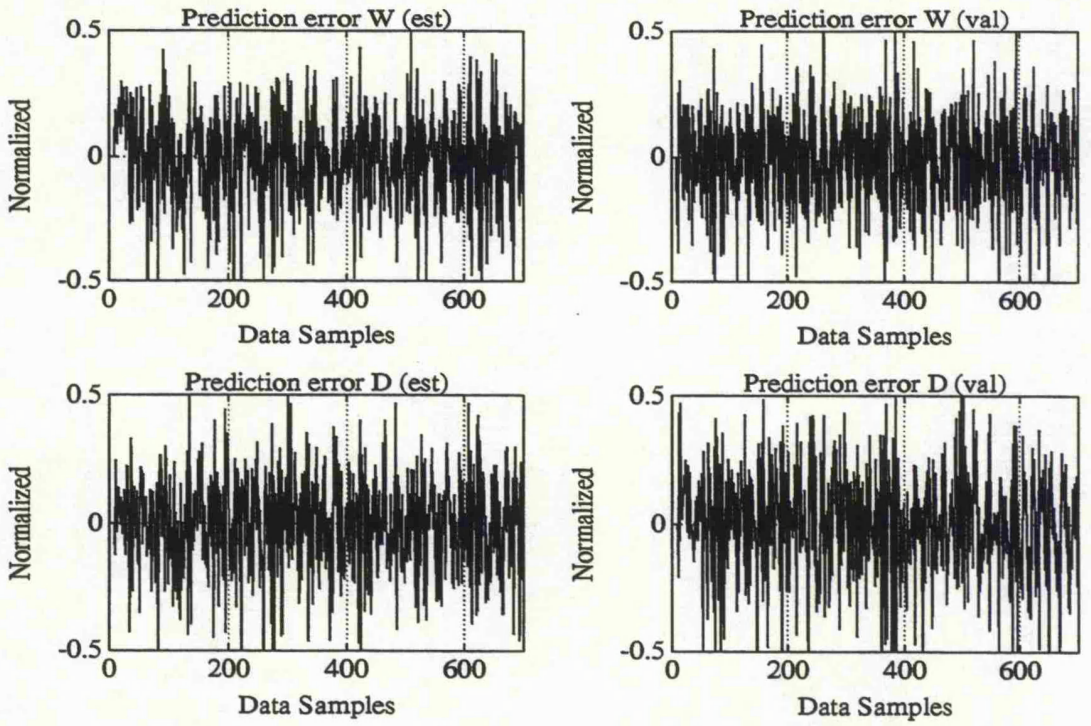

Figure 7.10: Prediction Error for Estimation (left) and Validation (right).

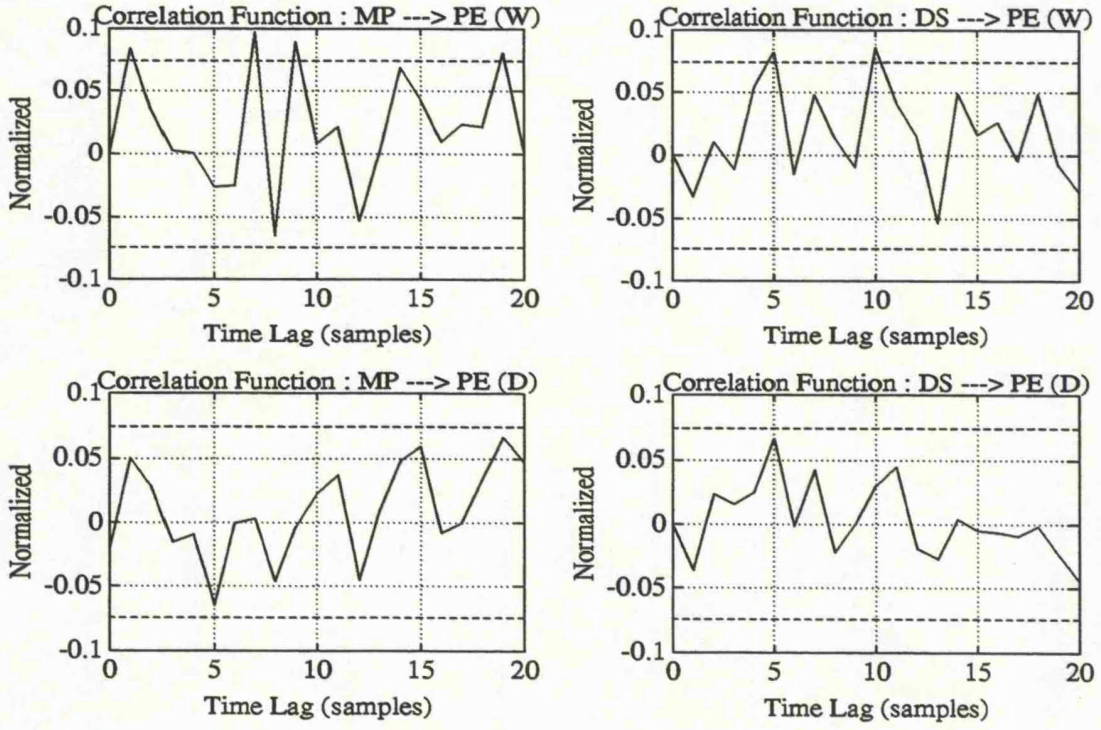

Figure 7.11: Cross-correlation between the Prediction Errors and the Process Inputs.

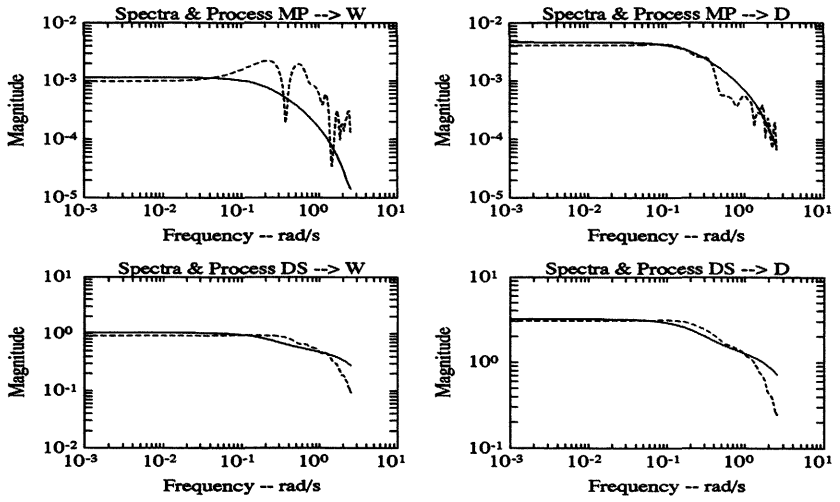

Figure 7.12: Magnitude Plots: Spectra of the Input-Output Data (dashed) and the Estimated Process Transfer Functions (solid).

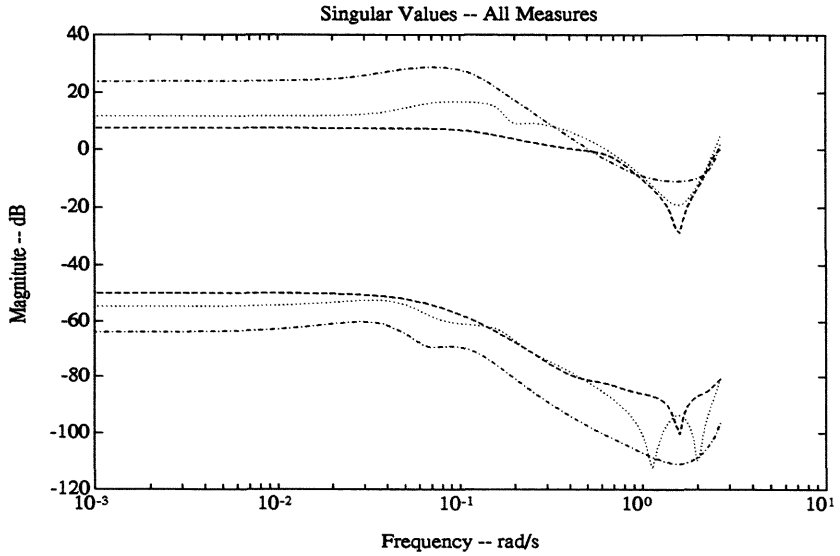

Figure 7.13: Magnitude Plots: Measure 1 (dashed) – Measure 2 (dotted) – Measure 3 (dash-dotted).

7.6 Summary

In this chapter, the principle of advanced multivariable process identification was briefly introduced and applied to an industrial glass tube production process. The problem of experiment design together with the principle of data pre-treatment were discussed and shown to be the most crucial steps towards extracting good and reliable information about the process dynamics, and towards repairing the data so as to avoid the problems of high frequency disturbances, spikes and outliers, low frequency disturbances such as drifts and offsets, and the numerical values of different inputs and outputs which are not in the same order of magnitude in the model estimation and validation steps. In the next chapter the identified models will be used for the design of robust IMC controllers.

Chapter 8

Applying Robust IMC Control to a Glass Tube Production Process

8.1 Introduction

Robust control system design is receiving considerable attention in the process industry due to the growing demands on the high quality of products and on the ease of flexibility towards changeovers. The old strategies based on classical control have proven to be inadequate for multivariable process control where a high degree of interaction exists between the inputs and outputs. Scalar techniques are only useful for primary single-input single-output (SISO) control, and hence more advanced control methodologies are necessary. In addition to the latter, novel control schemes are also being studied. The IMC scheme is the most popular scheme (over the classical feedback structure) in the process industry and the advantages of such a scheme were justified in Chapter 5.

The aim of this chapter is to demonstrate, on the basis of the different models derived from advanced multivariable identification, that a well performing and industrially applicable robust MIMO control system can be designed. The MIMO industrial process control problem will be the shaping part of the glass tube production process of which the description and the identification of this process has been discussed in Chapter 7. A mixture of time domain performance specifications and robust stability specifications are desired to be met. In order to satisfy both requirements, the 2-DOF IMC approach formulated in Chapter 5, together with the method of inequalities (MOI) discussed in Chapter 4, is applied. Both Type 1 and Type 2 controllers will be designed for three

operating points.

Notable attempts for designing controllers for the glass tube production problem can be found in [6, 81, 44]. In [6], Type 1 IMC controllers were designed *via* linear quadratic-implicit model following control (a model reference type of control system) as discussed in Chapter 5, but the controllers were designed for tube sizes (measures) that differ from the present ones. In [81], Type 1 multivariable PID controllers were designed. The PID parameters were tuned using a multi-objective optimization tuning algorithm that can provide a solution when different measures of quality are considered simultaneously and trade-offs are inevitable; however, this design approach failed to synthesize a satisfactory PID controller for large measures (3*rd* operating point). In [44], a Type 1 (1-DOF) $\mathcal{H}^\infty$ controller was designed based on the normalized right coprime factor design procedure proposed by [62].

The organization of this chapter is as follows. In Section 8.2 a detailed design study of the glass tube production process will be presented. Section 8.3 motivates the proposed control system design approach by comparing it with the results obtained from the present control system proposed in [6]. Section 8.4 outlines the controller design procedure used to synthesize the controllers. Section 8.5 presents the simulation results obtained from the proposed control system. Finally, a summary is given in Section 8.6.

8.2 Glass Tube Design Study

8.2.1 An Overview of the Control Problem

Each furnace in the glass tube production process is equipped with a MIMO control device which is used for controlling the wall thickness and external diameter of tubes. When these glass tubes are used in the production of gas-discharge lamps, the internal diameter is very important since the volume of gas to be filled in the lamp very much determines the characteristics of the lamp.

It is not possible to measure the internal diameter directly. Two external diameter sensors placed vertically on top of each other and four wall thickness sensors each displaced by 90 degrees with respect to each other are used for measuring the dimensions

of the glass tube. It is possible to deduce the internal diameter from the average of two external diameters and the average of four wall thicknesses. This process takes account of the fact that it is not possible for these dimensions to be measured at the same time.

The glass tube production process is presently used for the production of well over 300 different product types. Specifications of these products differ quite significantly and some of these products have to meet stringent specifications, which are beyond the limits of what can be realized at present. The specifications are on the external diameter and on the wall thickness of the tubes. Currently, the whole range of products is produced with a few very robust IMC schemes. These control systems do not perform well enough to enable production of the new products with narrow tolerances. High performance control systems have to be designed to enable production of these new products; however, these newly designed control systems have to be sufficiently robust to cope with model inaccuracies encountered over production runs.

The objective of this case study is to design and test three IMC controllers for controlling the average external diameter and the average wall thickness for tubes with three different measures which are used for the production of gas-discharge lamps.

8.2.2 Open-Loop Analysis of the Process

As discussed in Chapter 7, a PRBNS experiment has been carried out on the production process in order to obtain the required data for system identification. After performing some preliminary signal processing on the raw data, the desired output signals, average wall thickness and average external diameter, were constructed. The pre-processed data has then been used to estimate linear discrete-time state-space models of the process at three desired operating points using advanced multivariable identification, where a nominal model was identified for each operating point, mainly by using the Minimal Polynomial approach (MPI). Other models were also identified using the Subspace State-Space approach (N4SID), and the Robust Control Oriented approach (RCOM). Two extra models were identified for each operating point using N4SID. Table 8.1 lists the information needed regarding the state-space models. Figures 8.1-8.4 show the open-loop step responses of the outputs and the frequency response characteristics for all

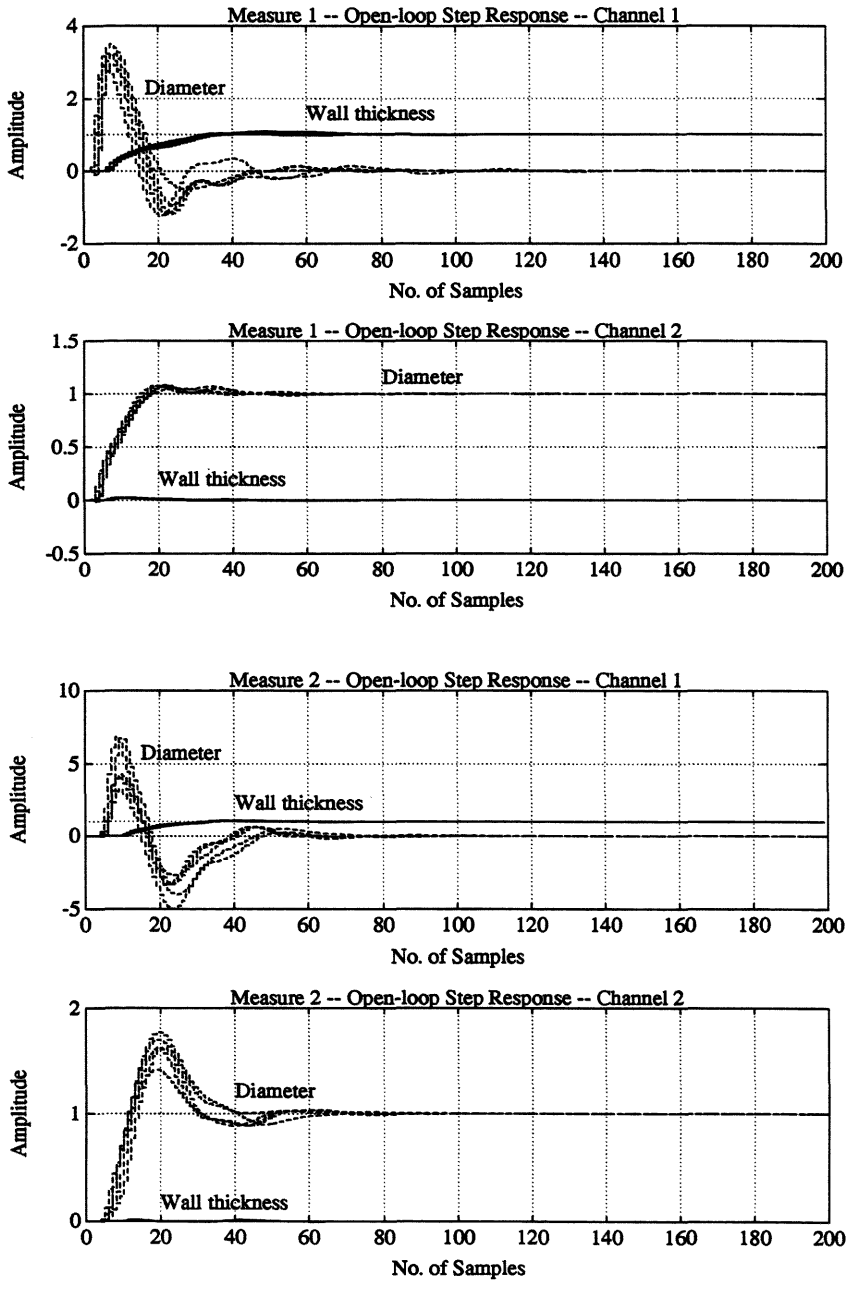

Figure 8.1: Open-loop step responses of the process outputs.

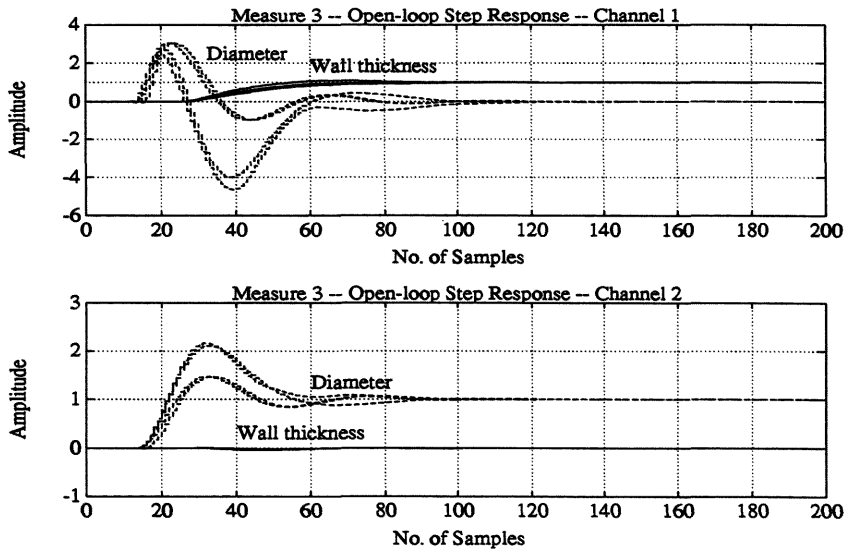

Figure 8.2: Open-loop step responses of the process outputs.

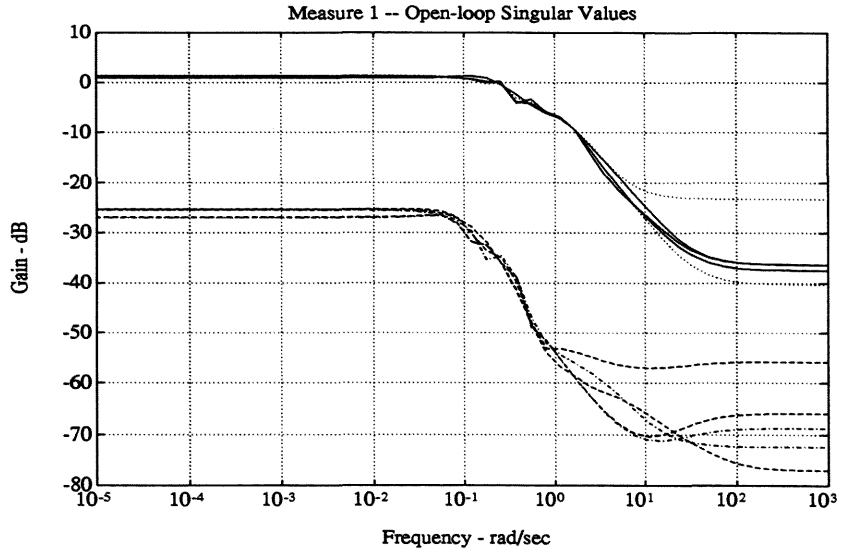

Figure 8.3: Open-loop frequency response characteristics.

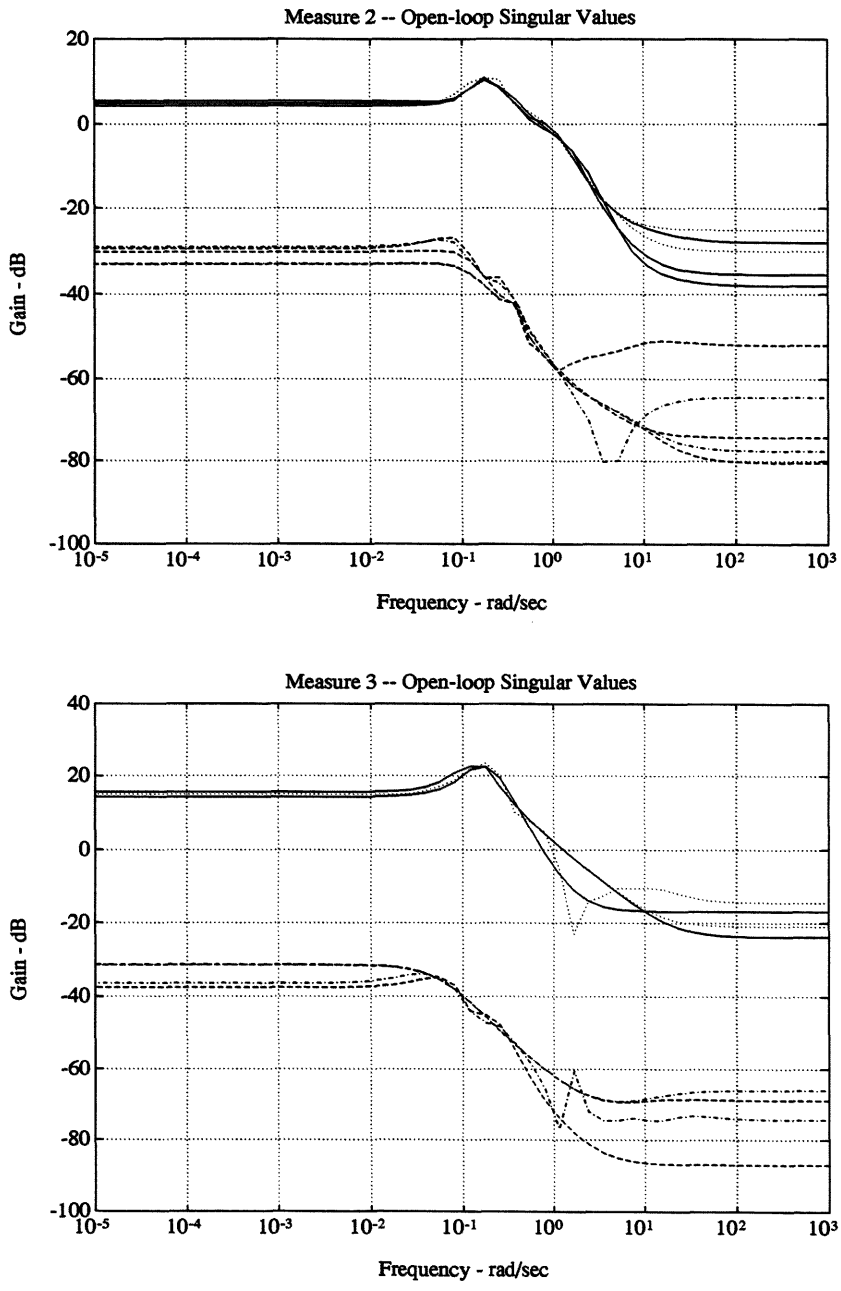

Figure 8.4: Open-loop frequency response characteristics.

Identification Approach	Order of State-Space Models					
	Measure 1		Measure 2		Measure 3	
	No Delays	With Delays	No Delays	With Delays	No Delays	With Delays
MPI	12	24	12	27	8	49
N4SID	10	20	7	22	3	44
RCOM	22	32	18	33	18	59

Table 8.1: Model Information.

three measures. The time responses are pre-multiplied with the inverse steady-state. These responses clearly indicate that overshoot, oscillatory characteristics, and high coupling have to be eliminated.

One important commonly used index of plant controllability is the condition number κ_a, which is the ratio of the largest to the smallest singular value. It is a measure of the relative difference between the strength and weaknesses of the system [15]. In terms of the process control problem, a large condition number indicates that it will be impractical, if not possible, to satisfy the entire set of control objectives, regardless of the control method used. In the physical sense, the condition number represents the ratio of the maximum and minimum open-loop decoupled gains of the system. A large condition number indicates that the relative sensitivity of the various multivariable dimensions is quite different. From a practical point of view, it means that at least one direction, in terms of all the sensors, is either too weak or too strong to be effectively controlled. Applying a multivariable control strategy that attempts to control the system in the direction of poor sensitivity may well result in a multivariable performance that is unsatisfactory even in those directions in which the sensitivity is good.

The condition numbers for the glass tube production process are listed in Table 8.2. These numbers show, on a relative basis, how much more difficult it will be to control the tube dimensions at the $3rd$ operating point than it would be to control the dimensions at operating points 1 & 2. However, it is difficult to assign condition numbers that separate the *well behaved* process from the *poorly behaved* process and the *difficult to*

Measure	κ_a
1	20.987
2	46.317
3	451.218

Table 8.2: Process Condition Number.

control process from the *impossible to control* process. A process might have a good condition number but have singular values too low or too high for good control.

The dynamics of the process are also very important in determining the ultimate difficulty of controlling a multivariable system. In [15] it has been noted that if a process has very well behaved dynamics and little noise in the sensor signals, it might be practical to attempt to control the system with a high condition number. If, on the other hand, the dynamics are poor (*i.e.* significant time delays), it might not be possible to successfully control the process with a low condition number. In general, the magnitude of the condition number cannot be used to make a final judgement on the multivariable problem, but it is a good first-pass screening. If the process characteristics are poorly behaved at steady-state, the situation is likely to get worse as other aspects of the problem are considered.

It is clear from Table 8.1 that the time delays have a relatively strong effect on the dynamics of the process, especially at the $3rd$ operating point. This can exert severe limitations on the so-called dynamic resilience, which is defined in [46] as: the quality of the regulatory and the servo behaviour which can be obtained for a plant (*i.e.* the final closed-loop performance). For a MIMO process, the analyses of dynamic resilience on the basis of time delays is not at all obvious. This is because not only the magnitudes of the time delays are important, but also their distribution within the transfer function matrix. Table 8.3 lists the time delays of each element of the transfer function matrix for the glass tube production process, where MP and DS are the process inputs (Mandrel Pressure and Drawing Speed), WT and OD are the process outputs (Wall thickness and Outer Diameter).

It was shown in [46] that the IMC scheme is very useful for the analysis of dynamic

	Tube Measure					
	1		2		3	
	MP	DS	MP	DS	MP	DS
WT	10	8	20	18	52	50
OD	6	4	12	10	26	24

Table 8.3: Process Time Delays (in seconds).

resilience. As shown in Chapter 5, the input and output transfer function in the absence of plant/model mismatch is given by

$$y_{p_k} = G_p Q r_k + (I - G_m Q) d_k \tag{8.1}$$

where perfect control can be achieved by selecting $Q(z) = G_p(z)^{-1}$. However, perfect control cannot be achieved if

1) $G_p(z)$ contains time delays, and/or

2) $G_p(z)$ contains transmission zeros outside the unit circle.

Even in the absence of those problems, it is undesirable to select the perfect controller since

1) its use may result in rippling behaviour of the control signals, resulting in output oscillations owing to the presence of transmission zeros of $G_p(z)$ close to the unit circle, and

2) a system equipped with a perfect controller is very sensitive to modelling errors.

To overcome the difficulties associated with perfect control, the approach that may be adopted [33] is to split the process transfer function matrix into two parts according to the factorization

$$G_p(z) = G_+(z) G_-(z) \tag{8.2}$$

where $G_+(z)$ accommodates any time delays such that $G_-(z)^{-1}$ is realizable. If $G_-(z)^{-1}$ is also stable, then $Q(z)$ is selected according to $Q(z) = G_-(z)^{-1}$. If $G_p(z)$ contains transmission zeros outside the unit circle, then $G_-(z)^{-1}$ will not be stable, in which case a further factorization will have to be carried out.

To determine $G_+(z)$, the multiple time delays must be factored out [46]. When the transfer function matrix contains unequal time delays, a diagonal factorization matrix $G_+(z)$ may be selected according to

$$G_+(z) = \textbf{diag}\left[z^{-(\tau_1+1)}, z^{-(\tau_2+1)}, \ \ldots\ , z^{-(\tau_r+1)}\right] \tag{8.3}$$

with

$$\tau_j = \max \max_i(0, \bar{\tau}_{ij}),\ j = 1,\ \ldots\ , r \tag{8.4}$$

where $z^{\bar{\tau}_{ij}+1}g_{ij}(z)$ are elements of the process inverse matrix $G_p(z)^{-1}$ such that $g_{ij}(z)$ are semi-proper. A ratio of polynomials $g_{ij}(z)$ that is semi-proper in z is one in which the order of the numerator $g_{ij}(z)$ is less than or equal to the order of its denominator. For the glass tube production process problem, the $3rd$ operating point will be considered as an illustrative example. Let $G_p(z)$ be given by

$$G_p(z) = \begin{bmatrix} z^{-26}g_{11}(z) & z^{-25}g_{12}(z) \\ z^{-13}g_{21}(z) & z^{-12}g_{22}(z) \end{bmatrix} \tag{8.5}$$

The inverse of (8.5) is

$$G_p(z)^{-1} = \frac{1}{g_{11}(z)g_{22}(z) - g_{12}(z)g_{21}(z)} \begin{bmatrix} z^{26}g_{22}(z) & -z^{13}g_{12}(z) \\ -z^{25}g_{21}(z) & z^{12}g_{11}(z) \end{bmatrix} \tag{8.6}$$

Thus,

$$\begin{aligned} \bar{\tau}_{11} &= 25,\ \bar{\tau}_{12} = 12,\ \bar{\tau}_{21} = 24,\ \bar{\tau}_{22} = 11 \\ \tau_1 &= \max\left[\max(0,25), \max(0,24)\right] = 25 \\ \tau_2 &= \max\left[\max(0,12), \max(0,11)\right] = 12 \end{aligned}$$

and

$$G_+(z) = \begin{bmatrix} z^{-25} & 0 \\ 0 & z^{-12} \end{bmatrix} \tag{8.7}$$

The significance of this result is that for a dynamically decoupled output the best response that can be achieved for the closed-loop system, no matter what type of controller is used, will have a time delay of 25 samples (50 seconds) in the wall thickness and 12 samples (24 seconds) in the diameter.

8.2.3 Design Specifications

The aim of the 2-DOF IMC design approach is to produce a controller (of two parts) which will meet typical robust performance and robust stability specifications on the basis of a nominal model taken from a bank of models around the same operating point. The time-domain specification is given in terms of a step response requirement and translated into a set of inequalities which must be met by the controller for all the models. It is required that the process signals satisfy the following constraints:

1) Closed-loop stability.

2) The wall thickness to a step demand $r(t)$ (t-minutes) $\begin{bmatrix} 0.2 \\ 0 \end{bmatrix}$ satisfies

Measure	$y_1(t)$		$\lvert y_2(t)\rvert$	$\lvert u_1(t), u_2(t)\rvert$
1	$\leq 0.2,\ \forall t$	$\geq 0.18,\ \forall t > 1.10$	$\leq 0.08,\ \forall t$	< 20
2	$\leq 0.2,\ \forall t$	$\geq 0.18,\ \forall t > 1.80$	$\leq 0.08,\ \forall t$	< 30
3	$\leq 0.2,\ \forall t$	$\geq 0.18,\ \forall t > 2.50$	$\leq 0.08,\ \forall t$	< 70

3) The diameter to a step demand $r(t)$ $\begin{bmatrix} 0 \\ 1.0 \end{bmatrix}$ satisfies

Measure	$\lvert y_1(t)\rvert$	$y_2(t)$		$\lvert u_1(t), u_2(t)\rvert$
1	$\leq 0.01\ \forall t$	$\leq 1.0,\ \forall t$	$\geq 0.90,\ \forall t > 1.10$	< 2
2	$\leq 0.01\ \forall t$	$\leq 1.0,\ \forall t$	$\geq 0.90,\ \forall t > 1.80$	< 3.5
3	$\leq 0.01\ \forall t$	$\leq 1.0,\ \forall t$	$\geq 0.90,\ \forall t > 2.50$	< 13

The main design objectives to be achieved by the IMC controller can be stated as follows:

1) The designed IMC based-control system has to be robustly stabilizable with respect to model inaccuracies encountered over production runs, that is about the desired and slightly different operating points.

2) Good product changeover properties. Changeover should be realized within a pre-defined time without excessive overshoot and undershoot, that is the process outputs (diameter and wall thickness) should follow step command inputs of the controlled process to a specified accuracy. Zero steady-state error and low interaction is also desired.

3) Good disturbance rejection properties in the sense that a trade-off between maximum bandwidth and amplification of the noise outside the bandwidth is desired, and good rejection of slow trends at very low frequencies where Type 2 control is required.

4) The control signals should be within reasonable limits and should be as smooth as possible. Fast variations in these signals are undesirable.

8.3 A Comparison with the Existing Control System

The purpose of this section is to compare the IMC design methods discussed in Chapter 5 (Section 5.3 and Section 5.5). The design methods will be applied to the glass tube production process. It will be demonstrated that the design method of Chapter 5 (Section 5.5) produces IMC controllers which give better robust performance.

In December 1989, the various identification experiments discussed in Chapter 7 were performed on the production process at two different operating points (Measure 1 and Measure 2), resulting in linear discrete-time state-space models. A multivariable identification approach formulated by [6] was used to identify the state-space models. The nominal model was chosen from Measure 1. Philips used the design approach of Chapter 5 (Section 5.3) to synthesize an IMC controller, whereas the new IMC controller was synthesized using the design approach of Chapter 5 (Section 5.5). In both designs the same nominal model was used. Figures 8.5-8.6 demonstrate the nominal and robust performance of the Philips' controller. They show the closed-loop output responses to a set-point change of 0.2 from $0 \rightarrow 13$ minutes, in wall thickness, and a set-point change of 1.0 from $13 \rightarrow 25$ minutes, in diameter. The nominal and perturbed closed-loop systems are stable. For a set-point change in wall thickness, there is 55% interaction in diameter

for the nominal case. For the perturbed case, there is 55% interaction with regards to Measure 1, and over a 100% interaction with regards to Measure 2. Figures 8.7-8.8 demonstrate the nominal and robust performance of the new controller. The nominal and perturbed closed-loop systems are stable. For a set-point change in wall thickness, there is at least 10% interaction in diameter for the nominal case. For the perturbed case, there is 15% interaction with regards to Measure 1, and 70% interaction with regards to Measure 2. For a set-point change in diameter, the interaction on the wall thickness for both, the nominal case and the perturbed case, with regards to Measures 1 & 2 and with both controllers, is small. The new controller clearly demonstrates better robust performance.

In July 1992, new identification experiments were carried out on the same process. The $1st$ operating point slightly differs from the $1st$ operating point of the 1989 process. So, to further test the robust performance of the control system, both IMC controllers were tested on the new identified models. Figures 8.9-8.10 demonstrate the robust performance of the Philips' controller. The perturbed closed-loop systems are stable. For a set-point change in wall thickness, the amount of interaction in diameter ranges from 30% to 90%. Figures 8.11-8.12 demonstrate the nominal and robust performance of the new controller. The perturbed closed-loop systems are stable. For a set-point change in wall thickness, the amount of interaction in diameter ranges from 10% to 40%. For a set-point change in diameter, the interaction on the wall thickness with both controllers, is small. Again, the new controller clearly demonstrates better robust performance. Figures 8.13-8.14 give the corresponding control requirements for the set-point changes. The magnitudes of the control signals are all within acceptable limits. It is clear that the new IMC controller produces non-aggressive control signals and low gain at high frequencies.

Plots of the sensitivity and complementary sensitivity are shown in Figures 8.15-8.16. As would be expected, the new IMC controller performs well here. Figure 8.17 shows that the new IMC controller is much more robust to the presence of high frequency additive and output multiplicative uncertainties than the Philips' IMC controller.

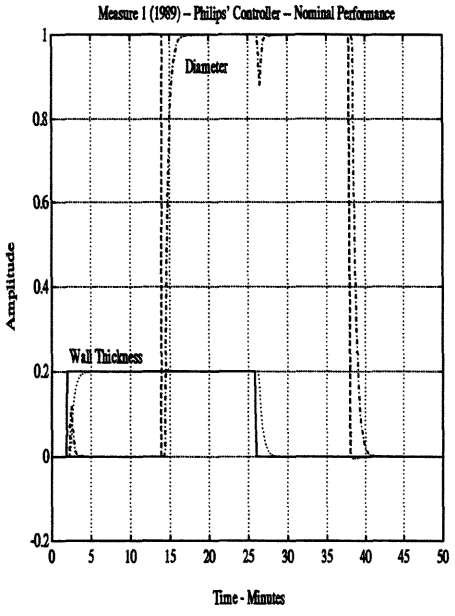

Figure 8.5: Closed-loop Responses due to Set-point Changes – Measure 1 (1989)

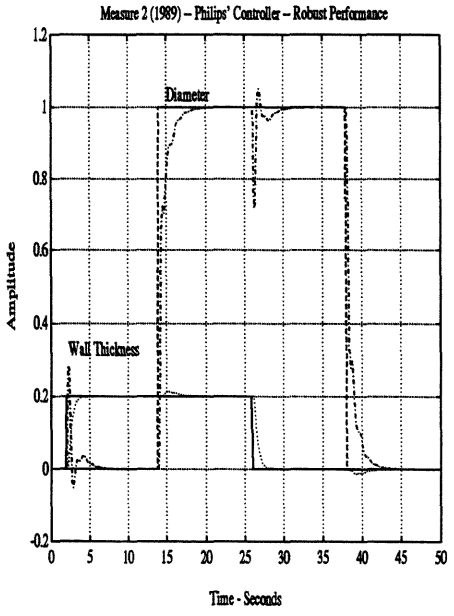

Figure 8.6: Closed-loop Responses due to Set-point Changes – Measure 2 (1989)

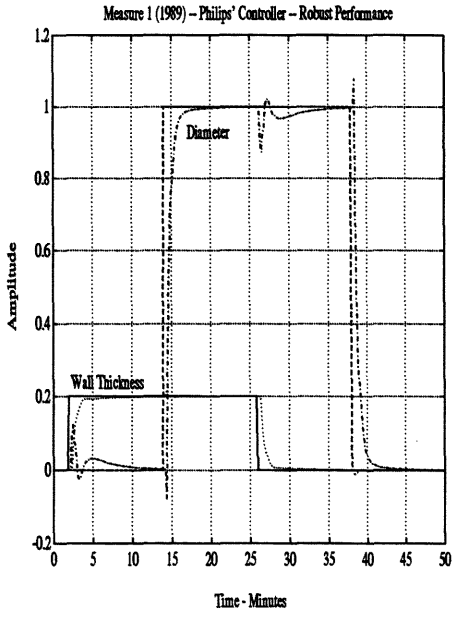

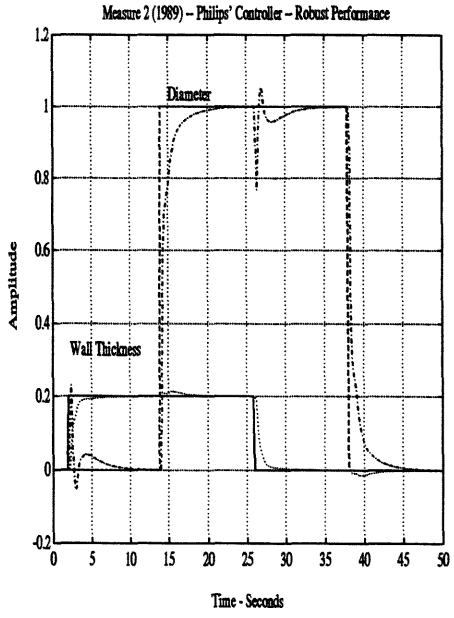

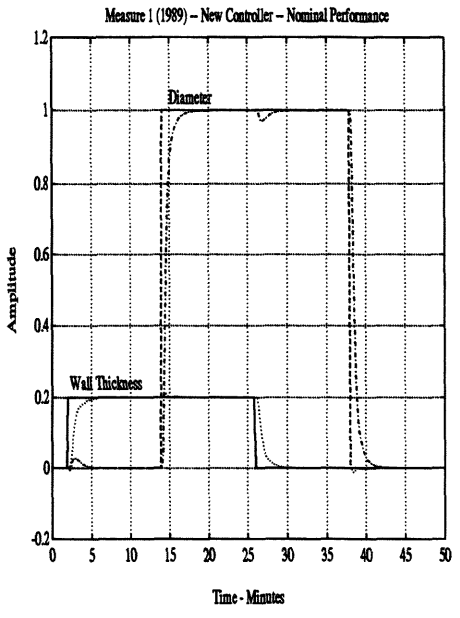

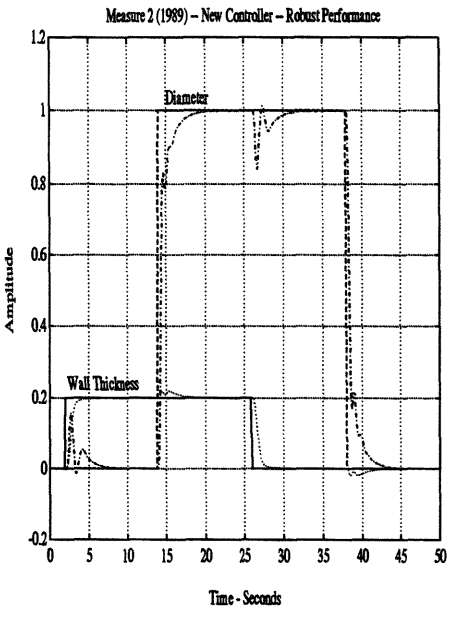

Figure 8.7: Closed-loop Responses due to Set-point Changes – Measure 1 (1989)

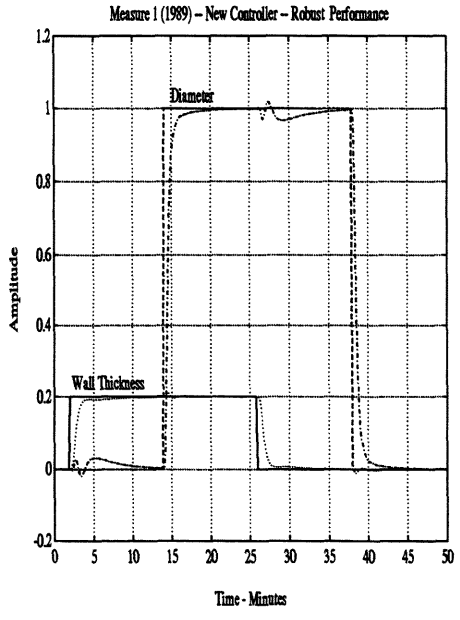

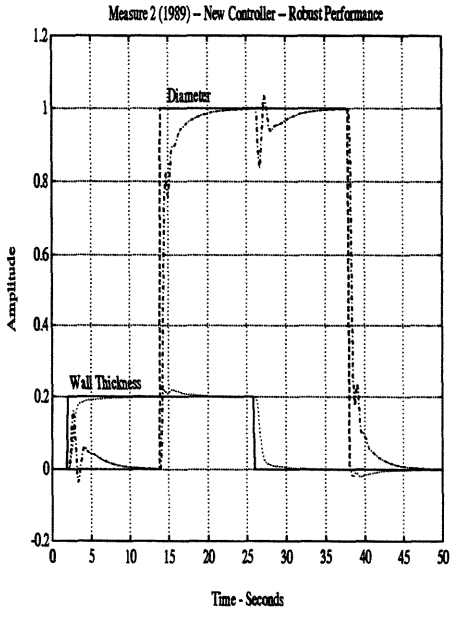

Figure 8.8: Closed-loop Responses due to Set-point Changes – Measure 2 (1989)

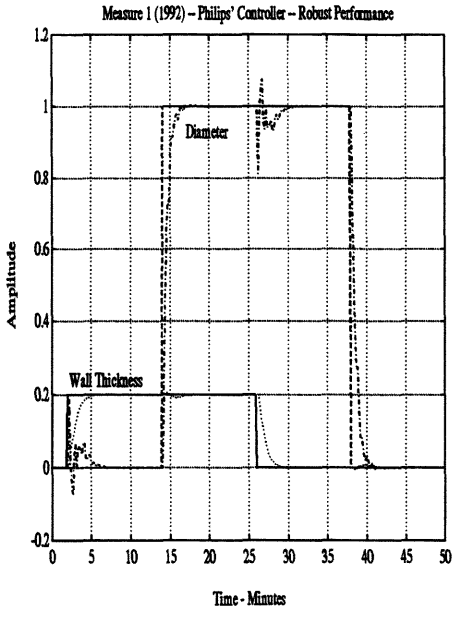

Figure 8.9: Closed-loop Responses due to Set-point Changes – Measure 1 (1992)

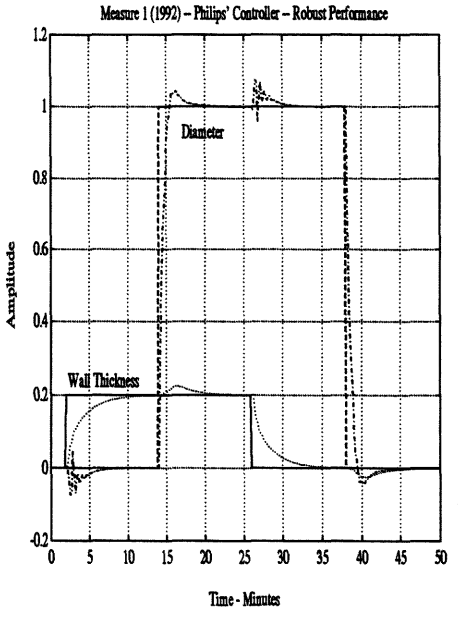

Figure 8.10: Closed-loop Responses due to Set-point Changes – Measure 1 (1992)

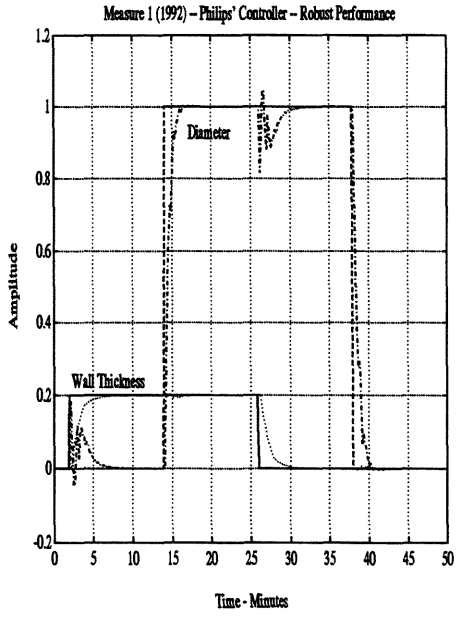

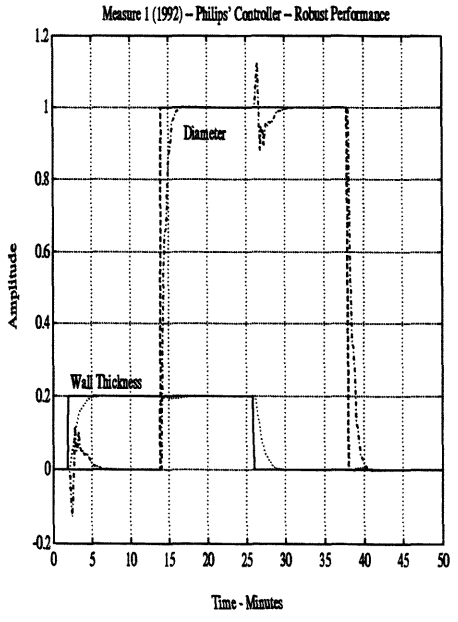

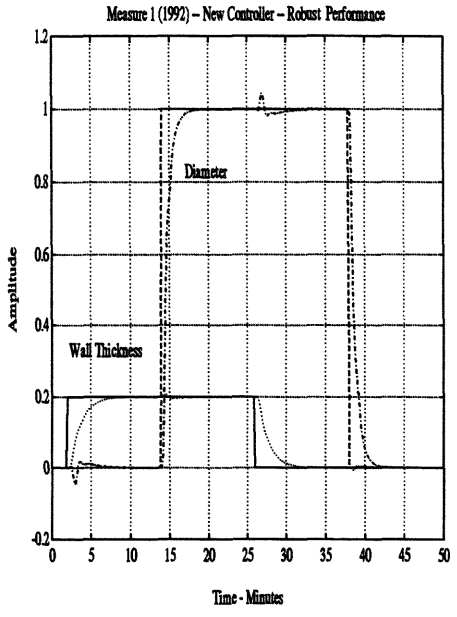

Figure 8.11: Closed-loop Responses due to Set-point Changes – Measure 1 (1992)

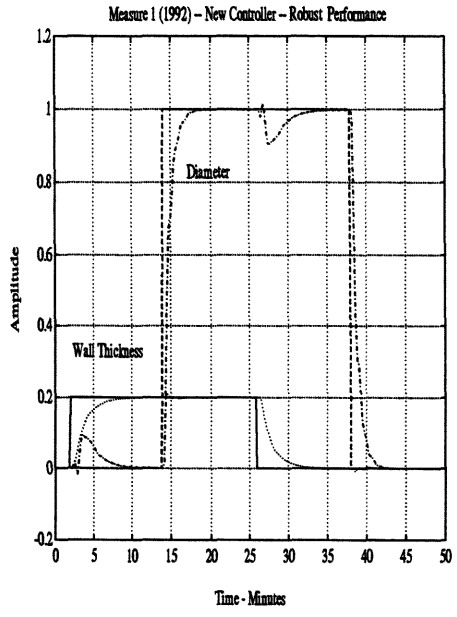

Figure 8.12: Closed-loop Responses due to Set-point Changes – Measure 1 (1992)

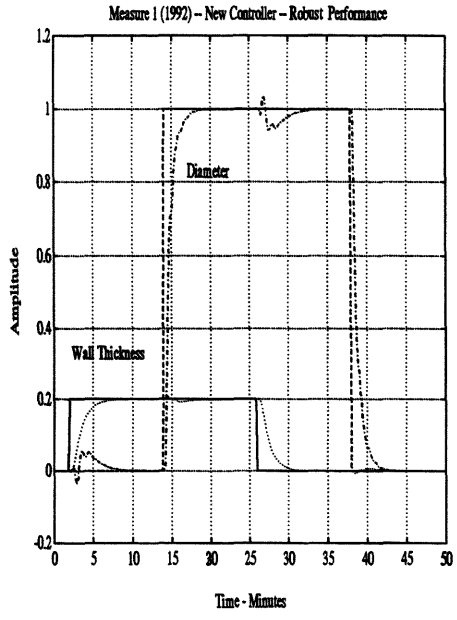

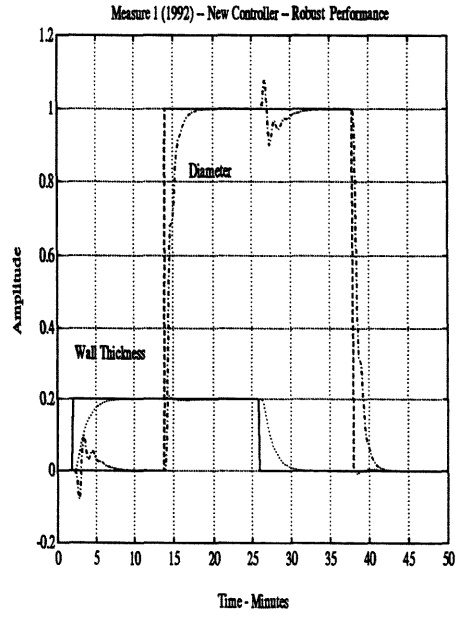

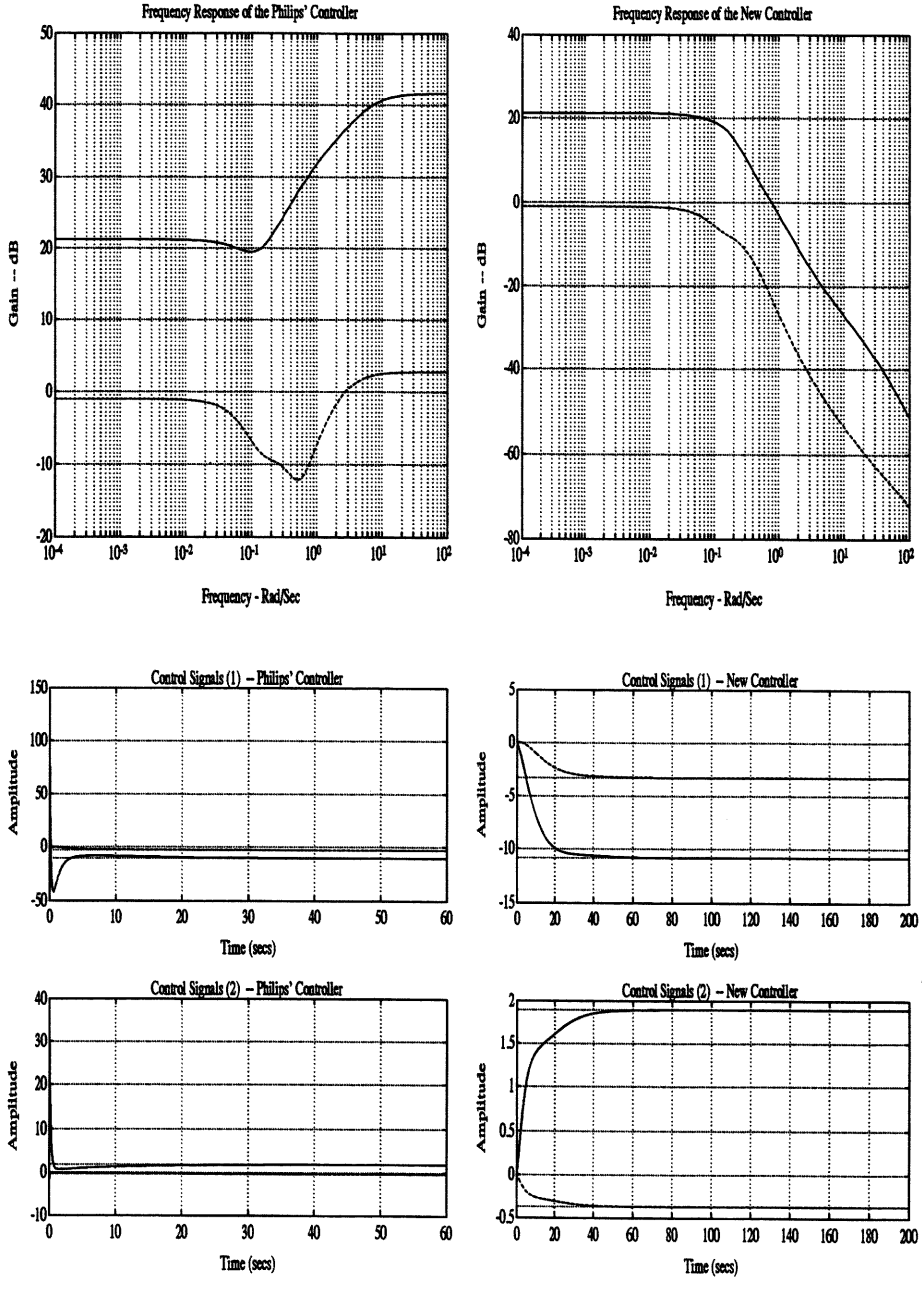

Figure 8.13: The Frequency and Time Responses of the Philips' IMC Controller

Figure 8.14: The Frequency and Time Responses of the New IMC Controller

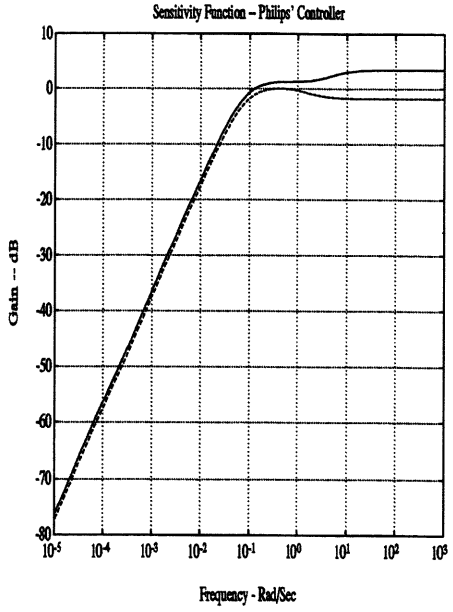

Figure 8.15: Sensitivity and Complementary Sensitivity Functions – Philips' Controller

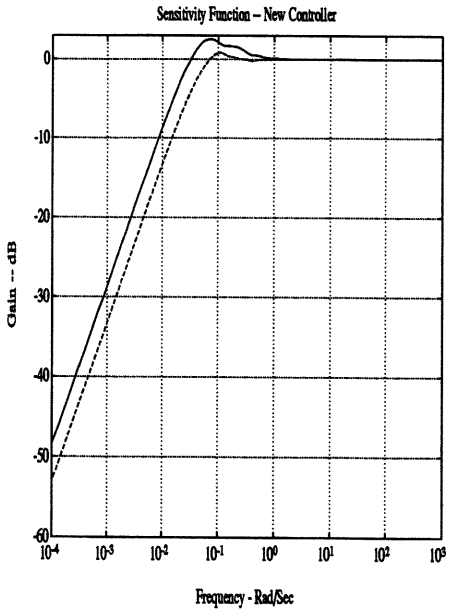

Figure 8.16: Sensitivity and Complementary Sensitivity Functions – New Controller

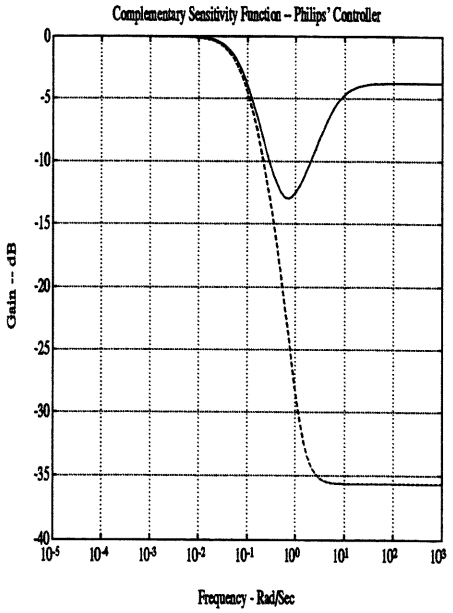

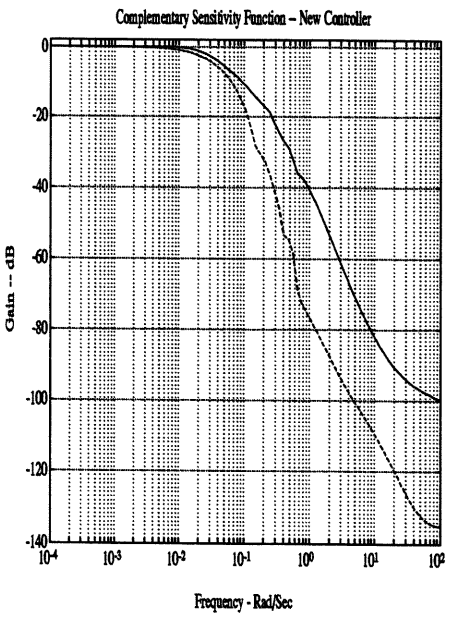

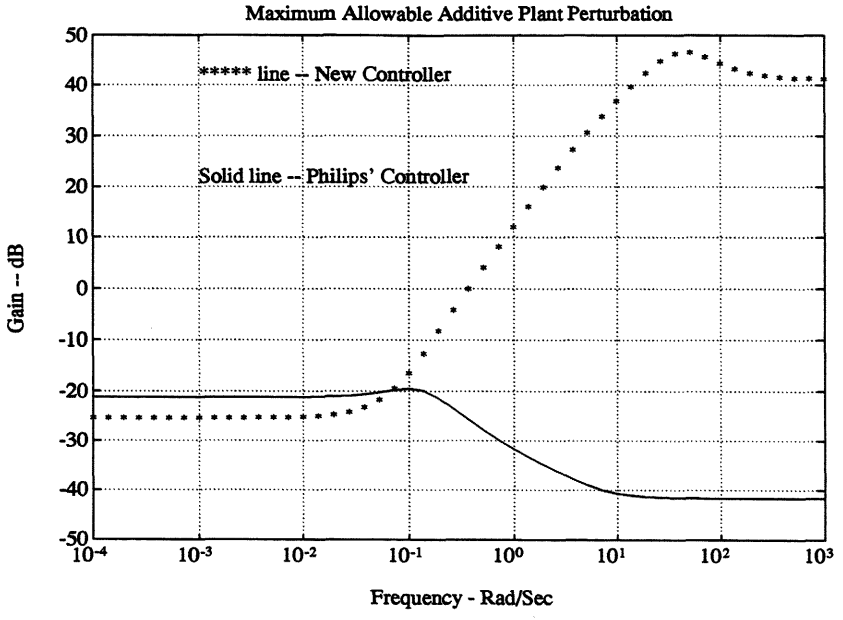

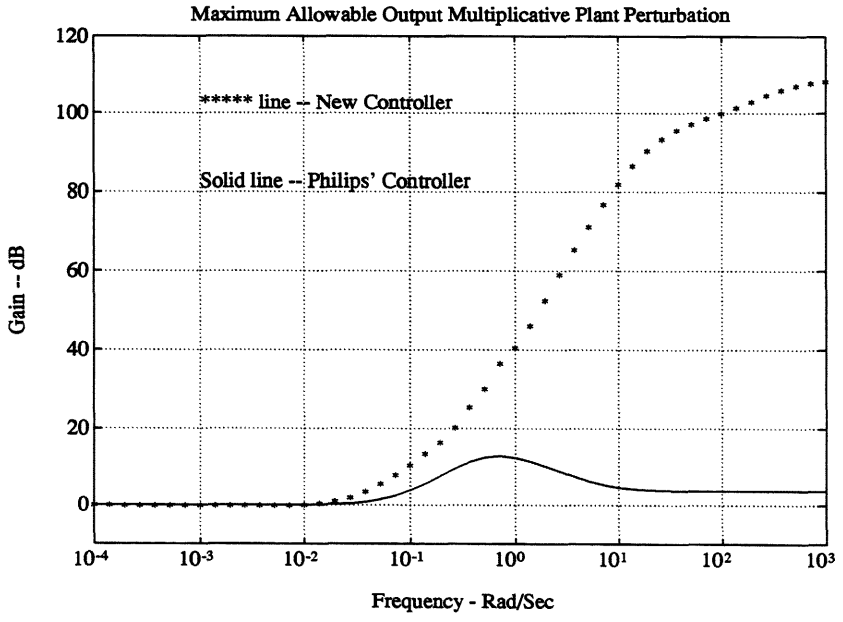

Figure 8.17: Maximum Allowable Additive and Output Multiplicative Plant Perturbation

8.4 Controller Design Procedure

In this section we present the design procedure followed to synthesize the Type 1 & 2 IMC controllers.

Problem

For the system of Figure 8.18, find a (W_1, W_2) such that

$$\gamma_o(W_1, W_2) \leq \epsilon_{\gamma_o} \tag{8.8}$$

$$\gamma_1(W_1, W_2) \leq \epsilon_{\gamma_1} \tag{8.9}$$

$$\phi_i(G_{p_j}, W_1, W_2) \leq \varepsilon_i \text{ for } i = 1, 2, ..., 10 \; j = 1, 2, ..., 5 \tag{8.10}$$

where plants G_{p_j} are the perturbed models shown in Figure 8.18, and (W_1, W_2) are the loop-shaping weights with real parameters $w^1 = (w_1^1, w_2^1, ..., w_q^1)$, also shown in Figure 8.18. The functionals defined in (8.10) are defined based on the design specifications given in Section 8.2; that is the functionals ϕ_1 to ϕ_{10} on the measures of the step response specifications on both the process measured outputs and control signals. The design

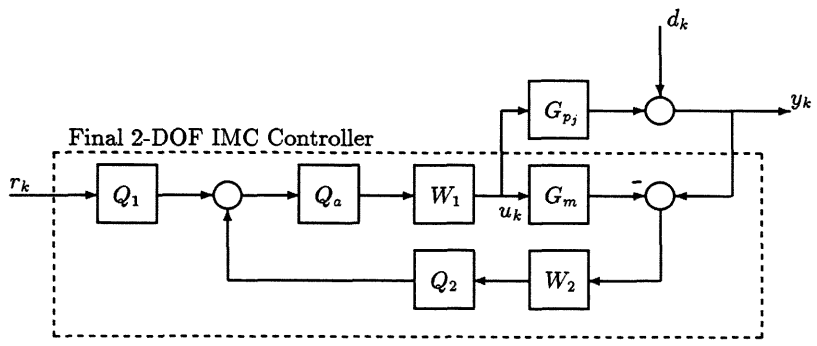

Figure 8.18: 2-DOF IMC Controller Implementation.

procedure comprises of the following main steps:

1) Define the nominal model G_m, the perturbed models G_{p_j}, and the functionals ϕ_i.

2) Define the values ϵ_{γ_0}, ϵ_{γ_1}, and ε_i.

3) Select the structure and order of the loop-shaping weights (W_1, W_2) for the open-loop process G_m. Bounds should be placed on the parameters w_i^1 to ensure that (W_1, W_2) are stable and minimum phase. Analyzing the singular values of the open-loop process G_m indicated the need for higher low frequency gain to achieve good tracking and disturbance rejection at these frequencies. The weighting function W_1 shall thus contain integral action. A stable approximation of an integrator is chosen due to the stability condition of the IMC scheme. Extra poles are introduced to reduce the roll-off rate at the cross-over frequency. The desired (W_1, W_2) in Figure 8.18 were given the following structure

$$W_1 = \begin{bmatrix} \frac{w_1^1}{(s+w_2^1)(s+w_3^1)} & 0 \\ 0 & \frac{w_4^1}{(s+w_5^1)(s+w_6^1)} \end{bmatrix}, \; W_2 = \begin{bmatrix} w_7^1 & 0 \\ 0 & w_8^1 \end{bmatrix}$$

For Type 2 control W_1 was augmented with double integral action, (stable approximations thereof) and the desired (W_1, W_2) in Figure 8.18 for Type 2 control were given the following structure

$$W_1 = \begin{bmatrix} \frac{w_1^1(s+w_2^1)}{(s+w_3^1)(s+w_4^1)(s+w_5^1)} & 0 \\ 0 & \frac{w_6^1(s+w_7^1)}{(s+w_8^1)(s+w_9^1)(s+w_{10}^1)} \end{bmatrix}, \; W_2 = \begin{bmatrix} \frac{w_{11}^1(s+w_{12}^1)}{(s+w_{13}^1)} & 0 \\ 0 & \frac{w_{14}^1(s+w_{15}^1)}{(s+w_{16}^1)} \end{bmatrix}$$

The zero in W_1 is chosen to moderate the effect of the double integrator. Both weighting functions are selected in continuous-time and then discretized, using the bilinear transformation described in Chapter 4, before cascading it with the discrete process model.

4) A desired reference model M_o is selected for the closed-loop system. Again the reference model is selected in continuous-time as

$$M_o = \begin{bmatrix} \frac{1}{(\tau s+1)} & 0 \\ 0 & \frac{1}{(\tau s+1)} \end{bmatrix}$$

The controlled outputs are thus desired to behave as simple first-order lags with no interaction. The reference model was discretized using ZOH, and the state-space realization of the generalized plant constructed.

5) The MBP, described in Chapter 4, is then implemented in conjunction with (3.55), (5.100), and (5.102) to find a (W_1, W_2) which satisfies inequalities (8.8),

(8.9) and (8.10). If a solution is found, the design is satisfactory. If no solution is found, either the order of the weighting functions is increased, one or more of the bounds ϵ_{γ_0}, ϵ_{γ_1} and ε_i increased, or the process is repeated with different initial values of w^1.

6) The IMC controller $Q = [\,Q_1 \quad Q_2\,]$ is cascaded with the weights (W_1, W_2) forming the final 2-DOF IMC controller

$$Q_f = [\,W_1Q_1 \quad W_1Q_2W_2\,]$$

The pre-filter W_1Q_1 is then scaled to achieve perfect steady-state model matching.

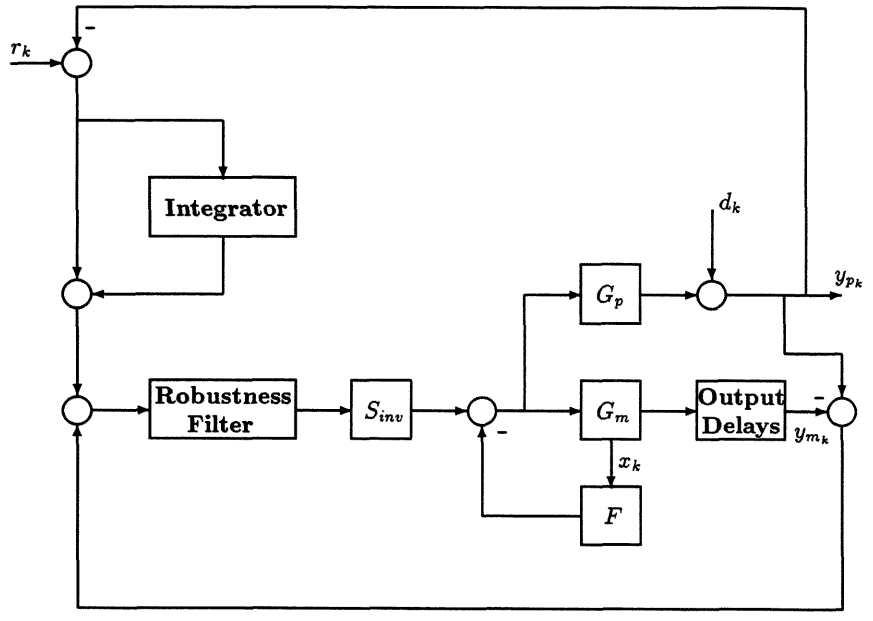

Figure 8.19: An IMC Type 2 Control Scheme.

The present IMC Type 2 control scheme is shown in Figure 8.19. The integrator block is explicitly included to provide Type 2 control so that when a slow trend disturbance (*i.e.*

a slow ramp type disturbance) occurs at d_k, the time constant of the explicit integrator is tuned until the trend is completely rejected. The main disadvantage of such a scheme is that the tracking performance will be degraded, and the only way to avoid this is to make sure that there are no set-point changes occurring during the rejection of the slow trend.

Since the Type 1 IMC controller was designed based on a nominal model excluding time delays, the block labelled "output delays" was tuned to match the delays of the real process. This had the advantage of designing IMC controllers with no delays in the nominal model, provided the time delays are not dominant. For the glass tube production process it was possible, for Measure 1 and Measure 2, to use a nominal model excluding time delays to design a 2-DOF IMC controller. An "output delay" block was augmented with the nominal model G_m shown in Figure 8.18 and was successfully tuned to maintain robust stability and good performance. Since the time delays for Measure 3 were very dominant, the scheme of Figure 8.18 went unstable.

8.5 Simulation Results

A set of closed-loop performance functionals

$$\phi_i(G_{p_j}, G_m, W, Q),\ i = 1, 2, ..., 10,\ j = 1, 2, ..., 5 \tag{8.11}$$

are defined based on the design specifications given in Section 8.2. Functionals ϕ_1 to ϕ_{10} are measures of the step response specifications. Functionals ϕ_1 and ϕ_8 are measures of the overshoot; ϕ_2 and ϕ_7 are measures of rise time; ϕ_4, ϕ_5, ϕ_9 and ϕ_{10} are measures of the control signal; and ϕ_3 and ϕ_6 are measures of the interaction. Denoting the process outputs and control signals of the closed-loop system with a plant G_p at a time t to a reference step command $r(t)$ by $y_i\left([r_1 \quad r_2]', t\right)$ and $u_i\left([r_1 \quad r_2]', t\right)$, respectively, for $i = 1, 2$. The step response functionals are

$$\phi_1 = \max_t y_1\left([0.2 \quad 0]', t\right) \tag{8.12}$$

$$\phi_2 = -\min_{t>t_r} y_1\left([0.2 \quad 0]', t\right) \tag{8.13}$$

$$\phi_3 = \max_t y_2\left([0.2 \quad 0]', t\right) \tag{8.14}$$

$$\phi_4 = \max_t \left|u_1\left([0.2 \quad 0]', t\right)\right| \tag{8.15}$$

$$\phi_5 = \max_t \left| u_2\left([0.2 \quad 0]', t\right)\right| \tag{8.16}$$

$$\phi_6 = \max_t y_1\left([0 \quad 1.0]', t\right) \tag{8.17}$$

$$\phi_7 = -\min_{t>t_r} y_2\left([0 \quad 1.0]', t\right) \tag{8.18}$$

$$\phi_8 = \max_t y_2\left([0 \quad 1.0]', t\right) \tag{8.19}$$

$$\phi_9 = \max_t |u_1\left([0 \quad 1.0]', t\right)| \tag{8.20}$$

$$\phi_{10} = \max_t |u_2\left([0 \quad 1.0]', t\right)| \tag{8.21}$$

The performance was calculated from linear time-invariant closed-loop responses for the perturbed plants G_{p_j}, all including time delays. The controller was synthesized using a desired nominal model G_m (with delays). The aim was to find design parameters which satisfied the inequalities for all perturbed plants.

8.5.1 Measure 1

The weighting functions and the desired reference model used to form the final Type 1 controller are given by

$$W_1 = \begin{bmatrix} \frac{1.5}{(s+10^{-6})(s+20)} & 0 \\ 0 & \frac{0.5}{(s+10^{-6})(s+30)} \end{bmatrix}, \; W_2 = \begin{bmatrix} 15 & 0 \\ 0 & 1.5 \end{bmatrix}, \; M_o = \frac{1}{(16s+1)} I_2$$

For the final Type 2 controller, the weighting functions and the desired reference model used are given by

$$W_1 = \begin{bmatrix} \frac{1.5(s+10^{-2})}{(s+10^{-6})^2(s+20)} & 0 \\ 0 & \frac{0.5(s+10^{-2})}{(s+10^{-6})^2(s+30)} \end{bmatrix}, \; W_2 = \begin{bmatrix} \frac{15(s+0.1)}{(s+1)} & 0 \\ 0 & \frac{1.5(s+0.1)}{(s+1)} \end{bmatrix}, \; M_o = \frac{1}{(25s+1)} I_2$$

The results of the time response simulations are shown in Figures 8.20-8.21. The Type 1 design met the performance specifications given in Section 8.2; however, the Type 2 design almost met all the specifications. The settling time was slightly slower. The sensitivity functions of both designs are shown in Figure 8.21.

8.5.2 Measure 2

The weighting functions and the desired reference model used to form the final Type 1 controller are given by

$$W_1 = \begin{bmatrix} \frac{3.5}{(s+10^{-6})(s+8)} & 0 \\ 0 & \frac{0.58}{(s+10^{-6})(s+45)} \end{bmatrix}, \; W_2 = \begin{bmatrix} 13 & 0 \\ 0 & 1.077 \end{bmatrix}, \; M_o = \frac{1}{(20s+1)} I_2$$

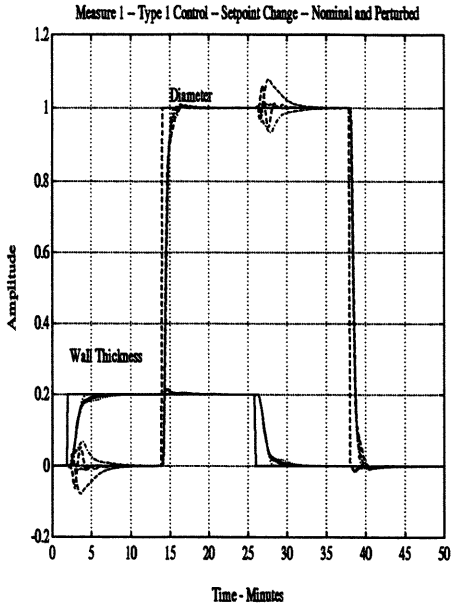

Figure 8.20: Closed-loop Responses due to Set-point Changes – Measure 1.

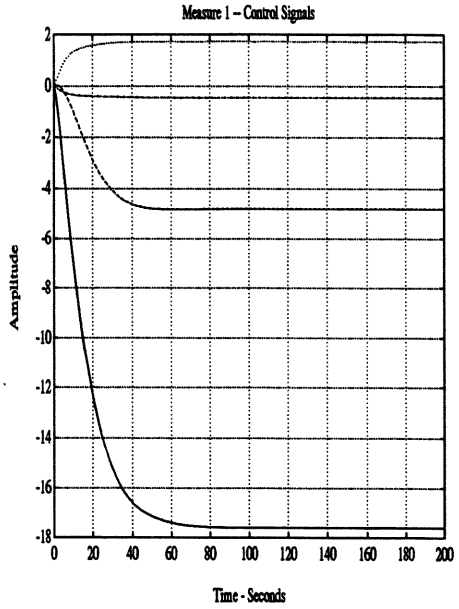

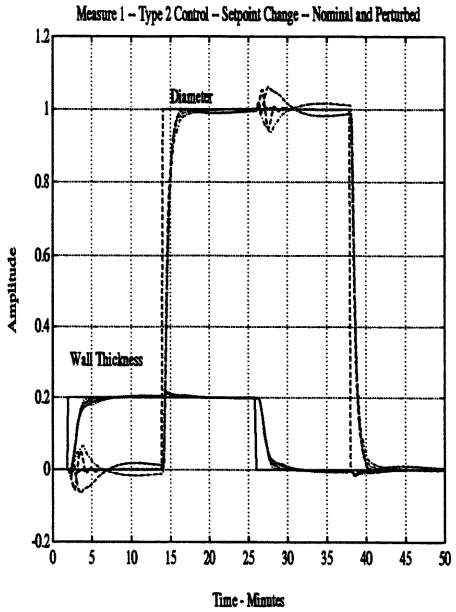

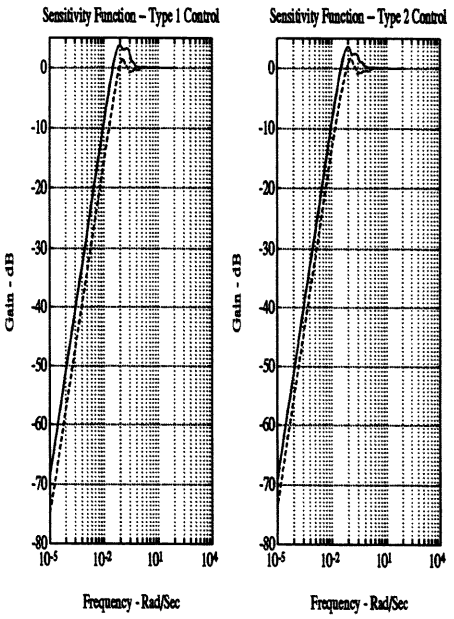

Figure 8.21: Control Signals and Sensitivity Functions – Measure 1.

For the final Type 2 controller, the weighting functions and the desired reference model used are given by

$$W_1 = \begin{bmatrix} \frac{3.5(s+10^{-2})}{(s+10^{-6})^2(s+8)} & 0 \\ 0 & \frac{0.58(s+10^{-2})}{(s+10^{-6})^2(s+45)} \end{bmatrix}, \; W_2 = \begin{bmatrix} \frac{13(s+0.1)}{(s+1)} & 0 \\ 0 & \frac{1.077(s+0.1)}{(s+1)} \end{bmatrix}, \; M_o = \frac{1}{(33s+1)} I_2$$

The results of the time response simulations are shown in Figures 8.22-8.23. The Type 1 design met almost all the performance specifications. The interaction was slightly exceeded. The Type 2 design didn't meet all the specifications. The rise and settling times were slower, and the interaction was slightly exceeded. The sensitivity functions of both designs are shown in Figure 8.23.

8.5.3 Measure 3

The weighting functions and the desired reference model used to form the final Type 1 controller are given by

$$W_1 = \begin{bmatrix} \frac{18}{(s+10^{-6})(s+20)} & 0 \\ 0 & \frac{0.62}{(s+10^{-6})(s+45)} \end{bmatrix}, \; W_2 = \begin{bmatrix} 7 & 0 \\ 0 & 1.072 \end{bmatrix}, \; M_o = \frac{1}{(40s+1)} I_2$$

For the final Type 2 controller, the weighting functions and the desired reference model used are given by

$$W_1 = \begin{bmatrix} \frac{18(s+10^{-2})}{(s+10^{-6})^2(s+20)} & 0 \\ 0 & \frac{0.62(s+10^{-2})}{(s+10^{-6})^2(s+45)} \end{bmatrix}, \; W_2 = \begin{bmatrix} \frac{7(s+0.1)}{(s+1)} & 0 \\ 0 & \frac{1.072(s+0.1)}{(s+1)} \end{bmatrix}, \; M_o = \frac{1}{(58s+1)} I_2$$

The results of the time response simulations are shown in Figures 8.24-8.25. The Type 1 and Type 2 designs met almost all the performance specifications. The interaction was slightly exceeded, and the rise and settling times were slightly slower. The sensitivity functions of both designs are shown in Figures 8.25.

Information regarding the orders of the final Type 1 and Type 2 IMC controllers for all tube measures are tabulated in Table 8.4. Using the model reduction approach of Chapter 6, lower-order controllers were obtained with performance indistinguishable from the high-order controllers. Figures 8.26-8.28 show the process output responses due to a slow trend disturbance for all measures.

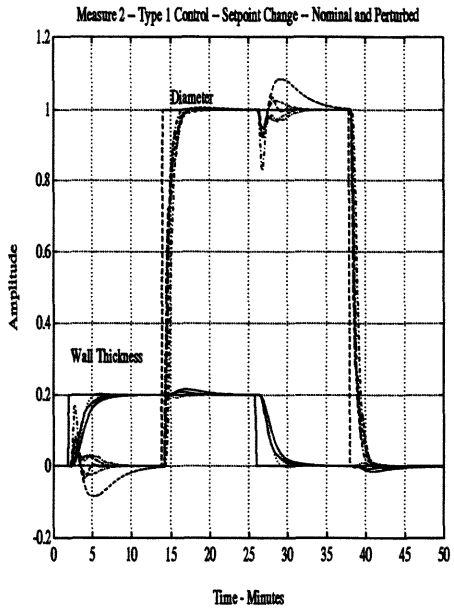

Figure 8.22: Closed-loop Responses due to Set-point Changes – Measure 2.

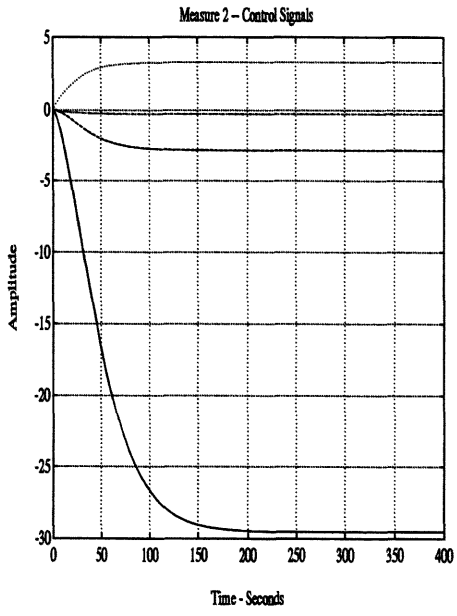

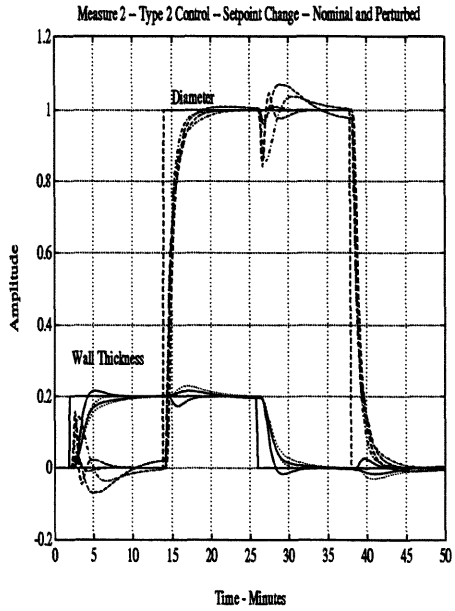

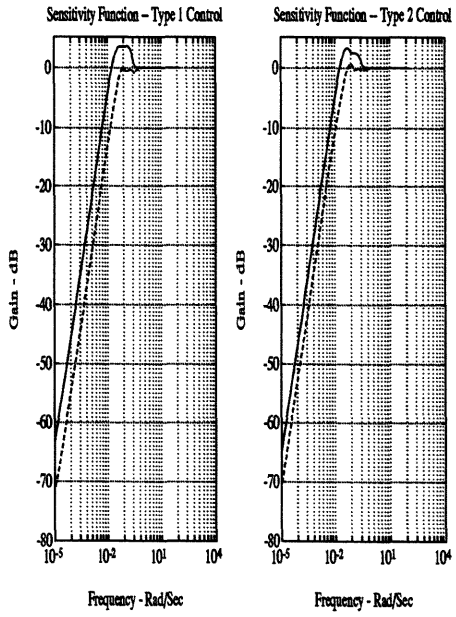

Figure 8.23: Control Signals and Sensitivity Functions – Measure 2.

Tube Measure	Order of 2-DOF IMC Controllers			
	Type 1		Type 2	
	High-order	Low-order	High-order	Low-order
1	58	15	66	20
2	64	15	72	20
3	108	18	116	20

Table 8.4: Controller Information.

The IMC controllers were also validated on their ability to suppress noise. The noise sequence was extracted from the freerun experiment described in Chapter 7. This noise sequence was then fed to the sensitivity function. The results for small measures (Measure 1) and large measures (Measure 3) are summarized in Table 8.5. The first two columns show the standard deviation of the noise in closed-loop. The last two columns contain the percentage improvement. The noise level for the open-loop process was 0.0058 mm for the wall thickness (WT) and 0.0508 mm for the diameter (D). Figures 8.30 and 8.31 show the output responses of the process (due to the noise sequence) for Measures 1 & 3. The solid line represents the open-loop response and the dashed line represents the closed-loop response.

Tube Measure	Noise Level		Improvement	
	WT (mm)	D (mm)	WT (%)	D (%)
1	0.0041	0.0177	29	65
3	0.0056	0.0309	3	39

Table 8.5: Noise Suppression.

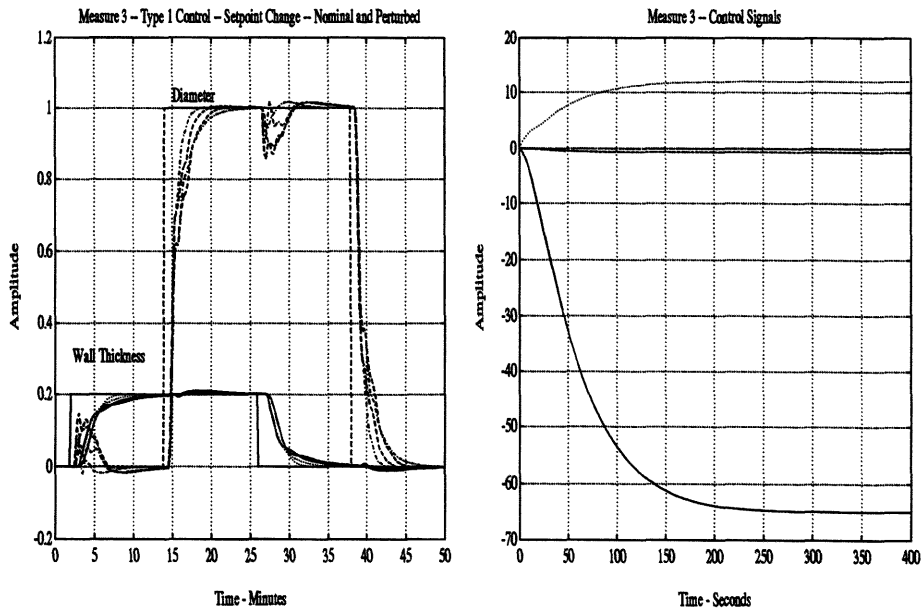

Figure 8.24: Closed-loop Responses due to Set-point Changes – Measure 3.

Figure 8.25: Control Signals and Sensitivity Functions – Measure 3.

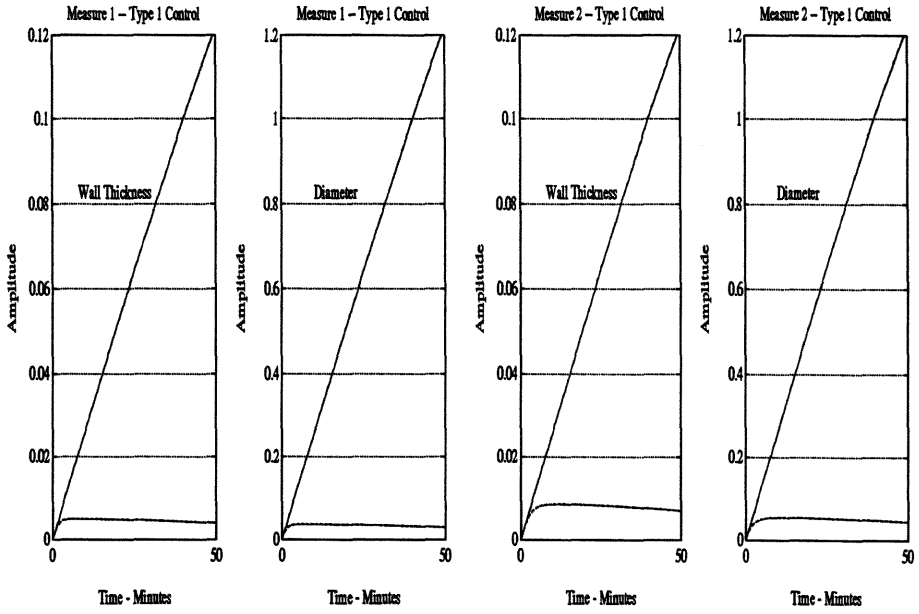

Figure 8.26: Closed-loop Responses due to Slow Trend Disturbances – Measure 1.

Figure 8.27: Closed-loop Responses due to Slow Trend Disturbances – Measure 2.

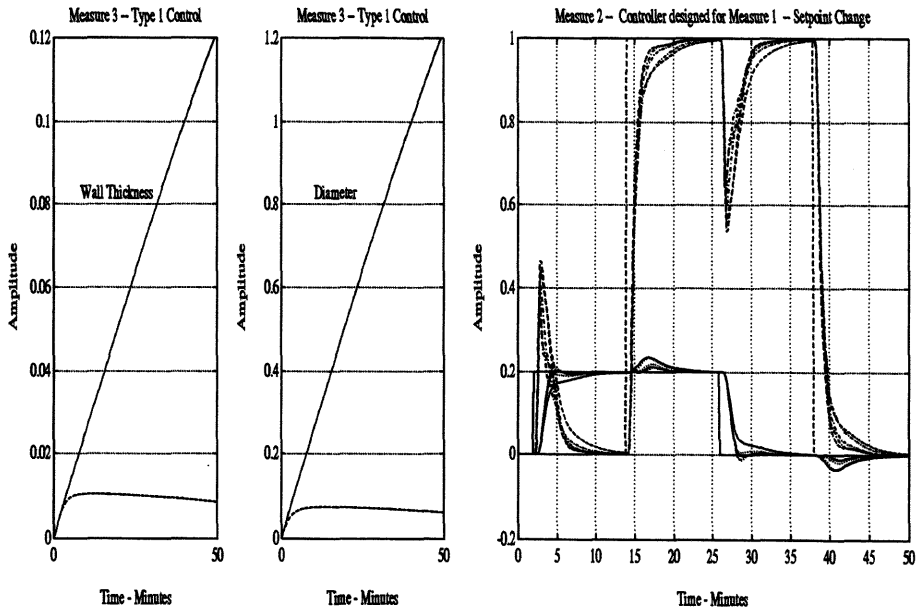

Figure 8.28: Closed-loop Responses due to Slow Trend Disturbances – Measure 3.

Figure 8.29: Closed-loop Responses due to Set-point Changes – Measure 2.

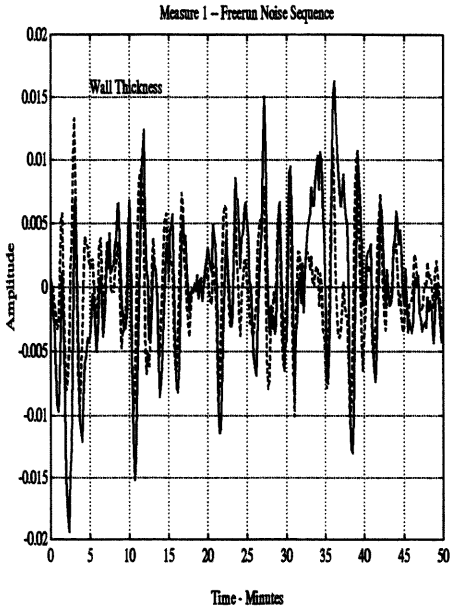

Figure 8.30: Closed-loop Responses due to Freerun Disturbance – Measure 1.

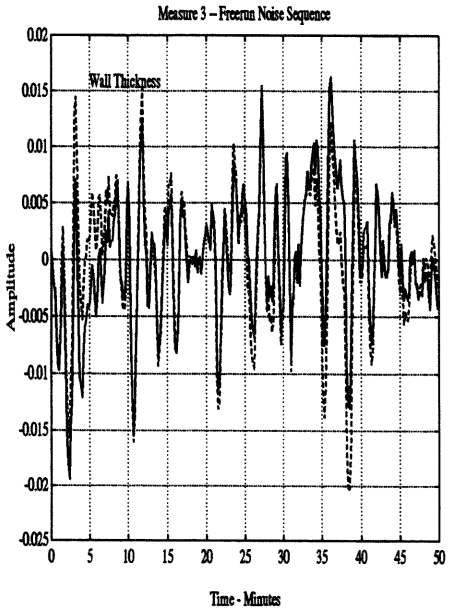

Figure 8.31: Closed-loop Responses due to Freerun Disturbance – Measure 3.

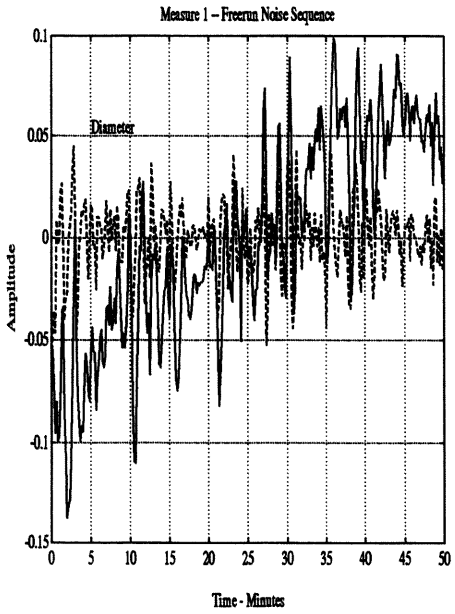

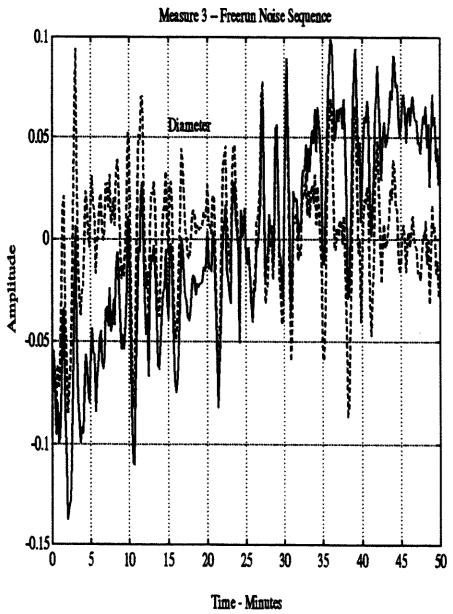

8.6 Summary

In this chapter 2-DOF IMC controllers have been designed for the glass tube production process at 3 different operating points.The IMC controller configuration considered appears to provide satisfactory designs for the production process. It is believed that the framework possesses desirable properties, yielding potentially good levels of performance. The combination of the 2-DOF IMC approach with the method of inequalities for formulating realistic problems to design explicitly for closed-loop performance and robust stability, is seen to provide a more flexible design procedure.

Significant low frequency trends had to be attenuated drastically, while some significant disturbances were present just outside the attainable bandwidth of the closed-loop system. Based on this knowledge, Type 1 and Type 2 controllers were designed. The Type 2 controller rejected the low frequency trends without excessive noise amplification outside the bandwidth; however, this controller was more sensitive to model errors compared to the Type 1 controller.

For all measures, the closed-loop responses from wall thickness set-point to diameter output were extremely sensitive to model errors. This can be understood from the relative large difference in gain between the diameter and the wall thickness in combination with the decreasing influence of the mandrel pressure on the process outputs. For Measure 3, problems have been encountered in the controller design because of the large time delays and of the large interaction between the wall thickness and the diameter. For Measure 1, the designed controller was also implemented on the models from Measure 2 with a large loss of performance in the interaction between the wall thickness and the diameter as shown in Figure 8.29. This was mainly due to the sensitivity of the process static gains when operating over a larger production range. Finally, their was no need to augment the final IMC controllers with a low-pass filter, as discussed in Chapter 5, in order to find a compromise between robustness and dynamic performance.

Chapter 9

A Robust Design Approach to Integrated Controls and Diagnostics

9.1 Introduction

This chapter is concerned with the design of integrated control and diagnostic systems. The four degrees-of-freedom (4-DOF) controller configuration will be introduced as a framework for addressing some interaction issues between a control system (control module) and a failure detection system (diagnostic module). This approach was first proposed in [77]. A robust control framework will be developed which will enable the design of an integrated control-diagnostic 4-DOF controller having both control and actuator failure detection capabilities.

In addition to robust stability of a system in the face of model uncertainty, robustness to loop failures which is sometimes called the integrity of the system, is also an important property of a multivariable feedback design. Also, the detection of failures is the subject of increased development because of the increasing demands on reliability and safety. An integrated approach to controls and diagnostics *via* the 4-DOF controller has been formulated in [77]. This controller has 2-vector inputs, 2-vector outputs and 4-matrix parameters. The additional controller output can be used to detect sensor and actuator failures, thereby providing the controller with diagnostic capabilities, in addition to its control capabilities. So, in this approach, the control and diagnostic modules of a reliable control system are designed together, instead of independently, thereby accounting for the interactions which occur between these two modules.

In the design of a Reliable Control System, two separate system modules are usually considered and designed independently: The Control Module and the Diagnostic Module. The fundamental problem with this approach is that the interactions which occur between these two modules are not accounted for, which may lead to the following disadvantages [77]:

1) A Diagnostic Module designed for an uncontrolled plant may not perform satisfactorily with the controlled plant.

2) A Diagnostic Module designed for a controlled plant may not perform satisfactorily due to inherent limitations imposed on the achievable diagnostic performance during the design of the control module.

To appreciate the undesirable effects of interaction between the control and diagnostic modules, consider the block diagram depicted in Figure 9.1, where the transfer function matrices G, K, and F are representative of the Plant, Control Module, and the Diagnostic Module, respectively. The objectives of this control system are to:

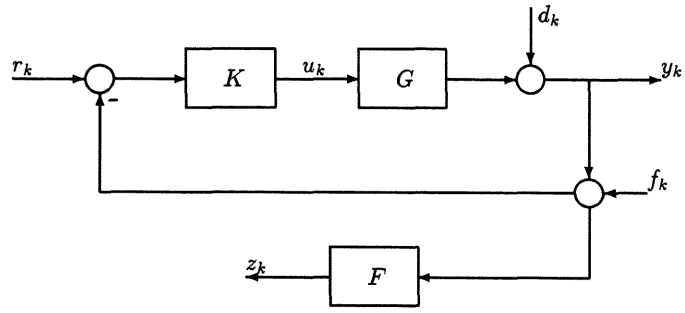

Figure 9.1: A Hypothetical Control System.

1) Control the plant.

2) Diagnose sensor failures.

(1) is taken to mean the tracking of references r_k and rejection of the disturbance d_k at the plant output y_k, and (2) is taken to mean the tracking, or identification of, the sensor failures f_k at z_k, the diagnostic output. With T_{ab} denoting the transfer function matrix from signal a_k to signal b_k, (1) and (2) require, respectively, that $T_{ry} - I$ and T_{dy}, and $T_{fz} - I$ be *small* in an appropriate sense. However, since $T_{fz} = F.T_{dy}$, these objectives are clearly seen to be in conflict with one another. Also, since $T_{fy} = T_{dy} - I$, achievement of the control objective may actually increase the critical nature of the diagnostic objective relative to the overall objective of reliable control, thus revealing the presence of interactions between the Control and Diagnostic Modules. Hence, the integrated design of the Control and Diagnostic Modules is necessary to achieve overall satisfactory control-diagnostic performance.

Notable attempts at formulating different synthesis methods for this control-diagnostic problem can be found in [77, 25, 98]. [77] proposes a four step design procedure where each controller parameter is synthesized independently. [25] introduces a design method whereby a nominal control module is synthesized with robust stability in an $\mathcal{L}^\infty$ framework, and then designs the diagnostic module on the resultant closed-loop. Finally, [98] proposes a single step design procedure for synthesizing the 4-DOF controller. They employ the results from $\mathcal{H}^\infty$ and μ-synthesis for the design of integrated control and diagnostic systems with the following properties:

1) The plant output signal tracks reference commands and is insensitive to actuator failures.

2) The diagnostic output signal is large only when an actuator failure has occurred.

3) Properties (1) and (2) hold in the presence of a bounded uncertainty.

The aim of this chapter is to introduce and formulate a systematic approach towards the synthesis of the 4-DOF controller that guarantees some level of robust control and diagnostic performance in the face of uncertainty by employing the results of $\mathcal{H}^\infty$-optimization with the following main properties:

1) The plant output signal tracks reference commands and is insensitive to actuator failures.

2) The diagnostic output signal tracks actuator failures (abrupt and slow ramp type failures) as suggested by [77].

3) Properties (1) and (2) hold in the presence of a bounded coprime factor uncertainty.

The organization of this chapter is as follows. In Section 9.2, different types of actuator and sensor failure models are introduced. Section 9.3 formulates the control and diagnostic design objectives by introducing and motivating the 4-DOF controller. Section 9.4 shows how the 4-DOF controller can simply be a special case of the standard regulator framework and how its parameterization is compatible with that of the Youla parameterization. Section 9.5 shows that by using the results from $\mathcal{H}^2$-optimal control, an optimal control module and an optimal diagnostic module can be designed separately. Section 9.6 formulates a design procedure for the integrated control and diagnostic. A suboptimal 4-DOF controller is synthesized in a single step approach *via* robust $\mathcal{H}^\infty$ control using a normalized coprime factor plant description. A design example will be presented to support the design approach. Finally, a summary will be given in Section 9.7.

9.2 Types of Failure Models

Two general classes of failures are considered here: actuator and sensor failures. It is thought that it is possible to model the failure of actuators and sensors as additive signals appearing at appropriate places in the model. Consider the plant depicted in Figure 9.2.

9.2.1 Actuator Failure

Let u_{d_k} be the ideal output of the actuator when no failures are present, that is $u_{d_k} = u_k$. Let u_k represent the actual output of the actuator. Then

$$u_k = u_{d_k} + a_k \tag{9.1}$$

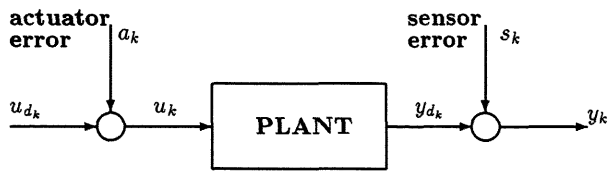

Figure 9.2: System with Sensor and Actuator Failure Models.

where a_k is the actuator error; it is a time-varying vector with elements a_{i_k}. By appropriate choice of a_{i_k}, one can capture various failure modes of the i-th channel of the actuator. For example, if the i-th actuator freezes at its zero position, producing no output at all, then $a_{i_k} = -u_{d_{i_k}}$; if there is a bias b_{i_k}, that is a drift in the correct output, then $a_{i_k} = b_{i_k}$. Two types of bias failure may occur, a step failure or a ramp type failure. Another type of failure occurs when the ith actuator is stuck at a constant value l_{i_k}, then $a_{i_k} = l_{i_k} - u_{d_{i_k}}$. Multiple failures can be captured in the above setting by specifying several elements of a_k to be non-zero.

9.2.2 Sensor Failure

Sensor failures are modelled in the same way. Let y_{d_k} and y_k represent the sensor ideal or true output and the actual output, respectively. Then

$$y_k = y_{d_k} + s_k \tag{9.2}$$

where s_k is the sensor error; it is a time-varying vector with elements s_{i_k} representing sensor failures. Complete failure of the i-th sensor can be modeled by setting $s_{i_k} = -u_{d_{i_k}}$, bias failures b_{i_k} by setting $s_{i_k} = b_{i_k}$, and failures where the sensor is stuck at a constant value k_{i_k} by setting $s_{i_k} = k_{i_k} - y_{d_{i_k}}$. Again, both single and multiple sensor failures can be modeled using this formulation.

9.3 Control and Diagnostic Design Objectives

Consider the following block diagram depicted in Figure 9.3. Any plant-controller inter-

Signal	*Definition*	*Examples*
e_k	Untilized plant output.	Sensor,actuator,and process states.
y_{p_k}	Utilized plant output.	Ideal sensor outputs.
u_k	Manipulated plant input.	Actuator inputs.
d_k	Unmanipulated plant input.	Disturbances,initial conditions, manual controls.
e_{d_k}	Unutilized controller output.	Controller states.
u_{c_k}	Utilized controller output.	Ideal actuator inputs.
y_k	Manipulated controller input.	Sensor outputs.
w_{c_k}	Unmanipulated controller input.	Commands,initial conditions, disturbances.
n_{a_k}, n_{s_k}	Exogenous inputs.	Noise,interference, loading, etc.

Table 9.1: Signals.

connection can be represented in terms of this control system interconnection structure while preserving the distinction between the plant and the controller. Table 9.1 lists the definitions and the interpretations of the various signals [77].

A block diagram of the 4-DOF controller is illustrated in Figure 9.4. The 4-DOF

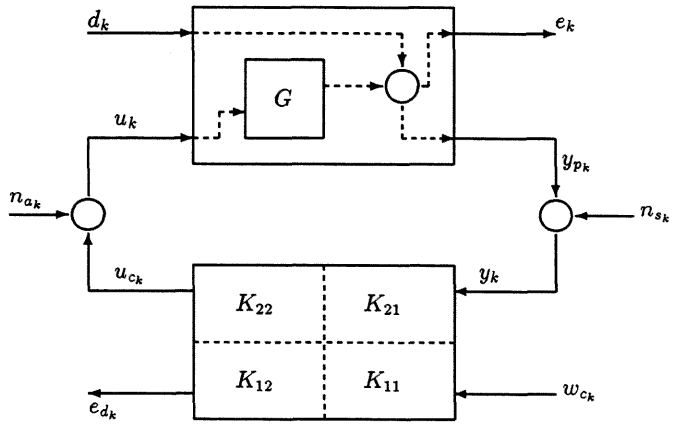

Figure 9.3: Control System Interconnection Structure with 4-DOF Controller.

controller can be thought of as a control/diagnostic module; there are no restrictions imposed on the structure of this control and diagnostic module. In addition, with K the 2×2 block–matrix comprised of K_{11}, K_{12}, K_{21}, and K_{22}, the 4-DOF controller depicted in Figure 9.4 can be viewed as an operator, represented by K, which maps commands and measurements into actuator commands and diagnostics. Since K_{11}, K_{12}, K_{21}, and K_{22} are unrestricted, K is unrestricted, and thus the set-up is completely general. The roles of the various controller parameters are summerized in Table 9.2 [77].

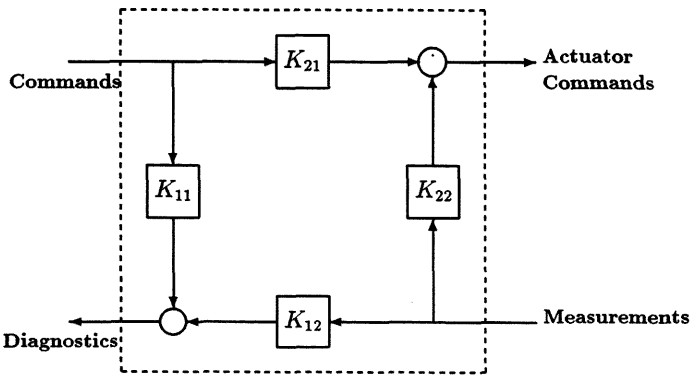

Figure 9.4: The 4-DOF Controller.

In the block diagram depicted in Figure 9.3, e_{d_k} will be used to detect sensor and/or actuator failures. These failures can be modelled using n_{a_k} and n_{s_k} in much the same way n_{a_k} and n_{s_k} are used to model sensor and actuator noise. The idea is to regard n_{a_k} and n_{s_k} as deviations from ideal sensor and actuator behaviour, respectively, where here ideal means unfailed and noiseless. To distinguish between noise and failures, we may write

$$n_{a_k} = f_{a_k} + \eta_{a_k} \tag{9.3}$$

and

$$n_{s_k} = f_{s_k} + \eta_{s_k} \tag{9.4}$$

and define f_{a_k}, f_{s_k} as failures and η_{a_k}, η_{s_k} as noise. Let us consider the block diagram depicted in Figure 9.5. The nominal system transfer function matrices in terms of K

Parameters	*Principal Roles*
K_{22}	Determines the effects of uncertainties occurring in the form of plant modelling errors, noise, and disturbances. It also determines noise/disturbance rejection and robust stability characteristics, control efforts, and both control and diagnostic sensitivities.
K_{11}	Determines nominal control/diagnostic interaction.
K_{21}	Determines control command following, nominal response characteristic, and control effort.
K_{12}	Determines nominal diagnostics in the absence of control.

Table 9.2: Roles of the Design Parameters.

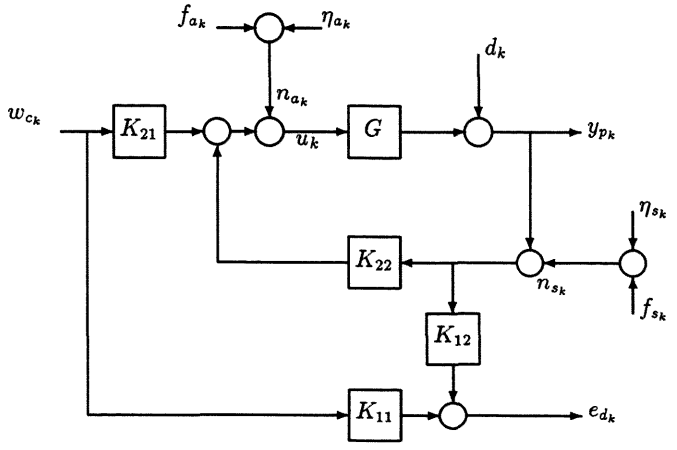

Figure 9.5: Figure 9.3 Re-drawn.

can be easily derived, and they are given by

$$T_{w_c y_p} = (I - GK_{22})^{-1}GK_{21},\ T_{n_a y_p} = (I - GK_{22})^{-1}G,\ T_{n_s y_p} = -(I - GK_{22})^{-1}GK_{22}$$

$$T_{d y_p} = (I - GK_{22})^{-1},\ T_{w_c e_d} = K_{11} + K_{12}(I - GK_{22})^{-1}GK_{21}$$

$$T_{n_a e_d} = K_{12}G(I - K_{22}G)^{-1},\ T_{n_s e_d} = K_{12}(I - GK_{22})^{-1},\ T_{d e_d} = K_{12}(I - GK_{22})^{-1} \quad (9.5)$$

The diagnostic objective is to mean follow, or identify $\tilde{f}_k$ at e_{d_k} where $\tilde{f}_k = \begin{bmatrix} f_{a_k} \\ f_{s_k} \end{bmatrix}$. Implicit in this is the need to reject, or attenuate at e_{d_k} all other system inputs and to account for plant modelling errors. So, in the face of plant modelling errors, the aim is to achieve closed-loop stability, and also make $T_{\tilde{f}e_d} - I$, $T_{\eta_a e_d}$, $T_{\eta_s e_d}$, $T_{w_c e_d}$, and T_{de_d} *small* in an appropriate sense.

The control objective is to mean follow, or track w_{c_k} at the plant output y_{p_k}, with reasonable control effort u_k. Implicit in this objective is the need to reject η_{a_k}, η_{s_k} and d_k at y_{p_k}, with reasonable u_k. Since failures which can be satisfactorily compensated for by the control need not be diagnosed, and vice versa, the remaining system inputs, f_{a_k}, f_{s_k}, are not considered in the control objective. So, in the face of plant modelling errors, the aim is to achieve closed-loop stability, and also make $T_{w_c y_p} - I$, $T_{\eta_a y_p}$, $T_{\eta_s y_p}$, and T_{dy_p} *small*, subject to the constraints on the size of $T_{w_c u_s}$, T_{du_s}, $T_{\eta_a u_s}$, and $T_{\eta_s u_s}$. A multitude of inherent limitations and tradeoffs are clearly exposed in the above nominal system transfer function matrices. Those pertaining only to the control objective are discussed in [23], so the concentration will be on those pertaining to the diagnostic objective and control-diagnostic interaction. As an example, the following two remarks are stated [77]:

Remark 9.3.1 Since $T_{f_s e_d} = T_{n_s e_d} = T_{de_d}$, simultaneous sensor failure diagnosis and disturbance rejection requires appropriate frequency shaping of this transfer function matrix to exploit differences in disturbance and sensor failure frequency content. Thus, sensor diagnostic performance and disturbance rejection performance must be traded off against one another in accordance with transfer function limitations. ■

Remark 9.3.2 Since $T_{f_a e_d} = T_{n_a e_d} = K_{12}G(I - K_{22}G)^{-1} = T_{n_s e_d}G = T_{f_s e_d}G$, it is clear that sensor diagnostic performance and actuator diagnostic performance must be traded off against one another. ■

If it wasn't for the fact that nominal performance, nominal diagnostic performance, and control-diagnostic interaction have to be traded off against one another, the blocks of Table 9.2, taken in order, would constitute a completely systematic 4-step design process for the 4-DOF controller. Though not completely systematic, this 4-step design

procedure is still a useful conceptual path for 4-DOF controller design where it has been successfully applied in the following references [77, 112, 99].

9.4 The Four Degrees-Of-Freedom Controller

9.4.1 A Generalized Regulator Framework

Consider the following block diagram depicted in Figure 9.6. which represents the two

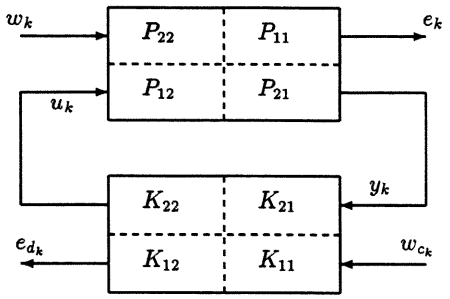

Figure 9.6: Control System Interconnection Structure.

equations:

$$\begin{bmatrix} e_k \\ y_k \end{bmatrix} = \begin{bmatrix} P_{11} & P_{12} \\ P_{21} & P_{22} \end{bmatrix} \begin{bmatrix} w_k \\ u_k \end{bmatrix}, \begin{bmatrix} e_{d_k} \\ u_k \end{bmatrix} = \begin{bmatrix} K_{11} & K_{12} \\ K_{21} & K_{22} \end{bmatrix} \begin{bmatrix} w_{c_k} \\ y_k \end{bmatrix} \tag{9.6}$$

By straightforward manipulation, the transfer function matrix $\begin{bmatrix} w_{c_k} \\ w_k \end{bmatrix} \rightarrow \begin{bmatrix} e_{d_k} \\ e_k \end{bmatrix}$ is given by

$$\begin{bmatrix} K_{11} + K_{12}P_{22}(I - K_{22}P_{22})^{-1}K_{21} & K_{12}(I - P_{22}K_{22})^{-1}P_{21} \\ P_{12}(I - K_{22}P_{22})^{-1}K_{21} & P_{11} + P_{12}K_{22}(I - P_{22}K_{22})^{-1}P_{21} \end{bmatrix} \tag{9.7}$$

which may be re-written as

$$\begin{bmatrix} e_{d_k} \\ e_k \end{bmatrix} = \tilde{P}_{11} + \tilde{P}_{12}\tilde{K}(I - \tilde{P}_{22}\tilde{K})^{-1}\tilde{P}_{21} \begin{bmatrix} w_{c_k} \\ w_k \end{bmatrix} \tag{9.8}$$

where

$$\tilde{P}_{11} = \begin{bmatrix} 0 & 0 \\ 0 & P_{11} \end{bmatrix}, \tilde{P}_{12} = \begin{bmatrix} I & 0 \\ 0 & P_{12} \end{bmatrix}, \tilde{P}_{21} = \begin{bmatrix} I & 0 \\ 0 & P_{21} \end{bmatrix}, \tilde{P}_{22} = \begin{bmatrix} 0 & 0 \\ 0 & P_{22} \end{bmatrix} \tag{9.9}$$

and

$$\tilde{K} = \begin{bmatrix} K_{11} & K_{12} \\ K_{21} & K_{22} \end{bmatrix} \tag{9.10}$$

Hence, the transfer function from $\begin{bmatrix} w_{c_k} \\ w_k \end{bmatrix} \rightarrow \begin{bmatrix} e_{d_k} \\ e_k \end{bmatrix}$ can be represented as a linear fractional map $\mathcal{F}_l(\tilde{P}, \tilde{K})$, where $\tilde{P} = \begin{bmatrix} \tilde{P}_{11} & \tilde{P}_{12} \\ \tilde{P}_{21} & \tilde{P}_{22} \end{bmatrix}$. So, the block diagram of Figure 9.6 can be redrawn as the block diagram depicted in Figure 9.7 below. This shows that all the inputs (outputs) are inputs (outputs) of the reconfigured system $\tilde{P}$ and the closed-loop systems of Figures 9.6 and 9.7 are equivalent. Hence,the problem is well-posed in the

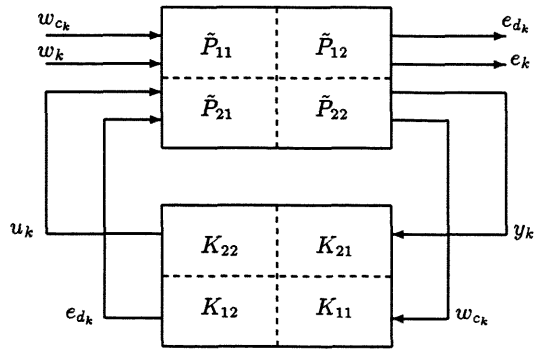

Figure 9.7: Equivalent 4-DOF Controller Interconnection Structure.

sense that an $\mathcal{H}^\infty$-synthesis problem can be posed to find a controller $\tilde{K}$ which achieves internal stability and solves $\min_{\tilde{K}} \left\| \mathcal{F}_l(\tilde{P}, \tilde{K}) \right\|_\infty$.

9.4.2 The Compatibility of the 4-DOF Controller Parameterization with the Youla Parameterization

The transfer function matrices $\tilde{P}$ and $\tilde{K}$ in Figure 9.7 are assumed to be proper. Let

$$\tilde{e}_k = \begin{bmatrix} e_{d_k} \\ e_k \end{bmatrix}, \ \tilde{w}_k = \begin{bmatrix} w_{c_k} \\ w_k \end{bmatrix}, \ \tilde{y}_k = \begin{bmatrix} y_k \\ w_{c_k} \end{bmatrix}, \text{ and } \tilde{u}_k = \begin{bmatrix} u_k \\ e_{d_k} \end{bmatrix} \tag{9.11}$$

Then the block diagram of Figure 9.7 represents the two equations

$$\begin{bmatrix} \tilde{e}_k \\ \tilde{y}_k \end{bmatrix} = \begin{bmatrix} \tilde{P}_{11} & \tilde{P}_{12} \\ \tilde{P}_{21} & \tilde{P}_{22} \end{bmatrix} \begin{bmatrix} \tilde{w}_k \\ \tilde{u}_k \end{bmatrix} \text{ and } \tilde{u}_k = \tilde{K}\tilde{y}_k \tag{9.12}$$

By adding the following two fictitious external signals $\tilde{n}_{1_k}$ and $\tilde{n}_{2_k}$, to $\tilde{u}_k$ and $\tilde{y}_k$, respectively, where

$$\tilde{n}_{1_k} = \begin{bmatrix} 0 \\ n_{a_k} \end{bmatrix} \text{ and } \tilde{n}_{2_k} = \begin{bmatrix} 0 \\ n_{s_k} \end{bmatrix} \tag{9.13}$$

the system is well-posed if the transfer function matrix from $\begin{bmatrix} \tilde{w}_k \\ \tilde{n}_{1_k} \\ \tilde{n}_{2_k} \end{bmatrix} \rightarrow \tilde{u}_k$ exists and is proper [19]. This results in the equations

$$\begin{aligned} \tilde{u}_k &= \tilde{n}_{1_k} + \tilde{K}\tilde{n}_{2_k} + \tilde{K}\tilde{y}_k \\ \tilde{y}_k &= \tilde{P}_{21}\tilde{w}_k + \tilde{P}_{22}\tilde{u}_k \end{aligned} \tag{9.14}$$

and these in turn imply that

$$(I - \tilde{K}\tilde{P}_{22})\tilde{u}_k = \tilde{n}_{1_k} + \tilde{K}\tilde{P}_{21}\tilde{w}_k + \tilde{K}\tilde{n}_{2_k} \tag{9.15}$$

Thus, well-posedness is equivalent to the condition that $(I - \tilde{K}\tilde{P}_{22})^{-1}$ exists and is proper, which implies that $\begin{bmatrix} I & -\tilde{K} \\ -\tilde{P}_{22} & I \end{bmatrix}^{-1}$ exists and is proper, which also implies that $(I - \tilde{P}_{22}\tilde{K})^{-1}$ exists and is proper.

Remark 9.4.1 For $(I - \tilde{K}\tilde{P}_{22})$ to be invertible, $(I - K_{22}P_{22})$ must be invertible since

$$(I - \tilde{K}\tilde{P}_{22})^{-1} = (I - K_{22}P_{22})^{-1} \begin{bmatrix} (I - K_{22}P_{22}) & K_{12}P_{22} \\ 0 & I \end{bmatrix}$$

■

This is equivalent to saying that the system is well-posed if, and only if, $(I - K_{22}P_{22})^{-1}$ exists and is proper. So, to analyze stability, we only need to consider the $\tilde{P}_{22}$ partition of $\tilde{P}$.

Let $P_{22} = N_{22}M_{22}^{-1} = \tilde{M}_{22}^{-1}\tilde{N}_{22}$. Then $\tilde{P}_{22}$ may be written as

$$\tilde{P}_{22} = \begin{bmatrix} 0 & 0 \\ 0 & N_{22}M_{22}^{-1} \end{bmatrix} = \begin{bmatrix} 0 & 0 \\ 0 & N_{22} \end{bmatrix} \begin{bmatrix} I & 0 \\ 0 & M_{22}^{-1} \end{bmatrix} \tag{9.16}$$

Let $\tilde{P}_{22}$ and $\tilde{K}$ have the fractional representations $\tilde{P}_{22} = \underline{N}_{22}\underline{M}_{22}^{-1} = \underline{\tilde{M}}_{22}^{-1}\underline{\tilde{N}}_{22}$ and $\tilde{K} = \underline{U}\underline{V}^{-1} = \underline{\tilde{V}}^{-1}\underline{\tilde{U}}$ such that

$$\begin{bmatrix} \underline{\tilde{V}} & -\underline{\tilde{U}} \\ -\underline{\tilde{N}}_{22} & \underline{\tilde{M}}_{22} \end{bmatrix} \begin{bmatrix} \underline{M}_{22} & \underline{U} \\ \underline{N}_{22} & \underline{V} \end{bmatrix} = \begin{bmatrix} I & 0 \\ 0 & I \end{bmatrix} \tag{9.17}$$

where

$$\underline{N}_{22} = \begin{bmatrix} 0 & 0 \\ 0 & N_{22} \end{bmatrix}, \underline{M}_{22} = \begin{bmatrix} I & 0 \\ 0 & M_{22} \end{bmatrix}, \underline{U} = \begin{bmatrix} 0 & 0 \\ 0 & U \end{bmatrix}, \underline{V} = \begin{bmatrix} I & 0 \\ 0 & V \end{bmatrix} \tag{9.18}$$

and so on.

Theorem 9.4.1 [61] Let $\tilde{K}_o = \underline{U}_o\underline{V}_o^{-1} = \underline{\tilde{V}}_o^{-1}\underline{\tilde{U}}_o$ be such that (9.18) holds. For any $\tilde{Q} \in \mathcal{RH}^\infty$ (that is, for any realizable, stable $\tilde{Q}$ of compatible dimensions), where

$$\tilde{Q} = \begin{bmatrix} Q_{11} & Q_{12} \\ Q_{21} & Q_{22} \end{bmatrix},$$

define

$$\begin{aligned} \underline{U} &= \underline{U}_o + \underline{M}_{22}\tilde{Q} \\ \underline{V} &= \underline{V}_o + \underline{N}_{22}\tilde{Q} \\ \underline{\tilde{U}} &= \underline{\tilde{U}}_o + \tilde{Q}\underline{\tilde{M}}_{22} \\ \underline{\tilde{V}} &= \underline{\tilde{V}}_o + \tilde{Q}\underline{\tilde{N}}_{22} \end{aligned}$$

Then $\underline{U}\underline{V}^{-1} = \underline{\tilde{V}}^{-1}\underline{\tilde{U}}$, and $\tilde{K} = \underline{U}\underline{V}^{-1} = \underline{\tilde{V}}^{-1}\underline{\tilde{U}}$ is a stabilizing controller for $\tilde{P}_{22} = \underline{N}_{22}\underline{M}_{22}^{-1} = \underline{\tilde{M}}_{22}^{-1}\underline{\tilde{N}}_{22}$. ■

The above theorem implies that all stabilizing controllers $\tilde{K}$ can be parameterized in terms of a stable

$$\tilde{Q} = \begin{bmatrix} Q_{11} & Q_{12} \\ Q_{21} & Q_{22} \end{bmatrix} \tag{9.19}$$

That is, an expression for the controller's transfer function matrix $\tilde{K}$ in terms of $\tilde{K}_o$ and $\tilde{Q}$ can be obtained:

$$\tilde{K} = (\underline{U}_o + \underline{M}_{22}\tilde{Q})(\underline{V}_o + \underline{N}_{22}\tilde{Q})^{-1} \tag{9.20}$$

After some mathematical manipulation we get the following expression for $\tilde{K}$ as

$$\tilde{K} = \tilde{K}_o + \underline{\tilde{V}}_o^{-1}\tilde{Q}(I + \underline{V}_o^{-1}\underline{N}_{22}\tilde{Q})^{-1}\underline{V}_o^{-1} \tag{9.21}$$

Hence, by partioning $\tilde{Q}$ as in (9.19) and substituting the coprime factorization of $\tilde{P}_{22}$ and $\tilde{K}_o$ given in (9.16) and (9.18) into (9.21), $\tilde{K}$ can be parameterized as a set of all proper controllers achieving internal stability, in terms of the factorization of $\tilde{P}_{22}$, resulting in

$$\tilde{K} = \begin{bmatrix} Q_{11} - Q_{12}(V_o + N_{22}Q_{22})^{-1}N_{22}Q_{21} & Q_{12}(V_o + N_{22}Q_{22})^{-1} \\ (\tilde{V}_o + Q_{22}\tilde{N}_{22})^{-1}Q_{21} & (U_o + M_{22}Q_{22})(V_o + N_{22}Q_{22})^{-1} \end{bmatrix} \tag{9.22}$$

where Q_{11}, Q_{12}, Q_{21}, and Q_{22} range over $\mathcal{RH}^\infty$, and $\tilde{K}$ has a similar controller parameterization to the one derived in [76].

It is interesting to note that the expression obtained for the 4-DOF controller which is given by (9.22) is restrictive. Although the controller is an internally stabilizing one, the parameters K_{11}, K_{12}, and K_{21} are not guaranteed to be stable as required. If a given plant is unstable and non-minimum phase, the unstable zeros will be contained in the parameter N_{22} as unstable zeros and the inverse function $(V_o + N_{22}Q_{22})^{-1}$ in each term might include unstable poles as a result. Also the parameter V_o might also contain unstable zeros if the plant is unstable, which increases the criticalness of the problem even more. But, if the plant is stable and minimum phase, then K_{11}, K_{12}, and K_{21} can be guaranteed to be stable.

From the above argument, we can conclude that such a parameterization is not suitable for physical implementation. Figure 9.5 may be re-arranged, after some algebra and block diagram manipulation, to the following physically implementable control system as shown in Figure 9.8. It is clear that all the unstable poles (if any) will be located in the feedback-loop, so all the designer has to do is to properly choose the stable $\tilde{Q}$ transfer function matrix to achieve the control and diagnostic objectives. Two major drawbacks about this re-configuration:

1) The controller will be considered a black box controller, that is the knowledge of each individual parameter will be completely lost and indistinguishable.

2) Since $T_{f_s e_d} = Q_{12}\tilde{M}$, Q_{12} is constrained to be stable, and $\tilde{M}$ contains the unstable poles of G in the form of right-half plane zeros, it follows that the unstable poles of G must be contained in $T_{f_s e_d}$ in a stable closed-loop system. Thus, the requirement of closed-loop stability imposes fundamental limitations on the achievable sensor diagnostic performance, and also, since $T_{f_a e_d} = Q_{12}\tilde{N}$,

the requirement of closed-loop stability imposes fundamental limitations on the achievable actuator diagnostic performance for non-minimum phase plants.

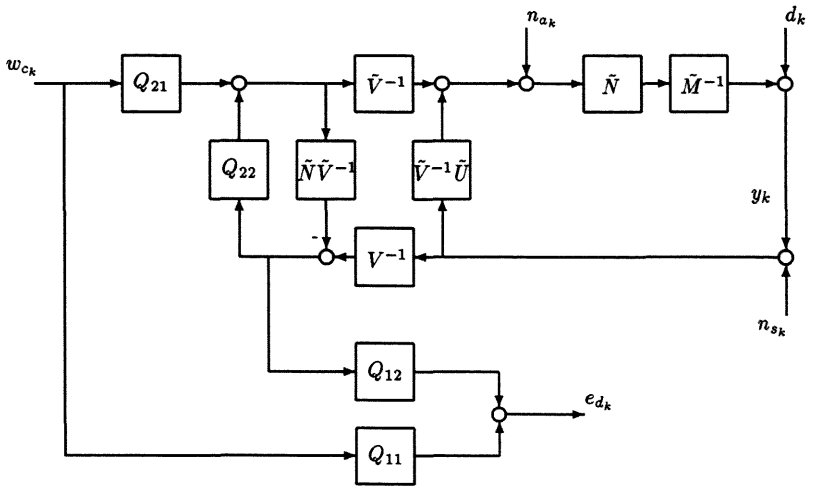

Figure 9.8: A Physically Implementable Reliable Control System.

9.5 $\mathcal{H}^2$-Optimal Control and Diagnostics

In this section, the problem of designing an optimal $\mathcal{H}^2$ controller which provides good nominal plant output regulation and good nominal failure tracking characteristics is considered. From the control system configuration shown in Figure 9.6, let the state-space realization of the transfer function matrix that maps $\begin{bmatrix} \hat{w}_k \\ u_k \end{bmatrix} \rightarrow \begin{bmatrix} e_k \\ \hat{y}_k \end{bmatrix}$ be given by

$$P_{con} \stackrel{s}{=} \left[\begin{array}{c|cc} A_c & B_{c_1} & B_{c_2} \\ \hline C_{c_1} & 0 & D_{c_{12}} \\ C_{c_2} & D_{c_{21}} & 0 \end{array}\right] \tag{9.23}$$

where $\hat{w}_k = \begin{bmatrix} w_{c_k} \\ w_k \end{bmatrix}$ and $\hat{y}_k = \begin{bmatrix} w_{c_k} \\ y_k \end{bmatrix}$. Recalling Chapter 2, assumptions A1-A7 and A9 still hold. Let the equations for the diagnostic module P_{diag} be given by

$$\begin{aligned} x_{d_{k+1}} &= A_d x_{d_k} + B_{d_1}\hat{w}_k + B_{d_2} e_{d_k} \\ z_{d_k} &= C_{d_1} x_{d_k} + D_{d_{12}} e_{d_k} \end{aligned} \tag{9.24}$$

This implies that the state-space realization of the diagnostic transfer function matrix that maps $\begin{bmatrix} \hat{w}_k \\ e_{d_k} \end{bmatrix} \rightarrow z_{d_k}$ is given by

$$P_{diag} \stackrel{s}{=} \left[\begin{array}{c|cc} A_d & B_{d_1} & B_{d_2} \\ \hline C_{d_1} & 0 & D_{d_{12}} \end{array}\right] \tag{9.25}$$

Amalgamating the control and diagnostic realizations of (9.23) and (9.25), the following control-diagnostic interconnection structure is obtained *via* the following state-space realization

$$\tilde{P} \stackrel{s}{=} \left[\begin{array}{c||c|c} \tilde{A} & \tilde{B}_1 & \tilde{B}_2 \\ \hline\hline \tilde{C}_1 & 0 & \tilde{D}_{12} \\ \hline \tilde{C}_2 & \tilde{D}_{21} & 0 \end{array}\right] \tag{9.26}$$

The system matrices for (9.26) are given by

$$\tilde{A} = \begin{bmatrix} A_c & 0 \\ 0 & A_d \end{bmatrix}, \tilde{B}_1 = \begin{bmatrix} B_{c_1} \\ B_{d_1} \end{bmatrix}, \tilde{B}_2 = \begin{bmatrix} 0 & B_{c_2} \\ B_{d_2} & 0 \end{bmatrix}$$

$$\tilde{C}_1 = \begin{bmatrix} C_{c_1} & 0 \\ 0 & C_{d_1} \end{bmatrix}, \tilde{C}_2 = [\, C_{c_2} \quad 0\,], \tilde{D}_{12} = \begin{bmatrix} 0 & D_{c_{12}} \\ D_{d_{12}} & 0 \end{bmatrix}, \tilde{D}_{21} = D_{c_{21}}$$

The optimal $\mathcal{H}^2$ controller given in (2.32) can be re-written as

$$\tilde{K}_{opt} \stackrel{s}{=} \left[\begin{array}{c|c} \tilde{A} + \tilde{B}_2\tilde{F} + \tilde{L}\tilde{C}_2 & -\tilde{L} \\ \hline \tilde{F} & 0 \end{array}\right] \tag{9.27}$$

where

$$\tilde{F} = -\tilde{B}_2^T \tilde{X} \left(I + \tilde{B}_2 \tilde{B}_2^T \tilde{X}\right)^{-1} \tilde{A} \tag{9.28}$$

$$\tilde{L} = -\left(\tilde{A}\tilde{Y}\tilde{C}_2^T + \tilde{B}_1\tilde{D}_{21}^T\right)\left(I + \tilde{C}_2\tilde{Y}\tilde{C}_2^T\right)^{-1} \tag{9.29}$$

and $(\tilde{X}, \tilde{Y})$ are, respectively, the solutions to the control and filter algebraic Riccati equations given by

$$\tilde{A}\tilde{X}\left(I + \tilde{B}_2\tilde{B}_2^T\tilde{X}\right)^{-1}\tilde{A} - \tilde{X} + \tilde{C}_1^T\tilde{C}_1 = 0 \tag{9.30}$$

and

$$\left(\tilde{A} - \tilde{B}_1\tilde{D}_{21}^T\tilde{C}_2\right)\tilde{Y}\left(I + \tilde{C}_2^T\tilde{C}_2\tilde{Y}\right)^{-1}\left(\tilde{A} - \tilde{B}_1\tilde{D}_{21}^T\tilde{C}_2\right)^T - \tilde{Y} + \tilde{B}_1\left(I - \tilde{D}_{21}^T\tilde{D}_{21}^T\right)\tilde{B}_1^T = 0 \tag{9.31}$$

By partitioning $\tilde{X}$ conformally with $\tilde{A}$, that is $\tilde{X} = \begin{bmatrix} X_{11} & X_{12} \\ X_{12}^T & X_{22} \end{bmatrix}$, (9.30) can be written as the following coupled equations

$$A_c^T\left(X_{11}Z_{11} + X_{12}Z_{21}\right)A_c - X_{11} + C_{c_1}^T C_{c_1} = 0 \tag{9.32}$$

$$A_d^T\left(X_{22}Z_{22} + X_{12}^T Z_{12}\right)A_d - X_{22} + C_{d_1}^T C_{d_1} = 0 \tag{9.33}$$

$$A_c^T\left(X_{11}Z_{12} + X_{12}Z_{22}\right)A_d - X_{12} = 0 \tag{9.34}$$

where

$$Z_{11} = \left(I + B_{c_2}B_{c_2}^T X_{11}\right)^{-1}\left[I + B_{c_2}B_{c_2}^T X_{12}Z_{22}B_{d_2}B_{d_2}^T X_{12}^T\left(I + B_{c_2}B_{c_2}^T X_{11}\right)^{-1}\right] \tag{9.35}$$

$$Z_{12} = -\left(I + B_{c_2}B_{c_2}^T X_{11}\right)^{-1} B_{c_2}B_{c_2}^T X_{12}Z_{22} \tag{9.36}$$

$$Z_{21} = -Z_{22}B_{d_2}B_{d_2}^T X_{12}^T\left(I + B_{c_2}B_{c_2}^T X_{11}\right)^{-1} \tag{9.37}$$

$$Z_{22} = \left[\left(I + B_{d_2}B_{d_2}^T X_{22}\right) - B_{d_2}B_{d_2}^T X_{12}^T\left(I + B_{c_2}B_{c_2}^T X_{11}\right)^{-1} B_{c_2}B_{c_2}^T X_{12}\right]^{-1} \tag{9.38}$$

It follows immediately from (9.34) to (9.38) that $X_{12} = 0$ is a solution to (9.34), and (9.32) and (9.33) can be re-written as

$$A_c^T X_{11}\left(I + B_{c_2}B_{c_2}^T X_{11}\right)^{-1} A_c - X_{11} + C_{c_1}^T C_{c_1} = 0 \tag{9.39}$$

$$A_d^T X_{22}\left(I + B_{d_2}B_{d_2}^T X_{22}\right)^{-1} A_d - X_{22} + C_{d_1}^T C_{d_1} = 0 \tag{9.40}$$

This implies that X_{11} and X_{22} can be solved independently, and (9.28) can be re-written as

$$\tilde{F} = -\begin{bmatrix} 0 & B_{d_2}^T X_{22}\left(I + B_{d_2}B_{d_2}^T X_{22}\right)^{-1} A_d \\ B_{c_2}^T X_{11}\left(I + B_{c_2}B_{c_2}^T X_{11}\right)^{-1} A_c & 0 \end{bmatrix} \tag{9.41}$$

Also, by partitioning $\tilde{Y}$ conformally with $\tilde{A}$, that is $\tilde{Y} = \begin{bmatrix} Y_{11} & Y_{12} \\ Y_{12}^T & Y_{22} \end{bmatrix}$, (9.31) can be written as the following coupled equations

$$R_{11}Y_{11}V_{11}R_{11}^T - Y_{11} + W_{11} = 0 \tag{9.42}$$

$$R_{11}Y_{12}R_{22}^T - Y_{12} + \left(R_{11}Y_{11}R_{12}^T + R_{11}Y_{11}V_{12}R_{22}^T + W_{12}\right) = 0 \tag{9.43}$$

$$R_{22}Y_{22}R_{22}^T - Y_{22} + \left[\left(R_{21}Y_{11} + R_{22}Y_{12}^T\right)\left(V_{11}R_{21}^T + V_{12}R_{22}^T\right) + R_{21}Y_{12}R_{22}^T + W_{22}\right] = 0 \tag{9.44}$$

where

$$\begin{bmatrix} R_{11} & R_{12} \\ R_{21} & R_{22} \end{bmatrix} = \begin{bmatrix} A_c - B_{c_1}D_{c_{21}}^T C_{c_2} & 0 \\ -B_{d_1}D_{c_{21}}^T C_{c_2} & A_d \end{bmatrix} \tag{9.45}$$

$$\begin{bmatrix} V_{11} & V_{12} \\ V_{21} & V_{22} \end{bmatrix} = \begin{bmatrix} \left(I + C_{c_2}^T C_{c_2} Y_{11}\right)^{-1} & -\left(I + C_{c_2}^T C_{c_2} Y_{11}\right)^{-1} C_{c_2}^T C_{c_2} Y_{12} \\ 0 & I \end{bmatrix} \tag{9.46}$$

$$\begin{bmatrix} W_{11} & W_{12} \\ W_{21} & W_{22} \end{bmatrix} = \begin{bmatrix} B_{c_1}\left(I - D_{c_{21}}^T D_{c_{21}}\right)B_{c_1}^T & B_{c_1}\left(I - D_{c_{21}}^T D_{c_{21}}\right)B_{d_1}^T \\ B_{d_1}\left(I - D_{c_{21}}^T D_{c_{21}}\right)B_{c_1}^T & B_{d_1}\left(I - D_{c_{21}}^T D_{c_{21}}\right)B_{d_1}^T \end{bmatrix} \tag{9.47}$$

It follows immediately from (9.42) to (9.44) that the solution to Y_{11} is independent of both, the Y_{12} term and any of the diagnostic terms. Equation (9.29) can be re-written as

$$\tilde{L} = -\begin{bmatrix} \left(A_c Y_{11} C_{c_2}^T + B_{c_1} D_{c_{21}}^T\right)\left(I + C_{c_2} Y_{11} C_{c_2}^T\right)^{-1} \\ \left(A_d Y_{12}^T C_{c_2}^T + B_{d_1} D_{c_{21}}^T\right)\left(I + C_{c_2} Y_{11} C_{c_2}^T\right)^{-1} \end{bmatrix} \tag{9.48}$$

For the optimal $\mathcal{H}^2$ solution, the optimal control module and the optimal diagnostic module are independent of each other, provided the interconnection structure described by (9.26) is considered. Hence, when a nominal model is considered, designing the control and diagnostic modules simultaneously is equivalent to designing them independently.

9.6 $\mathcal{H}^\infty$-Optimal Control and Diagnostics

In this section, the problem of designing, in a single step approach, an $\mathcal{H}^\infty$-suboptimal 4-DOF controller that robustly provides control and diagnostic objectives simultaneously in the face of coprime factor uncertainty is considered.

To motivate the need for synthesizing the 4-DOF controller in a single step using a robust synthesis method such as $\mathcal{H}^\infty$ optimization, the following block diagram shown in Figure 9.9 is considered. Suppose it is desired to track actuator failures (n_{a_k}) and reject step commands applied to the reference signal (w_{c_k}) at the diagnostic output (e_{d_k}). The diagnostic output is given by

$$e_{d_k} = T_{w_c e_d} w_{c_k} + T_{n_s e_d}(n_{s_k} + (G + \Delta)n_{a_k}) \tag{9.49}$$

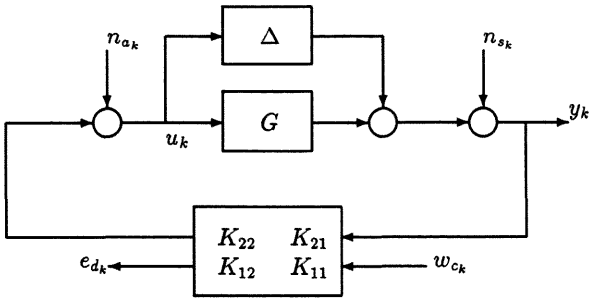

Figure 9.9: Control-Diagnostic Configuration with Additive Uncertainty.

where the perturbed transfer function matrices $T_{w_c e_d}$ and $T_{n_s e_d}$ are given by

$$T_{w_c e_d} = K_{11} + K_{12}(I - (G + \Delta)K_{22})^{-1}(G + \Delta)K_{21} \quad (9.50)$$

$$T_{n_s e_d} = K_{12}(I - (G + \Delta)K_{22})^{-1} \quad (9.51)$$

where $(I - (G + \Delta)K_{22})^{-1}$ is the perturbed sensitivity function $T_{d_{y_p}}$. In the nominal case, K_{11} and K_{12} can be designed separately, such that $T_{w_c e_d} \approx 0$ and $T_{n_a e_d} \approx I$, respectively. But according to (9.50) and (9.51) this suggests that additive model uncertainty will prohibit such a design, and these objectives will conflict with the control objectives, such as tracking of step commands and rejecting disturbances.

9.6.1 Robust Synthesis of the 4-DOF Controller

The approach proposed here allows the control parameters (K_{21} and K_{22}) and the diagnostic parameters (K_{11} and K_{12}) to be designed together in a single step *via* an extension of the $\mathcal{H}^\infty$-optimization framework covered in Chapter 3. For the control module, the feedback controller (K_{22}) is used to meet the robust stability and disturbance rejection specification, while the pre-filter (K_{21}) is used to shape the desired time responses of the closed-loop system. For the diagnostic module, the diagnostic controller (K_{12}) is used to robustly track actuator failures (step or ramp type failures), while the diagnostic controller (K_{11}) rejects step commands applied to the reference signal. The interconnection structure used for the 4-DOF design is shown in Figure 9.10. The control signal

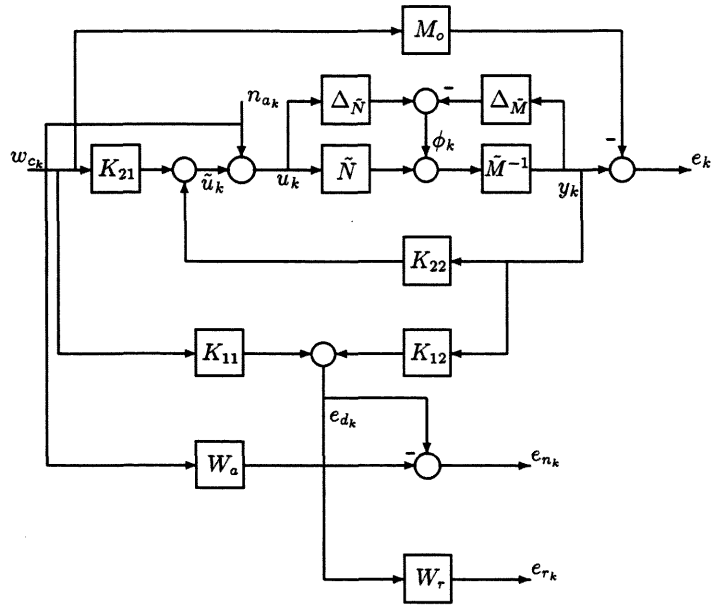

Figure 9.10: Control-Diagnostic Design Configuration under Coprime Factor Uncertainty.

is given by

$$\tilde{u}_k = \begin{bmatrix} K_{21} & K_{22} \end{bmatrix} \begin{bmatrix} w_{c_k} \\ y_k \end{bmatrix} \tag{9.52}$$

and the diagnostic signal is given by

$$e_{d_k} = \begin{bmatrix} K_{11} & K_{12} \end{bmatrix} \begin{bmatrix} w_{c_k} \\ y_k \end{bmatrix} \tag{9.53}$$

Simple algebra from Figure 9.10 shows that

$$\left[\begin{array}{c} u_k \\ y_k \\ e_k \\ \hline e_{n_k} \\ e_{r_k} \end{array}\right] = \left[\begin{array}{cc|c} (I - K_{22}G)^{-1} K_{21} & K_{22}T_{dy_p}\tilde{M}^{-1} & (I - K_{22}G)^{-1} \\ T_{n_a y_p}K_{21} & T_{dy_p}\tilde{M}^{-1} & T_{n_a y_p} \\ T_{n_a y_p}K_{21} - M_o & T_{dy_p}\tilde{M}^{-1} & T_{n_a y_p} \\ \hline K_{11} + K_{12}T_{n_a y_p}K_{21} & K_{12}T_{dy_p}\tilde{M}^{-1} & K_{12}T_{n_a y_p} - W_a \\ W_r\left[K_{11} + K_{12}T_{n_a y_p}K_{21}\right] & W_r K_{12}T_{dy_p}\tilde{M}^{-1} & W_r K_{12}T_{n_a y_p} \end{array}\right] \left[\begin{array}{c} w_{c_k} \\ \phi_k \\ \hline n_{a_k} \end{array}\right] \tag{9.54}$$

The (1,1) partition in (9.54) is associated with the control objective discussed in Chapter 3. The (1,1) element of the (2,2) partition is associated with the diagnostic objective. By appropriate choice of the weighting function W_a, K_{12} will be designed such that the diagnostic output tracks an actuator abrupt failure or a slow ramp type failure. Finally, the (2,1) element of the (2,1) partition is also associated with the diagnostic objective. By appropriate choice of the weighting function W_r, K_{11} will be designed such that the transfer function $T_{w_{ce}e_d}$ is made robustly small.

Setting the problem up in the standard regulator framework, the standard augmented plant will be given by

$$\begin{bmatrix} u_k \\ y_k \\ e_k \\ e_{n_k} \\ e_{r_k} \\ w_{c_k} \\ y_k \end{bmatrix} = \begin{bmatrix} 0 & 0 & I & 0 & I \\ 0 & \tilde{M}^{-1} & G & 0 & G \\ -M_o & \tilde{M}^{-1} & G & 0 & G \\ 0 & 0 & -W_a & I & 0 \\ 0 & 0 & 0 & W_r & 0 \\ I & 0 & 0 & 0 & 0 \\ 0 & \tilde{M}^{-1} & G & 0 & G \end{bmatrix} \begin{bmatrix} w_{c_k} \\ \phi_k \\ n_{a_k} \\ e_{d_k} \\ u_k \end{bmatrix} \tag{9.55}$$

where $G = \tilde{M}^{-1}\tilde{N}$ is the desired shaped plant (Chapter 3). A state-space realization for (9.55) can be easily derived, and may be passed to standard $\mathcal{H}^\infty$-algorithms, resulting in a suboptimal 4-DOF $\mathcal{H}^\infty$ controller.

9.6.2 Design Example

The following example is taken from [50], where the purpose is to demonstrate how the 4-DOF controller can be designed using the proposed single step approach to integrated controls and diagnostics. In this design example the diagnostics are required to detect, isolate and identify actuator failures.

The plant considered in this example is a jet engine. It has 3-inputs and 3-outputs, is stable and minimum phase, and has poles at $-4.8 \pm 3j$, -10.5, and -78.7. Further information on this model may be found in [64]. The control and diagnostic requirements are as follows:

1) **Control Objectives**: In tracking step commands at the plant output, there

should be zero steady-state error and less than 10% interaction. Also, the tracking bandwidth should be at least 5 rad/s. For robust stability, the maximum singular value of $T_{n_s y_p}$ should begin to roll-off at 10 rad/s and should be down -20 dB at 30 rad/s. It should also have good low frequency disturbance rejection.

2) **Diagnostic Objectives**: The diagnostic map $T_{n_a e_d}$ should be approximately I and $T_{w_c e_d}$ should be small up to a bandwidth of 10 rad/s, that is the diagnostic output must track actuator failures and reject step commands when the respective signal spectral content is concentrated below 10 rad/s.

Design procedure

The design procedure comprises of the following main steps:

1) Analyzing the singular values of the open-loop nominal model G indicated the need for higher low frequency gain to achieve good tracking and disturbance rejection at these frequencies. The weighting function W should thus contain integral action. Extra poles are introduced to reduce the roll-off at the cross-over frequencies. The desired W was chosen to become $\frac{1}{(s+10^{-6})(s+30)} I_3$. The weighting function is selected in continuous-time and then discretized before cascading it with the discretized nominal model. The sampling time used to discretize the nominal model was $T_s = 0.02$ seconds [64].

2) GW is next aligned at the approximate desired closed-loop bandwidth of 10 rad/s. The align gain k_a is the approximate real inverse of the system at the specified frequency. The cross-over is thus adjusted accordingly. The pre-compensator can now be expressed as $W_g = W k_a$. It is discretized, using the bilinear transformation discussed in Chapter 4, and then cascaded with G.

3) A desired reference model M_o is then selected for the closed-loop system. The reference model is selected in continuous-time as $\frac{1}{0.3s+1} I_3$ and then discretized. The controlled outputs are thus desired to behave as simple first order lags with no interaction.

4) To meet the diagnostic objectives, the desired weighting functions were selected as $W_a = \frac{1}{0.6s+1} I_3$ and $W_r = \frac{0.001(s+1)}{s+0.1} I_3$, and then discretized. The state-space realization of the generalized plant (9.55) is then constructed.

5) γ-iterations are performed, and a suboptimal controller achieving $\gamma = 4.355$ is obtained.

6) The 4-DOF controller is cascaded with the weight W_g, and the following controller parameters K_{11}, K_{12} and K_{21} were scaled to achieve the steady-state requirements. The Final 4-DOF controller was of order 32. By using the model reduction technique proposed in Chapter 6, a 13 state controller was obtained, with performance indistinguishable from the $32nd$ order controller.

Control Simulation Results

Figure 9.11 shows the open-loop shaped plant GW_g. Figures 9.12-9.13 present the maps T_{dy_p} and the input complementary sensitivity function $H_i = K_{22}G(I - K_{22}G)^{-1}$ which show that the design has good low frequency disturbance rejection characteristics and the desired robust stability requirements have been achieved, respectively. Figure 9.14 shows that the tracking of step commands at the plant output with less than 10% interaction has been achieved.

Diagnostic Simulation Results

Figure 9.15 shows the command and actuator failures. As shown in the figure, a step command is first applied to channel 2, a step or abrupt failure then occurs in actuator 1, and finally a slow ramp type failure occurs in actuator 3. The response of the diagnostic output under these conditions is shown in Figure 9.16. As can be seen from the figure, the step command is rejected with a small enough amplitude from the diagnostic output, and this output tracks nicely the actuator failures. Figure 9.17 shows the frequency response of the map $T_{n_a e_d}$ and Figure 9.18 shows the frequency response of the map $T_{w_c e_d}$. Both figures show that $T_{n_a e_d} \approx I$ and $T_{w_c e_d}$ small over the desired bandwidth.

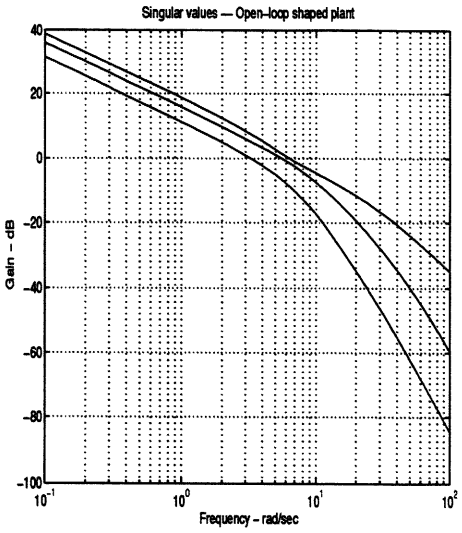

Figure 9.11: Frequency Response of the Open-loop Shaped Plant GW_g.

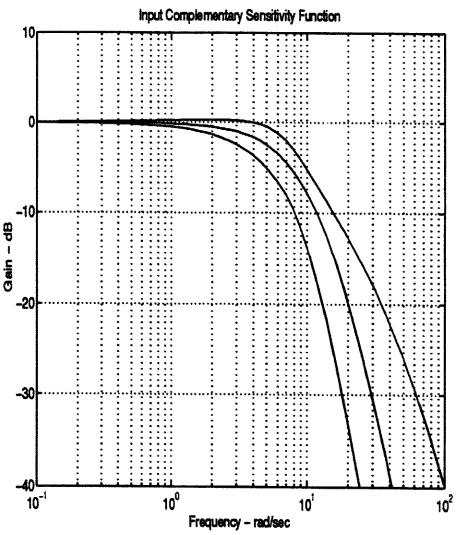

Figure 9.13: Frequency Response of the map H_i.

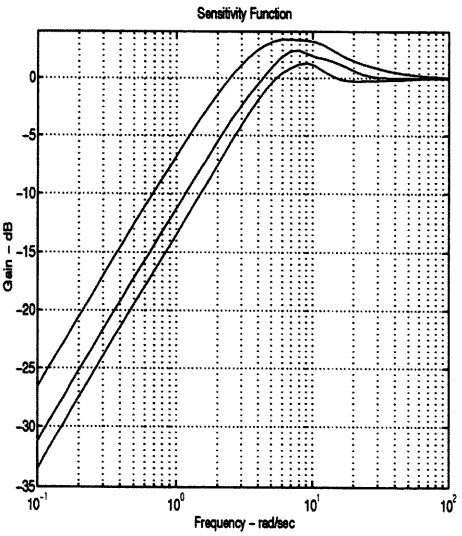

Figure 9.12: Frequency Response of the map T_{dy_p}.

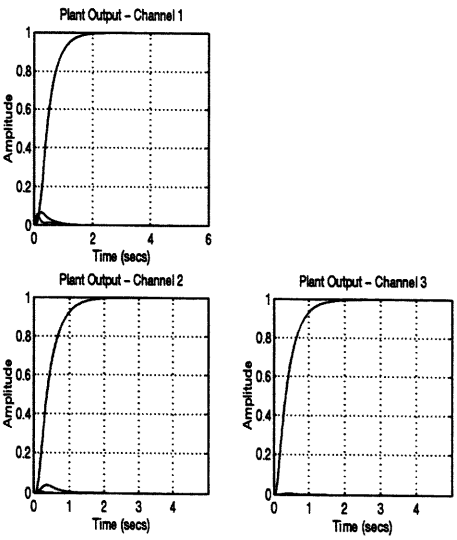

Figure 9.14: Closed-loop Step Responses of the map $T_{w_c y_p}$.

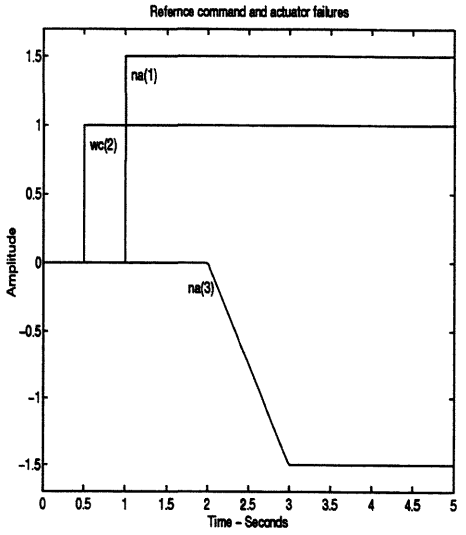

Figure 9.15: Step Command w_{c_k} and Actuator Failure n_{a_k} used in the Simulation.

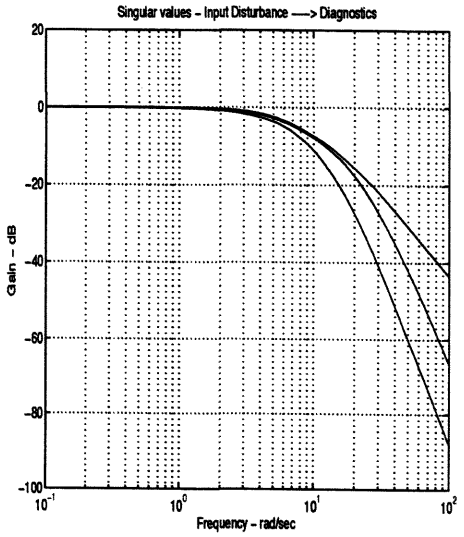

Figure 9.17: Frequency Response of the map T_{ae_d}.

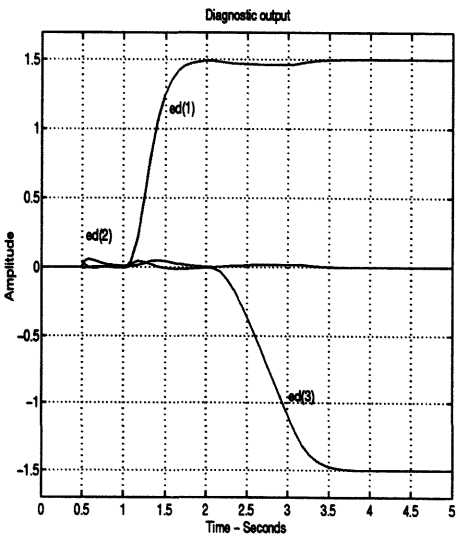

Figure 9.16: Diagnostic Output e_{d_k} Produced in the Simulation.

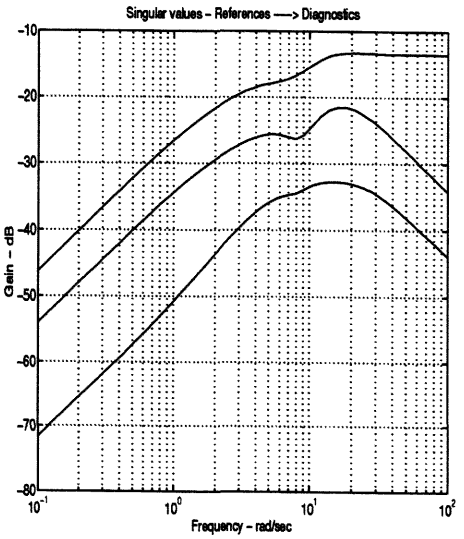

Figure 9.18: Frequency Response of the map $T_{w_c e_d}$.

9.7 Summary

In this chapter, a comprehensive treatment of the design of integrated control and diagnostic modules has been presented. The 4-DOF controller has been systematically parameterized in a single step approach. It was shown that the design can be approached using standard advanced multivariable control methods. For the nominal case, the control and diagnostic modules can be designed separately using $\mathcal{H}^2$-optimal control. However, since the diagnostic objective will limit the achieved performance in the face of uncertainty, robust $\mathcal{H}^\infty$ control theory was employed such that both modules can be designed simultaneously and frequency dependent weights used to reflect the sometimes conflicting objectives.

Chapter 10

Conclusions and Future Work

10.1 Concluding Remarks

In this thesis, a number of important practical issues on robust controller design for SISO and MIMO processes have been studied. We began by presenting some well known results on $\mathcal{H}^2$ and $\mathcal{H}^\infty$ control. Then the normalized coprime factor design procedure was investigated, and we formulated the discrete-time problem with respect to uncertainty in a normalized left coprime factor plant description. Suboptimal and optimal controllers were derived. A suboptimal controller was also derived for the 2-DOF framework. The strength of this 2-DOF framework is that the controller provides a degree of robust performance in the sense of making the closed-loop system match a pre-defined reference model in addition to its ability to provide robust stability against coprime factor uncertainty.

An industrial case study, based on an "unknown" plant (the IFAC 1993 benchmark) operating at 3 different stress levels, was then considered. The robust control methods discussed in Chapters 2 & 3, also known as analytical optimization methods, were combined with the MOI and applied to the benchmark to give fixed controllers which achieved good robust performance for stress levels 1 & 2. The performance at stress level 3 was less satisfactory, but some improvement was obtained with a variable gain adaptive scheme, although at the expense of some robustness.

Methods for synthesizing robust controllers that can be directly implemented in the Internal Model Control (IMC) scheme were formulated. First, the IMC scheme was

reviewed in the context of the Youla parameterization of all stabilizing controllers. We then showed how to put various $\mathcal{H}^\infty$ design methods into the IMC scheme. These methods included 1-DOF and 2-DOF $\mathcal{H}^\infty$ designs. Explicit state-space formulae for an $\mathcal{H}^\infty$ IMC based controller were derived. These included suboptimal and optimal IMC controllers for the 1-DOF case and a suboptimal IMC controller for the 2-DOF case, all in a coprime factor design framework.

We also presented a model reduction approach for reducing discrete-time stable/unstable non-minimal state-space systems. The approach combined existing algorithms resulting in a reliable method for computing a balanced singular perturbational approximation of a stable state-space system which may be close to being non-minimal. The approach circumvented the computation of possibly ill-conditioned balancing transformations. The algorithm was then used in a normalized coprime factor model reduction procedure which can be used for the reduction of stable as well as unstable systems. The proofs of the existing continuous-time results were directly extended to their discrete-time counterpart.

A MIMO industrial process, a glass tube production process was then introduced. Its physical behaviour was carefully studied, and mathematical models derived in state-space form using existing advanced identification methods. It was shown how to combine a variety of identification methods into an industrially applicable identification procedure. The application to the MIMO production process indicated that the combined identification approach gave good results and provided accurate low-order models for use in MIMO control schemes. The application of robust IMC control to the production process then followed. The design of a MIMO IMC control system was discussed in detail. The responses of the process output without the MIMO controller showed an unacceptable degree of interaction and a lot of overshoot. The responses of the controlled process were smooth, fast reacting and first-order. Both Type 1 and Type 2 IMC controllers were designed with predictable responses. Robustness was obtained within the accuracies of the different models, suggesting that the designs were reliable for practical implementation. However, problems were encountered for the larger measures because then the time delays became more dominant. Also, the sensitivity to process static gains increased the interaction between the wall thickness and the diam-

eter for incorrect estimates or when operating over a larger process range. Finally, the standard deviation of both the wall thickness and diameter were reduced considerably for small measures and reduced marginally for large measures.

An existing but relatively new theoretical foundation for an integrated approach to the design of controls and diagnostics was further developed. With a 4-DOF controller and a standard regulator framework, it was shown how to design the controls and diagnostics together using robust control theory. The main strength of this approach is that the 4-DOF controller can be synthesized in a single step approach into which model uncertainty is directly incorporated. This has the advantage of improving diagnostic performance when the plant is uncertain. Finally, with this approach the interactions that do occur between the control and diagnostic modules can be minimized to some extent.

10.2 Suggestions for Future Work

The robust control system design framework developed and studied in this thesis, and the industrial case studies suggest further research in the following areas:

Robust Adaptive Control – This concerns the integration of robust control and adaptive schemes. This particular problem was motivated in Chapter 4. It was shown that the main problems in designing a controller for the "unknown" plant (IFAC 1993 benchmark) arose at stress level 3 where the gain variation was such that some adaptive control was required. Some improvement was obtained but at the expense of robustness. This motivates the need of robust adaptation schemes and controllers that incorporate both robust and adaptive schemes.

IMC Control for Unstable Systems – The main reasons behind extending the IMC to open-loop unstable systems is that, firstly the stability of the IMC controller Q shown in Figure 5.1 (Chapter 5) does not guarantee the stability of the closed-loop system when the plant G_p is unstable, and secondly designing the controller for robust stability can be more difficult. That is, when the plant is stable the controller can be easily detuned, but when the plant is unstable there is a limit to how much the controller can be detuned. In this case, some controller gain is needed just to stabilize the system.

This is demonstrated in Figure 10.1.

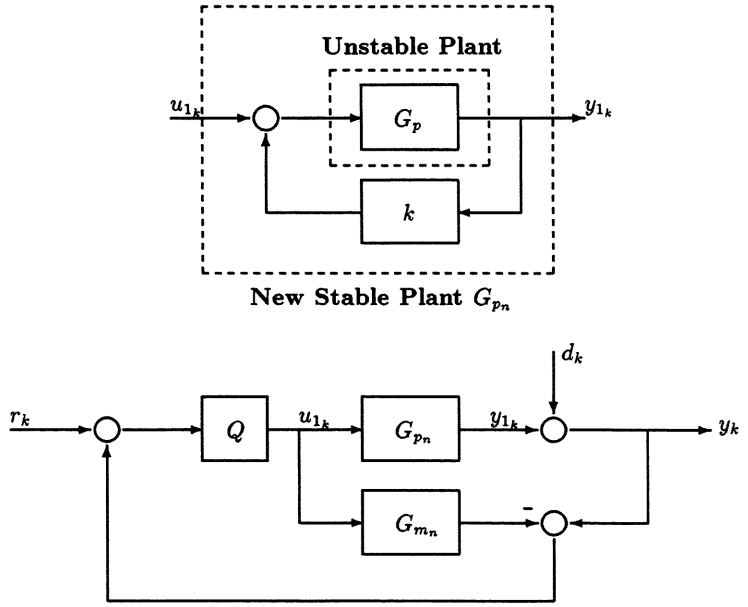

Figure 10.1: An IMC Scheme for Unstable Systems.

Moving to unstable systems, the IMC scheme of Figure 5.1 for control system implementation has to be abandoned. An alternative scheme is shown in Figure 10.2 where its clear that when $G_p = G_m$ (no plant/model mismatch) it simplifies to the classical feedback scheme. The main advantage of this scheme is that the IMC controller will include the nominal model G_m of the unstable plant, unlike the scheme shown in Figure 10.1. Furthermore, the restriction of having only stable parameters in the scheme is removed. We believe that designing the controller parameters Q_1 and Q_2 of Figure 10.2 in a single step approach is worthy of further investigation.

Discrete-time Model Reduction – This concerns the derivation of the following two error bounds: Firstly, a tight bound for the model error for the coprime factor order reduction of discrete-time systems based on balancing. The error bound given for $G - G_r = \tilde{M}^{-1}\tilde{N} - \tilde{M}_r^{-1}\tilde{N}_r$ in Chapter 6 by (6.78) is very weak and simple (too

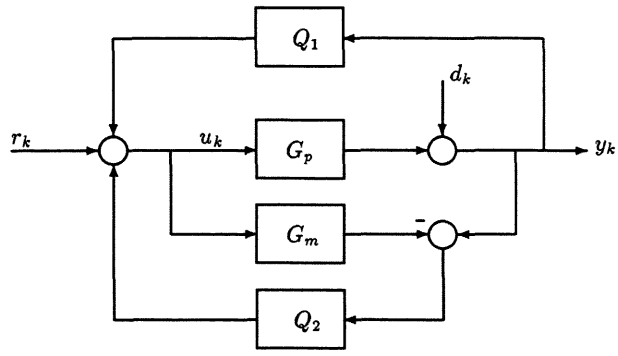

Figure 10.2: Proposed IMC Scheme for Unstable Systems.

conservative). Secondly, a reduced-order stability bound for the controller reduction error, of the suboptimal 2-DOF $\mathcal{H}^\infty$ controller derived in Chapter 3 and of the suboptimal 2-DOF $\mathcal{H}^\infty$ IMC based controller derived in Chapter 5, to guarantee closed-loop stability and to minimize the performance degradation when controller-order reduction is performed. We believe that the search for such bounds is therefore a worthy area for future research.

Control of the Glass Tube Production Process – This concerns the possibility of controlling the glass tube production process *via* the IMC scheme with one fixed gain controller over a larger process range, that is for example, controlling Measure 1 and Measure 2 with a single controller. It was shown in Figure 8.29 (Chapter 8) that the static gains of the process become more sensitive and therefore will increase the coupling between the wall thickness and the diameter when moving from Measure 1 to Measure 2 with a controller originally designed for Measure 1. A possible solution to this problem can be gain scheduling to ensure correct process static gains, or alternatively on-line adaptation of the process static gains. Finally, combining adaptation with the IMC scheme to obtain an adaptive IMC scheme is worthy of further investigation.

Integrated Controls and Diagnostics – This concerns the possibility of synthesizing the 4-DOF controller, in a single step approach, such that the diagnostic output identifies sensor and actuator failures. The framework presented in Chapter 9 will enable

the diagnostic output to identify actuator failures only. We believe that the diagnostic module must have the ability to distinguish between sensor failures and actuator failures. Finally, the development of a reconfiguration module, which is simply a controller reconfiguration strategy that allows the control performance to be maintained in the presense of failures, is very crucial and a worthy subject for future research.

Appendix A

Preliminary Mathematical Background

In this appendix a brief review is given on some useful definitions and well known results of discrete time linear time-invariant systems that may be necessary to understand the theoretical contents of this thesis. Section A.1 lists a table of standard notations together with their definitions. Section A.2, on basic system theory, includes transfer function matrices in state-space form, operations on linear systems, controllability and observability, and all-pass transfer function matrices. Section A.3 reviews the discrete-time algebraic Riccati equation (DARE), and some issues on solving the DARE are discussed. In section A.4, some definitions on coprime factorization are given. Finally, a definition of stability, including well-posedness and internal stability are presented.

A.1 Nomenclature

Notation	Meaning
z	A Complex variable. Given $F \in l^{p\times q}$, define $F(z) = \sum_{k=0}^{\infty} F_k z^{-k}$ as the Z-transform of F. $z = e^{j\theta}$ yields the frequency response.
s	Laplace operator.
$\mathcal{R}$	Field of real numbers.
$\mathcal{R}^m$	Space of m-component real vectors.
$\mathcal{R}^{p\times m}$	Space of $p \times m$ matrices with real elements.
R	Space of all real-rational transfer function matrices.
$\mathcal{C}$	Field of complex numbers.

$\mathcal{C}^m$	Space of m-component complex vectors.
$\mathcal{C}^{p\times m}$	Space of $p \times m$ matrices with complex elements.
A^{-1}	Inverse of a matrix A.
A^*	Complex Conjugate Transpose of a matrix A.
A^T	Transpose of a matrix A.
rank(A)	Rank of a matrix A.
det(A)	Determinant of a matrix A.
tr(A)	Trace of a matrix A.
diag(A)	Matrix A is diagonal.
$\rho(A)$	Spectral radius of a matrix A.
$\lambda_{max}(A), \lambda_{min}(A)$	Maximum, minimum eigenvalue of a matrix A.
$\bar{\sigma}(A), \underline{\sigma}(A)$	Maximum, minimum singular value of a matrix A.
$\tilde{\sigma}_i$	$i-th$ Hankel singular value.
$A > 0$	Matrix A is positive definite.
$A \geq 0$	Matrix A is semi-positive definite.
$G(z)$	Transfer function matrix.
$G^*(z)$	$G^T(z^{-1})$, the reciprocal transpose.
deg(G)	Degree of $G(z)$, *i.e.* the number of states of $G(z)$.
$\mathcal{D}$	The open unit disc.
$\mathcal{L}^\infty$	Lebesgue space with appropriate dimensions essentially bounded on the unit circle.
$\mathcal{H}^\infty$	Hardy space of complex valued functions analytic in $\mathcal{D}$ bounded on the unit circle.
$\mathcal{H}^2$	The Hilbert space of square integrable complex valued functions on the unit circle that have analytic continuation in the unit disc.
$\mathcal{H}^2_\perp$	Complementary part of $\mathcal{H}^2$ having analytic continuation outside the unit disc.
$\mathcal{RL}^\infty$	Real rational subspace of $\mathcal{L}^\infty$.
$\mathcal{RH}^\infty$,$\mathcal{RH}^\infty_\perp$	Real rational subspace of $\mathcal{H}^\infty$,$\mathcal{RH}^\infty_\perp$.
$\| G(z) \|_\infty$	$\mathcal{H}^\infty$ norm of $G(z)$.
$\| G(z) \|_2$	$\mathcal{H}^2$ norm of $G(z)$.

$\| G(z) \|_H$	Hankel norm of $G(z)$.
$\mathcal{R}(A)$	Symbol for the range of a matrix A.
I_m	$m \times m$ identity matrix.

A.2 Basic System Theory

A.2.1 Transfer Functions

Consider the linear time-invariant difference equation described by

$$\begin{aligned} x_{k+1} &= Ax_k + Bu_k \\ y_k &= Cx_k + Du_k \end{aligned} \tag{A.1}$$

where $x_k \in \mathcal{R}^n$ is the state, $u_k \in \mathcal{R}^m$ is the input and $y_k \in \mathcal{R}^p$ is the output. The A, B, C and D are appropriately dimensioned real matrices. The system described by (A.1) is given the notation

$$G \stackrel{s}{=} \left[\begin{array}{c|c} A & B \\ \hline C & D \end{array}\right] \tag{A.2}$$

The pulse response of the system is given by

$$G_k = \begin{cases} D & \text{for } k = 0 \\ CA^{k-1}B & \text{for } k > 0 \end{cases} \tag{A.3}$$

and the Z-transform, resulting in a transfer function given by

$$G(z) = C(zI - A)^{-1}B + D \tag{A.4}$$

A.2.2 Controllability and Observability

A system is controllable [51] if there always exists an input that takes the states from any initial condition to any prespecified final state in finite time.

Theorem A.2.1 The following are equivalent:

1) (A, B) is controllable.

2) The matrix $[B \quad AB \quad A^2B \quad \cdots \quad A^{n-1}B]$ has full row rank equal to n.

3) The matrix $[A - \lambda I \quad B]$ has full row rank equal to n for all $\lambda \in \mathcal{C}$.

4) The eigenvalues of $A + BF$ can be freely assigned by suitable choice of F.

■

The pair (A, B) is stabilizable if there exists an F such that $A + BF$ is stable.

A system is observable [51] if an initial condition can be exactly determined from observing the output for some finite time.

Theorem A.2.2 The following are equivalent:

1) (A, C) is observable.

2) The matrix $[C^T \quad A^TC^T \quad (A^2)^TC^T \quad \cdots \quad (A^{n-1})^TC^T]^T$ has full column rank equal to n.

3) The matrix $\begin{bmatrix} A - \lambda I \\ C \end{bmatrix}$ has column rank equal to n for all $\lambda \in \mathcal{C}$.

4) The eigenvalues of $A + HC$ can be freely assigned by suitable choice of H.

■

The pair (A, C) is detectable if there exists an H such that $A + HC$ is stable.

The degree of a controllable and observable realization (*i.e.* minimal realization) will be referred to as the McMillan degree.

A.2.3 All-Pass Transfer Function Matrices

The conjugate system of (A.4) is defined as

$$G^*(z) = G^T(z^{-1}) = B^T(z^{-1}I - A^T)^{-1}C^T + D^T \tag{A.5}$$

and a realization for G^* is given by

$$G^* \stackrel{s}{=} \left[\begin{array}{c|c} A^{-T} & A^{-T}C^T \\ \hline -B^TA^{-T} & D^T - B^TA^{-T}C^T \end{array}\right] \tag{A.6}$$

provided A^{-1} exists. The following lemma gives sufficient conditions for a discrete transfer function matrix to be all pass.

Lemma A.2.1 [106] Given $G(z) = C(zI - A)^{-1}B + D$ such that

$$\begin{aligned} D^TD + B^TQB &= I \\ D^TC + B^TQA &= 0 \\ Q - A^TQA &= C^TC \end{aligned} \tag{A.7}$$

then $G^*G = I$. Similarly, if

$$\begin{aligned} DD^T + CPC^T &= I \\ BD^T + APC^T &= 0 \\ P - APA^T &= BB^T \end{aligned} \tag{A.8}$$

then $GG^* = I$. ■

A.3 The Discrete-Time Algebraic Riccati Equation

A.3.1 Symplectic Matrices

An extensive discussion of the discrete-time algebraic Riccati equation can be found in the following references [83, 49, 8, 107]. A pair of matrices $S_1, S_2 \in \mathcal{C}^{2n\times 2n}$ is called symplectic if the following equation is satisfied

$$S_1JS_1^T = S_2JS_2^T \tag{A.9}$$

where

$$J = \begin{bmatrix} 0 & I \\ -I & 0 \end{bmatrix} \tag{A.10}$$

Let S denote the symplectic pair $[S_1, S_2]$ where

$$S_1 = \begin{bmatrix} A & 0 \\ -Q & I \end{bmatrix} \text{ and } S_2 = \begin{bmatrix} I & R \\ 0 & A^T \end{bmatrix} \tag{A.11}$$

with $Q = Q^T$ and $R = R^T$.

A complex number β is a generalized eigenvalue of S if there exist a vector x such that

$$S_1 x = \beta S_2 x \tag{A.12}$$

Equivalently, β is a root of the polynomial $\mathbf{det}\ (S_1 - \lambda S_2)$.

In the case where the pair S has no generalized eigenvalues inside the unit circle, then it has n generalized eigenvalues inside the unit disc. Let $\mathcal{X}_-(S)$ denote the n-dimensional spectral subspace associated with the generalized eigenvalues inside $\mathcal{D}$. This subspace can be represented as the span of the principal eigenvectors associated with each generalized eigenvalue. Stacking up these vectors gives

$$\mathcal{X}_-(S) = \mathcal{R}\begin{bmatrix} X_1 \\ X_2 \end{bmatrix} \tag{A.13}$$

where $X_1, X_2 \in \mathcal{C}^{n\times n}$. By definition it follows that

$$S_1 \begin{bmatrix} X_1 \\ X_2 \end{bmatrix} = S_2 \begin{bmatrix} X_1 \\ X_2 \end{bmatrix} T \tag{A.14}$$

where $T \in \mathcal{C}^{n\times n}$ satisfying $\rho(T) < 1$. If X_1 is non-singular, then

$$\mathcal{R}\begin{bmatrix} X_1 \\ X_2 \end{bmatrix} = \mathcal{R}\begin{bmatrix} I \\ X_2 X_1^{-1} \end{bmatrix} \tag{A.15}$$

A.3.2 The Riccati Operator

If X_1^{-1} exists, then a function $Ric(.)$ that maps the symplectic pair S to the matrix $X = X_2 X_1^{-1}$, can be defined. S is said to be in the domain of Ric, denoted by $dom(Ric)$ if

1) S has no generalized eigenvalues on the unit circle.

2) X_1^{-1} exists.

3) $(I + RX)$ is invertible.

In this case $Ric(S) = X$.

Theorem A.3.1 **[14]** Let $S \in dom(Ric)$ and $X = Ric(S)$. Then the following statements hold

1) $X = X^T$.

2) X satisfies the discrete Riccati equation

$$X = A^T X(I + RX)^{-1}A + Q \tag{A.16}$$

3) The matrix $(I + RX)^{-1}A$ is stable. ■

If A^{-1} exists, then it is possible to work with the symplectic matrix $S = S_2^{-1}S_1$ given by

$$S = \begin{bmatrix} A + RA^{-T}Q & -RA^{-T} \\ -A^{-T}Q & A^{-T} \end{bmatrix} \tag{A.17}$$

and it satisfies $S^T J S = J$.

Theorem A.3.2 [43] If S in (A.17) has no eigenvalues on the unit circle and $[A, R]$ is stabilizable, then the discrete-time algebraic Riccati equation (A.16) has a unique solution X such that the continuous-time algebraic Riccati equation

$$\tilde{A}^T X + X\tilde{A} - X\tilde{R}X + \tilde{Q} = 0 \tag{A.18}$$

is satisfied. This can be achieved by performing the following transformation

$$\begin{aligned} H &= (S + I)^{-1}(S - I) \\ &= \begin{bmatrix} \tilde{A} & -\tilde{R} \\ -\tilde{Q} & \tilde{A}^T \end{bmatrix} \end{aligned} \tag{A.19}$$

where H is a Hamiltonian matrix [3]. Also, H has no eigenvalues on the imaginary axis, because S has no eigenvalues on the unit circle. ■

A.4 Coprime Factorization

An extensive discussion of coprime factorization can be found in the following references [102, 103, 104, 62]. Here we present some basic definitions. Firstly, necessary and sufficient conditions for two matrices to be right and left coprime are given in the following two definitions.

Definition A.4.1 Suppose $N, M \in \mathcal{RH}^\infty$ have the same number of columns. Then N, M are right coprime if, and only if, there exists $U, V \in \mathcal{RH}^\infty$ such that

$$VM + UN = I \tag{A.20}$$

Definition A.4.2 Suppose $\tilde{M}, \tilde{N} \in \mathcal{RH}^\infty$ have the same number of rows. Then $\tilde{M}, \tilde{N}$ are left coprime if, and only if, there exists $U, V \in \mathcal{RH}^\infty$ such that

$$\tilde{M}V + \tilde{N}U = I \tag{A.21}$$

■

It is possible to represent any real-rational, proper transfer function in terms of a pair of asymptotically stable, real-rational, proper transfer function which are right or left coprime. This is called a right or left coprime factorization, and is defined next, together with normalized right and left coprime factorization.

Definition A.4.3 The pair (N, M), where $N, M \in \mathcal{RH}^\infty$, constitutes a normalized right coprime factorization of $G \in R$ if, and only if,

1) M is square, $\det(M) \neq 0$.

2) $G = NM^{-1}$.

3) N, M are right coprime.

4) $N^*N + M^*M = I$. ■

Definition A.4.4 The pair $(\tilde{M}, \tilde{N})$, where $\tilde{M}, \tilde{N} \in \mathcal{RH}^\infty$, constitutes a normalized left coprime factorization of $G \in R$ if, and only if,

1) $\tilde{M}$ is square, $\det(\tilde{M}) \neq 0$.

2) $G = \tilde{M}^{-1}\tilde{N}$.

3) $\tilde{M}, \tilde{N}$ are left coprime.

4) $\tilde{N}\tilde{N}^* + \tilde{M}\tilde{M}^* = I$. ■

A.5 Internal Stability and Well-Posedness

It is common in control system analysis to be concerned with input-output stability. A system is input-output stable if the output response to a bounded input signal is also bounded. However, a stronger notion of stability, is that of internal stability [16], which precludes the possibility of any unbounded signals existing in a closed-loop system. The condition of internal stability will be given in terms of the following framework shown in Figure A.1 [19]. The inputs and outputs of Figure A.1 are related as follows

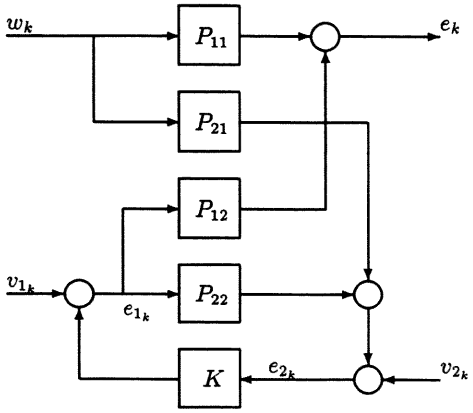

Figure A.1: Diagram for Internal Stability Definition.

$$\begin{bmatrix} I & -P_{12} & 0 \\ 0 & I & -K \\ 0 & -P_{22} & I \end{bmatrix} \begin{bmatrix} e_k \\ e_{1_k} \\ e_{2_k} \end{bmatrix} = \begin{bmatrix} P_{11} & 0 & 0 \\ 0 & I & K \\ P_{21} & 0 & 0 \end{bmatrix} \begin{bmatrix} w_k \\ v_{1_k} \\ v_{2_k} \end{bmatrix} \tag{A.22}$$

Definition A.5.1 The feedback loop in Figure A.1 is internally stable if the system mapping $[\, w_k^T \quad v_{1_k}^T \quad v_{2_k}^T \,]^T$ to $[\, e_k^T \quad e_{1_k}^T \quad e_{2_k}^T \,]^T$ is stable, or equivalently, the system mapping $[\, v_{1_k}^T \quad v_{2_k}^T \,]^T$ to $[\, e_{1_k}^T \quad e_{2_k}^T \,]^T$ is stable. ■

Definition A.5.2 The feedback loop of Figure A.1 is internally stable if, and only if,

$$\begin{bmatrix} I & K \\ -P_{22} & I \end{bmatrix}^{-1} \in \mathcal{RH}^\infty \tag{A.23}$$

■

For certain controllers, the 2×2 block matrix in (A.23) may not be proper, though P_{22} and K are. This means that for some inputs v_{1_k}, v_{2_k}, the algebraic loop cannot be solved and the feedback loop is said to be ill-posed. If either P_{22} or K is strictly proper, then the feedback loop is assured to be well-posed.

Definition A.5.3 In the case of state-space systems, the feedback loop of Figure A.1 is well-posed if $(I - P_{22}K)^{-1}$ can be represented as a state-space system. If P_{22} and K are the transfer function matrices of state-space systems, well-posedness is equivalent to $det(I - P_{22}(e^{j\theta})K(e^{j\theta})) \neq 0$ when $\theta = -\pi$. ■

An important stability result is based on what is called the Small Gain Theorem [116]. This theorem provides a sufficient condition for the stability of the feedback loop in Figure A.1.

Theorem A.5.1 Let $P_{22} : \mathcal{L}_n^2 \rightarrow \mathcal{L}_m^2$ and $K : \mathcal{L}_m^2 \rightarrow \mathcal{L}_n^2$ be stable operators of bounded $\mathcal{L}^2$-gain and assume that the closed loop system is well-posed. Then the closed loop system is stable if

$$\| P_{22} \|_\infty \| K \|_\infty < 1 \tag{A.24}$$

■

Appendix B

Proof of Results from Chapter 6

B.1 Proof of (6.18)

Lemma B.1.1 Let

$$G_r \stackrel{s}{=} \left[\begin{array}{c|c} E_{11} & F_1 \\ \hline G_1 & \tilde{H} \end{array}\right] \tag{B.1}$$

be a balanced continuous-time reduced-order model. Then by using bilinear transformation (defined in Chapter 1), the balanced discrete-time reduced-order model $\hat{G}_r$ is given by

$$\hat{G}_r \stackrel{s}{=} \left[\begin{array}{c|c} \hat{A}_{11} - \hat{A}_{12}(I+\hat{A}_{22})^{-1}\hat{A}_{21} & \hat{B}_1 - \hat{A}_{12}(I+\hat{A}_{22})^{-1}\hat{B}_2 \\ \hline \hat{C}_1 - \hat{C}_2(I+\hat{A}_{22})^{-1}\hat{A}_{21} & \hat{D} - \hat{C}_2(I+\hat{A}_{22})^{-1}\hat{B}_2 \end{array}\right] \tag{B.2}$$

Proof

The state-space realization for the balanced continuous-time model is given by

$$\left[\begin{array}{cc|c} E_{11} & E_{12} & F_1 \\ E_{21} & E_{22} & F_2 \\ \hline G_1 & G_2 & \tilde{H} \end{array}\right] \tag{B.3}$$

By using the bilinear transformation, the E-matrix will be given by

$$\begin{bmatrix} E_{11} & E_{12} \\ E_{21} & E_{22} \end{bmatrix} = \begin{bmatrix} I+\hat{A}_{11} & \hat{A}_{12} \\ \hat{A}_{21} & I+\hat{A}_{22} \end{bmatrix}^{-1} \begin{bmatrix} \hat{A}_{11}-I & \hat{A}_{12} \\ \hat{A}_{21} & \hat{A}_{22}-I \end{bmatrix} \tag{B.4}$$

where by applying the inverse of a block matrix, $\begin{bmatrix} I+\hat{A}_{11} & \hat{A}_{12} \\ \hat{A}_{21} & I+\hat{A}_{22} \end{bmatrix}^{-1}$ can be re-written as

$$\begin{bmatrix} (I+\hat{A}_{11}-\hat{A}_{12}\breve{A}_{22}^{-1}\hat{A}_{21})^{-1} & -(I+\hat{A}_{11}-\hat{A}_{12}\breve{A}_{22}^{-1}\hat{A}_{21})^{-1}\hat{A}_{12}\breve{A}_{22}^{-1} \\ -(I+\hat{A}_{22}-\hat{A}_{21}\breve{A}_{11}^{-1}\hat{A}_{12})^{-1}\hat{A}_{21}\breve{A}_{11}^{-1} & (I+\hat{A}_{22}-\hat{A}_{21}\breve{A}_{11}^{-1}\hat{A}_{12})^{-1} \end{bmatrix} \tag{B.5}$$

where $\breve{A}_{22} = (I + \hat{A}_{22})$ and $\breve{A}_{11} = (I + \hat{A}_{11})$. Now E_{11} can be expressed as

$$\begin{aligned} E_{11} &= (I + \hat{A}_{11} - \hat{A}_{12}\breve{A}_{22}^{-1}\hat{A}_{21})^{-1}(\hat{A}_{11} - I) - (I + \hat{A}_{11} - \hat{A}_{12}\breve{A}_{22}^{-1}\hat{A}_{21})^{-1} \\ &\quad \times \hat{A}_{12}\breve{A}_{22}^{-1}\hat{A}_{21} \\ &= (I + \hat{A}_{11} - \hat{A}_{12}\breve{A}_{22}^{-1}\hat{A}_{21})^{-1}[-2I + I + \hat{A}_{11} - \hat{A}_{12}\breve{A}_{22}^{-1}\hat{A}_{21}] \\ &= (I + \hat{A}_{11} - \hat{A}_{12}\breve{A}_{22}^{-1}\hat{A}_{21})^{-1}(-I + \hat{A}_{11} - \hat{A}_{12}\breve{A}_{22}^{-1}\hat{A}_{21}) \end{aligned} \tag{B.6}$$

For the F-matrix, we have

$$\begin{bmatrix} F_1 \\ F_2 \end{bmatrix} = \sqrt{2}\begin{bmatrix} I + \hat{A}_{11} & \hat{A}_{12} \\ \hat{A}_{21} & I + \hat{A}_{22} \end{bmatrix}^{-1}\begin{bmatrix} \hat{B}_1 \\ \hat{B}_2 \end{bmatrix} \tag{B.7}$$

Now F_1 can be expressed as

$$F_1 = \sqrt{2}(I + \hat{A}_{11} - \hat{A}_{12}(I + \hat{A}_{22})^{-1}\hat{A}_{21})^{-1}(\hat{B}_1 - \hat{A}_{12}(I + \hat{A}_{22})^{-1}\hat{B}_2) \tag{B.8}$$

For the G-matrix, we have

$$[G_1 \quad G_2] = \sqrt{2}[\hat{C}_1 \quad \hat{C}_2]\begin{bmatrix} I + \hat{A}_{11} & \hat{A}_{12} \\ \hat{A}_{21} & I + \hat{A}_{22} \end{bmatrix}^{-1} \tag{B.9}$$

Now G_1 can be expressed as

$$G_1 = \sqrt{2}(\hat{C}_1 - \hat{C}_2(I + \hat{A}_{22})^{-1}\hat{A}_{21})(I + \hat{A}_{11} - \hat{A}_{12}(I + \hat{A}_{22})^{-1}\hat{A}_{21})^{-1} \tag{B.10}$$

For the $\tilde{H}$-matrix, we have

$$\tilde{H} = \hat{D} - [\hat{C}_1 \quad \hat{C}_2]\begin{bmatrix} I + \hat{A}_{11} & \hat{A}_{12} \\ \hat{A}_{21} & I + \hat{A}_{22} \end{bmatrix}^{-1}\begin{bmatrix} \hat{B}_1 \\ \hat{B}_2 \end{bmatrix} \tag{B.11}$$

By using the bilinear transformation to map (B.1) to the discrete-time state-space system $(\hat{A}_r, \hat{B}_r, \hat{C}_r, \hat{D}_r)$, we obtain the following: For the $\hat{A}_r$-matrix

$$\hat{A}_r = (I + E_{11})(I - E_{11})^{-1} \tag{B.12}$$

where

$$\begin{aligned} (I - E_{11})^{-1} &= [I + 2(I + \hat{A}_{11} - \hat{A}_{12}(I + \hat{A}_{22})^{-1}\hat{A}_{21})^{-1} - I]^{-1} \\ &= \frac{1}{2}(I + \hat{A}_{11} - \hat{A}_{12}(I + \hat{A}_{22})^{-1}\hat{A}_{21}) \end{aligned} \tag{B.13}$$

and

$$\begin{aligned} (I + E_{11}) &= 2I - 2(I + \hat{A}_{11} - \hat{A}_{12}(I + \hat{A}_{22})^{-1}\hat{A}_{21})^{-1} \\ &= 2(\hat{A}_{11} - \hat{A}_{12}(I + \hat{A}_{22})^{-1}\hat{A}_{21})(I + \hat{A}_{11} - \hat{A}_{12}(I + \hat{A}_{22})^{-1}\hat{A}_{21})^{-1} \end{aligned} \tag{B.14}$$

We then have, from (B.12)

$$\hat{A}_r = \hat{A}_{11} - \hat{A}_{12}(I + \hat{A}_{22})^{-1}\hat{A}_{21} \tag{B.15}$$

For the $\hat{B}_r$-matrix, we have

$$\begin{aligned} \hat{B}_r &= \sqrt{2}(I - E_{11})^{-1}F_1 \\ &= \hat{B}_1 - \hat{A}_{12}(I + \hat{A}_{22})^{-1}\hat{B}_2 \end{aligned} \tag{B.16}$$

For the $\hat{C}_r$-matrix, we have

$$\begin{aligned} \hat{C}_r &= \sqrt{2}G_1(I - E_{11})^{-1} \\ &= \hat{C}_1 - \hat{C}_2(I + \hat{A}_{22})^{-1}\hat{A}_{21} \end{aligned} \tag{B.17}$$

For the $\hat{D}_r$-matrix, we have

$$\begin{aligned} \hat{D}_r &= \tilde{H} + G_1(I - E_{11})^{-1}F_1 \\ &= \hat{D} - [\hat{C}_1 \quad \hat{C}_2]\begin{bmatrix} I + \hat{A}_{11} & \hat{A}_{12} \\ \hat{A}_{21} & I + \hat{A}_{22} \end{bmatrix}^{-1}\begin{bmatrix} \hat{B}_1 \\ \hat{B}_2 \end{bmatrix} + (\hat{C}_1 - \hat{C}_2(I + \hat{A}_{22})^{-1}\hat{A}_{21}) \\ &\quad \times (I + \hat{A}_{11} - \hat{A}_{12}(I + \hat{A}_{22})^{-1}\hat{A}_{21})^{-1}(\hat{B}_1 - \hat{A}_{12}(I + \hat{A}_{22})^{-1}\hat{B}_2) \\ &= \hat{D} - [\hat{C}_1 \quad \hat{C}_2]\begin{bmatrix} I + \hat{A}_{11} & \hat{A}_{12} \\ \hat{A}_{21} & I + \hat{A}_{22} \end{bmatrix}^{-1}\begin{bmatrix} \hat{B}_1 \\ \hat{B}_2 \end{bmatrix} \\ &\quad + [\hat{C}_1 \quad \hat{C}_2]\begin{bmatrix} I \\ -(I + \hat{A}_{22})^{-1}\hat{A}_{21} \end{bmatrix}(I + \hat{A}_{11} - \hat{A}_{12}(I + \hat{A}_{22})^{-1}\hat{A}_{21})^{-1} \\ &\quad \times [I \quad -\hat{A}_{12}(I + \hat{A}_{22})^{-1}]\begin{bmatrix} \hat{B}_1 \\ \hat{B}_2 \end{bmatrix} \\ &= \hat{D} - [\hat{C}_1 \quad \hat{C}_2]\begin{bmatrix} I + \hat{A}_{11} & \hat{A}_{12} \\ \hat{A}_{21} & I + \hat{A}_{22} \end{bmatrix}^{-1}\begin{bmatrix} \hat{B}_1 \\ \hat{B}_2 \end{bmatrix} \\ &\quad + [\hat{C}_1 \quad \hat{C}_2]\left[\begin{bmatrix} I + \hat{A}_{11} & \hat{A}_{12} \\ \hat{A}_{21} & I + \hat{A}_{22} \end{bmatrix}^{-1} - \begin{bmatrix} 0 & 0 \\ 0 & I + \hat{A}_{22} \end{bmatrix}\right]\begin{bmatrix} \hat{B}_1 \\ \hat{B}_2 \end{bmatrix} \\ &= \hat{D} - \hat{C}_2(I + \hat{A}_{22})^{-1}\hat{B}_2 \end{aligned} \tag{B.18}$$

This completes the proof. ■

B.2 Proof of (6.20)

Lemma B.2.1 Let

$$G_r \stackrel{s}{=} \left[\begin{array}{c|c} E_{11} - E_{12}E_{22}^{-1}E_{21} & F_1 - E_{12}E_{22}^{-1}F_2 \\ \hline G_1 - G_2E_{22}^{-1}E_{21} & \tilde{H} - G_2E_{22}^{-1}F_2 \end{array}\right] \tag{B.19}$$

be a balanced singular perturbational low-order approximation of a continuous-time model. Then by using the bilinear transformation described in Chapter 1), the balanced singular perturbational low-order approximation of a discrete-time model $\hat{G}_r$ is given by

$$\hat{G}_r \stackrel{s}{=} \left[\begin{array}{c|c} \hat{A}_{11}+\hat{A}_{12}(I-\hat{A}_{22})^{-1}\hat{A}_{21} & \hat{B}_1+\hat{A}_{12}(I-\hat{A}_{22})^{-1}\hat{B}_2 \\ \hline \hat{C}_1+\hat{C}_2(I-\hat{A}_{22})^{-1}\hat{A}_{21} & \hat{D}+\hat{C}_2(I-\hat{A}_{22})^{-1}\hat{B}_2 \end{array}\right] \tag{B.20}$$

Proof

From (B.4), we have

$$\begin{aligned} E_{12} &= (I+\hat{A}_{11}-\hat{A}_{12}(I+\hat{A}_{22})^{-1}\hat{A}_{21})^{-1}\hat{A}_{12}-(I+\hat{A}_{11}-\hat{A}_{12}(I+\hat{A}_{22})^{-1}\hat{A}_{21})^{-1} \\ &\quad \times\hat{A}_{12}(I+\hat{A}_{22})^{-1}(\hat{A}_{22}-I) \\ &= 2(I+\hat{A}_{11})^{-1}\hat{A}_{12}(I+\hat{A}_{22}-\hat{A}_{21}(I+\hat{A}_{11})^{-1}\hat{A}_{12})^{-1} \end{aligned} \tag{B.21}$$

$$\begin{aligned} E_{21} &= -(I+\hat{A}_{22}-\hat{A}_{21}(I+\hat{A}_{11})^{-1}\hat{A}_{12})^{-1}\hat{A}_{21}(I+\hat{A}_{11})^{-1}(\hat{A}_{11}-I) \\ &\quad +(I+\hat{A}_{22}-\hat{A}_{21}(I+\hat{A}_{11})^{-1}\hat{A}_{12})^{-1}\hat{A}_{21} \\ &= 2(I+\hat{A}_{22})^{-1}\hat{A}_{21}(I+\hat{A}_{11}-\hat{A}_{12}(I+\hat{A}_{22})^{-1}\hat{A}_{21})^{-1} \end{aligned} \tag{B.22}$$

and

$$\begin{aligned} E_{22} &= -(I+\hat{A}_{22}-\hat{A}_{21}(I+\hat{A}_{11})^{-1}\hat{A}_{12})^{-1}\hat{A}_{21}(I+\hat{A}_{11})^{-1}\hat{A}_{12} \\ &\quad +(I+\hat{A}_{22}-\hat{A}_{21}(I+\hat{A}_{11})^{-1}\hat{A}_{12})^{-1}(\hat{A}_{22}-I) \\ &= (I+\hat{A}_{22}-\hat{A}_{21}(I+\hat{A}_{11})^{-1}\hat{A}_{12})^{-1}(-I+\hat{A}_{22}-\hat{A}_{21}(I+\hat{A}_{11})^{-1}\hat{A}_{12}) \\ &= I-2(I+\hat{A}_{22}-\hat{A}_{21}(I+\hat{A}_{11})^{-1}\hat{A}_{12})^{-1} \end{aligned} \tag{B.23}$$

From (B.7) and (B.9), we have

$$F_2=\sqrt{2}(I+\hat{A}_{22}-\hat{A}_{21}(I+\hat{A}_{11})^{-1}\hat{A}_{12})^{-1}(-\hat{A}_{21}(I+\hat{A}_{11})^{-1}\hat{B}_1+\hat{B}_2) \tag{B.24}$$

and

$$G_2=\sqrt{2}(-\hat{C}_1(I+\hat{A}_{11})^{-1}\hat{A}_{12}+\hat{C}_2)(I+\hat{A}_{22}-\hat{A}_{21}(I+\hat{A}_{11})^{-1}\hat{A}_{12})^{-1} \tag{B.25}$$

respectively. For the $\hat{A}_r$-matrix, we have

$$\hat{A}_r=(I+E_{11}-E_{12}E_{22}^{-1}E_{21})(I-E_{11}+E_{12}E_{22}^{-1}E_{21})^{-1} \tag{B.26}$$

where

$$\begin{aligned} E_{12}E_{22}^{-1} &= 2(I+\hat{A}_{11})^{-1}\hat{A}_{12}(I+\hat{A}_{22}-\hat{A}_{21}(I+\hat{A}_{11})^{-1}\hat{A}_{12})^{-1} \\ &\quad \times(I+\hat{A}_{22}-\hat{A}_{21}(I+\hat{A}_{11})^{-1}\hat{A}_{12})[(I+\hat{A}_{22}-\hat{A}_{21}(I+\hat{A}_{11})^{-1}\hat{A}_{12})-2I]^{-1} \\ &= 2(I+\hat{A}_{11})^{-1}\hat{A}_{12}(-I+\hat{A}_{22}-\hat{A}_{21}(I+\hat{A}_{11})^{-1}\hat{A}_{12})^{-1} \\ &= 2(-I+\hat{A}_{22}-\hat{A}_{21}(I+\hat{A}_{11})^{-1}\hat{A}_{12})^{-1}\hat{A}_{21}(I+\hat{A}_{11})^{-1} \end{aligned} \tag{B.27}$$

$(I-E_{11}+E_{12}E_{22}^{-1}E_{21})^{-1}=\hat{E}$, where

$$\begin{aligned} \hat{E} &= (I-I+2(I+\hat{A}_{11}-\hat{A}_{12}(I+\hat{A}_{22})^{-1}\hat{A}_{21})^{-1} \\ &\quad +4(I+\hat{A}_{11})^{-1}\hat{A}_{12}(-I+\hat{A}_{22}-\hat{A}_{21}(I+\hat{A}_{11})^{-1}\hat{A}_{12})^{-1} \\ &\quad \times(I+\hat{A}_{22})^{-1}\hat{A}_{21}(I+\hat{A}_{11}-\hat{A}_{12}(I+\hat{A}_{22})^{-1}\hat{A}_{21})^{-1})^{-1} \\ &= \frac{1}{2}(I+\hat{A}_{11}-\hat{A}_{12}(I+\hat{A}_{22})^{-1}\hat{A}_{21}) \\ &\quad \times[I+2(I+\hat{A}_{11}-\hat{A}_{12}(\hat{A}_{22}-I)^{-1}\hat{A}_{21})^{-1}\hat{A}_{12}(\hat{A}_{22}-I)^{-1}(\hat{A}_{22}+I)^{-1}\hat{A}_{21}]^{-1} \\ &= \frac{1}{2}(I+\hat{A}_{11}-\hat{A}_{12}(I+\hat{A}_{22})^{-1}\hat{A}_{21}) \\ &\quad \times(I+\hat{A}_{11}-\hat{A}_{12}(\hat{A}_{22}-I)^{-1}(\hat{A}_{22}+I-2I)(I+\hat{A}_{22})^{-1}\hat{A}_{21})^{-1} \\ &\quad \times(I+\hat{A}_{11}-\hat{A}_{12}(\hat{A}_{22}-I)^{-1}\hat{A}_{21}) \\ &= \frac{1}{2}(I+\hat{A}_{11}-\hat{A}_{12}(\hat{A}_{22}-I)^{-1}\hat{A}_{21}) \end{aligned} \tag{B.28}$$

$(I+E_{11}-E_{12}E_{22}^{-1}E_{21})=\check{E}$, where

$$\begin{aligned} \check{E} &= I+(I+\hat{A}_{11}-\hat{A}_{12}(I+\hat{A}_{22})^{-1}\hat{A}_{21})^{-1}(-I+\hat{A}_{11}-\hat{A}_{12}(I+\hat{A}_{22})^{-1}\hat{A}_{21}) \\ &\quad -4(I+\hat{A}_{11}-\hat{A}_{12}(I+\hat{A}_{22})^{-1}\hat{A}_{21})^{-1}\hat{A}_{12}(I+\hat{A}_{22})^{-1} \\ &\quad \times(-I+\hat{A}_{22}-\hat{A}_{21}(I+\hat{A}_{11})^{-1}\hat{A}_{12})^{-1}\hat{A}_{21}(I+\hat{A}_{11})^{-1} \\ &= (I+\hat{A}_{11}-\hat{A}_{12}(I+\hat{A}_{22})^{-1}\hat{A}_{21})^{-1} \\ &\quad \times[(2\hat{A}_{11}-2\hat{A}_{12}(I+\hat{A}_{22})^{-1}\hat{A}_{21})-4\hat{A}_{12}(I+\hat{A}_{22})^{-1} \\ &\quad \times(-I+\hat{A}_{22}-\hat{A}_{21}(I+\hat{A}_{11})^{-1}\hat{A}_{12})^{-1}\hat{A}_{21}(I+\hat{A}_{11})^{-1}] \\ &= 2(I+\hat{A}_{11}-\hat{A}_{12}(I+\hat{A}_{22})^{-1}\hat{A}_{21})^{-1} \\ &\quad \times[(\hat{A}_{11}-\hat{A}_{12}(I+\hat{A}_{22})^{-1}\hat{A}_{21})-2\hat{A}_{12}(\hat{A}_{22}+I)^{-1}(\hat{A}_{22}-I)^{-1} \\ &\quad \times\hat{A}_{21}(I+\hat{A}_{11}-\hat{A}_{12}(\hat{A}_{22}-I)^{-1}\hat{A}_{21})^{-1}] \\ &= 2(I+\hat{A}_{11}-\hat{A}_{12}(I+\hat{A}_{22})^{-1}\hat{A}_{21})^{-1} \\ &\quad \times[(I+\hat{A}_{11}-\hat{A}_{12}(I+\hat{A}_{22})^{-1}\hat{A}_{21})-I-2\hat{A}_{12}(\hat{A}_{22}+I)^{-1}(\hat{A}_{22}-I)^{-1} \\ &\quad \times\hat{A}_{21}(I+\hat{A}_{11}-\hat{A}_{12}(\hat{A}_{22}-I)^{-1}\hat{A}_{21})^{-1}] \end{aligned}$$

$$
\begin{aligned}
&= 2(I+\hat{A}_{11}-\hat{A}_{12}(I+\hat{A}_{22})^{-1}\hat{A}_{21})^{-1} \\
&\quad \times[I+\hat{A}_{11}-\hat{A}_{12}(I+\hat{A}_{22})^{-1}\hat{A}_{21} \\
&\quad -(I+\hat{A}_{11}-\hat{A}_{12}(I+\hat{A}_{22})^{-1}\hat{A}_{21})(I+\hat{A}_{11}-\hat{A}_{12}(\hat{A}_{22}-I)^{-1}\hat{A}_{21})^{-1}] \\
&= 2\left[I-(I+\hat{A}_{11}-\hat{A}_{12}(\hat{A}_{22}-I)^{-1}\hat{A}_{21})^{-1}\right] \\
&= 2\left[\hat{A}_{11}-\hat{A}_{12}(\hat{A}_{22}-I)^{-1}\hat{A}_{21}\right]\left[I+\hat{A}_{11}-\hat{A}_{12}(\hat{A}_{22}-I)^{-1}\hat{A}_{21}\right]^{-1} \qquad \text{(B.29)}
\end{aligned}
$$

From (B.26), the $\hat{A}_r$-matrix will be given by

$$\hat{A}_r = \hat{A}_{11}+\hat{A}_{12}(I-\hat{A}_{22})^{-1}\hat{A}_{21} \qquad \text{(B.30)}$$

For the $\hat{B}_r$-matrix, we have

$$\hat{B}_r = \sqrt{2}(I-E_{11}+E_{12}E_{22}^{-1}E_{21})^{-1}(F_1-E_{12}E_{22}^{-1}F_2) \qquad \text{(B.31)}$$

where $(F_1-E_{12}E_{22}^{-1}F_2)=\check{F}$, and

$$
\begin{aligned}
\check{F} &= \sqrt{2}[(I+\hat{A}_{11}-\hat{A}_{12}(I+\hat{A}_{22})^{-1}\hat{A}_{21})^{-1}(\hat{B}_1-\hat{A}_{12}(I+\hat{A}_{22})^{-1}\hat{B}_2) \\
&\quad +E_{12}E_{22}^{-1}(I+\hat{A}_{22}-\hat{A}_{21}(\hat{A}_{11}+I)^{-1}\hat{A}_{12})^{-1}(\hat{A}_{21}(\hat{A}_{11}+I)^{-1}\hat{B}_1-\hat{B}_2)] \\
&= \sqrt{2}(I+\hat{A}_{11}-\hat{A}_{12}(\hat{A}_{22}+I)^{-1}\hat{A}_{21})^{-1}[\hat{B}_1-\hat{A}_{12}(I+\hat{A}_{22})^{-1}\hat{B}_2+2\hat{A}_{12}(I+\hat{A}_{22})^{-1} \\
&\quad \times(-I+\hat{A}_{22}-\hat{A}_{21}(\hat{A}_{11}+I)^{-1}\hat{A}_{12})^{-1}(\hat{A}_{21}(\hat{A}_{11}+I)^{-1}\hat{B}_1-\hat{B}_2)] \\
&= \sqrt{2}(I+\hat{A}_{11}-\hat{A}_{12}(\hat{A}_{22}+I)^{-1}\hat{A}_{21})^{-1}[[I+2\hat{A}_{12}(I+\hat{A}_{22})^{-1} \\
&\quad \times(-I+\hat{A}_{22}-\hat{A}_{21}(\hat{A}_{11}+I)^{-1}\hat{A}_{12})^{-1}\hat{A}_{21}(I+\hat{A}_{11})^{-1}]\hat{B}_1-[\hat{A}_{12}(I+\hat{A}_{22})^{-1} \\
&\quad +2\hat{A}_{12}(I+\hat{A}_{22})^{-1}(-I+\hat{A}_{22}-\hat{A}_{21}(\hat{A}_{11}+I)^{-1}\hat{A}_{12})^{-1}]\hat{B}_2] \\
&= \sqrt{2}(I+\hat{A}_{11}-\hat{A}_{12}(\hat{A}_{22}+I)^{-1}\hat{A}_{21})^{-1}[(I+\hat{A}_{11}-\hat{A}_{12}(\hat{A}_{22}+I)^{-1}\hat{A}_{21}) \\
&\quad \times(I+\hat{A}_{11}-\hat{A}_{12}(\hat{A}_{22}-I)^{-1}\hat{A}_{21})^{-1}\hat{B}_1-(I+\hat{A}_{11}-\hat{A}_{12}(\hat{A}_{22}+I)^{-1}\hat{A}_{21}) \\
&\quad \times(I+\hat{A}_{11}-\hat{A}_{12}(\hat{A}_{22}-I)^{-1}\hat{A}_{21})^{-1}\hat{A}_{12}(\hat{A}_{22}-I)^{-1}\hat{B}_2] \\
&= \sqrt{2}(I+\hat{A}_{11}-\hat{A}_{12}(\hat{A}_{22}-I)^{-1}\hat{A}_{21})^{-1}(\hat{B}_1-\hat{A}_{12}(\hat{A}_{22}-I)^{-1}\hat{B}_2) \qquad \text{(B.32)}
\end{aligned}
$$

From (B.31), the $\hat{B}_r$-matrix will be given by

$$\hat{B}_r = \hat{B}_1+\hat{A}_{12}(I-\hat{A}_{22})^{-1}\hat{B}_2 \qquad \text{(B.33)}$$

For the $\hat{C}_r$-matrix, we have

$$\hat{C}_r = \sqrt{2}(G_1-G_2E_{22}^{-1}E_{21})(I-E_{11}+E_{12}E_{22}^{-1}E_{21})^{-1} \qquad \text{(B.34)}$$

where $G_1 - G_2E_{22}^{-1}E_{21} = \check{G}$, and

$$\begin{aligned}
\check{G} &= \sqrt{2}(\hat{C}_1 - \hat{C}_2(I+\hat{A}_{22})^{-1}\hat{A}_{21})(I+\hat{A}_{11}-\hat{A}_{12}(\hat{A}_{22}+I)^{-1}\hat{A}_{21})^{-1} \\
&\quad -\sqrt{2}[(-\hat{C}_1(I+\hat{A}_{11})^{-1}\hat{A}_{12}+\hat{C}_2)(I+\hat{A}_{22}-\hat{A}_{21}(\hat{A}_{11}+I)^{-1}\hat{A}_{12})^{-1}] \\
&\quad \times(-I+\hat{A}_{22}-\hat{A}_{21}(\hat{A}_{11}+I)^{-1}\hat{A}_{12})^{-1}(I+\hat{A}_{22}-\hat{A}_{21}(\hat{A}_{11}+I)^{-1}\hat{A}_{12}) \\
&\quad \times 2(I+\hat{A}_{22})^{-1}\hat{A}_{21}(I+\hat{A}_{11}-\hat{A}_{12}(\hat{A}_{22}+I)^{-1}\hat{A}_{21})^{-1} \\
&= \sqrt{2}[\hat{C}_1 - \hat{C}_2(I+\hat{A}_{22})^{-1}\hat{A}_{21} - 2(-\hat{C}_1(I+\hat{A}_{11})^{-1}\hat{A}_{12}+\hat{C}_2) \\
&\quad \times(I+\hat{A}_{22}-\hat{A}_{21}(\hat{A}_{11}+I)^{-1}\hat{A}_{12})^{-1}(-I+\hat{A}_{22}-\hat{A}_{21}(\hat{A}_{11}+I)^{-1}\hat{A}_{12})^{-1} \\
&\quad \times(I+\hat{A}_{22}-\hat{A}_{21}(\hat{A}_{11}+I)^{-1}\hat{A}_{12})^{-1}(I+\hat{A}_{22})^{-1}\hat{A}_{21}](I+\hat{A}_{11}-\hat{A}_{12}(\hat{A}_{22}+I)^{-1}\hat{A}_{21})^{-1} \\
&= \sqrt{2}[\hat{C}_1 - \hat{C}_2(I+\hat{A}_{22})^{-1}\hat{A}_{21} - 2(-\hat{C}_1(I+\hat{A}_{11})^{-1}\hat{A}_{12}+\hat{C}_2) \\
&\quad \times(-I+\hat{A}_{22}-\hat{A}_{21}(\hat{A}_{11}+I)^{-1}\hat{A}_{12})^{-1}(I+\hat{A}_{22})^{-1}\hat{A}_{21}](I+\hat{A}_{11}-\hat{A}_{12}(\hat{A}_{22}+I)^{-1}\hat{A}_{21})^{-1} \\
&= \sqrt{2}[\hat{C}_1[I+2(I+\hat{A}_{11})^{-1}\hat{A}_{12}(-I+\hat{A}_{22}-\hat{A}_{21}(\hat{A}_{11}+I)^{-1}\hat{A}_{12})^{-1}(I+\hat{A}_{22})^{-1}\hat{A}_{21}] \\
&\quad -\hat{C}_2[(I+\hat{A}_{22})^{-1}\hat{A}_{21}+2(-I+\hat{A}_{22}-\hat{A}_{21}(\hat{A}_{11}+I)^{-1}\hat{A}_{12})^{-1} \\
&\quad \times(\hat{A}_{22}+I)^{-1}\hat{A}_{21}]](I+\hat{A}_{11}-\hat{A}_{12}(\hat{A}_{22}+I)^{-1}\hat{A}_{21})^{-1} \\
&= \sqrt{2}[\hat{C}_1(I+\hat{A}_{11}-\hat{A}_{12}(\hat{A}_{22}-I)^{-1}\hat{A}_{21})^{-1}(I+\hat{A}_{11}-\hat{A}_{12}(\hat{A}_{22}+I)^{-1}\hat{A}_{21}) \\
&\quad -\hat{C}_2(\hat{A}_{22}-I)^{-1}\hat{A}_{21}(I+\hat{A}_{11}-\hat{A}_{12}(\hat{A}_{22}-I)^{-1}\hat{A}_{21})^{-1} \\
&\quad \times(I+\hat{A}_{11}-\hat{A}_{12}(\hat{A}_{22}+I)^{-1}\hat{A}_{21})(I+\hat{A}_{11}-\hat{A}_{12}(\hat{A}_{22}+I)^{-1}\hat{A}_{21})^{-1} \\
&= \sqrt{2}(\hat{C}_1 - \hat{C}_2(\hat{A}_{22}-I)^{-1}\hat{A}_{21})(I+\hat{A}_{11}-\hat{A}_{12}(\hat{A}_{22}-I)^{-1}\hat{A}_{21})^{-1} \qquad \text{(B.35)}
\end{aligned}$$

From (B.34), the $\hat{C}_r$-matrix will be given by

$$\hat{C}_r = \hat{C}_1 + \hat{C}_2(I-\hat{A}_{22})^{-1}\hat{A}_{21} \qquad \text{(B.36)}$$

For the $\hat{D}_r$-matrix, we have

$$\begin{aligned}
\hat{D}_r &= (\tilde{H} - G_2E_{22}^{-1}F_2) + (G_1 - G_2E_{22}^{-1}E_{21})(I - E_{11} + E_{12}E_{22}^{-1}E_{21})^{-1}(F_1 - E_{12}E_{22}^{-1}F_2) \\
&= [\hat{D} - \hat{C}(I+\hat{A})^{-1}\hat{B} - 2(-\hat{C}_1(I+\hat{A}_{11})^{-1}\hat{A}_{12}+\hat{C}_2) \\
&\quad \times(I+\hat{A}_{22}-\hat{A}_{21}(\hat{A}_{11}+I)^{-1}\hat{A}_{12})^{-1}(-I+\hat{A}_{22}-\hat{A}_{21}(\hat{A}_{11}+I)^{-1}\hat{A}_{12})^{-1} \\
&\quad \times(I+\hat{A}_{22}-\hat{A}_{21}(\hat{A}_{11}+I)^{-1}\hat{A}_{12})(I+\hat{A}_{22}-\hat{A}_{21}(\hat{A}_{11}+I)^{-1}\hat{A}_{12})^{-1} \\
&\quad \times(-\hat{A}_{21}(I+\hat{A}_{11})^{-1}\hat{B}_1+\hat{B}_2)] + \sqrt{2}(\hat{C}_1 - \hat{C}_2(\hat{A}_{22}-I)^{-1}\hat{A}_{21}) \\
&\quad \times(I+\hat{A}_{11}-\hat{A}_{12}(\hat{A}_{22}-I)^{-1}\hat{A}_{21})^{-1}\frac{1}{2}(I+\hat{A}_{11}-\hat{A}_{12}(\hat{A}_{22}-I)^{-1}\hat{A}_{21}) \\
&\quad \times\sqrt{2}(I+\hat{A}_{11}-\hat{A}_{12}(\hat{A}_{22}-I)^{-1}\hat{A}_{21})^{-1}(\hat{B}_1 - \hat{A}_{12}(\hat{A}_{22}-I)^{-1}\hat{B}_2) \\
&= [\hat{D} - \hat{C}(I+\hat{A})^{-1}\hat{B} - 2(\hat{C}_1(I+\hat{A}_{11})^{-1}\hat{A}_{12}-\hat{C}_2)(I+\hat{A}_{22}-\hat{A}_{21}(\hat{A}_{11}+I)^{-1}\hat{A}_{12})^{-1}
\end{aligned}$$

$$
\begin{aligned}
&\times(-I+\hat{A}_{22}-\hat{A}_{21}(\hat{A}_{11}+I)^{-1}\hat{A}_{12})^{-1}(\hat{A}_{21}(I+\hat{A}_{11})^{-1}\hat{B}_1--\hat{B}_2)]\\
&+(\hat{C}_1-\hat{C}_2(\hat{A}_{22}-I)^{-1}\hat{A}_{21})(I+\hat{A}_{11}-\hat{A}_{12}(\hat{A}_{22}-I)^{-1}\hat{A}_{21})^{-1}(\hat{B}_1-\hat{A}_{12}(\hat{A}_{22}-I)^{-1}\hat{B}_2)\\
=\ &[\hat{D}-[\hat{C}_1(I+\hat{A}_{11}-\hat{A}_{12}(\hat{A}_{22}+I)^{-1}\hat{A}_{21})^{-1}\hat{B}_1\\
&-\hat{C}_2(I+\hat{A}_{22}-\hat{A}_{21}(\hat{A}_{11}+I)^{-1}\hat{A}_{12})^{-1}\hat{A}_{21}(I+\hat{A}_{11})^{-1}\hat{B}_1\\
&-\hat{C}_1(I+\hat{A}_{11})^{-1}\hat{A}_{12}(I+\hat{A}_{22}-\hat{A}_{21}(\hat{A}_{11}+I)^{-1}\hat{A}_{12})^{-1}\hat{B}_2\\
&+\hat{C}_2(I+\hat{A}_{22}-\hat{A}_{21}(\hat{A}_{11}+I)^{-1}\hat{A}_{12})^{-1}\hat{B}_2]\\
&-2(\hat{C}_1(I+\hat{A}_{11})^{-1}\hat{A}_{12}-\hat{C}_2)(I+\hat{A}_{22}-\hat{A}_{21}(\hat{A}_{11}+I)^{-1}\hat{A}_{12})^{-1}\\
&\times(-I+\hat{A}_{22}-\hat{A}_{21}(\hat{A}_{11}+I)^{-1}\hat{A}_{12})^{-1}(\hat{A}_{21}(I+\hat{A}_{11})^{-1}\hat{B}_1-\hat{B}_2)]\\
&+(\hat{C}_1-\hat{C}_2(\hat{A}_{22}-I)^{-1}\hat{A}_{21})(I+\hat{A}_{11}-\hat{A}_{12}(\hat{A}_{22}-I)^{-1}\hat{A}_{21})^{-1}(\hat{B}_1-\hat{A}_{12}(\hat{A}_{22}-I)^{-1}\hat{B}_2)\\
=\ &\hat{D}+\hat{C}_2(I-\hat{A}_{22})^{-1}\hat{B}_2 \qquad \text{(B.37)}
\end{aligned}
$$

This completes the proof. ■

References

[1] U.M. Al-Saggaf and G.F. Franklin. An Error Bound for a Discrete Reduced Order Model of a Linear Multivariable System. *IEEE Transactions on Automatic Control*, 32(9):815–819, September 1987.

[2] U.M. Al-Saggaf and G.F. Franklin. Model Reduction via Balanced Realizations: An Extension and Frequency Weighting Techniques. *IEEE Transactions on Automatic Control*, 33(7):687–692, July 1988.

[3] B.D.O. Anderson, K.L. Hitz, and N.D. Diem. Recursive Algorithm for Spectral Factorization. *IEEE Transactions on Circuits and Systems*, CAS-21(6):742–750, November 1974.

[4] B.D.O. Anderson and J.B. Moore. *Optimal Control: Linear Quadratic Methods.* Prentice-Hall, 1989.

[5] K.J. Astrom and B. Wittenmark. *Computer Controlled Systems: Theory and Design.* Prentice-Hall, 1984.

[6] A.C.P.M. Backx. *Identification of an Industrial Process: A Parameter Approach.* PhD thesis, Eindhoven University of Technology, The Netherlands, 1987.

[7] G.J. Balas, J.C. Doyle, K. Glover, A. Packard, and R. Smith. *μ-Analysis and Synthesis Toolbox: User's Guide.* MUSYN Inc. and The Mathworks, Inc., 1993.

[8] S. Bittanti, A.J. Laub, and J.C. Willems. *The Riccati Equation.* Communications and Control Engineering. Springer-Verlag, 1991.

[9] H.W. Bode. *Network Analysis and Feedback Amplifier Design.* D. Van Nostrand, Princeton, N.J., 1945.

[10] S. Boyd. On Computing the $\mathcal{H}^\infty$-Norm of a Transfer Matrix. *ACC Proceedings*, pages 396–397, 1988.

[11] S. Boyd and C. Baratt. *Linear Controller Design: Limits of Performance.* Prentice-Hall, 1991.

[12] J.C. Doyle C.C. Chu and E.B. Lee. The General Distance Problem in $\mathcal{H}^\infty$ Optimal Control Theory. *International Journal of Control*, 44:565–596, 1986.

[13] B.C. Chang and J.B. Pearson. Optimal Disturbance Rejection in Linear Multivariable Systems. *IEEE Transactions on Automatic Control*, AC-29:880–887, 1984.

[14] M. A. Dahleh and I.J. Diaz-Bobillo. *Control of Uncertain Systems.* Prentice-Hall, 1995.

[15] P.B. Deshpande. *Multivariable Process Control.* Instrument Society of America, USA, 1989.

[16] C.A. Desoer and W.S. Chan. The Feedback Interconnection of Lumped Linear Time-invariant Systems. *Journal of the Franklin Institute*, 300(5 & 6):335–351, 1975.

[17] J.C. Doyle. Analysis of Feedback Systems with Structured Uncertainties. *IEE Proceedings - Part D*, 129(6):242–250, November 1982.

[18] J.C. Doyle. Performance and Robustness Analysis for Structured Uncertainty. *IEEE CDC Proceedings*, pages 629–636, December 1982.

[19] J.C. Doyle. Lecture Notes in Advanced Multivariable Control. ONR/Honeywell Workshop, Minneapolis, 1984.

[20] J.C. Doyle. Structured Uncertainty in Control System Design. *IEEE CDC Proceedings*, pages 260–265, December 1985.

[21] J.C. Doyle and K. Glover. μ and $\mathcal{H}^\infty$: A Short Course. Cambridge Control, June 1990. Held at Cambridge University, Department of Engineering.

[22] J.C. Doyle, K. Glover, P.P. Khargonekar, and B.A. Francis. State-Space Solutions to Standard $\mathcal{H}^2$ and $\mathcal{H}^\infty$ control problems. *IEEE Transactions on Automatic Control*, 34:831–847, August 1989.

[23] J.C. Doyle and G. Stein. Multivariable Feedback Design: Concepts for a Classical/ Modern Synthesis. *IEEE Transactions on Automatic Control*, 26:4–16, February 1981.

[24] C.G. Economou and M. Morari. Internal Model Control. 6. Multiloop Design. *Ind. Eng. Chem. Process Des. Dev*, 25:252–265, 1986.

[25] A. Elias-Juarez, A. Ajbar, and J.C. Kantor. Multiobjective l^∞ Design with Integrated Diagnostics. *ACC Proceedings*, pages 1671–1672, 1991.

[26] H. Falkus, P. Van Overschee, G. Murad, R. Hakvoort, and J. Ludlage. Advanced Identification and Robust Control of a Glass Tube Production Process. *Third Philips Conference on Applications of Systems and Control Theory*, November 1994.

[27] Heinz Falkus. *Parametric Uncertainty in System Identification.* PhD thesis, Department of Electrical Engineering, Eindhoven University of Technology, The Netherlands, 1994.

[28] K.V. Fernando and H. Nicholson. Singular Perturbational Approximation for Discrete-Time Systems. *IEEE Transactions on Automatic Control*, 28(2):240–242, February 1983.

[29] B.A. Francis. *A Course in $\mathcal{H}^\infty$ Control Theory*, volume 88 of *Control and Information Sciences.* Springer-Verlag, 1987.

[30] B.A. Francis, J.W. Hilton, and G. Zames. $\mathcal{H}^\infty$-Optimal Feedback Controllers for Linear Multivariable Systems. *IEEE Transactions on Automatic Control*, AC-29(10):888–900, October 1984.

[31] P.M. Frank. *Entwurf von Regelkreisen mit vorgeschriebenem Verhalten.* G. Braun, Karlsruhe, 1974.

[32] C.E. Garcia and M. Morari. Internal Model Control. 1. A Unifying Review and some New Results. *Ind. Eng. Chem. Process Des. Dev*, 21:308–323, 1985.

[33] C.E. Garcia and M. Morari. Internal Model Control. 2. Design Procedure for Multivariable Systems. *Ind. Eng. Chem. Process Des. Dev*, 24:472–484, 1985.

[34] C.E. Garcia and M. Morari. Internal Model Control. 3. Multivariable Control Law Computation and Tuning Guidelines. *Ind. Eng. Chem. Process Des. Dev*, 24:484–494, 1985.

[35] T.T. Georgiou and M.C. Smith. Optimal Robustness in the Gap Metric. *IEEE Transactions on Automatic Control*, 35(6):673–685, June 1990.

[36] K. Glover. All Optimal Hankel-norm Approximations of Linear Multivariable Systems and their l^∞-error Bounds. *International Journal of Control*, 39(6):1115–1193, 1984.

[37] K. Glover and J.C. Doyle. State-Space Formulae for all Stabilizing Controllers that satisfy an $\mathcal{H}^\infty$ Norm Bound and Relations to Risk Sensitivity. *Systems & Control Letters*, 11:167–172, 1988.

[38] K. Glover, D.J.N. Limebeer, J.C. Doyle, E.M. Kasenally, and M.G. Safonov. A Characterization of all Solutions to the Four Block General Distance Problem. *SIAM Journal of Control & Optimization*, 29(2):283–324, 1991.

[39] S.F. Graebe. Robust and Adaptive Control of an Unknown Plant: A Benchmark of New Format. *IFAC World Congress Proceedings*, 3:165–168, July 1993.

[40] M. Green, K. Glover, D.J.N. Limebeer, and J.C. Doyle. A J-spectral Factorization Approach to $\mathcal{H}^\infty$ Control. *SIAM Journal of Control & Optimization*, 28:1350–1371, 1990.

[41] M. Green and D.J.N. Limebeer. *Linear Robust Control.* Prentice-Hall, 1994.

[42] M. Green, D.J.N. Limebeer, and E. Kasenally. A Note on $\mathcal{H}^2$-Optimal Control. Department of Electrical Engineering, Imperial College, February 1988.

[43] D-W. Gu, M.C. Tsia, and I. Postlethwaite. State-Space Formulae for Discrete-Time Optimization. *International Journal of Control*, 49(5):1683–1723, 1989.

[44] R.G. Hakvoort. *System Identification for Robust Process Control: Nominal Models and Error Bounds.* PhD thesis, Department of Mechanical Engineering, Delft University of Technology, The Netherlands, 1994.

[45] S. Hammerling. Numerical Solution of the Discrete-Time, Convergent, Non-Negative Definite Lyapunov Equation. *Systems & Control Letters*, 17:137–139, 1991.

[46] B.R. Holt and M. Morari. Design of Resilient Processing Plants - V. The Effect of Deadtime on Dynamic Resilience. *Chemical Engineering Science*, 40(7):1229–1237, 1985.

[47] D. Hoyle, R. Hyde, and D.J.N. Limebeer. An $\mathcal{H}^\infty$ Approach to Two-Degree-Of-Freedom Design. *Proceedings of the IEEE CDC*, pages 1581–1585, December 1991.

[48] P.A. Iglesias. *Robust and Adaptive Control for Discrete-Time Systems.* PhD thesis, Cambridge University, U.K., 1991.

[49] P.A. Iglesias and K. Glover. State-Space Approach to Discrete-Time $\mathcal{H}^\infty$ Control. *International Journal of Control*, 54(5):1031–1073, 1991.

[50] C.A. Jacobson and C.N. Nett. An Integrated Approach to Controls and Diagnostics Using The 4-Parameter Controller. *IEEE Control System Magazine*, 11(6):22–29, October 1991.

[51] T. Kailath. *Linear Systems.* Information and System Sciences. Prentice-Hall, 1980.

[52] D. Kavranoglu. *Elementary Solutions for the $\mathcal{H}^\infty$-General Distance Problem-Equivalence of $\mathcal{H}^2$ and $\mathcal{H}^\infty$ Optimization Problems.* PhD thesis, California Institute of Technology, USA, 1989.

[53] V. Kucera. *Analysis and Design of Discrete Linear Control Systems.* Prentice-Hall, University Press, Cambride, 1991.

[54] H. Kwakernaak and R. Sivan. *Linear Optimal Control Systems.* Wiley, 1972.

[55] A.J. Laub. On Computing Balancing Transformations. *Proc. joint ACC*, pages FA8–E, 1980.

[56] A.J. Laub, M.T. Heath, C.C. Paige, and R.C. Ward. Computation of System Balancing Transformations and other Applications of Simultaneous Diagonalization Algorithms. *IEEE Transactions on Automatic Control*, 32(2):115–121, February 1987.

[57] D.J.N. Limebeer, B.D.O. Anderson, P.P. Khargonekar, and M. Green. A Game Theoretic Approach to $\mathcal{H}^\infty$ Control for Time-Varying Systems. *SIAM Journal of Control and Optimization*, 30(2):262–283, March 1992.

[58] D.J.N. Limebeer, M. Green, and D. Walker. Discrete Time $\mathcal{H}^\infty$ Control. *IEEE CDC Proceedings*, pages 392–396, December 1989.

[59] Yi Liu and B.D.O. Anderson. Singular Perturbation of Balanced Systems. *International Journal of Control*, 50(4):1379–1405, 1989.

[60] L. Ljung. *Sytem Identification: Theory For The User.* Information and System Sciences. Prentice-Hall, 1987.

[61] J. Maciejowski. *Multivariable Feedback Design.* Addison-Wesley, 1989.

[62] D. McFarlane and K. Glover. *Robust Controller Design Using Normalized Coprime Factor Plant Descriptions.* Information and Control Sciences. Springer-Verlag, 1990.

[63] D.G. Meyer. Fractional Balanced Reduction: Model Reduction via Fractional Representation. *IEEE Transactions on Automatic Control*, 35(3):1341–1345, 1990.

[64] A.T. Miller. Integrated Controls and Diagnostics: An Application to a Nonlinear Aircraft Engine Model. Master's thesis, Electrical and Computer Engineering Department, Northeastern University, U.S.A., 1989.

[65] B. C. Moore. Principle Component Analysis in Linear Systems: Controllability, Observability, and Model Reduction. *IEEE Transactions on Automatic Control*, 26(1):17–31, February 1981.

[66] M. Morari, S. Skogestad, and D.E. Rivera. Implications of Internal Model Control for PID Controllers. *American Control Conference*, pages 661–666, 1984.

[67] M. Morari and E. Zafiriou. *Robust Process Control.* Prentice-Hall, 1989.

[68] C.T. Mullis and R.A. Roberts. Round-off Noise in Digital Filters: Frequency Transformations and Invariants. *IEEE Transactions on Acoustics, Speech, and Signal Processing*, 24(6):538–550, December 1976.

[69] C.T. Mullis and R.A. Roberts. Synthesis of Minimum Roundoff Noise Fixed Point Digital Filters. *IEEE Transactions on Circuits and Systems*, 23(9):551–562, September 1976.

[70] G. Murad, I. Postlethwaite, and D.-W. Gu. Robust Control System Design Applied to a Glass Tube Shaping Process. *IFAC World Congress Proceedings*, 4:385–388, July 1993.

[71] G. Murad, I. Postlethwaite, D.-W. Gu, and R. Samar. On The Structure of an $\mathcal{H}^\infty$ Two-Degree-Of-Freedom Internal Model-Based Controller & Its Application to a Glass Tube Production Process. *1995 European Control Conference*, 1995.

[72] G. Murad, I. Postlethwaite, D.-W. Gu, and J.F. Whidborne. Robust Control of a Glass Tube Shaping Process. *Proceedings of the Second European Control Conference*, 4:2350–2355, June-July 1993.

[73] G. Murad, I. Potlethwaite, D.-W. Gu, and J.F. Whidborne. Robust Control of a Glass Tube Production Process. In IEE, editor, *Improvements in Furnace Control: Current Developments and New Technologies*, pages 7/1–7/4, U.K., January 1994. Professional Group C9 (Applied Control Techniques).

[74] Z. Nehari. On Bounded Bilinear Forms. *Annals of Mathematics*, 65(1):153–162, January 1957.

[75] J.A. Nelder and R. Mead. A Simplex Method for Function Minimization. *IEE Proceedings on Control and Science*, 7:308, 1965.

[76] C.N. Nett. Algebraic Aspects of Linear Control System Stability. *IEEE Transactions on Automatic Control*, AC-31(10):941–949, October 1986.

[77] C.N. Nett, C.A. Jacobson, and A.T. Miller. An Integrated Approach to Controls and Diagnostics: The 4-Parameter Controller. *ACC Proceedings*, June 1988.

[78] G.C. Newton, L.A. Gould, and J.F. Kaiser. *Analytical Design of Feedback Controls*. Wiley, 1957.

[79] W.Y. Ng. *Interactive Multi-Objective Programming As A Framework For Computer-Aided Control System Design.* Information and Control Sciences. Springer-Verlag, 1989.

[80] H. Nyquist. Regeneration Theory. *Bell System Technical Journal*, 11:126–147, 1932.

[81] P. Van Overschee. *Subspace Identification: Theory - Implementation - Application.* PhD thesis, Department of Electrical Engineering, Catholic University Leuven, Belgium, 1995.

[82] A. Packard and J.C. Doyle. The Complex Structured Singular Value. *Automatica, Special Issue on Robust Control*, 29, 1993.

[83] T. Pappas, A.J. Laub, and N.R. Sandell. On the Numerical Solution of the Discrete-Time Algebraic riccati Equation. *IEEE Transactions on Automatic Control*, AC-25(4):631–641, August 1980.

[84] L. Pernebo and L.M. Silverman. Model Reduction via Balanced State Space Representations. *IEEE Transactions on Automatic Control*, 27(2):382–387, April 1982.

[85] I. Postlethwaite, J. Whidborne, G. Murad, and D.-W. Gu. Robust Control of the Benchmark Problem Using $\mathcal{H}^\infty$ Methods and Numerical Optimization Techniques. *IFAC World Congress Proceedings*, 3:193–196, July 1993.

[86] I. Postlethwaite, J.F. Whidborne, G. Murad, and D.-W. Gu. Robust Control of the Benchmark Problem Using $\mathcal{H}^\infty$ Methods and Numerical Optimization Techniques. *Automatica*, 30(4):615–619, 1994.

[87] M. Redheffer. Inequalities for a Matrix Riccati Equation. *Journal of Mathematics and Mechanics*, 8(3):349–367, 1959.

[88] M. Redheffer. On a Certain Linear Fractional Transformation. *Journal of Maths and Physics*, 39:269–286, 1960.

[89] D.E. Rivera, M. Morari, and S. Skogestad. Internal Model Control. 4. PID Controller Design. *Ind. Eng. Chem. Process Des. Dev*, 25:252–265, 1986.

[90] H.H. Rosenbrock. An Automatic Method for Finding the Greatest or Least Value of a Function. *Computer Journal*, 3:175–184, 1960.

[91] M. Safonov, E. Jonckheere, M. Verma, and D.J.N. Limebeer. Synthesis of Positive Real Multivariable Feedback Systems. *International Journal of Control*, 45(3):817–842, 1987.

[92] M.G. Safonov and M.S. Verma. $\mathcal{L}^\infty$ Optimization and Hankel Approximation. *IEEE Transactions on Automatic Control*, AC-30:279–280, 1985.

[93] R. Samar, G. Murad, I. Postlethwaite, and D.-W. Gu. A Discrete Time $\mathcal{H}^\infty$ Observer-Based Controller & Its Application to an Aero-Engine. *ACC Proceedings*, 1995.

[94] J. Sefton and K. Glover. Pole-Zero Cancellations in the General $\mathcal{H}^\infty$ Problem with Reference to a Two Block Design. *Systems & Control Letters*, 14:295–306, 1990.

[95] O.J.M. Smith. Closer Control of Loops with Dead Time. *Chemical Engineering Progress*, 53(5):217–219, 1957.

[96] A. Stoorvogel. *The $\mathcal{H}^\infty$ Control Problem.* Systems and Control Engineering. Prentice-Hall, 1992.

[97] M.S. Tombs and I. Postlethwaite. Truncated Balanced Realization of a Stable Non-minimal State Space System. *International Journal of Control*, 46(4):1319–1330, 1987.

[98] M.L. Tyler and M. Morari. Optimal and Robust Design of Integrated Control and Diagnostic Modules. *ACC Proceedings*, pages 2060–2064, June 1994.

[99] K.P. Valavanis, C.A. Jacobson, and B. Gold. An Application of The 4-Parameter Controller to The Robot Playload Variation Problem. *Proc. IEEE CDC*, pages 244–250, December 1989.

[100] A. Varga. Balancing Free Square-Root Algorithm for Computing Singular Perturbation Approximations. *Proc. IEEE CDC*, pages 1062–1065, December 1991.

[101] A. Varga. Balancing Singular Perturbation Approximations of coinner transfer function matrices. *Proc. IEEE CDC*, December 1992.

[102] M. Vidyasagar. Coprime Factorizations and the Stability of Multivariable Distributed Feedback Systems. *SIAM Journal of Control*, 13:1144, 1975.

[103] M. Vidyasagar. *Control System Synthesis: A Coprime Factorization Approach.* MIT Press, 1985.

[104] M. Vidyasagar and H. Kimura. Robust Controllers for Uncertain Linear Multivariable Systems. *Automatica*, 22(1):85–94, 1986.

[105] M. Vidyasagar, H. Schneider, and B. Francis. Algebraic and Topological Aspects of Feedback Stabilization. *IEEE Transactions on Automatic Control*, 27:880–894, 1982.

[106] D.J. Walker. Robust Stabilizability of Discrete-Time Systems with Normalized Stable Factor Perturbation. *International Journal of Control*, 52(2):441–455, 1990.

[107] D.J. Walker. *Robust Control of Discrete-Time Systems.* PhD thesis, Department of Electrical Engineering, Imperial College of Science, Technology and Medicine, University of London, 1992.

[108] D.J. Walker. On the Structure of a 2-degree-of-freedom $\mathcal{H}^\infty$ Loop Shaping Controller. *To appear in the International Journal of Control*, 1996.

[109] J.F. Whidborne, G. Murad, D.-W. Gu, and I. Postlethwaite. Multi-Objective Robust Controller Design using a Mixed Optimization Approach. In IEE, editor, *Advances in the Application of Robust Controllers*, pages 1–3, U.K., November 1993. Professional Group C9 (Applied Control Techniques).

[110] J.F. Whidborne, G. Murad, D.-W. Gu, and I. Postlethwaite. Robust Control of an Unknown Plant – The IFAC 93 Benchmark. *International Journal of Control*, 61(3):589–640, 1994.

[111] J.F. Whidborne, I. Postlethwaite, and D.-W. Gu. Robust Controller Design Using $\mathcal{H}^\infty$ Loop-Shaping and the Method of Inequalities. *IEEE Transactions on Control Systems Technology*, 2:455–461, 1994.

[112] X. Wu and A. Cinar. Reliable Process Control by 4-Parameter Controllers. *ACC Proceedings*, pages 1860–1865, 1991.

[113] D.C. Youla, H.A. Jabr, and J.J. Bongiorno. Modern Weiner-Hopf Design of Optimal Controllers, Part ii: The Multivariable Case. *IEEE Transactions on Automatic Control*, 21:319–338, 1976.

[114] L.A. Zadeh. From Circuit Theory to System Theory. *Proceedings of the IRE*, 50:856–865, 1962.

[115] V. Zakian and U. Al-Naib. Design of Dynamical and Control Systems by the Method of Inequalities. *IEE Proceedings - Control & Science*, 120(11):1421–1427, November 1973.

[116] G. Zames. On the Input-Output Stability of Time-Varying Nonlinear Feedback Systems Part I: Conditions Derived Using Concepts of Loop Gain, Conicity, and Positivity. *IEEE Transactions on Automatic Control*, AC-11:228–238, 1966.

[117] G. Zames. Feedback and Optimal Sensitivity: Model Reference Transformations, Multiplicative Seminorms and Approximate Inverses. *IEEE Transactions on Automatic Control*, 26(2):301–320, 1981.

[118] Y. Zhu and T. Backx. *Identification of Multivariable Industrial Processes for Simulation, Diagnosis and Control.* Advances in Industrial Control. Springer-Verlag, 1993.

[119] J.G. Ziegler and N.B. Nichols. Optimum Settings for Automatic Controllers. *Trans. ASME*, 64:759–768, 1942.